THE GEOLOGY, MINERALIZATION, GEOCHEMISTRY, AND METALLOGENY OF THE PALEOPROTEROZOIC RAMAH GROUP, NORTHERN LABRADOR

SANDY MACKINTOSH ARCHIBALD

NOTICE

The quality of this microform is heavily dependent upon the quality of the original thesis submitted for microfilming. Every effort has been made to ensure the highest quality of reproduction possible.

If pages are missing, contact the university which granted the degree.

Some pages may have indistinct print especially if the original pages were typed with a poor typewriter ribbon or if the university sent us an inferior photocopy.

Reproduction in full or in part of this microform is governed by the Canadian Copyright Act, R.S.C. 1970, c. C-30, and subsequent amendments.

AVIS

La qualité de cette microforme dépend grandement de la qualité de la thèse soumise au microfilmage. Nous avons tout fait pour assurer une qualité supérieure de reproduction.

S'il manque des pages, veuillez communiquer avec l'université qui a conféré le grade.

La qualité d'impression de certaines pages peut laisser à désirer, surtout si les pages originales ont été dactylographiées à l'aide d'un ruban usé ou si l'université nous a fait parvenir une photocopie de qualité inférieure.

La reproduction, même partielle, de cette microforme est soumise à la Loi canadienne sur le droit d'auteur, SRC 1970, c. C-30, et ses amendements subséquents.

Canada

THE GEOLOGY, MINERALIZATION, GEOCHEMISTRY, AND METALLOGENY OF THE PALEOPROTEROZOIC RAMAH GROUP, NORTHERN LABRADOR

by

© Sandy Mackintosh Archibald, B.Sc. (Hons.)

A thesis submitted to the School of Graduate Studies in partial fulfilment of the requirements for the degree of Master of Science

Department of Earth Sciences

Memorial University of Newfoundland

February 1995

St. John's Newfoundland

ISBN 0-612-01835-0

Canada

ABSTRACT

The Paleoproterozoic (ca. 2000 Ma) Ramah Group represents a relatively undeformed cover sequence developed on the Nain craton, northern Labrador. The group is 1.7 km thick, 65 km long and up to 16 km wide, and is most extensive between Nachvak and Saglek Fiords. Six formations make up the group, of which the two basal formations represent a shallow shelf sequence, while the upper four represent deep marine sequences. The dolomite unit capping the shelf sequence is metallogenically the most interesting as it hosts the majority of base metal mineralization present within the Ramah Group.

Two types of metallic mineralization are represented within the Ramah Group, namely syngenetic and epigenetic. The syngenetic mineralization formed due to rapid basin deepening which resulted in the formation of anoxic bottom waters. These bottom waters were enriched in sulphur-reducing bacteria which led to the precipitation of a two metre thick pyrite bed, and to the consequential ^{34}S enrichment of the remaining seawater in the basin. Further sedimentation led to the trapping of this ^{34}S-enriched water as a pore fluid within shales of the Nullataktok Formation. Following the deposition of the sedimentary formations, the Ramah Group was intruded by numerous gabbro-diabase sills which resulted in the formation of Cu and Ni mineralization within or adjacent to the sills.

The main metallogenic event to affect the Ramah Group resulted from the collision of the Nain and Rae Structural Provinces during the Torngat Orogeny (1860 Ma). The

collision caused the early migration of hydrocarbons, followed by large volumes of evolved basin brines. These brines contained metal chloride complexes, and ^{34}S-enriched pore water (in the form of dissolved sulphates) which migrated from deeper parts of the group to the basin margins. Precipitation of sulphides occurred in areas of increased porosity, such as collapse breccia zones, within the Reddick Bight Dolomite Member when the expelled sulphate and metal rich fluids mixed with resident hydrocarbons. Further epigenetic mineralization was formed due to remobilization of sulphides within fault zones as the Torngat Orogen deformation front progressed eastwards.

Mineralization within the Reddick Bight Dolomite Member is analogous to the Mississippi Valley-type (MVT) and as such represents the second oldest occurrence of this style of mineralization identified to date.

ACKNOWLEDGEMENTS

Sincere thanks to my supervisor, Dr. Derek Wilton, for his academic guidance and financial support. His use of the English language improved this thesis immeasurably, and his ever present sense of humour provided relief from something, but I'm not exactly sure what. ☺

Dr. Mark Wilson and Dr. George Jenner were very helpful with discussions on the use and abuse of stable isotopes and REE patterns, respectively. Dr. Ian Knight is thanked for discussion on carbonate textures within the dolomites, as is Dr. Peter Davenport for drawing my attention to the Archean as a potential metal source area. Adrian Timbal competently performed, and offered advice on stable isotope extraction methods. Adam Szybinski unselfishly allowed me the use of his printer and also discussed many aspects of igneous geochemistry. Gerry Kilfoil is thanked for acquiring stream sediment data. Dr. Jamie Jamison is thanked for unpublished structural data.

Fellow graduate students Pablo Valverde Vaquero and Richard Cox (as well as countless others) are thanked for sensible and not so sensible discussion on anything and everything apart from my thesis.

Peter Tallman (Black Pine Ltd) is thanked for the opportunity to go back to the Ramah Group in the summer of 1994 and re-examine the mineralization. Mike Cullen is thanked for stimulating discussions on carbonate brecciation.

Transportation and accommodation was provided by the good ship *M.V. Robert Bradford* captained by Kevin and Urias (Roy) Normore from Lanse-au-Loup. Field assistance was ably provided by Roland Butler (Jr.) with support from Andrew Hussey, and Merlin Gates.

Special thanks are owed to Rod Churchill for helping to produce the two fine maps that grace the back of this thesis, the many computer tutorials he has given, and countless bovine discussions.

Robyn Jamieson is thanked for the patience she has shown during the many good and ugly faces (or phases) of this thesis. Her ability to find many spelling mistakes and grammatical errors in the penultimate copy of the thesis was annoying, but also greatly appreciated. ☺

Finally, I would like to thank my parents for all the financial support and encouragement they have given me during my education.

TABLE OF CONTENTS

CHAPTER 3

MINERALIZATION

CHAPTER 4

RESULTS

CHAPTER 5

METALLOGENIC MODELS AND CONCLUSIONS

CHEMICAL ANALYSIS

ANALYTICAL TECHNIQUES

LIST OF TABLES

LIST OF FIGURES

LIST OF PLATES

CHAPTER 1

INTRODUCTION

General Statement

This study constitutes the first detailed description of mineralization within the Paleoproterozoic Ramah Group, northern Labrador. Results from field observations and geochemical analysis are used to place the Ramah Group mineralization into a metallogenic model.

The Ramah Group (Gp.) is a narrow (16 km wide, 190 km long) linear belt of north-south trending mainly meta-sedimentary rocks which occurs along the boundary between the Nain and Rae Structural provinces in northern Labrador (Taylor, 1971; Hoffman, 1988). The best preserved section of the Ramah Group extends for approximately 60 km between Saglek and Nachvak Fiords (Figure 1.1). Rocks to the east of the Ramah Gp. are Archean whereas those to the west are Archean gneisses that were reworked during the Lower Proterozoic (Morgan, 1975).

1.1 Location, Access and Physiography

1.1.1 Location and Access

The study area is situated in the easternmost part of the Torngat Mountains, about 300 km east of Kuujjuaq (Ft. Chimo), 450 km north-east of Schefferville, Quebec and 600 km north-north-west of Goose Bay, Labrador (Figure 1.1). Daily flights are available to Happy Valley - Goose Bay from St. John's, Halifax, and Montreal. Lab Air offers a year

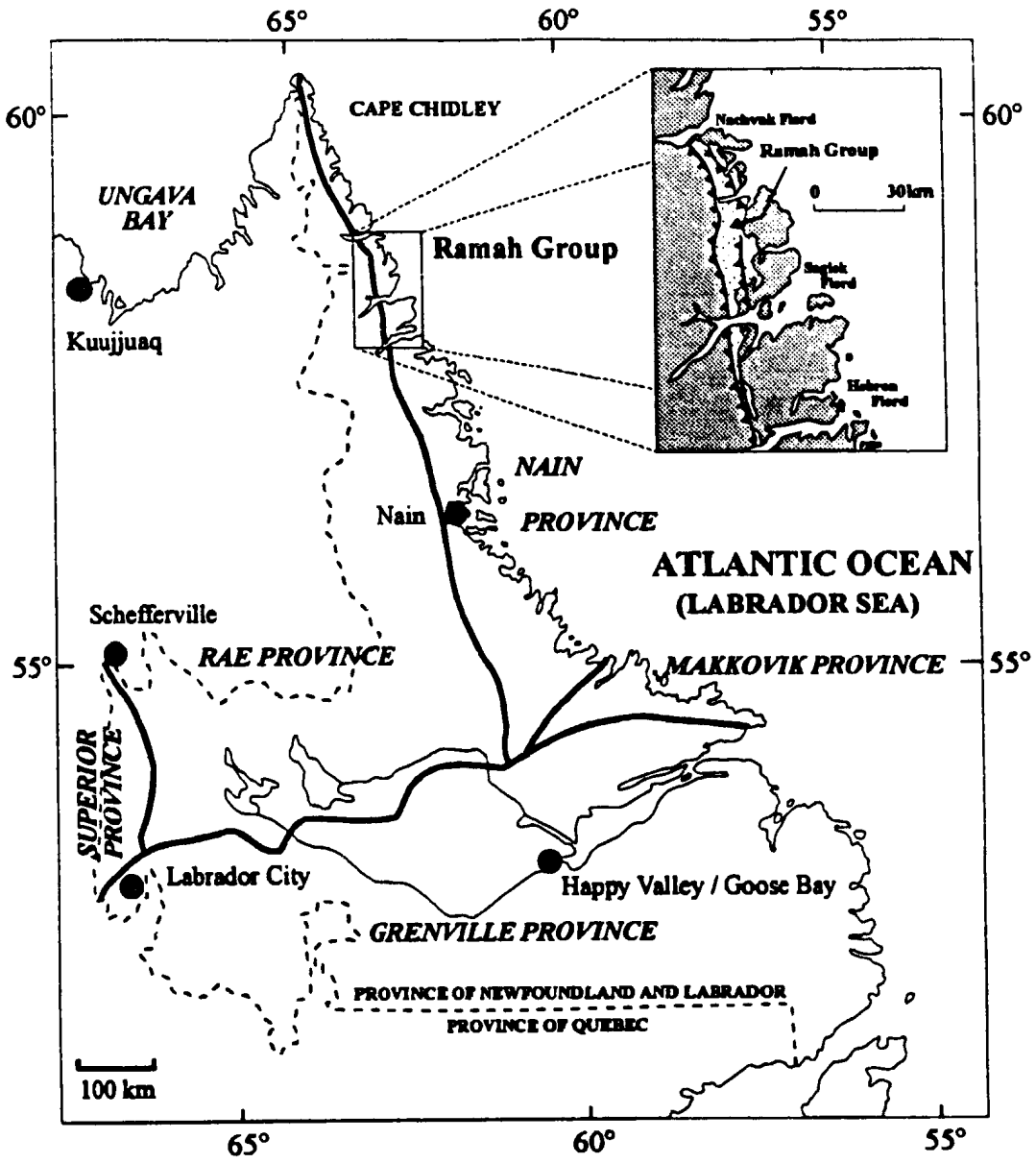

Fig 1.1: Location of Ramah Group and geological provinces in Labrador. After Greene (1972).

round service to many Labrador communities including Nain. A coastal boat service is also available to settlements as far north as Nain between June and November. Transportation to and from the field-area was provided by a chartered 17 m vessel from Lanse-aux-Loup, the *M.V. Robert Bradford*. The voyage from Nain to the field area took 5 days with a brief stop in the Mugford Group. During field work, accommodation was supplied by the *M.V. Robert Bradford*, but on two occasions temporary base camps were set up in the Bears Gut and Rowsell Harbour areas. Access to the area was achieved throughout by the use of a *Zodiac* inflatable boat, thus enabling deep penetration into parts of the shallow fiords and bays. Excellent anchorages are present in most of the deep bays and fiords. Once on shore, investigation was carried out by foot traverses.

1.1.2 Physiography

The Torngat Mountains have an alpine, glaciated topography, with heights varying from 760 to 1370 m above sea level in the field area. Glaciated features include arêtes, hanging valleys and spectacular fiords. Outcrop exposure is exceptional, especially along the fiords, where the Archean and Proterozoic sequences are exposed. Felsenmeer is abundant both on the flat mountain tops, and at the base of most of the arêtes. Vegetation is very sparse, due to the harsh Alpine climate. Trees are absent and only small areas of grass are present, such as at the head of Ramah and Delabarre Bay and Rowsell Harbour.

Northern Labrador is noted for its inclement weather and short summers. Dense fog, rain, low cloud, high winds and snow occur throughout the field season, with high

winds persisting from mid-August onwards, and therefore field work was undertaken from July 28th until August 26th. Out of a total of 29 days in the field, 2 were lost due to low visibility and rain, with the rest of the days being warm, with low winds, and clear skies with no precipitation. The weather encountered during the field work was atypical for northern Labrador.

1.2 Previous Work

The earliest geological description of the Ramah Bay area was published by Steinhauer (1814) based on the observations made by two Moravian missionaries journeying through northern Labrador a year earlier. Ramah Bay had previously been known to the Inuit as Nulletarktok Bay before the establishment of a Moravian mission there in 1871. Bell (1884,1895) briefly described the slaty rocks which occur at Ramah Bay and extend northwards to Nachvak Fiord over a distance of 23 km. A Brown-Harvard expedition in 1900, lead by Daly (1902), named the rocks in the Ramah area, the "Ramah Sedimentary Series" and described the geology in the vicinity of Nachvak Fiord. Delabarre (1902) walked from Hebron Fiord to Nachvak Fiord with a small party and mapped the extent of the Ramah Group.

More detailed work was carried out in 1915 and 1916 by Coleman (1921), who described a volcanic unit near the base of the Ramah Group and measured two stratigraphic sections. Coleman also noted the occurrence of paragneiss, hypersthene gneiss, crystalline limestone and psuedotachylyte in the Archean rocks.

Milligan and Goodman (in Douglas, 1953) produced detailed stratigraphic columns, and cross-sections of the Ramah Group between Ramah Bay and Rowsell Harbour. They also studied the Archean rocks that had been thrust over the Ramah Group north of Rowsell Harbour, and recognized several other western dipping thrust faults during fieldwork in 1946 and 1947.

Christie (1952) mapped the coast at the scale of one inch to four miles in 1951, and measured stratigraphic sections on the north shore of Ramah Bay. Christie also observed that the Ramah Group extended to the south shore of Saglek Fiord, that the western boundary of the unit was probably fault bounded, and that gneiss to the east and west of the Ramah Group had different compositions. His map shows intermediate hypersthene and pyroxene gneiss to the west of the Ramah Group and granitoid gneisses to the east.

A large scale, helicopter-assisted, reconnaissance geological mapping program of northern Labrador and north-eastern Quebec was carried out by Taylor (1969, 1970) in 1967 and 1969. This study afforded the first opportunity to examine inland parts of the Ramah Group. The most interesting feature found was that the Ramah Group was fault-bounded to the west by a thin strip of Archean rocks, which are fault bounded further to the west by Proterozoic granulites.

Detailed stratigraphic and sedimentological mapping of the Ramah Group was carried out by Morgan (1975), Knight and Morgan (1976) and Knight and Morgan (1981) in 1971 and 1972. As a result of this mapping, six formations were identified within the

Ramah Group and a 1: 50 000 geological map was produced of the area between Saglek and Nachvak Fiords (Morgan, 1979). In conjuction with Morgan's early work a study of the Warspite Formation dolomite was carried out by Jefferson (1973) as part of his B.Sc. at Ottawa University.

During the 1980's and 1990's renewed interest in northern Labrador tectonics and mineralization prompted detailed study by the Newfoundland Department of Mines and Energy (NDME) and workers at Memorial University of Newfoundland. Structural studies of the Nain-Churchill boundary in the area (Wardle, 1983, 1984) and the Archean-Proterozoic boundary (Ryan *et al.*, 1983,1984) constituted the first detailed mapping of the Archean and Proterozoic basement rocks. Mengel (1988) examined the structural and metamorphic character of the Ramah Group in the Lake Kiki area, and on the south side of Saglek Fiord. Meyer and Dean (1988) examined the industrial mineral potential of the Ramah Gp., and concluded that chert would make a good source for silica, while the 10 - 15 m thick Reddick Bight Dolomite Member would be a poor source of dolomite due to quartz carbonate veining. Stream sediment and stream water data were obtained for the northern Ramah Group (the Adam's Lake area) as part of a study by the NDME in 1992, and Pb, Zn, Au and U anomalous areas were detected (McConnell & Honarvar, 1993). The structural evolution of the most westerly part of the Ramah Group and the tectonic implications of this complex fold and thrust belt have been described by Calon and Jamison (1992, 1993). As part of a B.Sc. study at Memorial University of Newfoundland, Hussey (1994) completed research into the origin of the sulphides and

oxides present within the mafic and ultramafic sills cutting the Ramah Group. Structural work is presently being conducted in the Lake Kiki area by John Smith, as part of a M.Sc. at Memorial University of Newfoundland.

1.3 Industrial Exploration History

The exploration for natural resources in the Ramah Group has had a long and fragmented history. Archaeological artefacts made from Ramah chert have been found as far south as New York, Delaware, and even Florida (Lazenby, 1980). These artefacts indicate that the Maritime Archaic people were quarrying the chert at least 4100-3800 years B.P., from several quarries. No evidence exists that any form of metal extraction was ever carried out in the area by the Inuit.

Early exploration of the Ramah Group was chiefly concerned with the massive pyrite and chert horizons discovered at the turn of the century. The first account of exploration of the pyrite bed was by Du Pont geologists (Snelgrove, 1938), who investigated the bed around Rowsell Harbour in 1901 as a potential source of sulphur for sulphuric acid and its many by-products (Carlsson, 1901; Carter, 1902; Marsters, 1902). In 1906 J. Pippy of St. John's was given a fee simple mining grant of the Rowsell Harbour pyrite prospects, and work included the digging of eight pits and two adits (Carter, 1902). In 1934-1935 an attempt was made to mine the pyrite at Rowsell Harbour (Snelgrove, 1938; Blackwell, 1976), but the production figures are unknown.

BRINEX carried out an investigation of the quartz potential of Ramah Group cherts in the Ramah Bay, Reddick Bight and Rowsell Harbour areas in 1959 (Blackwell, 1976); results of which were inconclusive. Newfoundland & Labrador Corporation Ltd. (NALCO) examined the pyrite bed in 1966, tracing it over a distance of 16 km (Fogwill, 1966). NALCO concluded that the pyrite was a stratiform syngenetic deposit, but carried out no further work. In 1969, BRINEX had Questo Surveys carry out an EM-Magnetometer survey over the Ramah Group. More than 3600 line miles at 1/8 mile intervals were flown, however, extreme relief made the results of questionable value. Some ground follow-up was recommended (*in* Blackwell, 1976), but was never carried out.

The first major effort to carry out exploration for base-metals (copper, lead, zinc), as opposed to pyrite only, was carried out by COMINCO in 1976 as part of a preliminary reconnaissance program (Blackwell, 1976). The results suggested that the pyrite deposit had formed in small pools within a starved minor basin (Blackwell, 1976), and that "Low values coupled with relatively restricted dimensions of the basin make the probability of economic Pb, Zn, or Cu mineralization in the graphitic shale - massive pyrite - chert interval an unattractive exploration bet at this time." Blackwell (1976), however, also thought that "changes in geological thinking about clastic shale basin-hosted Pb-Zn deposits may lead to the development of new ideas for the area and more work may be needed in the future."

It was these changes in geological thinking that prompted ESSO Minerals to carry out reconnaissance geological work and geochemical stream sediment heavy mineral sampling during 1984 (MacLeod, 1984). Results obtained were very promising, with several base metal anomalies detected. Follow-up work in 1985 (MacLeod, 1985), resulted in the discovery of several base metal showings. MacLeod (1985) found that, as well as mineralization being present within the shale formation (Nullataktok Formation), lead-zinc mineralization was also present in Reddick Bight Formation dolomites, and that several ultramafic sills showed signs of copper mineralization. MacLeod (1985) concluded that no further field work should be carried out as the massive pyrite bed did not grade into accumulations of base metals as envisaged by their Sedimentary Exhalative (SEDEX) exploration model (Large, 1983).

In 1990 Falconbridge Limited acquired a reserved area license and carried out a three day, helicopter supported reconnaissance program to assess the nickel potential of the Ramah Group sills (McLean, 1991). Follow-up fieldwork was carried out in 1992, but results have not been released at this time (Osmond, 1992). Portions of the licence were dropped in September 1993, and the remainder in December 1994.

As a result of the fieldwork carried out in this study (Wilton et al., 1993a; 1993b) staking was initiated in the area between Nachvak Fiord and Ramah Bay by a number of individuals. Black Pine Ltd optioned these claims to Newfoundland Goldbar in 1994, resulting in one week of fieldwork, in mid August. Their program targeted the mineralization within the Reddick Bight Dolomite Member (Tallman, 1995).

1.4 Purpose and Scope

The aim of this study was to carry out a comprehensive investigation of the geology and metallogeny of the Ramah Group, in northern Labrador. The present study forms the final part of a detailed program to investigate mineralization developed within Paleoproterozoic basins, on the northern Nain Craton, led by Dr. D.H.C. Wilton (Memorial University). Previous basins studied by Wilton and co-workers include the Snyder-Falls Brook (Wilton and Phillips, 1992) and Mugford groups (Wilton *et al.*, 1993b; Wilton, 1994). The projects were funded by grants from the Comprehensive Labrador Cooperation Agreement (ACOA) and Enterprise Newfoundland and Labrador.

This study constitutes the first detailed description and synthesis of the mineralization found within the Ramah Group. The initial stage of this study consisted of three weeks of reconnaissance mineral exploration within the Ramah Group. Mineralization encountered was carefully documented with grab samples of mineralization, and representative lithological samples taken for further analysis. Subsequent geochemical analyses were carried out at the Department of Earth Sciences, Memorial University (XRF, ICP-MS, oxygen, carbon, ans sulphur stable isotope studies), Newfoundland Department of Natural Resources (ICP-OES), Ottawa-Carleton Geoscience Centre (sulphur isotopes), and Geotop Labs, Montreal (Pb isotopes). Polished thin sections were studied under transmitted and reflected light, and fluid inclusion studies were performed on samples associated with the carbonate-hosted mineralization.

The most significant mineralization found within the Ramah Group was present within the Reddick Bight Dolomite Member, the uppermost member of the Reddick Bight Formation. The bulk of this thesis is a metallogenic, petrographic, and geochemical study of sulphide mineralization within this stratigraphic unit, although other mineralization is also examined in some detail. This data is then used to construct a possible local and regional metallogenic model for all forms of mineralization encountered within the Ramah Group.

The results from this study document that mineralization within the Reddick Bight Dolomite Member is one of the earliest examples of Mississippi Valley-type Pb-Zn mineralization in the geological record.

CHAPTER 2

TECTONIC EVOLUTION OF NORTHERN LABRADOR

2.1 Ramah, Mugford, and Snyder Groups

There are three Paleoproterozoic basins in northern Labrador, which are, in order of size, the Ramah, Mugford, and Snyder - Falls Brook Groups (Figure 2.1). They all rest with marked unconformity on the Archean Nain craton, and are believed to have been deposited ca 2.0 Ga.. No precise ages for any of these groups have been derived, but they have been correlated on the basis of stratigraphic similarities (Smyth and Knight, 1978). A brief synopsis of the Mugford and Snyder groups are given below, with a detailed account of the Ramah Group.

The Ramah Group (Knight and Morgan, 1981; Morgan, 1975) is the most extensive Paleoproterozoic basin, with a thickness of 1700m and outcropping over a 65 by 16 km area (Figure 2.1). The base of the group consists of quartzites, dolomitic sandstones, and pelites (Rowsell Harbour and Reddick Bight formations) deposited in a shelf environment, which in turn are unconformably overlain by graphitic, and pyritic shales of the Nullataktok Formation (Figure 2.2). The Nullataktok Formation also contains widespread members, viz. a pyrite and overlying chert bed, up to two and thirty metres receptively. The presence of the pyritic shales seems to indicate the end of shelf-type deposition, and the initiation of basin deepening. Subsequent formations are the Warspite Formation, consisting of dolomitic breccias and debris flows, and the Typhoon

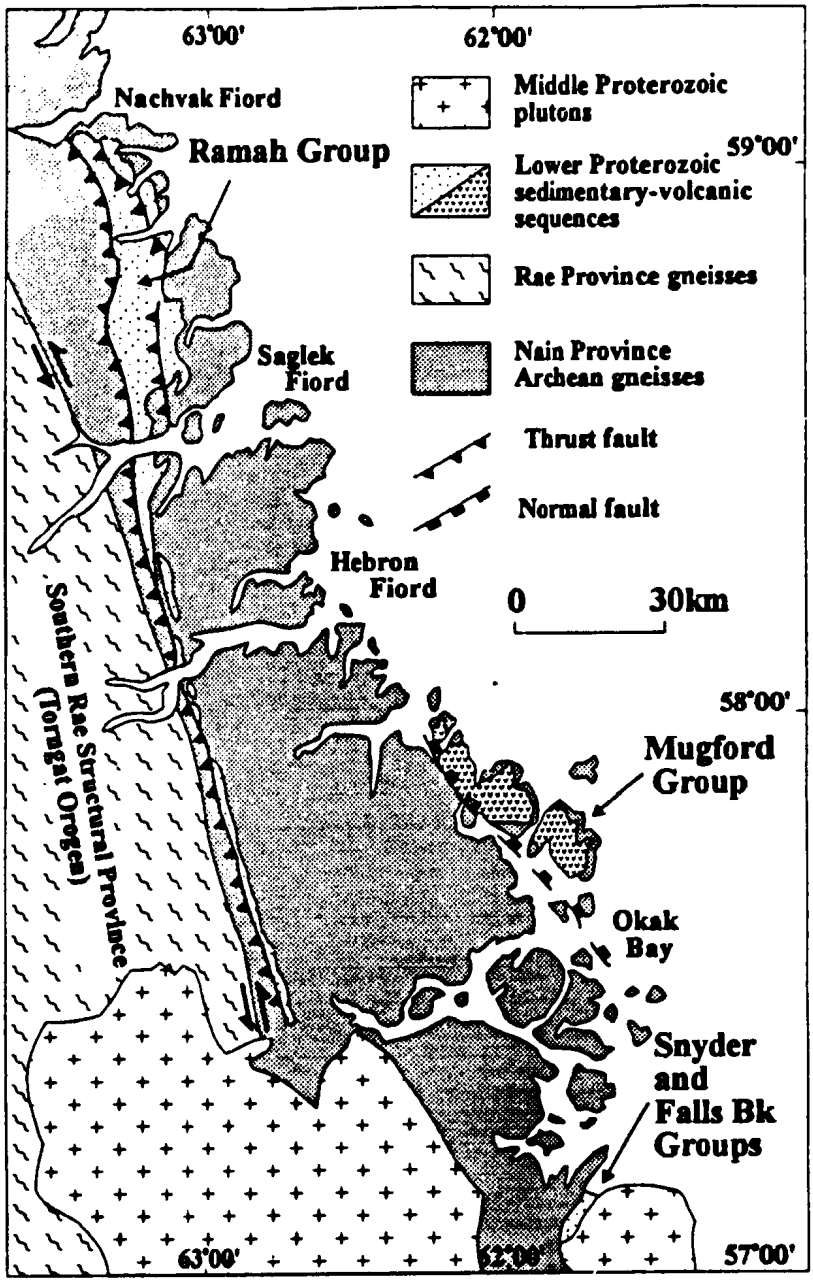

Fig 2.1: Geological setting of the Ramah, Mugford, and Snyder-Falls Brook groups in northern Labrador. After Swinden *et al.* (1991).

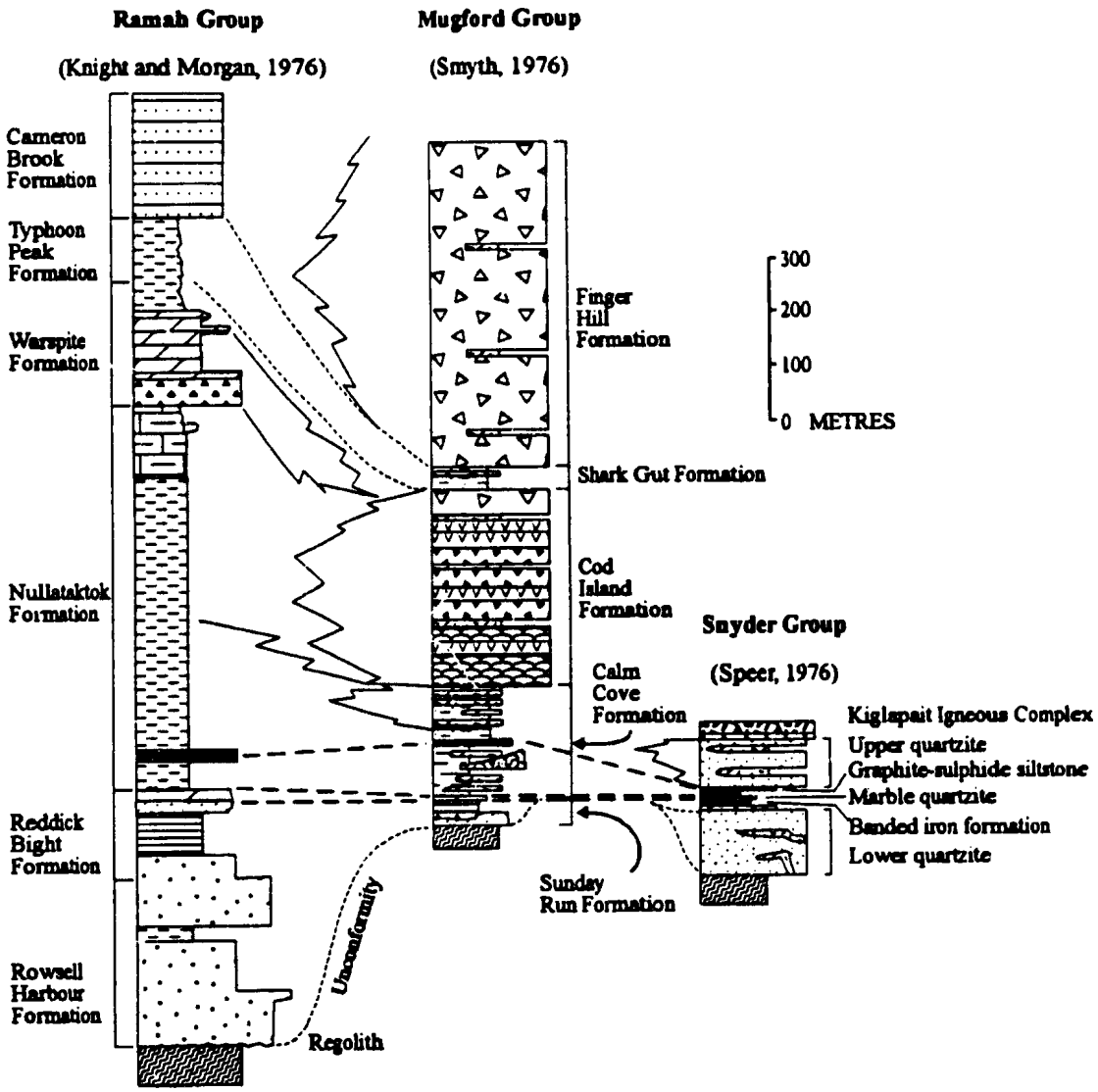

Figure 2.2: Simplified stratigraphic sections of the Ramah, Mugford, and Snyder groups (after Smyth and Knight, 1978). See text for explanation of the stratigraphy. Gabbro sills which are abundant in both the Ramah and Mugford groups have not been shown.

Peak and Cameron Brook formations turbidite sequences. Hoffman (1987) interpreted the Nullataktok, Warspite, Typhoon Peak, and Cameron Brook formations to represent eastward prograding foredeeps (subduction related basins). The Ramah Group was intruded by diabase-gabbro sills, which together with the sedimentary lithologies were subsequently deformed in the Torngat Orogeny (1860 Ma) to produce an east-verging fold-and-thrust belt (Hoffman, 1988; Calon and Jamison, 1992; Bertrand, 1993).

The Mugford Group is 1225 m thick and is situated approximately 100 km to the southeast of the southern-most part of the main exposure of the Ramah Group, and 60 km east of the highly deformed representation of the group (Figure 2.1). Basal portions of the Mugford Group (Sunday Run and Cod Island formations), with a combined thickness of 155 m, rest unconformably on the underlying Nain craton (Figure 2.2) and are fault-bounded to the west by a normal fault, downthrown to the east (Smyth, 1976). The basal lithologies consist of conglomerates, sandstones, and black shales, which are quite similar to the Reddick Bight and Nullataktok formations within the Ramah Group. Due to the presence of an impure dolomite marker bed at the top of the Sunday Run Formation and its similarities to the Reddick Bight Dolomite Member, Smyth and Knight (1978) correlated the two groups (Figure 2.2). Following deposition of the basal sedimentary units in the Mugford Group, voluminous volcanic products were erupted. The base of the volcanic sequence consists of a 430 m thick pillowed basalt, overlain by mixed basalt flows, breccias, and agglomerate of the Calm Cove Formation. The volcanic rocks are interrupted by a thin (40m thick), siliceous and calcareous argillite and tuff sequence, the

Shark Gut Formation, before the deposition of 600 m of basaltic breccia and agglomerate, belonging to the Finger Hill Formation. The Torngat Orogeny, 1860 Ma, (Van Kranendonk, 1993), folded the Mugford Group into an open upright, north-south trending syncline (Smyth, 1976). Wilton *et al.* (1993) noted several sulphide occurrences within the basal sediments and the overlying volcanics.

Sulphides occur as fragments within a debris flow on the north shore of Mugford Tickle. It is surmised that they were eroded and transported from more extensive exhalative sulphide horizons developed on the basin-floor. The occurrence of the sulphides and the basement block and listric faults led Wilton *et al.* (1993b) to postulate a SEDEX model for the basal Mugford mineralization.

The Snyder Group (Smyth and Knight, 1978) is preserved in the metamorphic aureole of the Middle Proterozoic Kiglapait layered intrusion (Figure 2.1). Metamorphic grade reaches hornblende and pyroxene hornfels facies (Speer, 1976). Relict sedimentary features are preserved within the main sedimentary rock lithologies. The Snyder Group is divided into five main units which are, in succession from bottom to top: lower quartzite, iron formation, quartzite-marble, graphite-sulphide siltstone, and the upper quartzite (Berg, 1981). Smyth and Knight (1978) correlated these formations with the basal formations of the Ramah and Mugford groups (Figure 2.2), however Berg (1981) questioned the accuracy of these correlations, due to the omission of the Falls Brook Group by Smyth and Knight (1978). The Snyder-Falls Brook Gp. appears to have formed in the same shelf environment as the lower formations of the Ramah and Mugford groups.

Lying unconformably above the Snyder Group, is the Falls Brook Group which contains in succession the following units: basal conglomerate, mafic granulite (with spinel peridotite sub unit), conglomerate, banded iron formation, calc-silicate unit, mafic granulite (pillowed metabasalt), metagranulite, and pyroxene paragranulite. Berg (1981) interpreted the Falls Brook Group to represent two main igneous sequences (sills, dykes, and flows) separated by banded iron formations and carbonates (calc-silicates). Metamorphic grade increases towards the Kiglapait intrusion making interpretation more difficult. Wilton and Phillips (1992) studied the mineral potential of the Snyder Group and postulated that the SEDEX potential was low, as the geochemistry of shales indicated that they represent deposition during continental margin type rifting (Maynard, 1991).

2.2 Nain Structural Province

The Nain Structural Province constitutes the westernmost representation of the North Atlantic Craton (Hoffman, 1988), remnants of which occur in Labrador, Greenland, northern Scotland, and Scandinavia. In Labrador, the Nain Structural Province is bounded by the Rae Province to the west, the Burwell Province to the north, and the Makkovik Province to the south (Hoffman, 1988). The Archean gneiss complexes making up the Nain Province consist principally of quartzofeldspathic rocks with granodioritic to tonalitic composition. The Nain craton is distinct from other Archean cratons in northeast Laurentia (Hoffman, 1988) as it contains very old Archean rocks, dated at between ~ 3.9 and 3.62 Ga. in the Uivak gneiss complex (Schiøtte *et al.*, 1989; Nutman and Collerson,

1991; Collerson *et al.*, 1992). The Uivak gneisses are interlayered with subordinate metasedimentary rocks of at least two ages and meta-igneous units intruded by mafic igneous rocks (Goodwin, 1991). Geochemical studies indicate several isotopically distinct terranes were present during the late Archean history from ~ 2.78 to 2.5 Ga which amalgamated to form the North Atlantic Craton (Nutman *et al.* 1989; Nutman and Collerson, 1991; Bridgewater and Schiøtte, 1991). The gneiss complex was affected by several regional metamorphic events during the Archean, with the latest at ca. 2.8 Ga, producing amphibolite to granulite metamorphic facies (Mengel *et al.*, 1991). In the Early Proterozoic, the gneiss complex formed a stable cratonic block that was cut by east-west trending swarms of mafic dykes, at ~ 2450 Ma (Napaktok dykes, Ermanovics *et al.*, 1989; K-Ar age from Taylor, 1974), and ~ 2200 ± 50 Ma (Kikkertavak dykes; Rb-Sr whole rock age, in Ermanovics, 1993). The Archean gneiss complex is overlain by the Lower Proterozoic, Ramah, Mugford, Snyder - Falls Brook supracrustal groups.

An abbreviated geological history of the Saglek Bay - Hebron Fiord area, northern Labrador as described by Nutman *et al.* (1989) is:

(1) Formation of sialic rocks, now present as components of the Uivak gneisses, which probably represent basement to the Nulliak assemblage, ca. 3850 - 3900 Ma

(2) Formation of the Nulliak (supracrustal) assemblage - 3800 Ma

(3) Intrusion of tonalitic precursors of the Uivak I gneisses, with high grade metamorphism, deformation and intrusion of granite veins - 3800 - 3600 Ma

(4) Intrusion of the granite precursors of the Uivak II gneisses - 3400 Ma

(5) Intrusion of several generations of mafic dykes - Saglek

(6) Formation of the Upernavik supracrustals

(7) Deformation, intrusion of tonalite sheets, and metamorphism culminating in granulite facies conditions- 3000 - 2800 Ma

(8) Deformation, intrusion of granitic sheets, and metamorphism under amphibolite facies conditions - 2800 - 2600 Ma

(9) Intrusion of Igukshuak granite - 2500 Ma

(10) Intrusion of at least two generations of mafic dykes - 2450 - 2200

(11) Deposition of the Ramah and Mugford groups

(12) Deformation and metamorphism. Restricted to local faulting and retrogression under greenschist facies conditions - 1900 - 1800 Ma

2.3 Southeast Rae Structural Province

The Southeast Rae Structural Province (SRSP) occurs to the west of the Nain Structural Province (Figure 2.1) from which it is separated by the Komaktorvik and Abloviak shear zones (Van Kranendonk *et al.*, 1993). The SRSP contains late Archean rocks of different ages, including; ~ 2922 - 2668 Ma granites and migmatites of the de Pas batholith in the north (Machado *et al.*, 1989); ~ 2807 and 2657 Ma basement gneisses, a 2597 ± 16 Ma charnockite deformed at 2572 ± 9 Ma in the middle-western part of the Torngat orogen (Ryan *et al.*, 1991); and ~ 2682-2663 Ma orthogneisses in the southern part of the province (Nunn *et al.*, 1990).

Archean and Paleoproterozoic magmatic and sedimentary rocks of the SRSP are unconformably overlain by Paleoproterozoic shelf and turbiditic sediments, carbonates and siliciclastics of the Lake Harbour Group (Van Kranendonk *et al.*, 1993). These sedimentary rocks pass eastwards into a distinctive unit of garnet-feldspar-quartz-biotite-sillimanite paragneiss and diatexite known as the Tasiuyak gneiss (Wardle, 1983). The Lake Harbour - Tasiuyak gneiss transition is thought to represent a depositional change from a shelf (Lake Harbour) to a slope (Tasiuyak) environment (Van Kranendonk *et al.*, 1993). The eastern margin of the SRSP is deformed as a result of the Torngat Orogeny at ~ 1860 Ma (Bertrand *et al.*, 1993); there was also deformation of the western margin in the New Quebec Orogeny, at or prior to, ~ 1803 Ma, with final deformation occurring before 1758 Ma, as indicated by post-tectonic stitching pegmatites (St-Onge *et al.*, 1992).

2.4 Evolution of the Torngat Orogen

The suturing of the Nain and Southern Rae Structural Provinces is termed the Torngat Orogeny (Hoffman, 1988) and occurred at ~ 1860 Ma (Bertrand *et al.* 1990, 1993) The orogenic Wilson cycle was initiated with the rifting of the Nain cratonic margin to form a passive continental margin with shelf sequences, sometime after the intrusion of the Napaktok dykes, ca. 2450 Ma (Ermanovics *et al.*, 1989). In the SRSP a similar shelf sequence, the Lake Harbour Group, formed during rifting.

Calc-alkaline magmatism (charnockite - enderbite suite) on the eastern edge of the SRSP, predating the Torngat tectonism, suggests the presence of a magmatic arc. This magmatism is thought to have been caused by westward subduction (Van Kranendonk, 1990, 1992). The oldest zircons in the enderbite have been dated at 1876.9 ± 1.1 Ma, which is interpreted to be the age of arc magmatism in the Torngat Orogen (Bertrand *et al.* 1993). The Nain - Rae continent - continent collision resulted in crustal thickening between ca. 1859 and 1853 Ma (Bertrand *et al.* 1993), causing the formation of a fold and thrust belt within the Ramah Group (Calon and Jamison, 1992) and the metamorphism and deformation in the Lake Harbour Group - Tasiuyak Gneiss.

Between ca. 1845 and 1820 Ma, as indicated by granulite-facies metamorphism and structural features, sinistral transpressional shear occurred across the Torngat Orogen, with strain intensity decreasing from east to west (Van Kranendonk, 1992). This transcurrent shear zone is known as the Abloviak Shear Zone and forms a splay to the east of the Burwell Terrane which constitutes the Komaktorvik Shear Zone. The main

high-grade transcurrent regime has been dated at ca. 1844 Ma within the Abloviak Shear Zone, with evidence for a discrete intrusive event at 1837.5 ± 1.1 Ma in the Torngat Orogen (Van Kranendonk *et al.*, 1993). Continued shearing along the Abloviak Shear Zone at amphibolite facies is evident from metamorphic zircon overgrowths, which yield U-Pb ages between 1826 - 1822 Ma. (Bertrand *et al.* 1993). Post - shearing granitic stocks intrude reworked Nain gneisses along the Abloviak Shear Zone. These granites give ages of ca. 1806 Ma, indicating the minimum age for shearing along the Abloviak Shear Zone. Uplift ages of ca. 1795 - 1740 Ma in the Torngat Orogen have been established using U-Pb and $^{40}Ar/^{39}Ar$ methods (Mengel *et al.* 1991; Bertrand *et al.* 1993). The wide spread in ages is either the result of episodic uplift movement along the Abloviak Shear Zone, or the result of differential orogenic cooling through the closure temperature of monazite at different times (Bertrand *et al.* 1993).

2.5 Geology of the Ramah Group

2.5.1 Introduction

The Ramah Group is a 1700m thick sequence of Lower Proterozoic (Paleoproterozoic) sedimentary strata resting unconformably on peneplained Nain Province Archean basement rocks along the Nain - Rae Structural Province boundary (Plate 2.1). The group consists of two contrasting sequences reflecting a change upwards from shallow siliciclastic shelf to deep basinal deposition (Morgan, 1975; Knight and Morgan, 1976; Knight and Morgan, 1981). The Ramah Gp. can be traced for

PLATE 2.1: Ramah Group unconformably resting on the Archean gneisses to the east of Little Ramah Bay. Note the presence of the black, Napaktok (2450 Ma) and Kikkertvak (2200 Ma) dykes within the Archean rocks. Unconformity marked by arrow.

approximately 190km south from Nachvak Fiord until it is incorporated into Mesoproterozoic anorthosite intrusions in the Okak Bay region. The largest extent of the Ramah Gp. is found between Nachvak and Saglek Fiords (Figures 2.1 and 2.3), a distance of 60 km, where it attains a width of up to 16 km. Structural deformation in the Torngat Orogen resulted in the formation of a doubly plunging synclinorium (Morgan, 1975) which underwent sub-greenschist to greenschist facies metamorphism in the east and up to amphibolite facies metamorphism on the thrust fault-bounded western margin. The resulting isograds make nomenclature of the lithologies awkward. Rocks in the western limb of the synclinorium include slate, quartzite, pelite, and phyllite due to greater than greenschist facies metamorphism, while the corresponding greenschist - subgreenschist facies rocks in the east would be characterised as shale, quartz sandstone, siltstone, and mudstone respectively. Generally if the members within a formation have been defined as quartzites, then the reader should be aware that depending on the metamorphic facies, these rocks could quite conceivably be termed quartz sandstones.

Preservation of the Ramah Gp. between Saglek Fiord and Okak Bay is very poor, where only the highly deformed and metamorphosed lower part of the formation is preserved (Morgan, 1975). As a result of its poor preservational potential and time limitations, this area was not studied.

Knight and Morgan (1976) divided the Ramah Gp. into six formations, viz.: Rowsell Harbour, Reddick Bight, Nullataktok, Warspite, Typhoon Peak, and Cameron

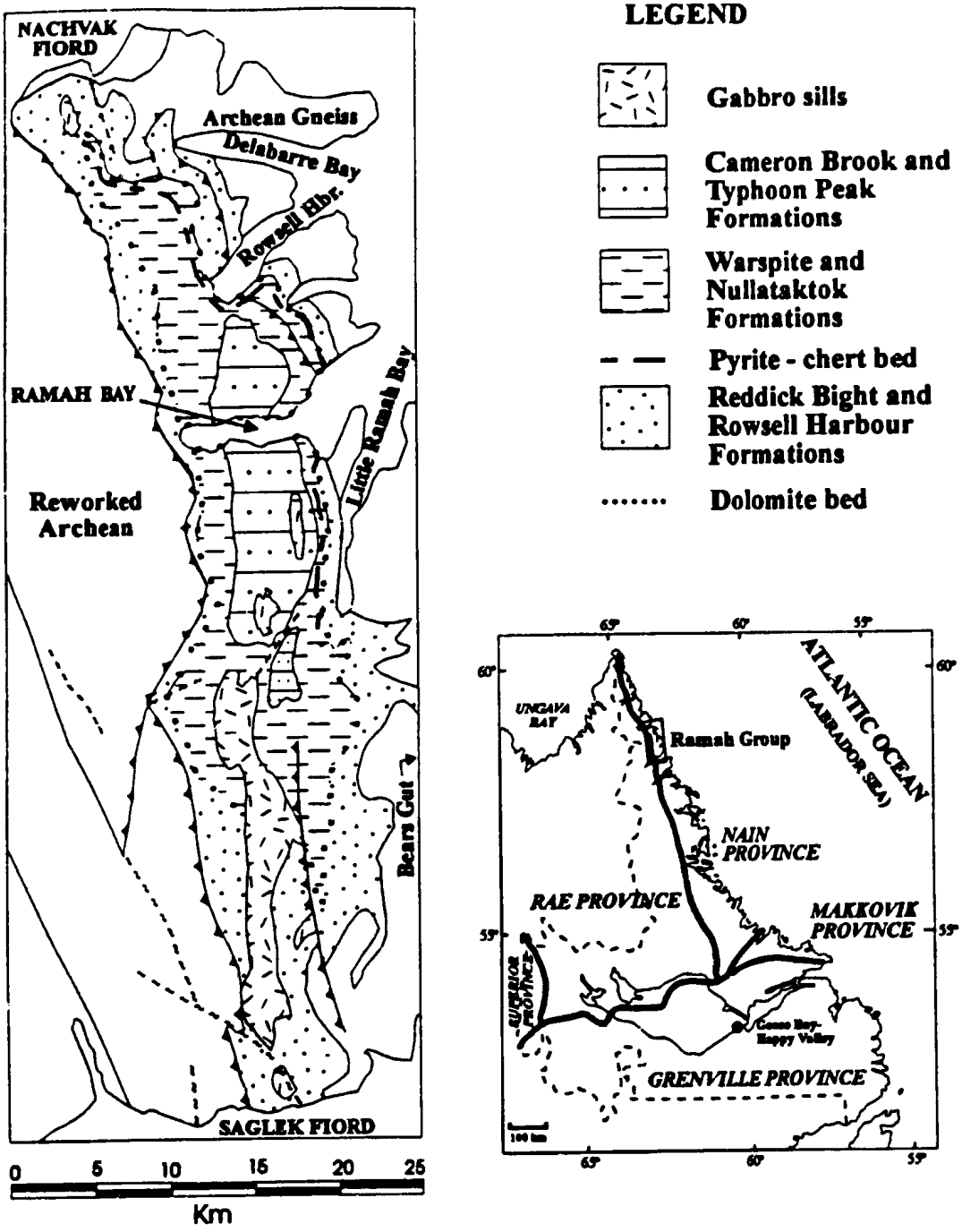

Fig. 2.3: Simplified geological map of the Ramah Group. Geology after Morgan (1975).

Brook formations (Figure 2.4, Plate 2.2, and Figure 2.5)). The uppermost of these formations have been extensively intruded by diabase to gabbro sills.

The six formations which make up the Ramah Gp. can be divided into two distinct sequences which are separated by a sequence boundary (unconformity). The three sequences are (1) the Shelf sequence, containing the Rowsell Harbour and Reddick Bight formations, (2) the Sequence Boundary, an unconformity between the Reddick Bight and Nullataktok formations, (3) the Basin sequence, consisting of the Nullataktok, Warspite, Typhoon Peak, and Cameron Brook formations

A geological map (Map 1) and sample location map (Map 2) of the Ramah Gp. can be found in the pocket at the back of this thesis, together with sample descriptions and locations (Table I.1, Appendix I).

2.5.2 Shelf Sequence

The shelf sequence is composed of two formations, Rowsell Harbour and Reddick Bight, which have a combined thickness between 304 and 613 m. The lower and middle portions of the Rowsell Harbour Formation are characterized by the abundance of quartzite and quartz sandstones, with a thin alkali basalt flow near the base, while the upper portion of the formation contains phyllites and further quartzites. The interpreted paleoenvironment is one of shallow marine processes with some fluvial processes taking place to introduce mudstones (phyllites). The shallow marine environment is supported by the common occurrence of ripple marks, cross-bedding, and coarsening upwards

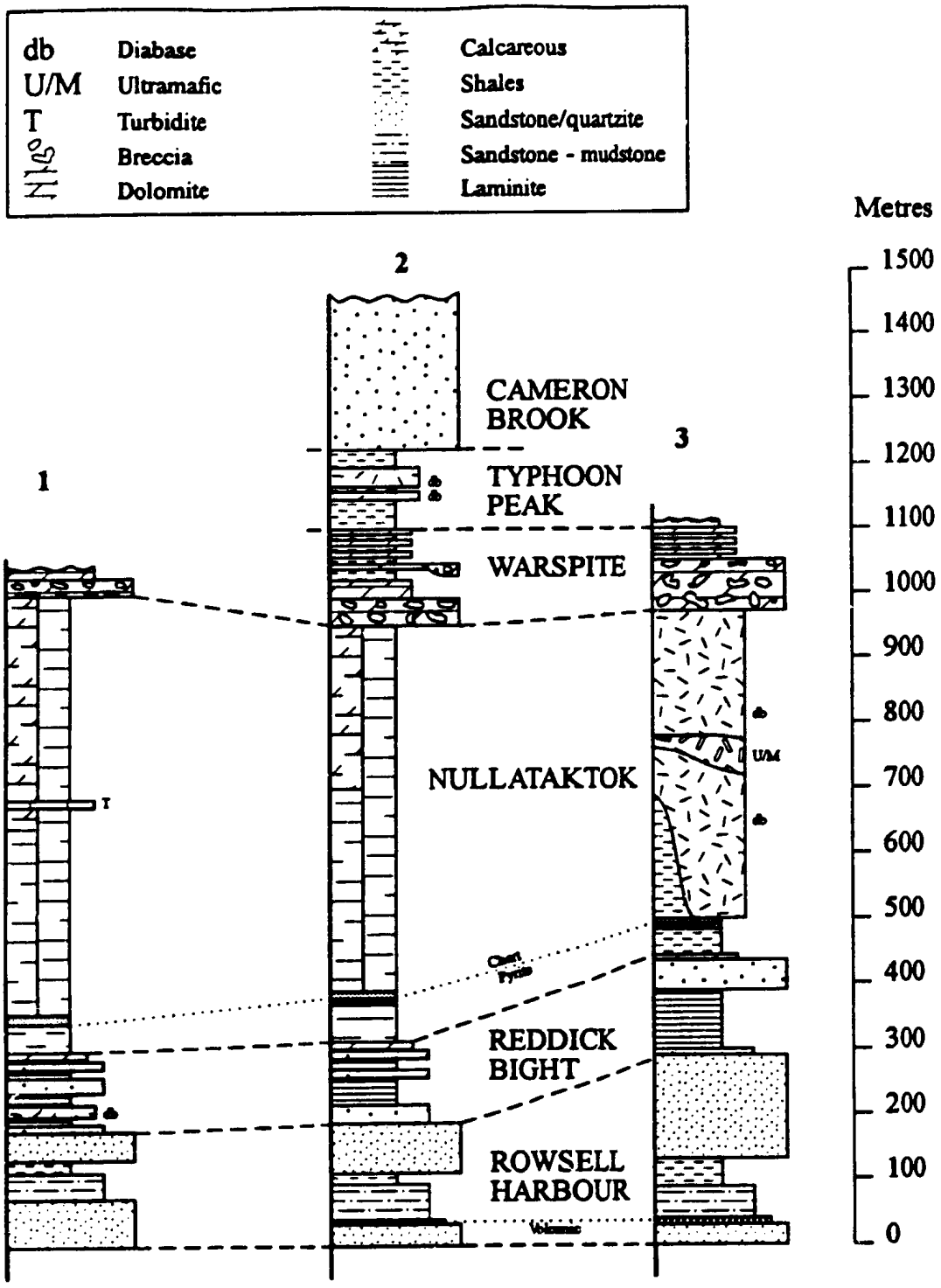

Fig. 2.4: Stratigraphic sections of the Ramah Gp. at: 1 - Delabarre Bay; 2 - Ramah Bay; 3 - Little Ramah Bay. Taken from Knight and Morgan (1981).

PLATE 2.2: Stratigraphy of the lower formations within the Ramah Gp. Note the conspicuous white Reddick Bight Dolomite Member (RBDM) at the centre of the photograph.

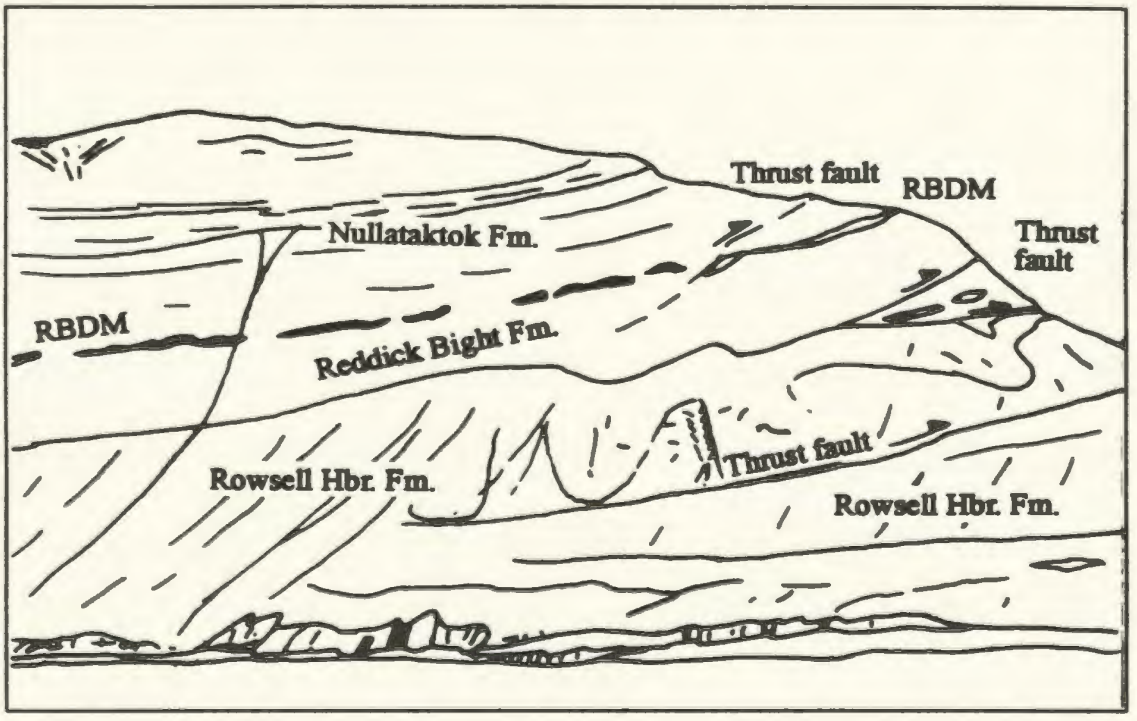

Fig 2.4: Explanation sketch to PLATE 2.2.

sequences within the uppermost member of the formation. The Reddick Bight Formation conists mainly of sandstones, siltstones and black quartzites and is capped by a conspicuous dolomite member. Knight and Morgan (1981) interpret the depositional environment of the Reddick Bight Formation as a tidal delta, based on shallowing upwards sequences, mudcracks, cross-bedding, and flame structures.

2.5.2.1 Rowsell Harbour Formation

The Rowsell Harbour Formation varies in thickness from 251 m to 470 m, measured on various sections by Knight and Morgan (1976, 1981), and can be subdivided into 5 members: viz; the Lower White Quartzite, Volcanic, Purple Quartzite and Mudstone, Phyllite, and Upper White Quartzite members. All but the volcanic unit can be traced throughout the synclinorium.

2.5.2.1.1 Lower White Quartzite Member

The Lower White Quartzite Member has a thickness of 31 to 97 m and consists mainly of quartzite overlying a granite wash, and local conglomerates, such as those on the south shore of Delabarre Bay. Morgan (1975) noted that the granite wash and pebble conglomerate rarely exceeds 6 m in thickness. The conglomerate is overlain by a laminated, trough cross-bedded quartzite which contains heavy mineral laminations, consisting of approximately 90 % magnetite with some amphiboles (Knight and Morgan, 1981). The bulk of the member is composed of yellow weathering, white quartzite, and

where the member is less metamorphosed, quartz sandstone which fines upwards. The quartzite is dominantly trough cross bedded with symmetrical and asymmetrical ripple marks (Knight and Morgan, 1981). At Naksaluk Cove, 8 to 75 cm beds of pure quartzite are separated by 9 to 45 cm of dolomite-rich quartzite. Due to the presence of gradational and irregular boundaries in the quartzites, Knight and Morgan (1981) considered the dolomite to be a secondary feature.

2.5.2.1.2 Volcanic Member

The Volcanic Member is a 6 to 18 m, highly altered grey basalt lava flow (Morgan, 1975, 1978; Knight and Morgan, 1981) which rests upon pebbly sandstones of the Lower Quartzite Member; it is the only volcanic unit in the Ramah Gp.. The flow is present from south of Rowsell Harbour, to the west of Bears Gut (Morgan, 1975). Macleod (1985) reported that the flow occurs near Saglek Fiord.

The altered, fine-grained flow is composed of carbonate, sericitized plagioclase, tremolite, chlorite, muscovite, quartz, and opaques, with few microscopic textures preserved (Knight and Morgan, 1981). The Volcanic Member at Schooner Cove and Bears Gut contains pillow structures (Plate 2.3) with glass rims (Douglas, 1953; Wilton *et al.* 1994), while north of Ramah Bay the flow has the general appearance of a subaerial flow due to the presence of pahoehoe toes (Knight and Morgan, 1981). Christie (1952) described the flow as latite, Taylor (1969) as an andesite, while Morgan (1978) described the flow as tholeiitic. Archibald and Wilton (in prep.) consider the flow to represent a

alkali-basalt which has undergone slight crustal contamination by the quartzofeldspathic Archean basement.

2.5.2.1.3 Purple Quartzite and Mudstone Member

This unit is between 75 and 157 m thick, and contains intercalated units of typical pink to purple quartzite and grey to purple grey mudstone (Knight and Morgan, 1976). The unit thickens away from an area near Reddick Bight, indicating a possible basement high at the time of sedimentation, which Knight and Morgan (1981) termed the Reddick Arch. Ripple marks with amplitudes of 20 cm and wavelengths of 112 cm are common in this unit.

2.5.2.1.4 Phyllite Member

The Phyllite Member has a variable thickness of 15 to 44 m, with the thinnest units over the Reddick Arch and near Nachvak Fiord. It is composed of beds of purplish grey and yellowish pink mudstones, with ripple laminations (Knight and Morgan, 1976, 1981).

2.5.2.1.5 Upper White Quartzite Member

The thickness of this unit varies from 46 to 68 m over the Reddick Arch, and up to 267 m at Bears Gut. The unit is generally composed of monotonous fine- to medium-grained white quartzites, exhibiting coarsening upwards sequences. Some conglomerates

are present at the top of the coarsening upwards sequence and are locally capped by mudcracked units (Knight and Morgan, 1976, 1981).

2.5.2.2 Reddick Bight Formation

The Reddick Bight Formation overlies the Rowsell Harbour Formation, and varies in thickness between 53 and 143 m. The predominant lithologies within the formation are grey sandstones, shales, brown laminites, black quartzites, a mud flow, and an upper dolomite member. The formation thins northwards and westward, and decreases in thickness from greater than 100 m in the south to less than 60 m over Reddick Arch, to less than 20 m at Naksaluk Cove (Knight and Morgan, 1981). The lower unit is composed mainly of a turbiditic sandstone and contains numerous sedimentary features such as graded bedding, neptunian dykes, load casts, and flames structures. This unit is succeeded by cross-bedded sandstones and shaly sandstones or siltstone laminae alternated with silty shale laminae (Knight and Morgan, 1981). Between Reddick Bight and Delabarre Bay, 12 to 35 m of black quartzite are interbedded with beds of shale and thin sandstones. Present throughout the clastic sequence of the Reddick Bight Formation are grit and pebble beds. Shale drapes, mudcracks and large scale cross-bedding indicate a shallowing upwards sequence similar to present day tidal deltas (Knight and Morgan, 1981). The whole sequence is capped by the Reddick Bight Dolomite Member.

2.5.3 Sequence Boundary

The sequence boundary is defined as the top of the Reddick Bight Dolomite Member (RBDM), and delineates the change from a supra-tidal (sub-aerial) environment to a postulated deep water basin. The boundary is marked by an undulating, smooth contact between the dolomite of the Reddick Bight Formation, and pyritic and graphitic shales of the Nullataktok Formation. The age of the sub-aerial exposure, and the amount of erosion, cannot be calculated, but this exposure led to ground preparation (an increase in brecciation and porosity) of the dolomite for subsequent mineralizing fluids.

2.5.3.1 Dolomite Member

The Reddick Bight Dolomite Member (RBDM) forms one of the most conspicuous units in the Ramah Gp. (Plate 2.2), and can be traced from Nachvak to Saglek Fiords, a distance of 65 km (Figure 2.3). The dolomite is 4 to 17 m thick and has a characteristic bright yellow to buff coloured weathering surface. It has an irregular gradational base with an upper 3 to 4 m of pure dolomite. Original bedding features are visible on the weathered surface of some of the outcrops (Plate 2.4). A secondary porosity is present at most of the outcrops, and brecciation is not uncommon. Brecciation is thought to have occurred as a result of tepee formation in a peritidal environment, similar to those presently forming in Western Australia, Abu Dhabi, and the Bahamas (Assereto and Kendall, 1977; Kendall and Warren, 1987). Tepee formation seems to have occurred at several times during the deposition of the carbonate unit (Plate 2.5) indicating

PLATE 2.3: Pillowed alkali basalt from the Rowsell Harbour Fm. Volcanic Member, near Schooner Cove.

PLATE 2.4: Bedding within the RBDM, between Naksaluk Cove and Adams Lake. The dark brown layers of calcilutite are the only evidence of an original bedded carbonate precursor to the dolomite.

PLATE 2.5: Brecciation and tepee structures present at the top of the RBDM at the Panda Showing.

fluctuations in sea level and depositional rates. An outcrop between Little Ramah Bay and Bears Gut shows evidence that solution collapse brecciation occurred between two periods of tepee formation. Solution collapse was probably a consequence of fresh water dissolving the calcite cement in the voids of the tepee structure, resulting in the formation of a rubble breccia (Plate 2.6) at the maximum dissolution site, and a mozaic breccia (Plate 2.7) at the periphery. As solution brecciation was occurring, coarse grained, rounded dolomite grains, probably aeolian in derivation (Knight, pers. commun., 1994), decended from the surface, through tepee ruptures, into the cavities where it formed the matrix to the rubble breccia. Cathodoluminescence has indicated that there have been several pulses of dolomite-forming fluid that passed through the carbonate sequence. The dolomite always exhibits quartz - dolomite veining of late fractures (Plate 2.8). Present within these veins and vugs are sulphides (galena, sphalerite, and pyrite), and at several localities, pyrobitumen.

2.5.4 Basin Sequence

The basin sequence is comprised of four distinct formations (Nullataktok, Warspite, Typhoon Peak, and Cameron Brook) with a combined thickness up to 1090 m. The Nullataktok Formation represents rapid basin deepening as it is unconformably developed on a shelf-carbonate unit, and is dominated by black, graphitic and pyritic shales. The presence of a two meter thick pyrite bed and overlying chert bed further supports the deep nature of the basin, as they suggest no clastic material was being

PLATE 2.6: Rubble breccia present near the base of the RBDM at the Panda Showing. The grey matrix surrounding the dolomite clast is composed of rounded dolomite particles interpreted to be aeolian in origin.

PLATE 2.7: Mosaic breccia within the RBDM at the Panda Showing. The dark brown mineral present within the surrounding matrix, above the hammer, is sphalerite.

PLATE 2.8: Secondary porosity and pervasive quartz-carbonate veining within the RBDM at the Saor Alba showing.

deposited into the basin at that time. Warspite Formation sedimentation is dominated by dolomitic breccias and sandstones, signifying that the carbonates have been transported from a nearby shelf environment. Overlying the Warspite Formation is the Typhoon Peak Formation which is dominated by shales, sandstones, and siltstones denoting the return of quiescent conditions with infrequent coarse clastic input. The uppermost formation preserved in the Ramah Group is the turbidite dominated Cameron Brook Formation, which probably formed through shelf instability caused by the early phase of the Torngat Orogeny (Hoffman, 1988).

2.5.4.1 Nullataktok Formation

The Nullataktok Formation consists of up to 595 m of shales, varicoloured mudstones, calcareous and dolomitic mudstones, thin dolomitic sandstones, intraformational breccias, sedimentary chert, pyrite iron formation, siliceous dolomite and argillite (Knight and Morgan, 1976, 1981). It is present from north of Adams Lake (Naksaluk Cove) to as far south as the north shore of Saglek Fiord. The stratigraphy of the Nullataktok Formation is illustrated in Figure 2.4.

The unit appears to unconformably rest on the underlying RBDM suggesting that basinal conditions were established rapidly. Pyritiferous, graphitic, sulphurous black shales form the basal 12 to 20 m of the formation. The maturation of this organic-rich unit may be responsible for the formation of the pyrobitumen that is present within the RBDM. This unit was followed (Figure 2.4) by the deposition of the varicoloured

mudstones, up to 350 m in thickness, of which 60 m lies below the pyrite - chert beds (Knight and Morgan, 1976, 1981).

2.2.4.1.1 Pyrite-Pyrrhotite Bed

The pyrite - pyrrhotite bed is a very distinctive unit that can be traced from east to west across the synclinorium axis, and from the north shore of Saglek Fiord to the south shore of Adams Lake. The base of this unit is marked by a green siltstone unit which is composed of quartz and plagioclase detritus, set in a carbonate - sericite - chlorite matrix. The thickness of the bed varies considerably from a few tens of centimetres to about 2 m, with an average thickness of around 40 to 57 cm. This thickening (and thinning) is predominantly due to thrusting. The bed is composed of brassy, granular pyrrhotite south of Little Ramah Bay (Plate 2.9), where the unit is proximal to later gabbro-diabase sills, and silvery grey pyrite to the north (Knight and Morgan, 1976, 1981). When metamorphosed the bed takes on a more granular appearance, with remobilization of pyrite resulting in the presence of quite coarse pyrite (up to 4 to 5mm) in en echelon veins (Plate 2.10). Oxidation of the bed is very common which causes the bed to take on a very rusty brown appearance (Plate 2.9). Clasts within the deformed bed are mainly quartz and slate in composition, and vary from a few millimetres to centimetres in diameter. In less deformed and metamorphosed areas the pyrite bed does not contain any lithoclasts. Streams flowing over the pyrite bed are very iron rich, with limonite sand developing at meander bends (such as on the south shore of Delabarre Bay).

PLATE 2.9: Pyrite-pyrrhotite bed at the Near Miss Showing. The sulphides have been extensively oxidized due to the presence of a diabase sill occuring above the chert bed. The thickness of the bed at this locality is approximately 45 cm.

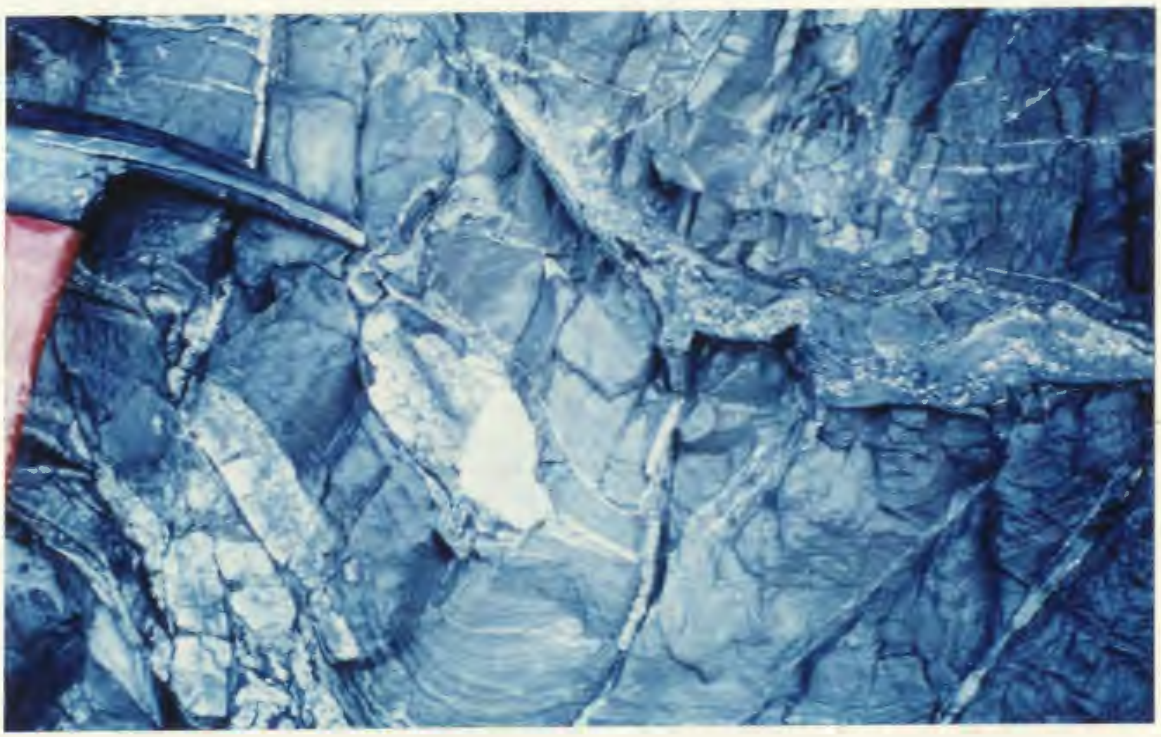

PLATE 2.10: Fine grained, bedded pyrite displaying deformation. Coarse pyrite (bright luster) is a result of en echelon fractures due to deformation associated with duplex formation within the pyrite bed. South shore of Rowsell Harbour.

2.5.4.1.2 Chert Bed

Overlying the pyrite - pyrrhotite unit is the Ramah Chert (Plate 2.11), which has an average thickness on the order of 4.5 m, and is up to 17m thick north of Adams Lake (Knight and Morgan, 1976, 1981). The chert can be white, grey, or black, vitreous, and (rarely) granular texture, containing intercalations of various colours of chert in the order of 6 to 45 cm (Knight and Morgan, 1981). Locally present within the chert, are lenses of pyrite, dolomite, green pyritic shale, and mudstone. Directly above the chert bed is a thin (~ 2 m) rusty weathered, siliceous dolomite (Plate 2.12), and green and white striped argillite unit which contains minor sulphide mineralization at certain localities.

The upper 220 to 250 m of the Nullataktok Formation is comprised of calcareous and dolomitic mudstones interbedded with less calcareous mudstones. Structures present in this unit are laminations, cross-laminations, convolute bedding, slump folds, neptunian dykes, boudinage and slump breccias (Knight and Morgan, 1976, 1981).

2.5.4.2 Warspite Formation

The Warspite Formation is between 110 to 165 m thick (Figure 2.4), and is comprised of a lower sequence of stratified fine dolomites, dolomite breccias, dolomitic sandstones, and mudstones, and an upper sequence of argillites and mudstones, with minor dolomite and sandstones. The boundary between the Warspite Formation and the Nullataktok Formation is characterised by basal breccia (Plate 2.13) which contains clasts of Nullataktok Formation set in a sandy dolomite matrix (Knight and Morgan, 1981).

PLATE 2.11: Nullataktok Fm. pyrite bed (at hammer) with the overlying chert bed, and the underlying green siltstone visible. Sandman Occurrence, south shore of Reddick Bight.

PLATE 2.12: Thin dolomite bed occurring above the Nullataktok Fm. chert bed near Reddick Bight. Mineralization is present in this unit when the underlying chert bed has been fractured.

Sedimentary structures present within the formation include cross-bedding, ripple marks, and rip-up beds. Sedimentary structures indicate paleocurrent flow directions from east to west during deposition of the Warspite Formation, with a westward change from matrix-supported breccias to graded and ungraded breccias (Knight and Morgan, 1981). Open porosity, similar to that within the RBDM, was not observed.

2.5.4.3 Typhoon Peak Formation

The Typhoon Peak Formation has a thickness of 85 to 130 m (Figure 2.4), and is poorly exposed due to the nature of the lithologies. The dominant lithology is rusty weathered pyritic slates, north of Ramah Bay, while sandstones, siltstones, quartzites, and grey limestones are interbedded with the slates south of Ramah Bay (Knight and Morgan, 1976, 1981). The sandstones are commonly boudinaged. This formation was extensively intruded by late stage diabase to gabbroic sills. This formation was not studied in detail.

2.5.4.4 Cameron Brook Formation

This formation was not examined during the field work, but Morgan (1975), and Knight and Morgan (1976, 1981) described it as a 200 m thick unit (Figure 2.4) composed of cleaved grey to black, argillaceous, turbiditic sandstones, alternating with black to grey shale. The sandstones are subarkosic to lithic subarkoses, which exhibit Bouma cycles dominated by A > B > E and A > E sequences (Knight and Morgan, 1981). Sedimentary

structures include load casts, flame structures, undulose or irregular bases, some faint, flat stratification is also present.

2.5.5 Interpretation of Depositional Environment

Knight and Morgan (1981) interpret the Rowsell Harbour Formation as representing a shallow shelf sequence with marine, and possibly some fluvial, processes dominating. During deposition of the Reddick Bight Formation, fluvial processes dominated which led to a prograding, shallowing upward, deltaic complex (event A, Figure 2.6). This deltaic complex was a product of regression and it blanketed the shallow shelf. The RBDM formed as a result of the shallow-lying, partially lithified carbonate sediments being dolomitized, perhaps in a sabka-like environment, due to either tidal pumping, reflux, or Kohout convection (cf. Land, 1985). Evidence exists that this sabka environment received aeolian carbonate sediments (due to the presence of rounded dolomite grains) perhaps from a previously formed carbonate sequence that was undergoing erosion (event B, Figure 2.6). Subaerial exposure of the carbonates lead to brecciation of the host rock, probably by the dissolution of calcite cements by meteoric water. The exact duration the RBDM was subaerial exposed cannot be postulated.

Following the sabkha deposition period, rapid subsidence of the shelf occurred resulting in deposition of black graphitic and pyritic shale of the Nullataktok Formation in a deep basin. The pyrite - pyrrhotite bed indicates that the basin was a very anoxic, low energy environment, which favoured pyrite production. Upper units of the Nullataktok

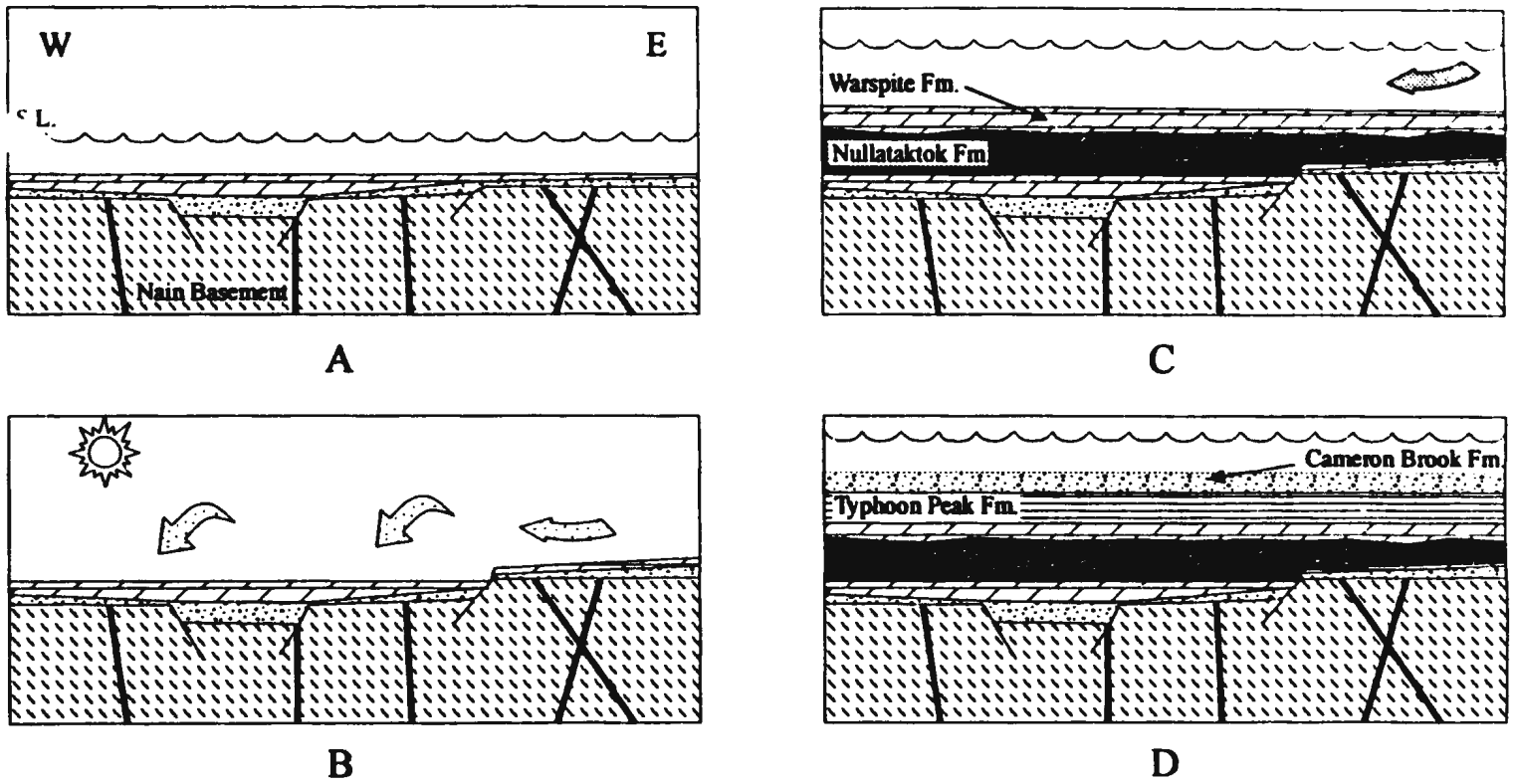

Fig. 2.6: Depositional history of the Ramah Group. (A) Faulting of Archean basement and deposition of Rowsell Harbour and lower-middle Reddick Bight formations. (B) Supratidal (Sabkha) conditions resulting in tepee structures. Aeolian sediments derived from erosion of shelf carbonates. (C) Transgression and rapid deepening during Nullataktok Fm. deposition. Carbonate turbidites formed during Warspite Fm. times. (D) Quiescent conditions prevailed during Typhoon Peak times, before being disrupted by greywacke turbidites of the Cameron Brook Fm. Note figures are not to scale.

Formation became progressively more arenaceous and calcareous indicating that a shelf source must have existed nearby. Paleoflow studies indicate sedimentary provenance from the east (Knight and Morgan, 1981). The presence of thin, planar, stratified, calcareous, dolomitic and noncalcerous mudstones over the deep basin deposits indicate a shelf slope environment encroaching into the shale basin (Knight and Morgan, 1981). By the time the Warspite Formation was deposited, channels had cut the carbonate shelf slope deposits, shedding their load to produce deep water fan deposits (event C, Figure 2.6). Slates of the Typhoon Peak Formation indicate that the basin returned to a quiescent phase, before being disturbed by turbidites of the Cameron Brook Formation (event D, Figure 2.6) which brought in clasts of basement and fresh basaltic volcanics, perhaps derived from the Mugford Gp. (Knight and Morgan, 1981), as this is the only known basaltic source area to the east of the Ramah Gp..

2.5.6 Intrusive Rocks

Massive, altered diabase, and amphibolitized (on the western margin) sills cut the Ramah Gp. at all stratigraphic levels, throughout its length (Nachvak to Saglek Fiords). The diabase generally has a rusty brown weathering colour, ranges in thickness from a few metres up to 175 m, and is conformable to semi-conformable with the Ramah Gp. (Plate 2.14). The sills contain a variety of different phases including medium to coarse-grained meta diabasic gabbros and pyroxenites (with minor orthopyroxene, and olivine), and locally minor peridotites and dunites (Osmond, 1992). Ultramafic phases, generally less

PLATE 2.13: Dolomitic intraformation breccia present within the Warspite Fm, west of Rowsell Harbour. Although brecciated, this unit does not display a good secondary porosity, and therefore lacks mineralization.

PLATE 2.14: Relatively thin diabase sill intruding contact between the Rowsell Harbour and Reddick Bight formations, north shore of Rowsell Harbour.

than 20 m thick, are typically websterites, with a clinopyroxene (cpx) rich base, and becoming more orthopyroxene (opx) rich upwards. A diabasic gabbro phase occurs above the opx and cpx pyroxenite, with a sharp transition (Osmond, 1992). Hussey (1994) indicated two generations of sill emplacement; (1) intrusion of a thick transgressive, subalkaline mafic-ultramafic sill, (2) differentiation of this sill and the parental magma, following a tholeiitic Fe-enrichment trend, to form smaller, and later sills.

2.5.7 Structural Geology

Several workers (Mengel *et al.*, 1991; Van Kranendonk *et al.*, 1993) have proposed that there have been two phases of deformation affecting the Ramah Gp ; (1) initial development of a fold and thrust belt, followed by (2) transpressional shearing within the Abloviak Shear Zone. Recent work by Calon and Jamison (1993) indicate that the western margin of the Ramah Gp. between Saglek and Nachvak fiords does not appear to have been affected by transpresional shearing.

The major structural feature exhibited by the Ramah Gp. is the relatively open, doubly plunging synclinorium. Deformation associated with the folding produced a pronounced axial planar cleavage within the Ramah Gp. sedimentary rocks. Thrust faulting, with eastern vergence, is common on the western side of the Ramah Gp. (Nachvak Brook and Kiki Lake Thrusts), and caused Nain Province basement to be thrust over the Ramah Gp., thus marking the contact between the basement and the cover sequence (Morgan, 1975; Calon and Jamison, 1993). Calon and Jamison (1993) also noted

that the contact of the Ramah Gp. and the underlying basement between Kiki Lake and the north shore of Saglek Fiord is unconformable, and not a tectonic contact as previously reported by Morgan (1975). Deformation zones within the Ramah Gp. have been defined as the Inner Borderland, Ramah Fold and Thrust Belt, and the Outer Borderland (Figure 2.7; Calon and Jamison, 1993). The Inner Borderland occurs immediately to the west of the Ramah Gp., and is characterised by the presence of reworked amphibolite gneisses which are overprinted at greenschist grade by large folds and associated thrust-sense shear zones (Calon and Jamison, 1993). The boundary between the Inner Borderland and the Ramah Fold and Thrust Belt is demarked by the Kiki Lake Thrust. The Ramah Fold and Thrust Belt, as the name implies, is the zone where the Ramah Gp. rocks have undergone extensive greenschist facies folding and faulting. The Outer Borderland, bounded to the west by the Branigan Thrust, displays less deformation and does not show evidence for structural incorporation of Nain Province basement with the Ramah Gp. cover (Calon and Jamison, 1993). Footwall synclines and hangingwall anticlines associated with the Ramah Fold and Thrust Belt thrust structures, are particularly visible near Schooner Cove (Plate 2.15), and on the south side of Adams Lake. High angle reverse faults have been interpreted as reactivation features of normal faults, which formed early in the deposition of the Ramah Gp. (Calon and Jamison, 1993). The best coastal exposure of the structures present within the Ramah Gp. can be seen on the north shore of Saglek Fiord (Plate 2.16).

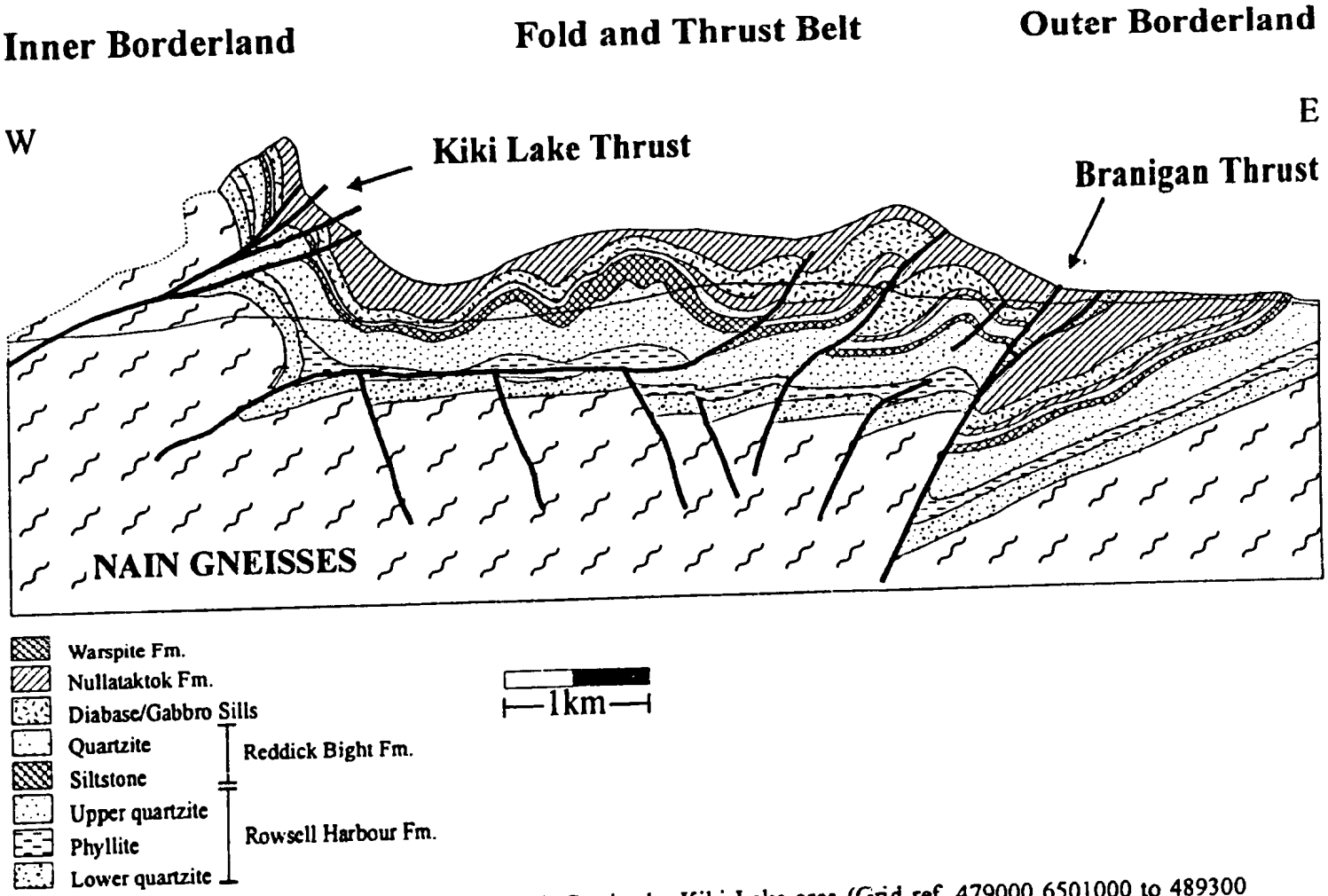

Fig. 2.8: Cross section through the Ramah Gp. in the Kiki Lake area (Grid ref. 479000 6501000 to 489300 6502100). The main tectonic subdivisions of the Ramah Gp. are illustrated on the diagram, viz. Inner Borderland, Fold and Thrust Belt, and Outer Borderland. Section after Calon and Jamison (unpublished work).

PLATE 2.15: Footwall syncline present within the Warspite Fm., near Schooner Cove.

PLATE 2.16: Deformation of the Ramah Group due to the Torngat Orogeny, north shore of Saglek Fiord. The predominant black unit is a gabbro sill, which has been displaced by a thrust (top right). A pre-Ramah Gp. diabase dyke is truncated by the unconformity (centre right).

CHAPTER 3

MINERALIZATION

3.1 Introduction

Fieldwork for this study, carried out in 1993, encountered several different styles of mineralization within all stratigraphic levels of the Ramah Gp.. Sulphide mineralization discovered or re-examined in the Ramah Gp. included: polymetallic veins within the basement; detrital hematite and fuchsite in conglomerates and quartzites; chalcopyrite rich quartz veins; volcanogenic Cu; carbonate-hosted lead-zinc in the RBDM (and remoblized equivalents); the syngenetic Nullataktok Formation pyrite bed (subsequently altered to pyrrhotite at certain localities); lead-zinc mineralization occurring within the chert bed or the thin overlying dolomite unit; Cu-Pb quartz veins in the Warspite Formation; and magmatic Cu associated with the diabase-gabbro sills (Wilton *et al.*, 1993, 1994). The most spectacular mineralization is the epigenetic lead - zinc mineralization associated with the RBDM which forms the main focus of this thesis.

The nine classes of mineralization encountered within the Ramah Gp., are spatially illustrated on a schematic cross-section (Figure 3.1), and the temporal distribution illustrated in Figure 3.2. The classification of each showing or occurrence is given in Table 3.1. A location map of the mineralization encountered during the study is found within the pocket at the back of the thesis. Assay values for the majority of showings are given in Table I.1 (Appendix I).

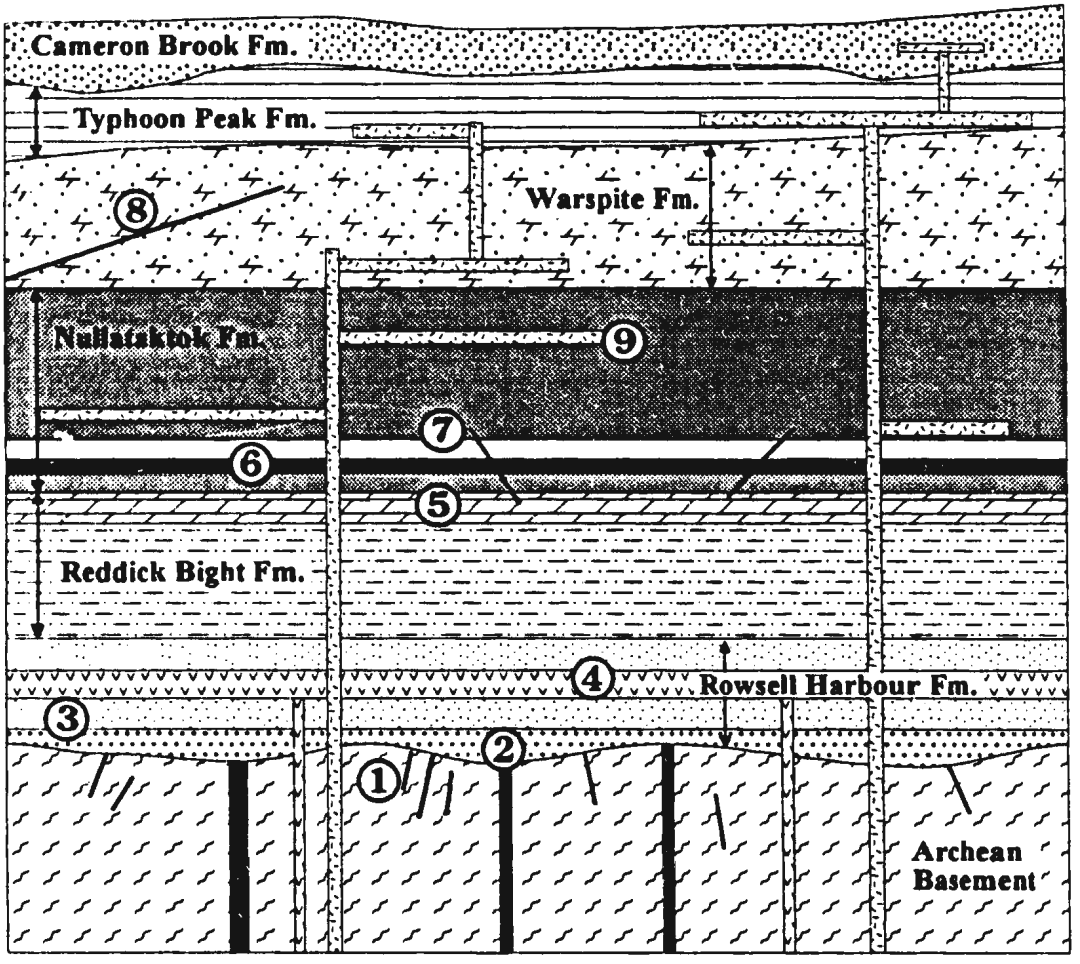

Fig. 3.1: Schematic cross-section of the mineralization within the Ramah Gp.. Key to minerlaization types: 1. veins in basement; 2. Detrital; 3. Cu-rich quartz vein; 4. volcanogenic Cu; 5. Carbonate hosted (MVT or remobilized MVT); 6. Syngenetic pyrite bed (unaltered or altered to pyrrhotite); 7. Zn-Pb sulphides in chert bed or overlying dolomite unit; 8. Cu and Pb rich quartz veins; 9. Magmatic Cu associated with the diabase-gabbro sills.

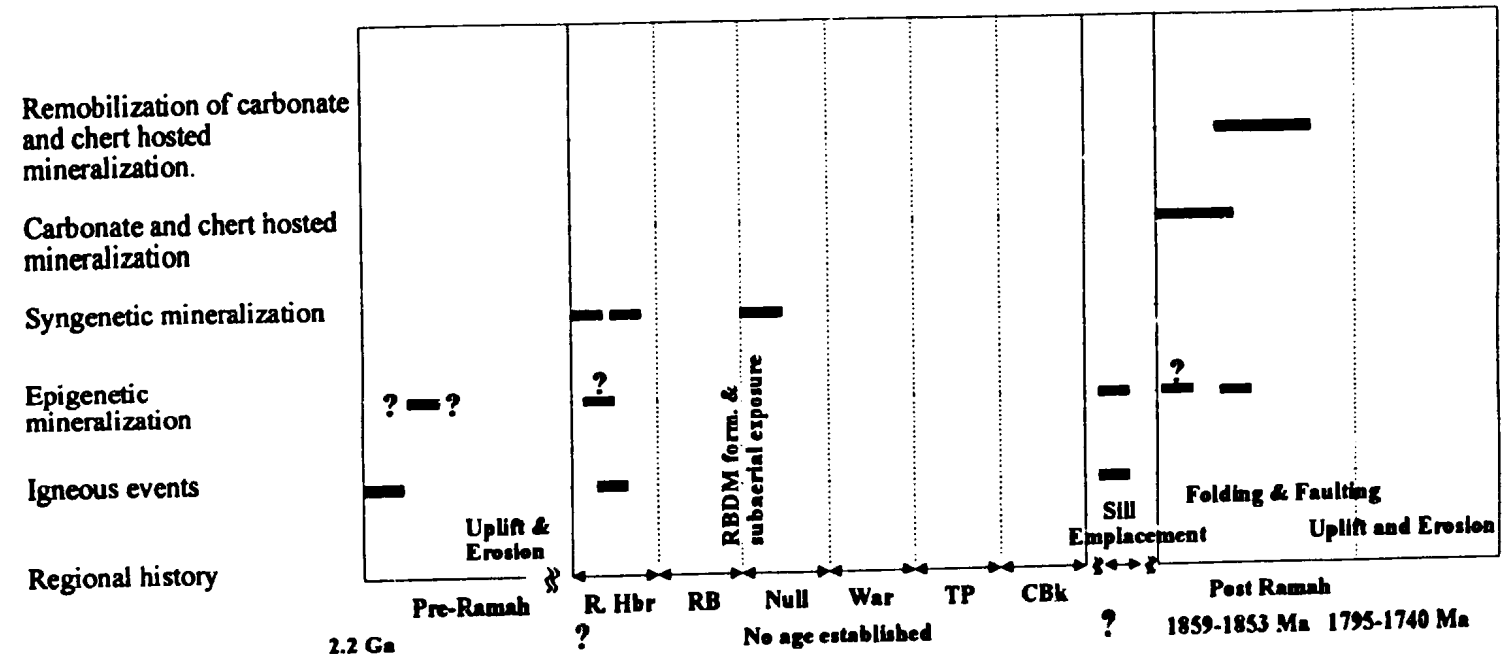

Fig. 3.2: Temporal distribution of mineralization within the Ramah Gp.. Epigenetic mineralization includes polymetallic veins in the basement, quartz vein hosted Cu in the Rowsell Harbour Fm., magmatic Cu, and Cu and Pb quartz veins.. Syngenetic mineralization includes detrital, volcanogenic Cu, and pyrite bed deposition. Key: R. Hbr - Rowsell Harbour Fm., RB - Reddick Bight Fm., Null - Nullataktok Fm., War - Warspite Fm., TP - Typhoon Peak Fm., CBk - Cameron Brook Fm. Ages from Mengel *et al.*, 1991; Collerson *et al.*, 1992; Bertrand *et al.*, 1993.

Table 3.1: Mineral occurrence classification

Occurrence / Showing	Host rock (Formation)	Syngenetic / epigenetic Mineralogy	Classification
Morgan's Archean Vein	Archean Gneiss	Epigenetic Cpy-Gn-Sph	Basement veins
Archibald Archean	Archean Gneiss	Epigenetic Gn	Basement veins
Normore	Quartz vein (RH Fm.)	Epigenetic Cpy-Py	Quartz vein hosted cpy
Naksaluk Cove	Conglomerate (RH Fm.)	Syngenetic Fe	Detrital
Zambia	Alkali basalt (RHVM)	Syngenetic Cpy	Volcanogenic Cu
Panda	Dolomite (RBDM)	Epigenetic Sph-Gn-Py	MVT
Daniel's Point	Dolomite (RBDM)	Epigenetic Sph-Gn-Py	MVT
V-8	Dolomite (RBDM)	Epigenetic Gn	MVT
Blue Sky	Dolomite (RBDM)	Epigenetic Sph-Py	MVT
Godot	Dolomite (RBDM)	Epigenetic Sph	MVT
MacLeod No.1	Dolomite (RBDM)	Epigenetic Sph-Gn-Py	MVT
Pine Harbour	Dolomite (RBDM)	Epigenetic Sph-Py	MVT
RB North Shore	Dolomite (RBDM)	Epigenetic Py-Sph	MVT
Saor Alba	Dolomite (RBDM)	Epigenetic Sph-Py	MVT
Three-nil	Dolomite (RBDM)	Epigenetic Py-Sph	MVT
Black Jack	Dolomite (RBDM)	Epigenetic Sph-Gn-Py	MVT remobilized
Galloway	Dolomite (RBDM)	Epigenetic Sph-Gn-Py	MVT remobilzed
Loch Bears Gut	Dolomite (RBDM)	Epigenetic Sph-Gn-Py	MVT remobilzed
Char	Dolomite (RBDM)	Epigenetic Py-Gn	MVT thermally altered

Table continued overleaf with key.

Table 3.1 cont.: Mineral Occurrence classification

Pyrite Bed	Pyrite bed (Null. Fm.)	Syngenetic Py	Pyrite bed
Near Miss	Pyrr.-pyrite bed near sills (Null. Fm)	Syngenetic Py altered to Pyrr.	Thermally altered pyrite bed
Adams Lake	Chert bed (Null. Fm.)	Syn-Epigentic Sph-Py	Zn-Pb sulphides in chert bed
Gates	Chert bed (Null. Fm.)	Epigenetic Sph	Zn-Pb sulphides in chert bed
Large	Dolomite associated with the Chert bed	Epigenetic Sph-Gn	Zn-Pb sulphides in chert bed
Sandman/Walsh	Chert bed (Null. Fm.)	Epigenetic Sph-Gn	Zn-Pb sulphides in chert bed
Wilton No.1	Quartz vein cutting W. Fm	Epigenetic Cpy	Vein hosted chalcopyrite within the Warspite Fm.
Wilton No.2	Quartz vein cutting W. Fm	Epigenetic Gn	Vein hosted galena within the Warspite Fm.
Butter and Butter Extension	Diabase sill cutting Null. Fm.	Epigenetic Cpy-Pyrr-Py	Magmatic Cu

Key: Gn - Galena, Sph - Sphalerite, Py - Pyrite, Pyrr - Pyrrhotite, Cpy - Chalcopyrite, Fm - Formation, RH-Rowsell Harbour, RHVM - Rowsell Harbour Volcanic Member, RBDM - Reddick Bight Dolomite Member, W - Warspite, ppt - precipitation.

3.2 Archean Basement

3.2.1 Basement Polymetallic Veins

3.2.1.1 Morgan Basement occurrence

The basement lithologies were not examined in any great detail in this study, except in the vicinity of the northern entrance to Ramah Bay, where Morgan (1975) reported the presence of galena-sphalerite-chalcopyrite mineralization (Plate 3.1). The mineralized outcrop, hosted in migmatitic metagranite, occurs in the bed of a small stream flowing south into Ramah Bay (Grid Ref. 486 460, 652 9900; Figure 3.3). Quartz veins/pods, ~2 m long and up to 0.4 m wide, are filled by intergrowths of chalcopyrite, sphalerite, and galena. The veins seem to define the intersection of conjugate fracture cleavage sets. One set has an orientation of 154°/ 83°E, while the other set is 098°/75°N (Wilton *et al.*, 1993; 1994). Further deformation is indicated by the contorted nature of the galena cleavage.

3.2.1.2 Archibald Archean occurrence

Two hundred metres to the east of Morgan's mineral occurrence are a series of smaller quartz veins which contain minor galena mineralization at the centre of the veins. The trend of the mineralized veins is 134° (90° dip). This occurrence is known as the Archibald Archean occurrence (Grid Ref. 489 600, 652 9990). Although of limited extent the mineralization indicates the presence of sulphides in the Archean basement to the east of the Ramah Gp..

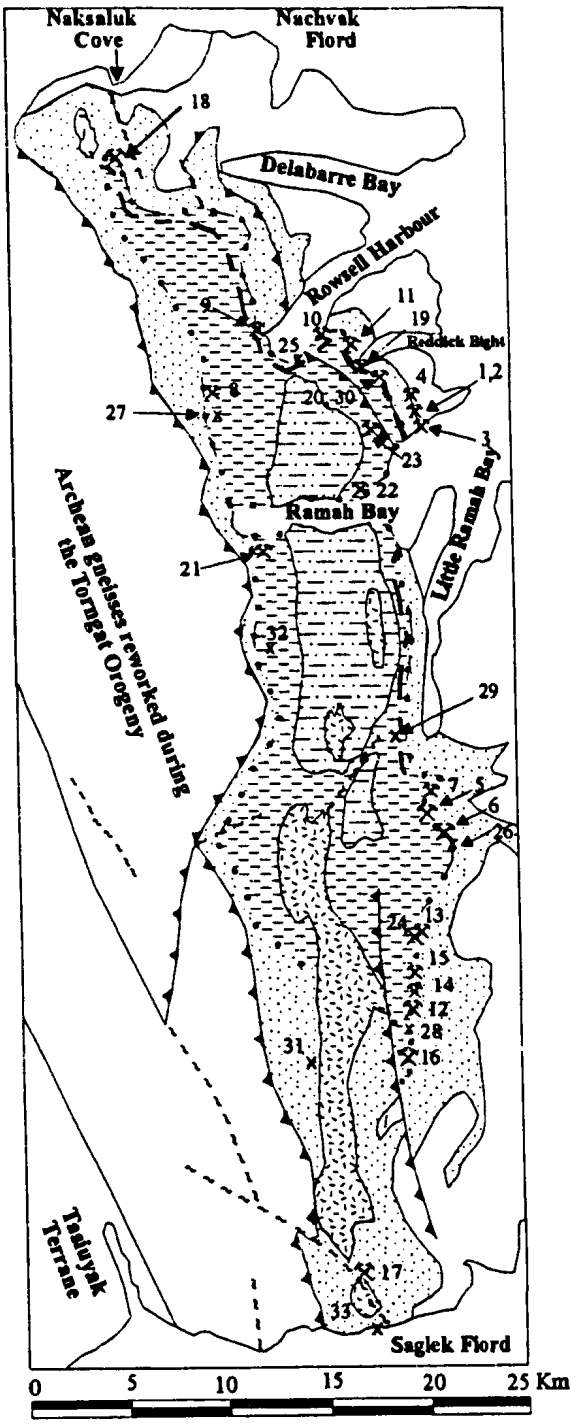

LEGEND

- Gabbro sills
- Cameron Brook and Typhoon Peak Formations
- Warspite and Nullataktok Formations
- Pyrite - chert bed
- Reddick Bight and Rowsell Harbour Formations
- ..... Dolomite bed

⚒ Mineralization encountered during this study

1. Morgan's Archean Vein
2. Archibald Archean
3. Normore
4. Zambia
5. Panda
6. Daniel's Point
7. V-8
8. Blue Sky
9. Godot
10. Pine Harbour
11. Reddick Bight North Shore
12. Black Jack
13. Saor Alba
14. Galloway
15. Three-nil
16. Loch Bears Gut
17. Char
18. Adams Lake
19. Gates
20. Sandman/Walsh
21. Butter & Butter Extension
22. Wilton No. 1
23. Wilton No. 2
24. Near Miss

X Previously Discovered Occurrences

25. Rowsell Harbour Pyrite Bed
26. Morgan (1975)
27. MacLeod No. 1
28. MacLeod No. 2
29. Large
30. Walsh No. 1
31. Walsh No. 2
32. Perrin
33. Morgan Cu

Fig. 3.3: Geological map of the Ramah Gp. with the location of mineralized outcrops. Previously discovered occurrences after Morgan (1975), MacLeod (1984, 1985). Geology after Morgan (1975).

3.3 Rowsell Harbour Formation

3.3.1 Detrital Mineralization

At several localities within the Rowsell Harbour quartzites, and especially near Naksaluk Cove (Grid Ref. 474 350, 654 5730), detrital heavy mineral grains are abundant. A green staining (Plate 3.2) is present on fractures and joints of quartzites above the unconformity at several localities, such as the south shore of Reddick Bight and Naksaluk Cove. The staining is believed to represent remoblization of Cr rich fluids leading to the precipitation of fuchsite (Cr- rich mica); the Cr was probably dervived from Archean ultramafic intrusions (Morgan, 1975).

3.3.2 Cu-rich quartz vein

3.3.2.1 Normore Showing

A 1.5 m thick east-west (096/54°N) trending quartz vein containing chalcopyrite, pyrite and malachite occurs at the Normore Showing (Grid Ref. 489 350, 652 9500; Figure 3.3). The showing is located 200 m south-south-west of the Morgan (1975) basement galena occurrence, 3.n above the unconformity between the Rowsell Harbour Formation quartzites and the Archean basement (Plate 3.3). The vein, although brecciating the quartzites, is relatively undeformed and has minor sericite associated with it. Abundant pyrite occurs within the host quartzites proximal to the vein. The vein does not extend for any great distance into the overlying Rowsell Harbour Formation quartzites, and seems to be confined to the lower part of the Rowsell Harbour Formation.

PLATE 3.1: Galena, sphalerite, and chalcopyrite present within a quartz-lined vein. The mineralization occurrs in basement between Reddick Bight and Ramah Bay, at the intersection of two joint sets (Morgan, 1975).

PLATE 3.2: Green virginite/fuchsite (?) staining within the basal Rowsell Harbour Fm. quartzites at Naksaluk Cove.

PLATE 3.3: Quartz vein with chalcopyrite mineralization at the Normore showing, north shore of Ramah Bay.

3.3.3. Volcanogenic Cu

3.3.3.1 Zambia Occurrence

The Zambia Occurrence (Grid Ref. 489 100, 653 0850; Figure 3.3) is located 1 km north of Morgan's Archean galena occurrence, in a 10 m thick exposure of the Rowsell Harbour basalt member (Plate 2.3). Mineralization consists exclusively of small blebs of chalcopyrite disseminated through the massive middle portion of the altered, amygdaloidal, basalt member, where abundant feldspar phenocrysts are present. Outcrop exposure is less than 15 m and is obscured by overburden to the north.

3.4 Reddick Bight Formation

3.4.1 Carbonate Hosted

3.4.1.1 Panda Showing

The Panda Showing (Grid Ref. 489 855, 650 8935; Figure 3.3) is located within a 2.5 km continuous exposure of the RBDM, between Little Ramah Bay and the head of Bears Gut. Throughout the exposure, the dolomite contains a pronounced secondary porosity with minor sphalerite and galena. The base of the dolomite bed along the outcrop length is demarked by a gradational boundary with brecciation of a relatively coarse-grained dolomitic arenite, which has been infilled by a fine grained micritic dolomite. The top of the dolomite horizon is composed of brecciated and thinly stratified, pinkish-brown, fine dolomite, cemented by white sparry dolomite, and is overlain by graphitic and pyritic shales of the Nullataktok Formation. All of the dolomite along this

exposure is cut by pervasive quartz carbonate veins, with most veins containing a soft, black material, resembling graphite that was subsequently identified as pyrobitumen.

The showing itself is approximately 30 m in length, and 15 m thick, and contains sphalerite, galena, and pyrite intergrown with quartz, saddle dolomite, and calcite in secondary porosity spaces. Mineralization is best developed in the lower portions of the dolomite as vugs up to 5 cm across (Plate 3.4).

3.4.1.2 Daniel's Point Showing

The Daniel's Point Showing (Grid Ref. 490 255, 650 8540; Figure 3.3) lies on the same ridge as the Panda Showing, but 400 m further to the south, in a zone of increased secondary porosity. The sulphide mineralogy and carbonate textures are similar to those in the Panda Showing (Wilton *et al.*, 1993; 1994). Between the Daniel's Point and Panda Showings there appears to be an off-set and a slight depression in the dolomite horizon, which may indicate the presence of a small fault with a dextral sense of motion.

3.4.1.3 V-8 Occurrence

Galena is the only sulphide mineral present at this occurrence which is approximately 2.5 km north of the Panda Showing (Grid Ref. 489 395, 651 0735; Figure 3.3). The mineralization is found as quartz void fillings in brecciated dolomite. The presence of this occurrence in the same stratigraphic horizon as the Panda, Daniel's Point, and Morgan's (1975) original showing (0.5 km and 60 m higher to the east southeast from

the Panda showing) indicates that scattered sphalerite-galena mineralization is present in broken outcrop and subcrop over a lateral distance of at least 3 km (Plate 3.5).

3.4.1.4 MacLeod No. 1 Showing

This showing was originally discovered by ESSO Minerals Ltd. geologists in 1985 (MacLeod, 1985) and occurs 5 km north from the head of Ramah Bay (Grid Ref. 478 920, 652 9460; Figure 3.3). Re-examination during fieldwork in 1993 revealed that the mineralization was restricted to the ~ 6 m dolomite bed over a strike length of over 320 m with mineralization present only in the southern 150 m. Textures present within the yellow weathered dolomite at this showing range from massive dolomite, to grey aeolian derived dolomite (Wilton *et al.*, 1993; 1994). The dolomite is overturned at this locality, contrary to the mapping of Morgan (1975), indicating the effects of thrusting to the west or the possibility that an inclined fold is present. A secondary porosity is present in the dolomite with quartz, calcite and saddle dolomite filling and lining the voids. The void centres were subsequently filled by sphalerite, galena, and pyrite. Pyrobitumen (graphite) is also present within the voids. Linear quartz veins cut the dolomite-filled voids, and contain sulphides, suggesting that remobilization of the sulphides may have occurred (Wilton *et al.*, 1993; 1994). The outcrop has abundant hydrozincite staining caused by the alteration of the sphalerite mineralization.

PLATE 3.4: Brown sphalerite (Sph) and grey galena (Gn) mineralization in voids of a mosaic breccia within the RBDM at the Panda showing. Late stage calcite and quartz form the centre of the voids.

PLATE 3.5: Exposure of the RBDM between Morgan's (1975) Pb-Zn mineralization (A), Daniels Point showing (B), and Panda showing (C), with the photograph taken from the V-8 occurrence. Exposed outcrop length is 5km. RB Fm - Reddick Bight Formation, Null Fm - Nullataktok Fm.

3.4.1.5 Blue Sky Occurrence

The Blue Sky Occurrence (Grid Ref. 478 575, 653 0850; Figure 3.3) occurs 1.4 km north of the MacLeod No. 1 Showing and is partially exposed in a river bed. Mineralization is very scarce, with minor sphalerite and pyrite at the northern end of the 50 m exposure, and galena present at the southern end in the stream bed. The host lithology is dolomite with the characteristic quartz - carbonate veining present (Wilton *et al.*, 1993; 1994).

3.4.1.6 Godot Showing

The Godot Showing (Grid Ref. 481 230, 653 4760; Figure 3.3) occurs in a waterfall on the northern side of the head of Rowsell Harbour, where the dolomite is exposed. The occurrence consists of a quartz-carbonate cement to a breccia of grey dolomite fragments. The cement contains 1-2 % disseminated sphalerite. Silicification of the host dolomite is more pronounced here than at other showings, resulting in a decrease of the dolomites porosity. Pyrobitumen is present in some of the vugs and cavities (Wilton *et al.*, 1993; 1994).

3.4.1.7 Reddick Bight North Shore Occurrence

The Reddick Bight North Shore Occurrence (Grid Ref. 486 075, 653 3455; Figure 3.3) is present as 20 m of subcrop of RBDM along the shoulder of the ridge between Reddick Bight and Rowsell Harbour (Wilton *et al.*, 1993a). The dolomite exhibits a

good secondary porosity and is cut by quartz carbonate veins. Present within the voids are pyrite, minor sphalerite, pyrobitumen, and quartz (Plate 3.6).

3.4.1.8 Saor Alba Occurrence

Mineralization at the Saor Alba Occurrence (Grid Ref. 488 645, 6503780; Figure 3.3) occurs in the lower portions of the 10-12 m thick RBDM and outcrops over a distance of 15 m before being obscured by grass and felsenmeer. At this locality the dolomite is pinkish brown and contains quartz in small vugs and thin veins (Plate 2.8). A secondary porosity is developed, but is not as well developed as that at the Panda or MacLeod No. 1 showings.

Sphalerite, with minor amounts of pyrite, constitutes the sulphide mineralization, and is usually present at the margins of the 1 - 2 cm wide quartz veins or vugs. Mineralization was absent in the upper part of the dolomite bed, although the presence of pyrobitumen was noted.

3.4.1.9 Pine Harbour Showing

This showing is situated on the southern shore of Rowsell Harbour (Grid Ref. 484 805, 653 4100; Figure 3.3) and is the 1993 "discovery" outcrop for the carbonate-hosted mineralization. Outcrop length is on the order of 30 m. The overlying Nullataktok Formation pyritiferous graphitic shales at this locality are highly sheared and contorted with minor quartz veining, indicating the presence of a thrust fault. In the upper 3 m of

PLATE 3.6: Quartz filled void displaying colloformal texture, within the Reddick Bight Dolomite Member, at the Reddick Bight North Shore showing.

the dolomite, quartz-filled patches, up to 20 - 30 cm across, are present and are rimmed by secondary dolomite. These quartz-filled voids are zoned with outer dark grey quartz rims, millimetre-scale colloformal sphalerite bands, and white quartz cores. Some voids also contain minor pyrite and pyrobitumen (Plate 3.7).

3.4.1.10 Three - nil (3-0) Occurrence

Six hundred and fifty metres, north-north east along stratigraphy from the dolomite bed at the Galloway Occurrence is the Three-nil occurrence (Grid Ref. 489 000, 650, 0400; Figure 3.3). The contact between the Reddick Bight Formation quartzite and the Dolomite Member is very diffuse. Dolomitization and quartz veining have penetrated into the coarse grained quartzites, but no sign of brecciation is present near the base. The dolomite tends to have a more orange appearance than normal (probably indicating more ferrodolomite), while the quartzites appear to have been bleached (removal of hematite cement). Mineralization is present within quartz veins and vugs, 3 - 5 cm thick, which parallel primary bedding features and consists of pyrite and sphalerite as small "clots" in the centres of the veins. Small quantities of disseminated pyrite are also present in the areas of orange dolomite.

PLATE 3.7: Pyrobitumen within a quartz-carbonate vug at the Pine Harbour showing, south shore of Rowsell Harbour.

3.4.2 Carbonate hosted vein (remobilized)

3.4.2.1 Black Jack Showing

The Black Jack Showing (Grid Ref. 488 665, 649 9620; Figure 3.3) occurs in the basal 2-3 m of the RBDM, and has an area of 1.45 x 0.4 x >0.45 m. The predominant form of mineralization is sphalerite, with lesser amounts of silver-rich galena (93ppm Ag, Table II.1, Appendix II), and very minor chalcopyrite, hosted in a quartz-coated cavity (Wilton *et al.*, 1993a). The straw brown coloured dolomite host rock has a well developed secondary porosity, a coarse grain size, and extensive quartz veins. Quartz, dolomite, and calcite veins in the immediate vicinity do not appear to have been mineralized. Plate 3.8 shows sulphide mineralization found within a void which might be related to the development of two sets of quartz veins (trend; 065°-245°, 090°-279°).

3.4.2.2 Galloway Occurrence

The Galloway Occurrence (Grid Ref. 488 850, 649 9750; Figure 3.3) is located 300 m north-east of the Black Jack Showing, and is hosted in buff coloured RBDM that has a relatively low porosity. Sphalerite, galena and pyrite are present as cores to well zoned quartz and saddle dolomite vertical veins that are up to 10 cm wide (Plate 3.9). The growth banding of the veins indicate repeated changes in fluid geochemistry. The main vein cuts the dolomite and was infilled by an early quartz, followed by galena, a 1 - 2 cm zone of pinkish-orange dolomite and finally a late sphalerite zone that is up to 6 cm in width, Plate 3.9. Most veins follow a trend of 090°-270°.

PLATE 3.8: Large void infilled by sphalerite (brown) at the Blackjack showing. Argentiferous galena at this showing contains the highest concentrations of silver (93 g/tonne) within the Ramah Group.

PLATE 3.9: Sphalerite (dark brown) occurs in the centre of quartz-carbonate veins at the Galloway showing.

3.4.2.3 Loch Bears Gut Showing

The Loch Bears Gut Showing (Grid Ref. 488 330, 649 8180; Figure 3.3) occurs within a stream bed 400 m south of the MacLeod No. 2 Showing (MacLeod, 1985). The MacLeod No. 2 Showing was reported by MacLeod (1985) to have 2700 ppm Pb and 2300 ppm Zn, but on re-examination for this study only a local secondary porosity, with pyrobitumen and quartz veining, was found in the dolomite. At the Loch Bears Gut showing, dolomite in the stream bed exhibits secondary porosity filled with calcite, dolomite, and/or quartz. The colour of the dolomite varies from the typical light yellow to grey-black colour. The occurrence consists of polymetallic sphalerite-galena-pyrite veins composed of almost 90 to 100% sulphides, which are subparallel to bedding with vertical connections (Plate 3.10). Mineralization is concentrated where the veins pinch and swell into pods, up to 6 x 15 cm. Overlying the dolomite are contorted and fragmented pyritiferous shales of the Nullataktok Formation which indicate the probable presence of a thrust plane directly above the dolomite unit. Evidence of the thrust plane and the polymetallic nature of the sulphides suggests that the mineralization may be a product of remobilization, perhaps from mineralization in the dolomite.

3.4.2.4 Char Showing

The Char Showing (Grid Ref. 485 775, 648 6985; Figure 3.3) is the most southerly example of sulphide mineralization found in the RBDM. The dolomite outcrop and subcrop extend for a distance of over 100 m to the south and 20 m to the north of the

stream where the Char Showing is located. The dolomite is highly altered here due to the proximity of overlying diabase sills. Sulphides are present in highly oxidised, deformed quartz veins, as pyrite with lesser galena (Plate 3.11). A vague secondary porosity is present, but is poorly preserved.

Approximately 500 m west of the Char showing, the dolomite member is cut by a high angle fault which resulted in silicification of the dolomite. In this zone, sulphide mineralization is present within silicified vugs in the dolomite, consisting of pyrite, pyrrhotite, and vaesite (NiS_2). The nickel is probably derived by remobilization of sulphides from within the common diabase sills in the area.

3.5 Nullataktok Formation

3.5.1 Syngenetic Pyrite

3.5.1.1 Pyrite-Pyrrhoitite Bed

The Pyrite-Pyrrhotite bed, although attracting a great deal of exploration attention due to its thickness (up to 2 m) and lateral extent (65 km by up to 16 km), has been found to contain no elevated base metal concentrations. Samples collected from several different outcrops of this bed indicate a biogenic origin and will be discussed further in chapters 4 and 5.

PLATE 3.10: Polymetallic veins (Sphalerite-Galena-Pyrite) within the RBDM at the Loch Bears Gut showing.

PLATE 3.11. Oxidized galena veins (A and arrow) at the Char showing represent the most southernly occurrence of mineralization hosted within the RBDM.

3.5.2 Zn-Pb sulphides associated with chert and thin dolomite unit

3.5.2.1 Large Occurrence

This occurrence was originally discovered by ESSO Mineral Ltd. geologists in 1985. MacLeod (1985, p.18) described it as "isolated blebs of sphalerite and galena" within "brecciated chert", a grab sample of which assayed 14 ppm Pb and 330 ppm Zn.

The occurrence is located on a ridge, above the north side of a river that flows into Little Ramah Bay (Grid Ref. 488 035, 651 3070; Figure 3.3), in a 3-5 m thick zone of brecciated chert (above the pyrite bed). A thin dolomite bed lies above the brecciated zone, and the breccia is cemented by a dolomite cement (Plate 2.12). Evidence exists for the presence of a thrust zone in the general vicinity of mineralization.

3.5.2.2 Adams Lake Occurrence

Sulphide mineralization at the Adams Lake Occurrence (Grid Ref. 474 175, 654 3700; Figure 3.3) was found as a piece of chert float in a stream bed about 10 m upstream from where the RBDM outcrops. The pyrite bed seems to be absent (also noted by Morgan, 1975 and Knight and Morgan, 1981), but the chert bed is easily located. Scree and felsenmeer is assumed to obscure the pyrite bed. Mineralization consists of massive sphalerite and euhedral pyrite in a brecciated white to grey, sugary chert, indicating possible recrystallization.

3.5.2.3 Gates Occurrence

The Gate Occurrence (Grid Ref. 485 955, 653 2145; Figure 3.3) is located within the stream flowing into Reddick Bight, in the brecciated top of the chert bed. The occurrence consists of small patches of sphalerite in black, brecciated chert.

3.5.2.4 Sandman/Walsh

This occurrence is located in a river valley flowing north into Reddick Bight (Grid Ref. 487 075, 653 1440; Figure 3.3). Sulphides were found as float in the river bed, and consist of small blebs of sphalerite and galena in brecciated chert. The source of this float is almost certainly in the same valley, and probably originates from the chert bed.

3.6 Warspite Formation

3.6.1 Cu-Pb quartz veins

3.6.1.1 Wilton No. 1 and Wilton No. 2 Occurrences

Both occurrences are located on the north shore of Ramah Bay. The Wilton No. 1 (Grid Ref. 486 520, 652 6040; Figure 3.3) is located in the lower part of the Warspite Formation, and consists of a small quartz vein containing chalcopyrite with malachite staining. The Wilton No. 2 (Grid Ref. 486 855, 652 6900; Figure 3.3) occurrence occurs near the top of the Warspite Formation, and consists of a deformed quartz vein with

galena at the core. The deformed nature of the vein indicates that mineralization occurred prior to deformation.

3.7 Diabase and Ultramafic Sills

3.7.1 Magmatic Copper

3.7.1.1 Butter and Butter Extension Occurrences

Both these occurrences are found on the south shore at the head of Ramah Bay (Grid Refs. 481 385, 652 3455, and 481 070, 652 3590; Figure 3.3). The host lithologies are Nullataktok slates which have been intruded by an 8 m thick diabase sill. Mineralization consists of chalcopyrite, pyrrhotite, and pyrite with a malachite staining present within quartz veins that cut the slate. Mineralization is a localised effect and the 30 - 60 cm quartz veins do not extend for more than 30 cm beyond the diabase sill.

3.7.1.2 Related Mineralization

Chalcopyrite, pyrrhotite and pyrite are present within the mafic and ultramafic rocks in the Ramah Gp.. Examination of these sulphide occurrences within the sills is beyond the scope of this thesis, but Hussey's (1993) work suggests that the economic potential for PGE's, nickel and copper at the present erosional level is low. This conclusion (Hussey, 1993) was reached through the use of geochemical data which demonstrated that if a sulphide segregation event occurred it would have been at depth.

The PGE-Ni-S depleted magma, of subalkaline basaltic composition, continued its assent to intrude the Ramah Gp. as diabase sills.

CHAPTER 4

RESULTS

4.1 Introduction

Several different styles of sulphide and placer mineralization occur within the Ramah Gp., all of which will be discussed in this chapter. Particular attention will be paid to the sulphide mineralization within the Reddick Bight Dolomite Member (RBDM), as it is the most economically significant. The Nullataktok Fm. pyrite - pyrrhotite bed will also be discussed in detail as there has been some considerable debate concerning its mode of origin since its discovery in the early 1900's. Other types of mineralization are also described , are briefly described.

Methods employed to characterise the mineralization include determination of sulphur, carbon, oxygen, and lead isotopic ratios, thermometric measurements on fluid inclusions, polished thin section microscopy, cathodoluminescence, and X-ray fluorescence (Tables II.2 and II.3, Appendix II). Analytical methods used are described in Appendix IV. The data obtained are used to quantify the mineralization process and to postulate a metallogenic model for the Ramah Gp..

4.2 Archean Sulphide Mineralization

Sulphide mineralization at the Morgan Vein and Archibald Archean occurrences consists of galena, sphalerite and chalcopyrite within Archean rocks. Galena and

sphalerite separates from both occurrences were analysed for their sulphur and lead isotopic compositions; the results are shown in Tables III.1, and III.2 (Appendix III) respectively.

4.2.1 Sulphur Isotopes

The sulphur isotopic ratios of the sulphides are ~ 0‰ (Table III.1, Appendix III), which correlate closely with values expected for a magmatic source (Rye and Ohmoto, 1974; Ohmoto and Rye, 1976). The values indicate that there was little fractionation of the sulphur source, which is suggestive of high temperature processes (Taylor, 1987). The initial origin of the sulphur was probably magmatic, perhaps due to leucocratic granite or pegmatite intruding the host gneisses. Leucocratic granite and pegmatites are common in the gneisses east of the Ramah Gp. (Morgan, 1975). Subsequent metamorphism of these gneisses (and intrusives) resulted in the remobilization of the sulphides to form vein mineralization.

4.2.2 Lead Isotopes

Lead isotope data for the galena separates (Table III.2, Appendix III; Figures 4.1 and 4.2) signifies that the lead is very non radiogenic, i.e. separated from a low Mu (μ) source region, and hence plots beneath Doe and Zartman's (1979) model growth curves for the lower crust. Model age (Stacey and Kramers, 1975) values are 2460 and 2446 Ma. Nuk gneisses comprise a portion of the Archean gneiss to the east of the Ramah

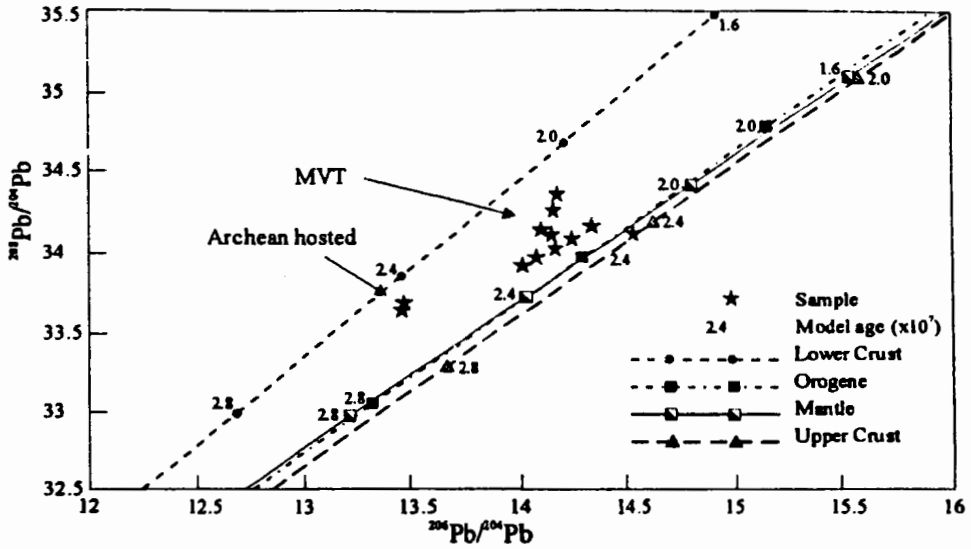

Fig. 4.1: $^{208}Pb/^{204}Pb$ vs $^{206}Pb/^{204}Pb$ plot with Doe and Zartman (1979) growth curves superimposed. The plot indicates that the lead mineralization formed from a source enriched in ^{232}Th relative to ^{238}U and ^{235}U, such as the lower crust.

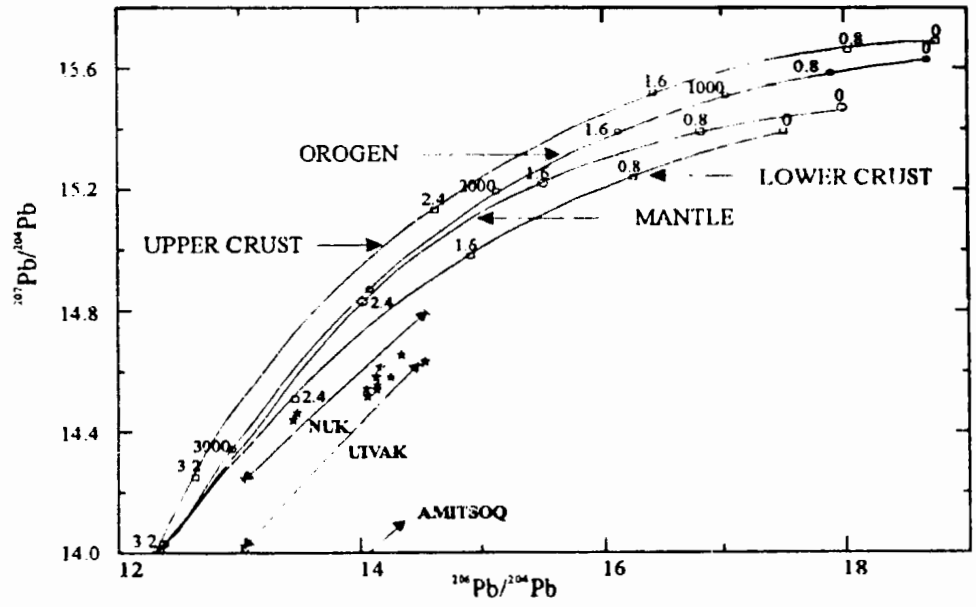

Fig. 4.2: $^{207}Pb/^{204}Pb$ vs $^{206}Pb/^{204}Pb$ plot with Doe and Zartman (1979) growth curves superimposed. The plot indicates that the lead is non-radiogenic (plots below lower crust values) and is similar to values obtained from the Archean gneisses (Nuk and Uivak) to the east of the Ramah Group Values for the Nuk, Uivak and Amitsoq gneisses from Ashwal *et al.* (1987).

Group and it is conceivable that these low μ values are a result of metamorphic reworking. The reworking led to a loss of ^{238}U, ^{235}U, and ^{232}Th, and as a consequence, less radiogenic lead was produced. The model is used to explain lead isotope ratios for rocks of the same age in Greenland (Moorbath *et al.*, 1973) and the Nain craton further south (Ashwal *et al.*, 1987; Wilton, 1991). The isotope data suggest that the galena was derived from the Archean gneisses. Lead isotopes will be discused further in section 4.6.7.

4.3 Detrital Mineralization

The oldest type of mineralization that formed in the Ramah Gp. is the detrital, heavy mineral sands, present within the basal formation (Rowsell Harbour Fm.). The heavy minerals were derived from weathering of the basement Archean gneisses, but the dimensions of these placer style mineral concentrations are not of any great significance. A conglomerate in the lower part of the Rowsell Harbour Fm. at Naksaluk Cove contained hematite (11.98 wt.%, Fe_2O_3; Plate 4.1) and elevated barium, vanadium, and chromium concentrations (sample SA93-070 in Table II.2, Appendix II), relative to other Rowsell Harbour samples analysed. The euhedral nature of the hemetite grains in the conglomerate suggest that it was derived locally, and was not transport any great distance. At several localities along the unconformity surface, green staining is present in the quartzite which can probably be attributed to the weathering of ultramafic zones within the basement. Due to the limited extent of this mineralization no further geochemical work was undertaken.

4.4 Rowsell Harbour Volcanic Member

The Rowsell Harbour Volcanic Member is between 6 and 18m thick and occurs throughout the Ramah Group. A description of the flow is given in Chapter 2 (2.5.2.1.2), but the actual geochemistry of the flow has remained problematic since first being described by Douglas (1953). Douglas (1953) simply described it as an amygdaloidal basalt, Christie (1952) as a latite (trachyandesite or trachybasalt), Taylor (1969) as an andesite. Morgan (1978) described the flow as a tholeiitic basalt, but questioned his own interpretation due to the altered nature of the sample. Work on the flow during this study indicates that it is in fact an alkali basalt, according to the classification of Meschede (1986), Figure 4.3. Six samples were analysed: base, middle, and top of a massive flow at the Zambia Occurrence; glass rim and core of pillow lava near Schooner Cove; and a deformed pillow near Bears Gut. The data for the six samples are presented in Table II.3 (Appendix II). Figure 4.3 also contains representative samples of alkali basalt from the Huri Hills, northern Kenya (Class *et al.*, 1994) for comparison. Samples from Kenya were chosen, because complete rare-earth element patterns were available which allowed better comparison with the RHVM samples. The only sample which failed to plot within a field was the volcanic glass rim of the pillow lava (SA93-048A), probably due to hydrothermal alteration during formation. Rare-earth element (REE) analysis, Figure 4.4, indicates that the RHVM samples have the same overall trend as the Kenyan samples (Class *et al.*, 1994), with heavy REE depletion relative to light REE which is indicative of within plate alkali basalts (Wilson, 1989). The extended REE plot, Figure 4.5, shows minor niobium

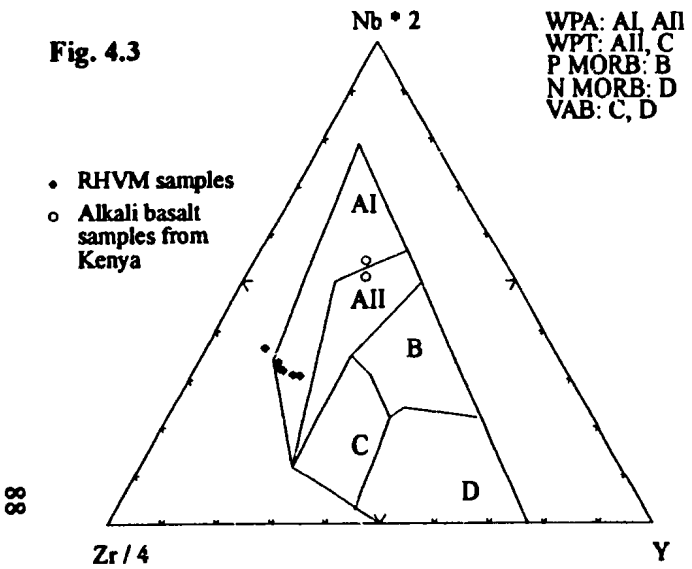

Fig. 4.3: Samples from the RHVM plot in the within plate alkali basalt field of Meschede (1986). Kenyan samples from Class *et al.* (1994).

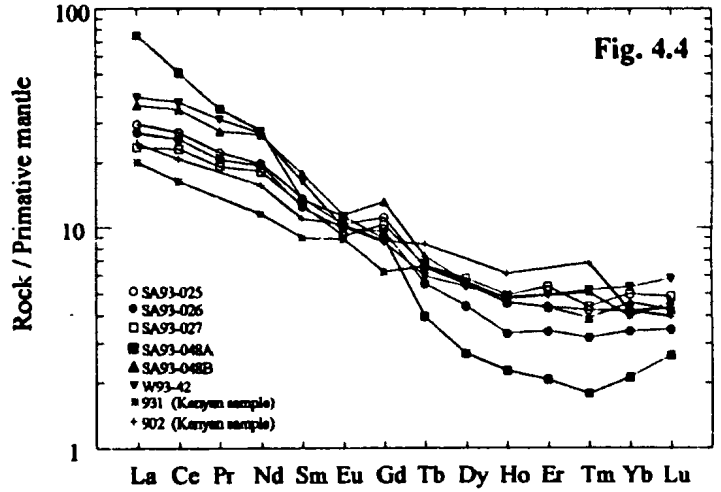

Fig. 4.4: REE plot of RHVM samples and alkali basalts from Kenya for reference (931 and 902) (Class *et al.*, 1994). The plot has been normalized to primative mantle values of Hofmann (1988).

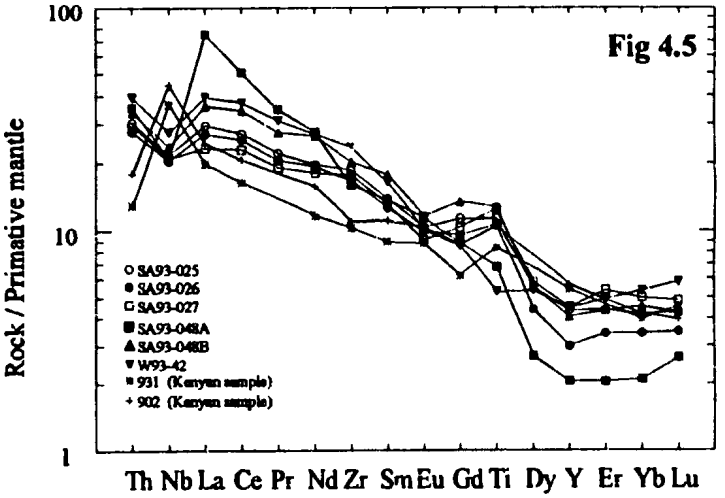

Fig. 4.5: Primitive mantle normalized extended REE plot of RHVM basalts with Kenyan samples for reference (Class *et al.*, 1994).

(Nb) depletion. The Nb depletion corresponds to assimilation of the upper crust by the ascending alkali magma (Sun, 1980; Wilson, 1989). Therefore, it seems likely that the RHVM is actually an alkali basalt which underwent minor crustal contamination, most likely by the quartzofeldspathic gneisses of the Nain Structural Province, during the ascent of the magma prior to eruption.

4.4.1 Zambia Occurrence

Although not a large occurrence, the chalcopyrite mineralization within the alkali basalt flow at the Zambia occurrence is interesting. Petrography indicates that the only sulphide mineral present is chalcopyrite which forms blebs up to 3mm in size within the host amygdaloidal basalt (Plate 4.2). The host rock has been extensively altered to form chlorite, epidote, and remnant feldspars (greenschist assemblage).

4.4.1.1 Sulphur Isotopes

Sulphur isotope ratios have been used to distinguish between the source areas for sulphur. Derived data for sulphide minerals are reported in the δ (del or delta notation), where :

$$\delta^{34}S = \frac{\left(^{34}S/^{32}S\right)_{sample} - \left(^{34}S/^{32}S\right)_{standard}}{\left(^{34}S/^{32}S\right)_{standard}} \times 1000$$

and the standard is the Cañon Diablo Troilite (CDT), with a $^{34}S/^{32}S$ ratio of 0.0450045 (Macnamara and Thode, 1950; Ault and Jensen, 1963). Values for the $\delta^{34}S$ ratio are expressed as parts per thousand, or per mil (‰).

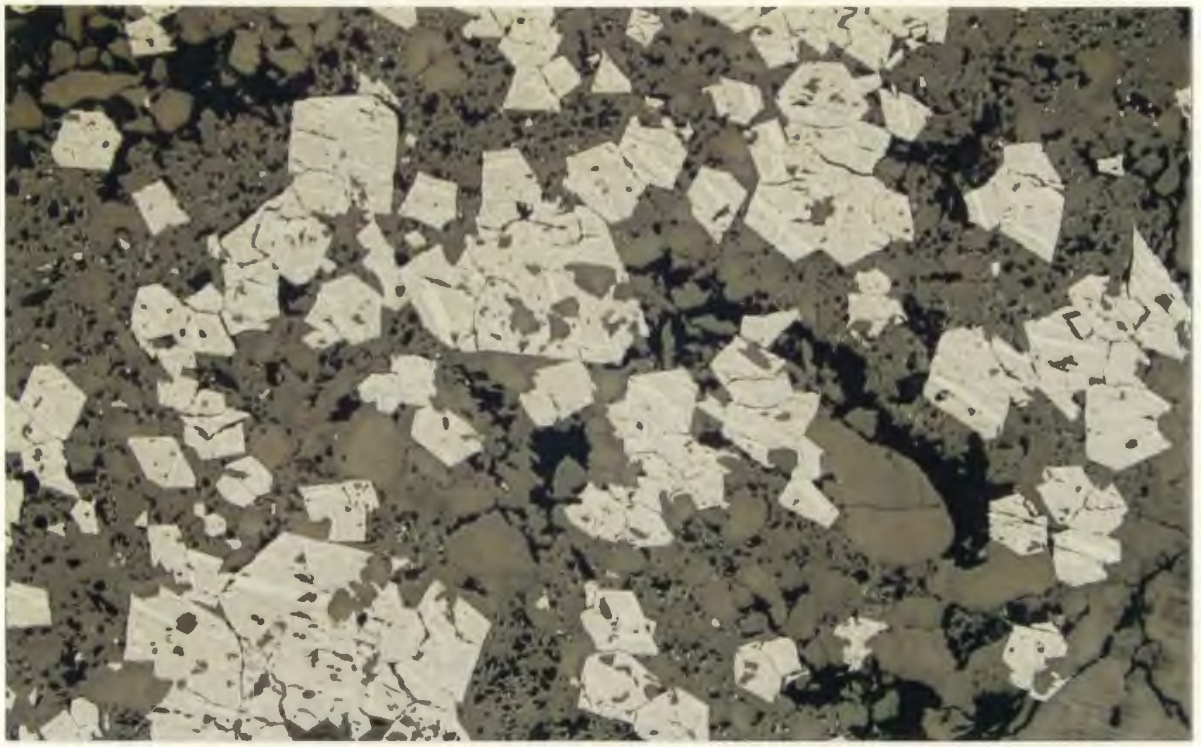

PLATE 4.1: Euhedral hematite found within conglomerate float at Naksaluk Cove. x 2.5 magnification, reflected light.

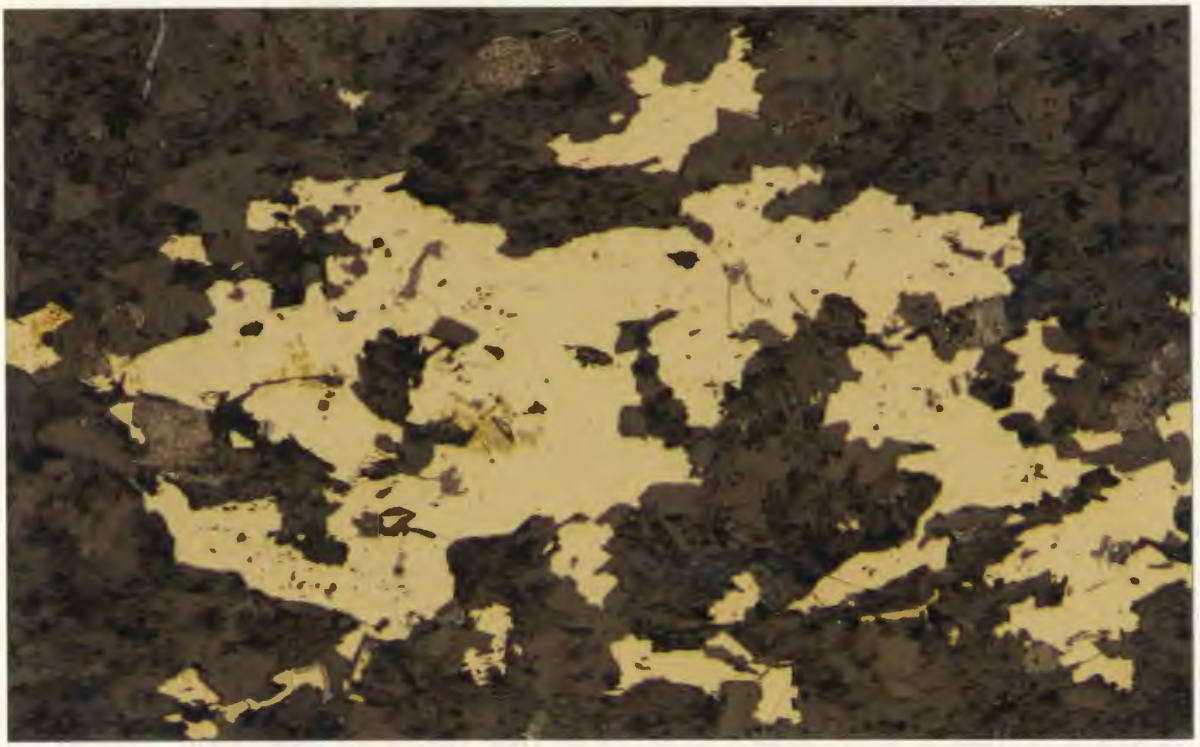

PLATE 4.2: Chalcopyrite from the Rowsell Harbour Volcanic Member at the Zambia showing. x 10 magnification, reflected light.

There are three main terrestrial sulphur sources viz., biogenic ($\delta^{34}S$ ~ 0‰), magmatic ($\delta^{34}S$ » 0 ± 2‰), and seawater ($\delta^{34}S$ 0‰, typically ~ 12‰ during Paleoproterozoic times) (Ohmoto and Rye, 1979; Taylor, 1987; Faure, 1986; Hayes *et al.*, 1992). A comparison of natural sulphur isotope reservoirs and their $\delta^{34}S$ values are given in Figure 4.6.

A single sulphur isotope ratio of + 12‰ was obtained for the chalcopyrite mineralization (Table III.1, Appendix III). This value would seem to indicate that the sulphide formed from the modification of seawater sulphate, perhaps similar to the process described by Rye and Ohmoto (1974) and Ohmoto and Rye (1976), where seawater is reduced by reaction with Fe^{2+} in hot volcanic rock. The H_2S so produced would react with any copper-iron complexes to produce the chalcopyrite. Sangster (1968) noted that most volcanogenic hosted massive sulphide deposits had $\delta^{34}S$ values approximately 17‰ lower than contemporaneous seawater. If this is the case then seawater sulphate present in the Ramah basin 2.0 Ga would have had an isotopic composition of 29‰, which is more than twice the estimated value of 12‰ from the literature (Hayes *et al.*, 1992). A value of +29‰ may indicate the presence of evaporites at this stage of basin development, proximal to the volcanic flow. Although the flow was extruded into a shallow marine environment, as indicated by the ripple marks present in the Rowsell Harbour Fm., no evidence exists for evaporites, or evaporite dissolution. The sulphur isotopic evidence for the Rowsell Harbour Volcanic Member remains problematic, but may be resolved through analysis of more sulphide samples.

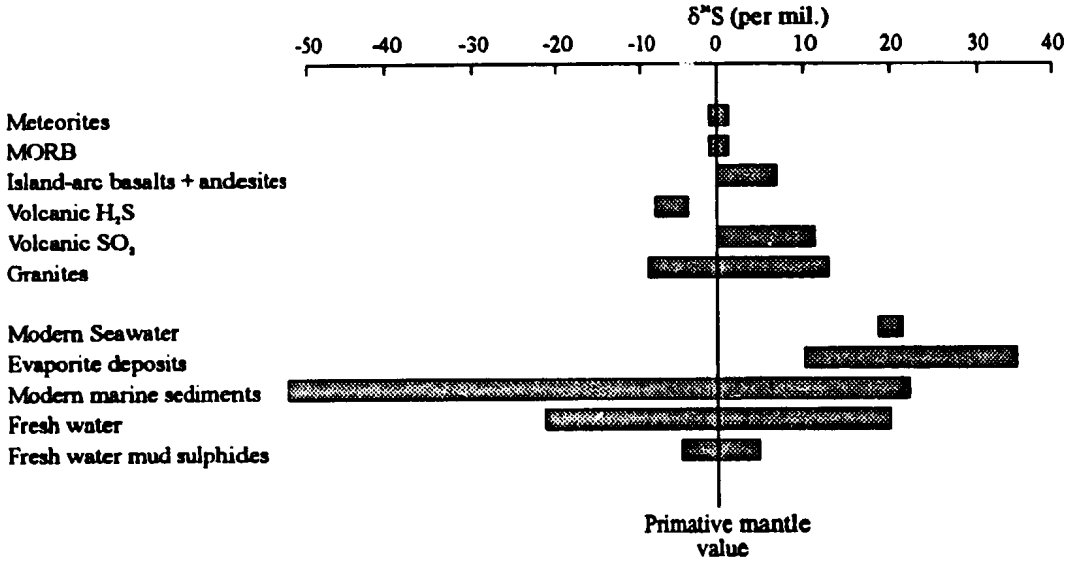

Fig. 4.6: Natural sulphur isotope reservoirs and their $\delta^{34}S$ values. Figure redrawn from Rollinson (1993).

4.5 Pyrite - Pyrrhotite Bed

This unit has a very wide distribution, occurring from Delabarre Bay (Grid Ref. 476500, 6540700) in the north, to Saglek Fiord in the south, and is present on both the eastern and western margins of the fold and thrust belt synclinorium. With an average thickness of about 50 cm, but up to 2m, it is an easily recognised and persistent unit in the Ramah Gp.. Early mineral exploration in the Ramah Gp. centred on determining the extent, composition, and genesis of this unit, especially in the vicinity of Rowsell Harbour. Carter (1902) considered the unit to be a vein associated with the overlying chert bed which he thought was quartz or flint. Douglas (1953) examined the bed and concluded that there had been two phases of mineralization, the first causing silicification of a dolomite unit to produce the chert bed, and in the second, sulphide-rich fluids precipitated pyrite beneath the chert bed. Fogwill (1966) and Blackwell (1976) concluded that the pyrite bed was stratiform, and probably formed in an anoxic basin. Blackwell (1976) noted differences in the geochemical characteristics of the pyrite bed, and attributed these to exhalative deposition in a series of sub-basins present within the larger Ramah basin. Macleod (1984, 1985) considered the pyrite bed to represent an exhalative product similar to the Sedimentary Exhalative (SEDEX) class of deposit. SEDEX deposits are characterised by synsedimentary faults and zoned copper, lead, and zinc mineralization (Large, 1983); Macleod's results indicated that zonation was absent, but that the pyrite may still represent some form of SEDEX mineralization.

Three principal methods were employed to resolve whether the pyrite - pyrrhotite bed resulted from hydrothermal exhalation or was biogenic, including examination of sulphur isotope ratios, Co/Ni ratios, and trace element concentrations within the pyrite.

4.5.1 Polished thin section microscopy

The pyrite within the bed, when not metamorphosed, is generally 10-20μm in diameter and consists mainly of anhedral to subhedral crystals of pyrite which define bedding (Plate 4.3). The matrix between the pyrite grains is a dark, fine grained substance which may represent a minor organic constituent. All but one of the eight unmetamorphosed samples studied contain 100% pyrite as the sulphide mineral; the exception is the bed south of Schooner Cove where the pyrite also contains trace amounts of chalcopyrite and sphalerite in a 100μm void (Plate 4.4).

Samples that were thermally metamorphosed by the sills are generally coarser grained, ~ 50μm, and contain greater than 90% pyrrhotite (Plate 4.5). Some secondary euhedral pyrite is also present ranging from 0.3 - 0.75mm in diameter. Other sulphides present, in order of abundance, include pyrite, chalcopyrite, and, rarely, arsenopyrite. Arsenic present in the unmetamorphosed pyrite bed occurs within the structure of the pyrite, but in the metamorphosed bed it has been remobilized producing distinct arsenopyrite crystals. Metamorphosed sulphide samples contain more quartz (recrystallized chert) and shale fragments (Plate 4.6), than the unmetamorphosed samples, ranging up to 10% of the sample.

PLATE 4.3: Bedded pyrite from Schooner Cove. When undeformed the pyrite has this typical fine grained appearance. The dark layers are organic rich. x 2.5 magnification, refelcted light.

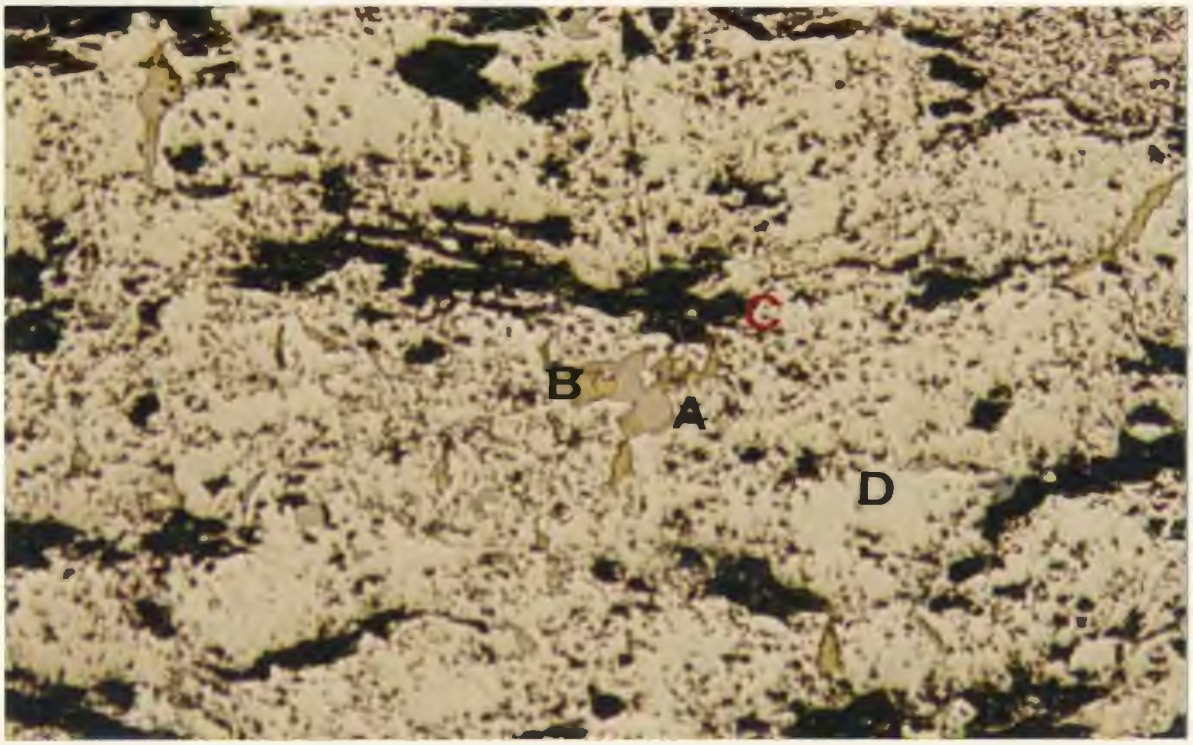

PLATE 4.4: Sphalerite (A) and chalcopyrite (B) present in an organic rich area (C) within the bedded pyrite (D) from Schooner Cove. x 20 magnification, reflected light.

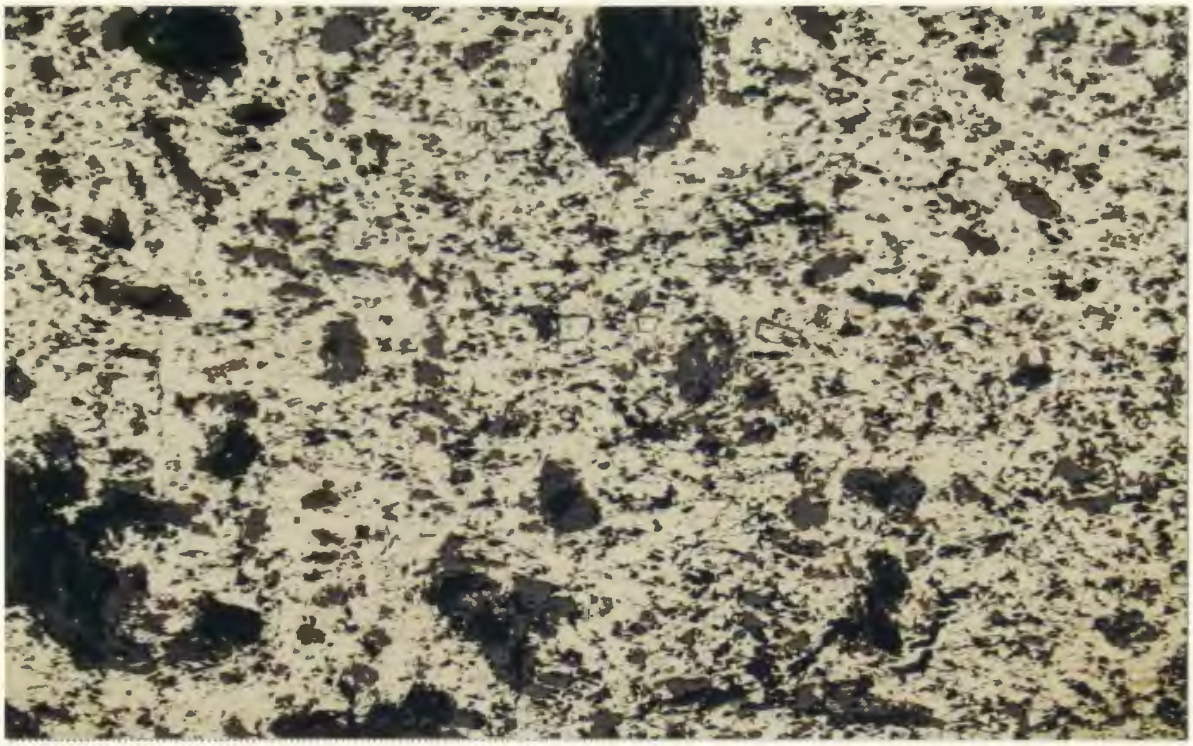

PLATE 4.5: Pyrrhotite (pinkish) with pyrite (cubic, silverly yellow) and quartz (grey) in the thermally metamorphosed pyrite bed at the Near Miss Showing. x 2.5 magnification, reflected light.

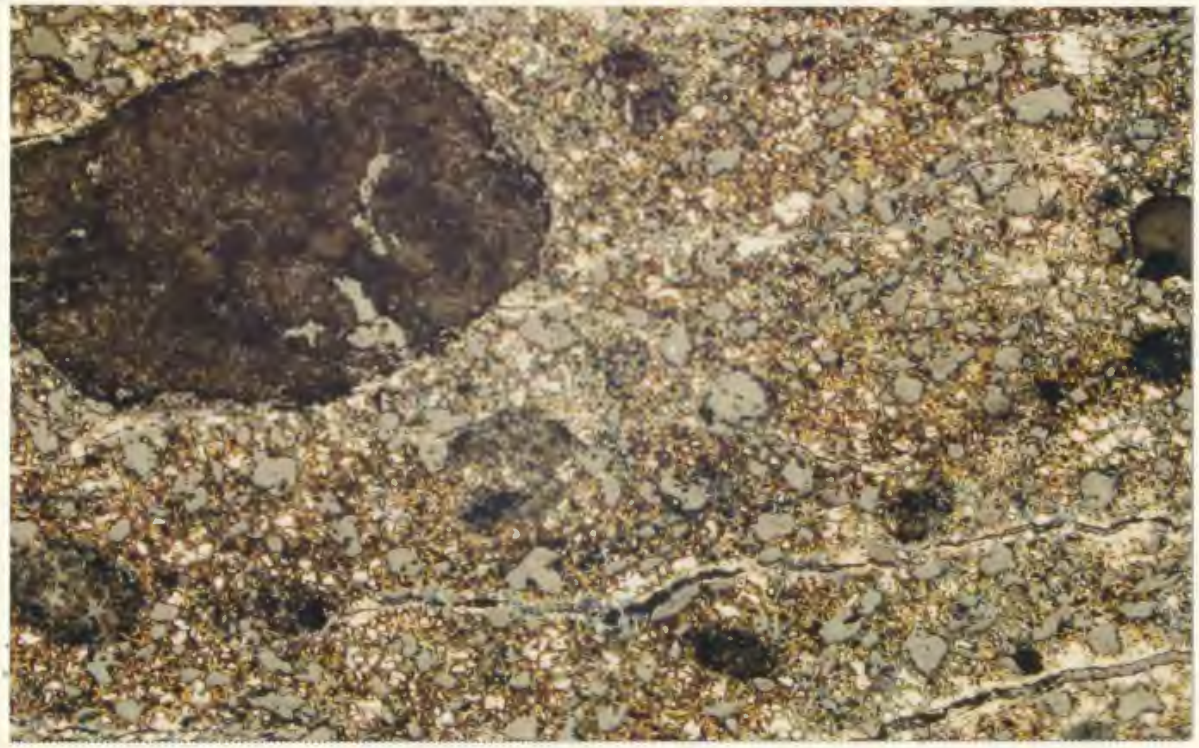

PLATE 4.6: Oxidised pyrite-pyrrhotite bed near the Panda Showing. The large clast in the top left corner is a chert fragment, small grey cubes are pyrite, and the brownish groundmass is oxidised pyrrhotite. x 2.5 magnification, reflected light.

4.5.2 Pyrite trace element composition

Samples from the pyrite bed group into two chemically distinct populations (Table II.2, Appendix II). The two populations were identified as either distal or proximal to diabase - gabbroic sills. South of Ramah Bay, mafic sills are generally more common and have altered the pyrite to pyrrhotite. No sills are proximal to the pyrite bed beyond the north shore of Ramah Bay. Elements analysed were V, Cr, Ni, Cu, Zn, As, Ba, and Pb, and metal concentrations for the altered and unaltered pyrite bed are plotted against their geographical occurrence in Figures 4.7 and 4.8. Trace elements commonly associated with igneous basic intrusions are V, Cr, Ni, Cu, and Zn, while biogenically produced pyrite contains As, Ba, and Pb (Goldschmidt, 1958; Raiswell and Plant, 1980; Pandalai *et al.*, 1983; Huerta-Diaz and Morse, 1992).

From Figure 4.7 it is obvious that the unaltered pyrite bed is not associated with igneous activity, as As concentrations are relatively high, but there is a slight Ni enrichment aiso present. There is no discernible geographical trend to the geochemical data from the sample sites. The high As concentrations in the pyrite are to be expected as As substitutes for Fe in the mineral structure as a result of biogenic activity (Goldschmidt, 1958). The concentrations of the other elements are relatively low.

Samples of the pyrrhotite-pyrite bed proximal to the mafic sills (Figure 4.8) show enrichments in V, Ni, Cu, Zn, Ba, and relative depletions in As. Again no recognisable geographical trend is observed in the trace element concentrations. When comparing both figures it appears that the presence of the mafic sills has resulted in an addition of V, Cr,

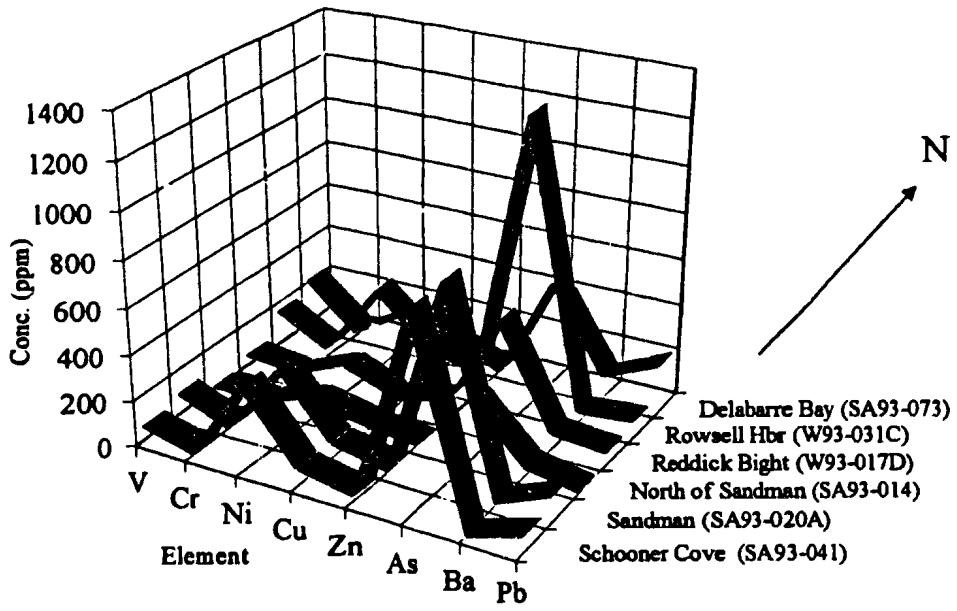

Fig. 4.7: Trace element concentrations of the unaltered Nullataktok Fm. pyrite bed plotted against lattitude. Note the high As, indicative of organically produced pyrite.

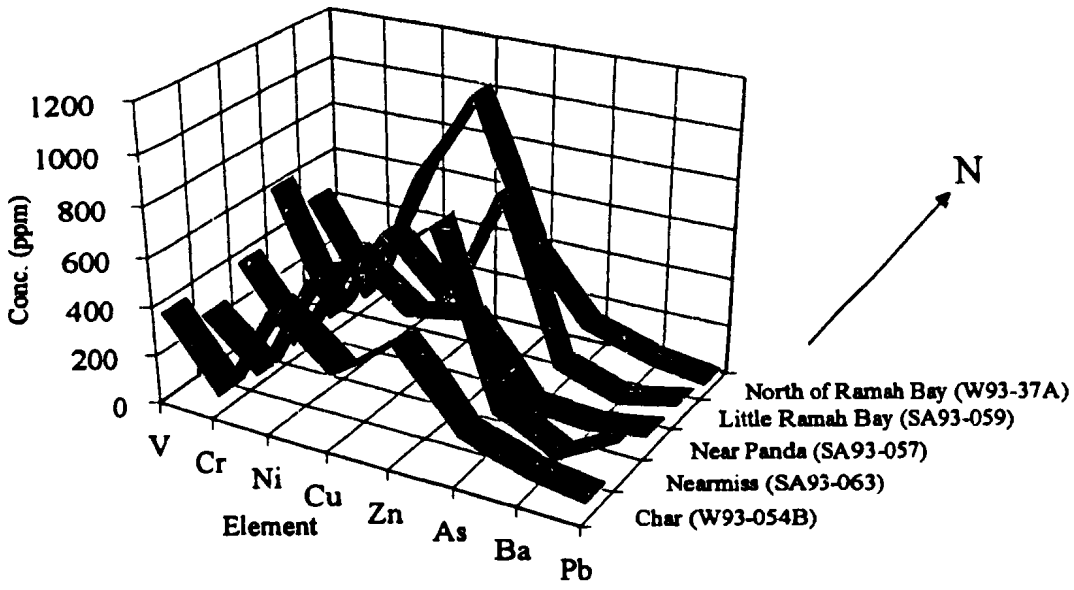

Fig. 4.8: Trace element concentration of the Nullataktok Fm. pyrite bed proximal to diabase/gabbro sills. Note that V, Cr, Ni, Cu, and Zn have been enriched relative to samples from Fig. 4.7, and As has been depleted.

Ni, Cu, and Zn, and a removal of As. Pb and Ba concentrations are variable for both groups, probably resulting from their large, incompatible size in the pyrite structure. Barium enrichment in the pyrite bed near the Char showing seems to not only affect the pyrite bed but is also present within the underlying RBDM; the reason for this anomaly cannot be satisfactory explained at present.

The presence of elevated As concentrations within the unaltered pyrite bed indicates that the pyrite bed probably formed biogenically. Elevated Ni, Cu, and V concentrations within the pyrrhotite-pyrite bed proximal to the sills indicate these elements were derived from the sillsduring metamorphic recrystallization of the pyrite bed.

4.5.3 Cobalt - Nickel ratios

Another means for discriminating between biogenic and volcanogenic pyrite is determination of the Co/Ni ratio of the pyrite (Loftus-Hills and Solomon, 1967; Bralia *et al.* 1979; Bajwah *et al.* 1987). Pyrite with a biogenic origin has a Co/Ni ratio of < 1, whereas pyrite of a volcanic exhalative origin has a Co/Ni ratio > 1. Co and Ni data obtained from the pyrite bed are in Table III.3 (Appendix III) and illustrated in Figure 4.9. The data indicate that the average Co/Ni ratio is 0.5, well within the boundary values for biogenic pyrite. Cobalt - nickel ratios of slightly > 1 in this study are probably due to Co enrichment by the mafic sills during emplacement. In the case of the ratios 1.3 and 3.3, the samples were collected within 5 m of the footwall of a thrust fault on the south shore of Delabarre Bay. The thrust faults may have acted as fluid conduits during deformation,

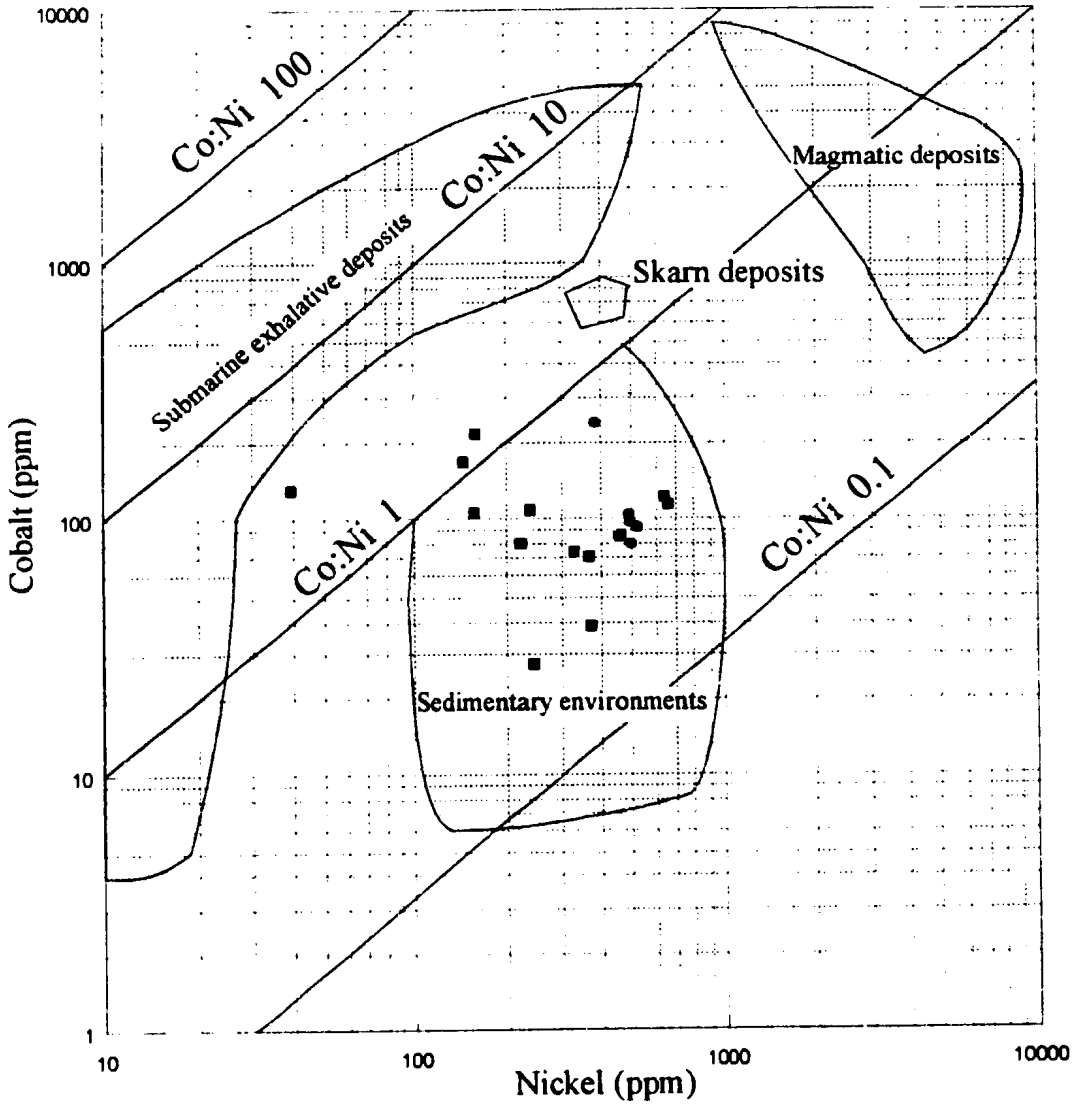

Fig. 4.9: Co:Ni distribution diagram for pyrite from various ore deposits and geological environments (Bajwah *et al.*, 1987). Samples from the Nullataktok Fm. pyrite bed (black squares), and altered pyrite-pyrrhotite bed (black circles) generally occur within the sedimentary environment field with Co:Ni <1.

resulting in addition of Co or removal of Ni. Samples collected where the pyrite bed has been altered by overlying sills (forming pyrrhotite), display little variation from the unaltered samples (Figure 4.8) except for minor nickel enrichment. The Co/Ni ratios suggest that the pyrite bed formed by a biogenic process and has not been influenced by any volcanic activity, except in the vicinity of the later diabasic intrusions.

4.5.4 Sulphur Isotopes

The sulphur isotopic signature of seawater has apparently changed through geological time. Present day seawater sulphate has a $\delta^{34}S$ value of +20‰, whereas Archean seawater sulphate had a value of 0‰ due to the lack of free oxygen (Hayes *et al.*, 1992; Holmden and Muehlenbachs, 1993). Seawater sulphate is believed to have had a sulphur isotopic composition of ~ +12‰ during Paleoproterozoic times (Hayes *et al.*, 1992; and Lambert and Donnelly, 1992). The characteristically negative $\delta^{34}S$ ratios for biogenic material result from the preferential incorporation of ^{32}S in sulphides derived from bacterial reduction of seawater sulphate, especially by such species as *Desulfovibrio desulphuricans*, at the sediment water interface (Ohmoto *et al.*, 1990). Figure 4.10 shows the distribution of sulphur isotopes within the pyrite bed at several localities. The majority of samples plot between -1 and -4‰ indicating a biogenic source. Three pyrrhotite ($Fe_{1-n}S$, n = 0-0.2) rich samples plot between 5 and 7‰ on Figure 4.10 (Table III.1, Appendix III) and were collected close to overlying mafic sills. It appears that intrusion of the sills may have caused removal of ^{32}S relative to ^{34}S, due to increased heat and

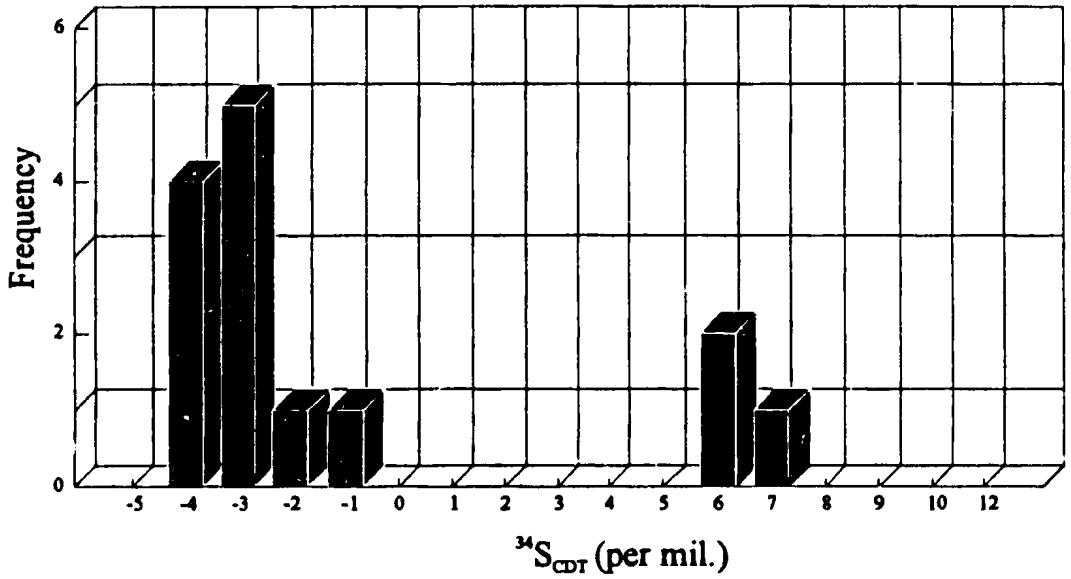

Fig. 4.10: Distribution of sulphur isotopes within the Nullataktok Fm. pyrite bed. The data indicates a biogenic origin (< 0 per mil.) for the unit, with positive values attributed to the metasomatic effects of the late sills.

fluid-rock interaction. The intrusion of the mafic sills resulted in the alteration of a significant proportion of pyrite (FeS_2) to pyrrhotite ($Fe_{1-n}S$, n = 0-0.2), either by sulphur loss or iron gain. It is conceivable that a sulphur loss resulted in the removal of the lighter isotope (^{32}S).

The sulphur isotope ratios suggest that some form of Rayleigh type fractionation was active during the deposition of the pyrite bed (Figure 4.11). Rayleigh fractionation generally occurs in a closed system, such as a restricted marine basin. ^{32}S was preferentially removed due to biogenic activity, continually enriching the remaining water in ^{34}S. A sample taken from the middle portion of the pyrite bed at Rowsell Harbour gave a $\delta^{34}S$ value of -3.2‰, while a sample from the hangingwall of the outcrop gave a value of -0.6‰. Diagenetic pyrite higher in the Nullataktok Formation yielded a value of 10.1‰. If we assume that a Rayleigh type fractionation process (with a sulphate-sulphide fractionation factor of 1.025) was operating in the restricted basin during the deposition of the pyrite bed, the $\delta^{34}S$ composition of contemporaneous seawater sulphate can be calculated from Figure 4.11. During the early deposition of the pyrite bed, sulphide values were approximately -4‰, corresponding to the formation of +18‰ seawater sulphate (example a, Figure 4.11), while the top of the pyrite bed contains sulphides with $\delta^{34}S$ values of -0.6‰ suggesting that seawater had evolved to an isotopic composition of +23‰ (example b, Figure 4.11). Diagenetic pyrite stratigraphically higher in the Nullataktok Fm. had a $\delta^{34}S$ value of 10.1‰, indicating that contemporaneous seawater had reached $\delta^{34}S$ values greater than 30‰ (example c, Figure 4.11). To modify seawater

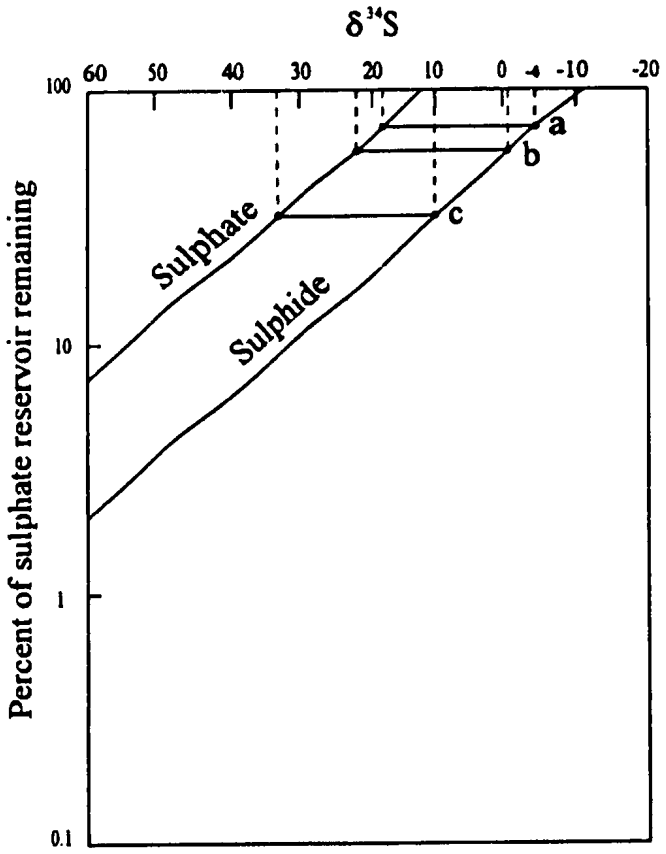

Fig. 4.11: The proposed model for the production of enriched sulphate where Rayleigh-type fractionation occurs in a closed system using a fractionation factor of 1.025 (sulphate-sulphide), and a starting sulphate composition of +12 per mil (after Hoefs, 1987). Labels a, b, and c refer to examples of fractionation discribed in the text. Note logarithmic scale on y-axis

from +12‰ to greater than +30‰ requires at least 60% of the sulphate reservoir in the Ramah Basin to have undergone fractionation. It is conceivable that this ^{34}S-seawater was trapped in the sediments as pore water, and later removed to form epigenetic sulphide mineralization.

4.6 Reddick Bight Dolomite Member

The RBDM is the most economically significant unit within the Ramah Group as it contains appreciable galena, sphalerite and pyrite mineralization. As mentioned previously the sulphides occur where a secondary porosity is exhibited by the dolomite, or where these sulphides have been remobilized into later veins. The sulphide mineralization filling the porous dolomite has been studied using sulphur, carbon, oxygen, and lead isotope geochemistry, fluid inclusions, polished thin section microscopy, and cathodoluminescence.

4.6.1 Preparation (brecciation) of dolomitic host rock

The most abundant mineralization is associated with areas where the host rock has been brecciated. Examples where the brecciation and mineralization are well developed include the Panda - Daniels Point and the Macleod #1 showings. The Panda - Daniels Point showings are particularly well exposed and will be discussed in some detail in this section. The base of the dolomite at these showings shows a characteristic gradation from a coarse grey quartzite into a fine-grained, cream coloured dolomite. Within the first few

metres from the base of this unit, tepee structures (Assereto and Kendall, 1977; Kendall and Warren, 1987) are present which indicate that desiccation of the dolomite occurred. Further dolomite (or carbonate precursor) was deposited with tepee structures again present at the top of the sequence. Dissolution of calcite-rich areas, probably by meteoric water, resulted in the formation of breccias in the host rock. Figure 4.12 indicates that when the tepees were open (during sub-aerial exposure), aeolian-derived dolomitic sand was deposited through the upper fractures and subsequently filled the void, forming the rubble breccia in the central area of the cavity. The aeolian nature of the matrix is indicated by the rounded appearance of the clasts and the absence of geopetal structures which would form through aqueous processes. Brecciation at the sides of this cavity would be classified as mosaic breccias (Leznicka, 1988) that have less space between clasts, and therefore were not subsequently infilled by the coarse dolomitic sand. Following this influx of aeolian-derived sediment, dolomite deposition seems to have resumed (Plate 2.6) due a sea level rise, causing several more tepee structures to form (especially near the top of the sequence), before the transgression represented by the Nullataktok Fm. The mosaic breccia is the most significant lithology for mineralization due to the remnant open porosity .

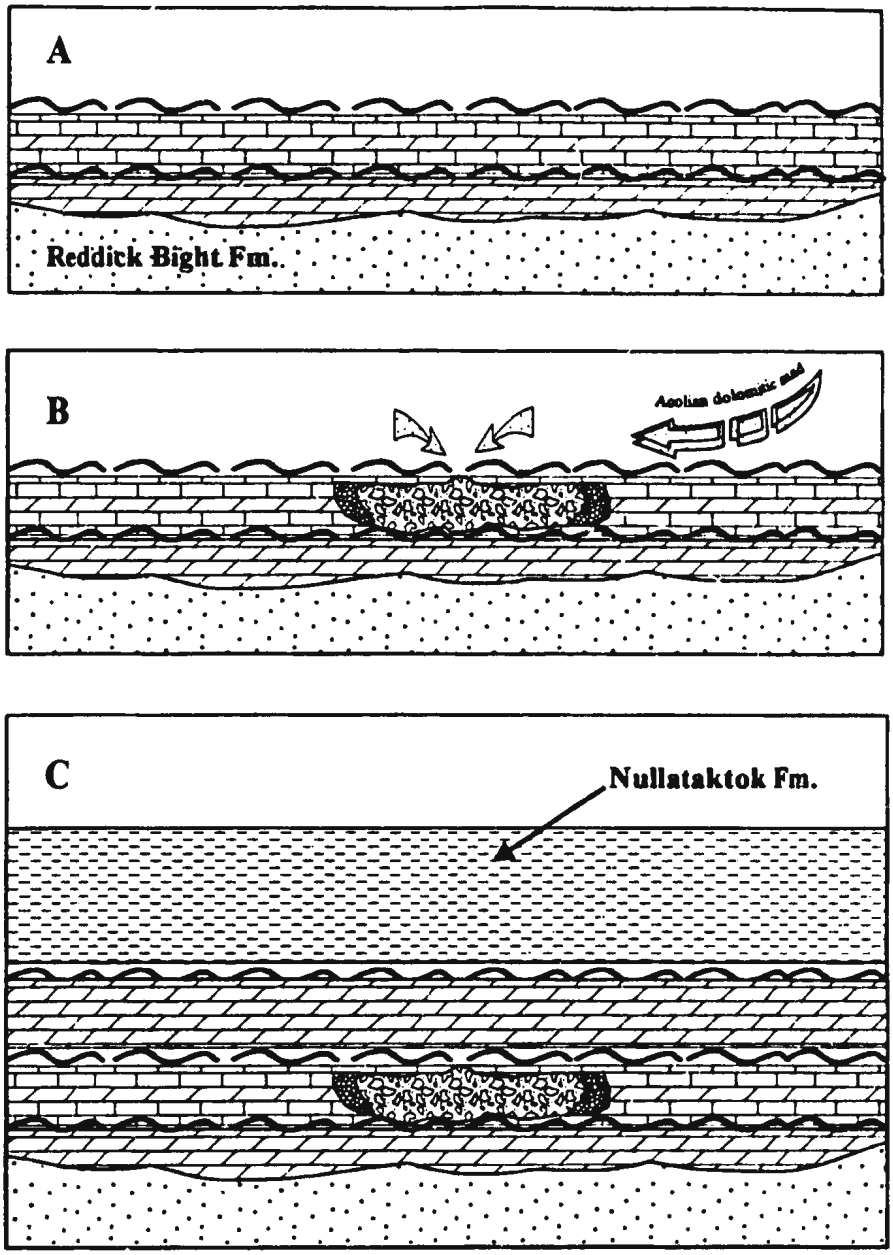

Fig. 4.12: Schematic representation for the formation of the RBDM. (A) Supratidal conditions developed over the siliciclastic shelf, resulting in desiccation of carbonate units and tepee structure formation. (B) Dissolution of calcite/evaporite rich zones, resulting in rubble and mosaic breccias. Voids in-filled by aeolian derived sediment (see PLATE 2.6). (C) Further dolomite deposition and tepee formation, followed by transgression of the Nullataktok Fm..

4.6.2 Ore Petrology

4.6.2.1 Polished thin section microscopy

Mineralized zones from the Panda and Daniels Point showings were used to document the petrography of the RBDM occurrences due to the grade of sulphide concentrations and lack of deformation present at these showings. The mineralogy of the showings and occurrences is relatively simple as the main sulphides are sphalerite, galena, and pyrite. Gangue associated with the mineralization is calcite, dolomite, quartz, and feldspar (microcline, and albite).

The paragenetic sequence and metal ratios (derived from XRF) present within the RBDM showings are illustrated in Figures 4.13 and 4.14. The host dolomite was overgrown by a fine-grained dolomite, a coarse pre-ore dolomite, and finally by a thin euhedral pyrite zone of mineralization (Plate 4.7). Pyrobitumen is common (Plate 4.8). The pyrite generally appears on only one side of the vug or cavity, indicating preferential mineralization at the bottom of the cavity (Plate 4.9 and 4.10), the appearance could be analogous to Oder and Hook's (1950) "snow-on-roof" texture (Leach and Sangster, 1993). Pyrite formation was concurrent with more pre-ore dolomite formation before the main stage sphalerite and galena mineralization commenced. Both sphalerite and galena appear to be contemporaneous, and sometimes contain euhedral pyrite grains within them. The sphalerite is generally dark brown to reddish brown in appearance (Plate 4.9) indicating a high iron content, subsequently proven by SEM analysis (Table III.4, Appendix III). No evidence of chalcopyrite disease is evident in the sphalerites, indicating

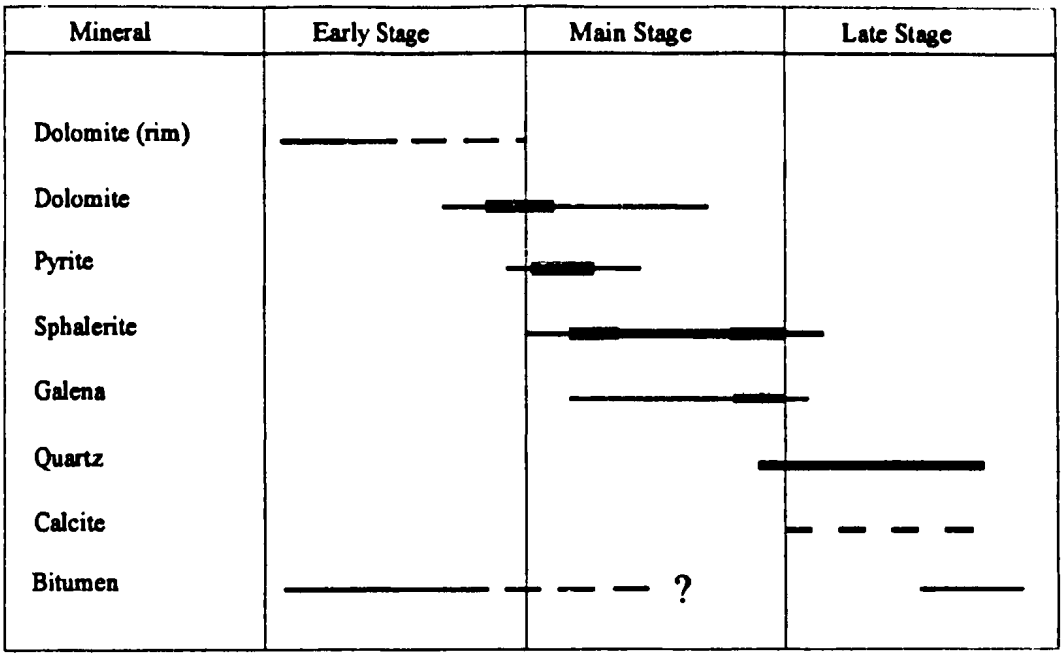

Fig. 4.13: Paragenetic sequence present within the RBDM at mineralized outcrops. Thickness of lines schematically represents the degree of mineralization.

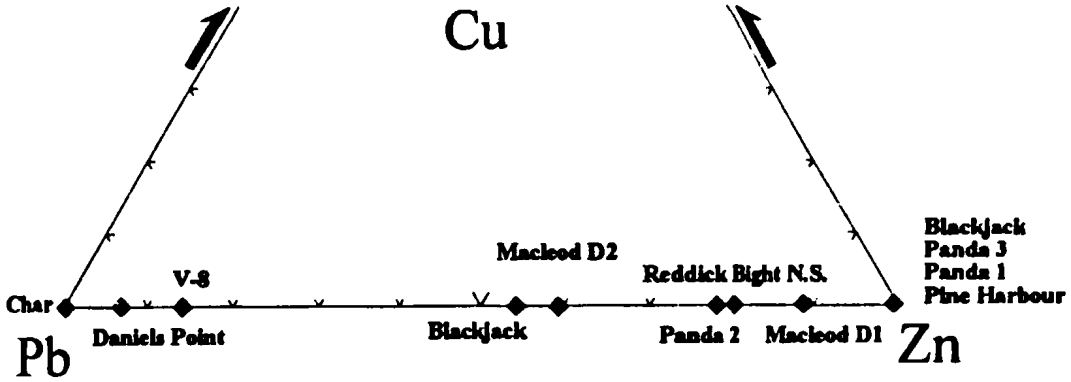

Fig. 4.14: Metal concentrations of showings within the RBDM. The majority of the showings are zinc-rich, and none are elevated in copper.

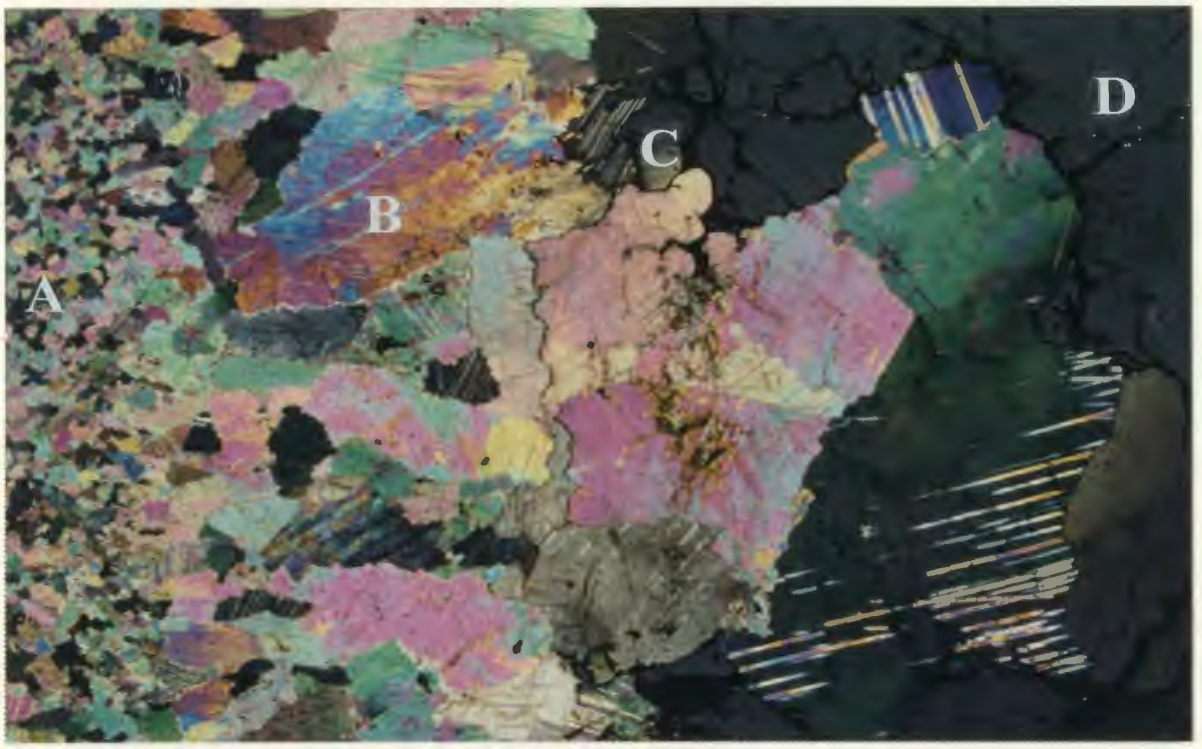

PLATE 4.7: Paragenetic sequence at the Panda Showing, earliest on the left and latest on the right. Host dolomite (A), pre-ore dolomite (B), pyrite (C), and sphalerite (D). x2.5 magnification, transmitted and reflected light with polarizer in.

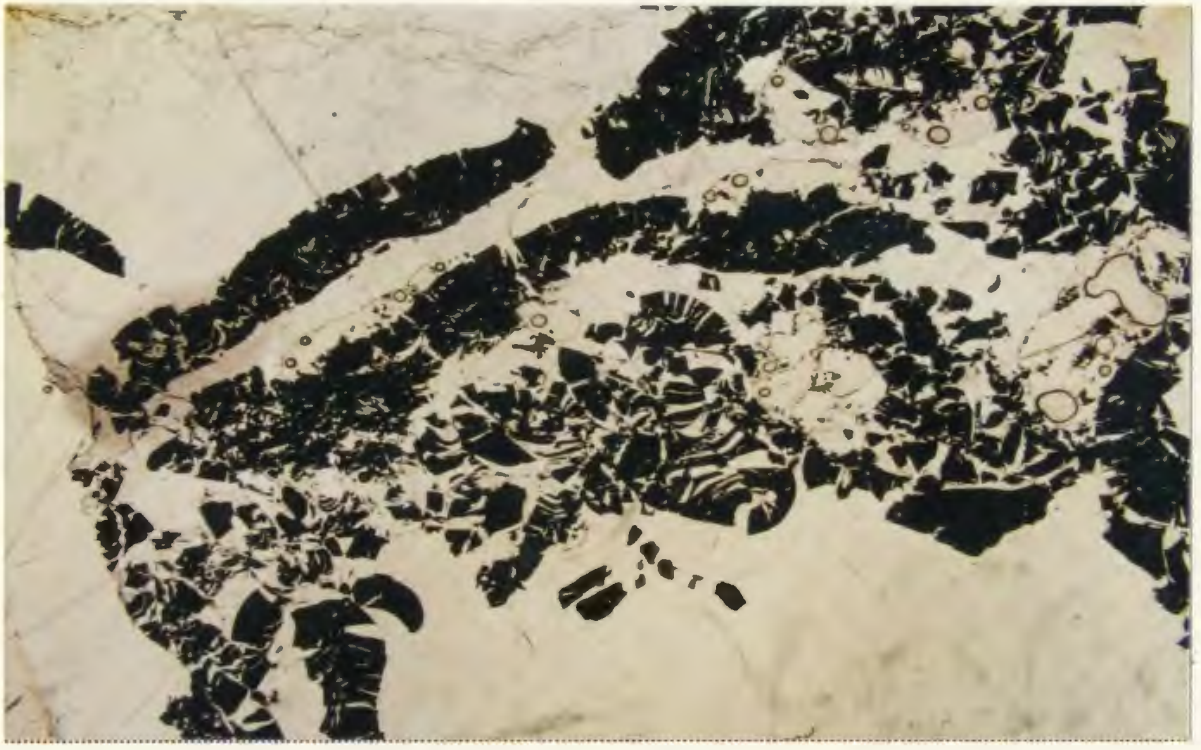

PLATE 4.8: Pyrobitumen from the RBDM at the Reddick Bight North Shore Occurrence (SA93-044). x 1.5 magnification, transmitted light.

PLATE 4.9: Paragenetic sequence and "snow on roof" texture from Panada Showing. Host dolomite (A), pre-ore dolomite (B), pyrite (C), and sphalerite (D). x 1.5 magnification, transmitted light.

PLATE 4.10: Same field of view as PLATE 4.9 with polarizer in. Note the presence of pyrite on one side of the cavity which can be used to indicate way-up during mineralization.

deposition from Cu-poor, low temperature (< 200°C) solutions (Barton and Bethke, 1987). Colloformal sphalerite has not been seen in thin section, but the Reddick Bight North Shore occurrence displays what appears to be colloformal sphalerite in outcrop.

Post-dating the main mineralization period was deposition of the gangue minerals quartz (with undulose extinction) and feldspars (Plates 4.11 and 4.12). Two types of feldspar have been identified, albite by X-ray diffraction techniques and microscopy, and microcline by microscopy. The quartz and feldspars were then overgrown by the latest mineral phase, calcite, which occurs in late vugs and cavities in outcrop.

4.6.2.2 Cathodoluminescence

Cathodoluminescence analyses of RBDM carbonates and gangue minerals were carried out on several of the Zn-Pb showings, especially the Panda, Daniels Point, and Saor Alba. Cathodoluminescence is a very useful tool for determining the zonation and growth histories of cements, particularly in carbonates (Marshall, 1988). Cathodoluminescence in dolomite is usually considered to be controlled by the concentration of Mn^{2+}, although $Pb^{2+}$and rare earth elements (especially Ce^{2+}) can also act as activators, whereas Fe^{2+}, and to a lesser extent Ni^{2+}, Co^{2+}, and Fe^{3+}, act as a quencher (Mendlin, 1961, 1968; Machel, 1985). Plates 4.13 and 4.14 show a traverse across the host, early, and pre-ore dolomites, and sphalerite. The host dolomite luminesces, indicating a high Mn^{2+} (or Pb^{2+}, and REE) content, but the early dolomite has the highest fluorescence in the section, indicating an even more elevated Mn^{2+} content. The pre-ore

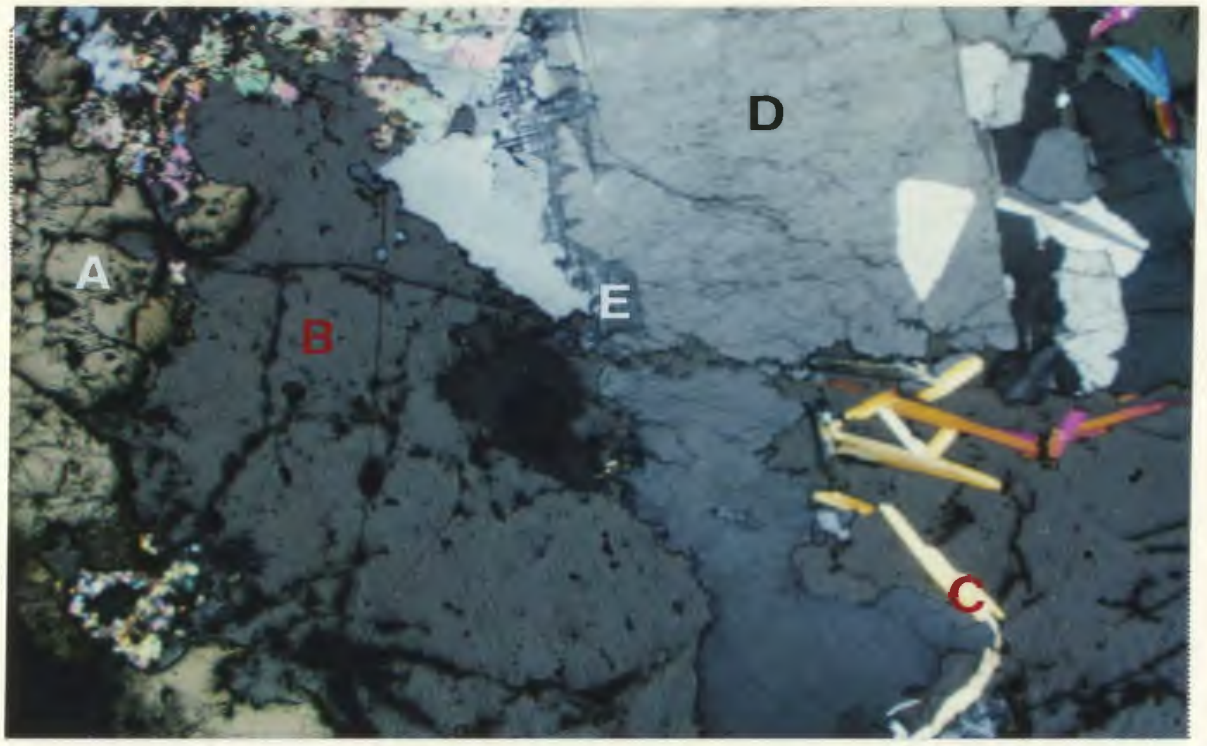

PLATE 4.11: Late stage mineralization from the Panda Showing containing pyrite (A), sphalerite (B), muscovite (C), quartz (D) and perthite (E). x 2.5 magnification, transmitted and reflected light with polarizer in.

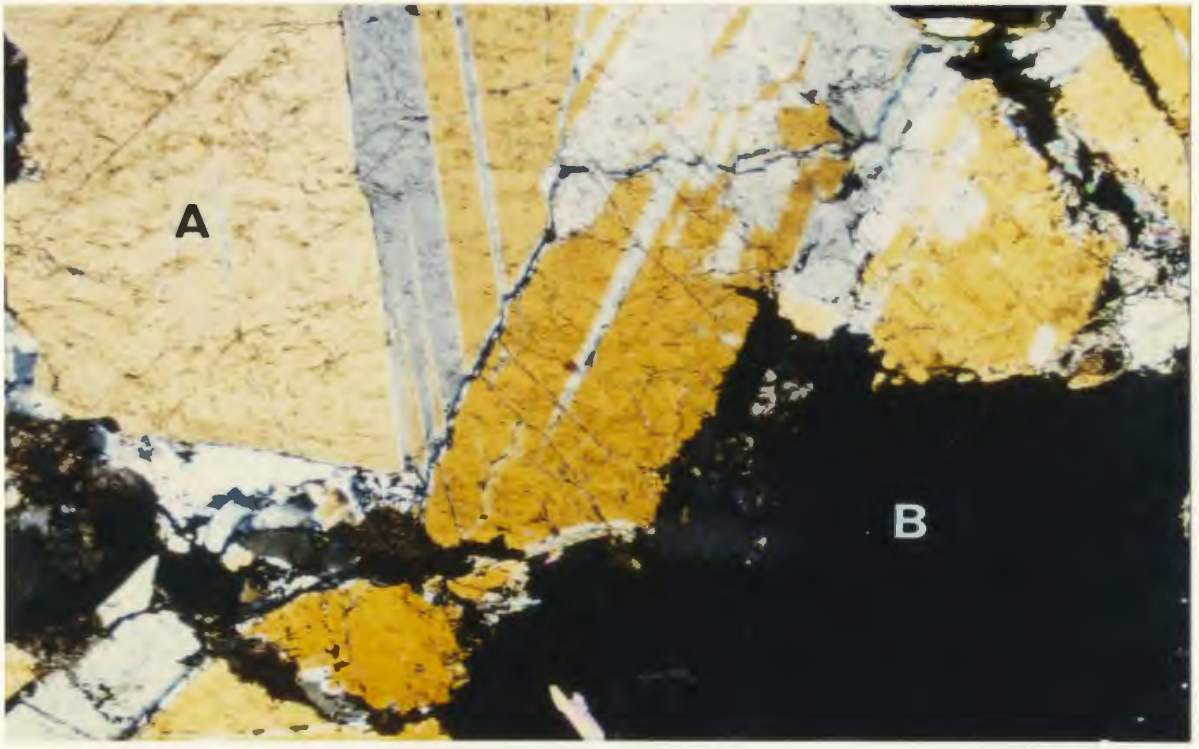

PLATE 4.12: Albite feldspar (A) overgrowing sphalerite (B) mineralization at the Panda Showing. x 2.5 maginification, reflected light with polarizer in.

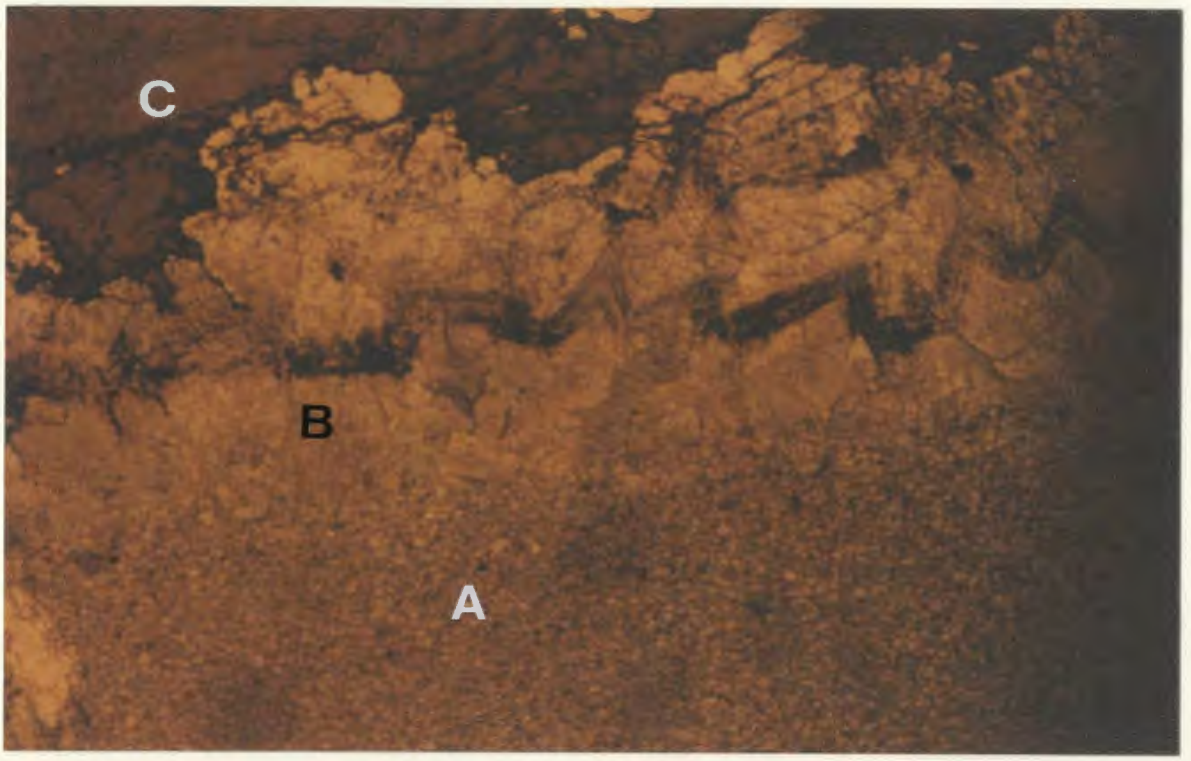

PLATE 4.13: Early paragenetic sequence of the RBDM at the Panda Showing. The paragenetic sequence is: host dolomite (A), pre-ore dolomite (B), and sphalerite (C). x 6.3 magnification, transmitted light.

PLATE 4.14: Same field of view as PLATE 4.13 in cathodoluminescence light. The bright areas are due to enrichment in Mn^{2+} within the carbonate, while the dark areas are probably due to ferrodolomite (Fe^{2+}-rich) acting as an inhibitor. The zoning represents changes in fluid chemistry.

dolomite generally has a low fluorescence, indicating that the dolomite is probably ferrodolomite, as the presence of the Fe^{2+} would quench or suppress the Mn^{2+} fluorescence. Changing fluid chemistry is indicated by a thin, highly fluorescent crystal face, which passes into ferrodolomite. In this study it was only possible to look at the relative abundances of Fe^{2+} and Mn^{2+}, as visual cathodoluminescence alone cannot quantify the abundances of Mn^{2+} and Fe^{2+} (or the other activators and inhibitors) in the dolomite (Marshall, 1988). The fluid composition must have changed throughout the deposition of the carbonate gangue and ultimately the sulphides.

4.6.3 Fluid Inclusions

Fluid inclusion analyses were carried out on pre-ore dolomite from the Saor Alba showing, and sphalerite and quartz from the Panda showing. Results are presented in Tables III.5, III.6, and III.7 (Appendix III). Homogenization temperatures and salinity data are illustrated in Figures 4.15a and 14.5b.

Twelve fluid inclusions present in the sphalerite from the Panda Showing were studied to determine homogenization temperatures and salinities. Inclusions were scarce but, two two phased ($H_2O_{(l)}$-$CO_{2(g)}$), primary inclusions were identified by their equant crystal shape, solitary occurrence, and absence of necking. The average size of the inclusions was 4 μm, making salinity measurements impractical. Homogenization temperatures (T_H) for these inclusions were 126 8 and 170.0°C. Pseudosecondary inclusions were more common than primary ones and were easier to identify due to their

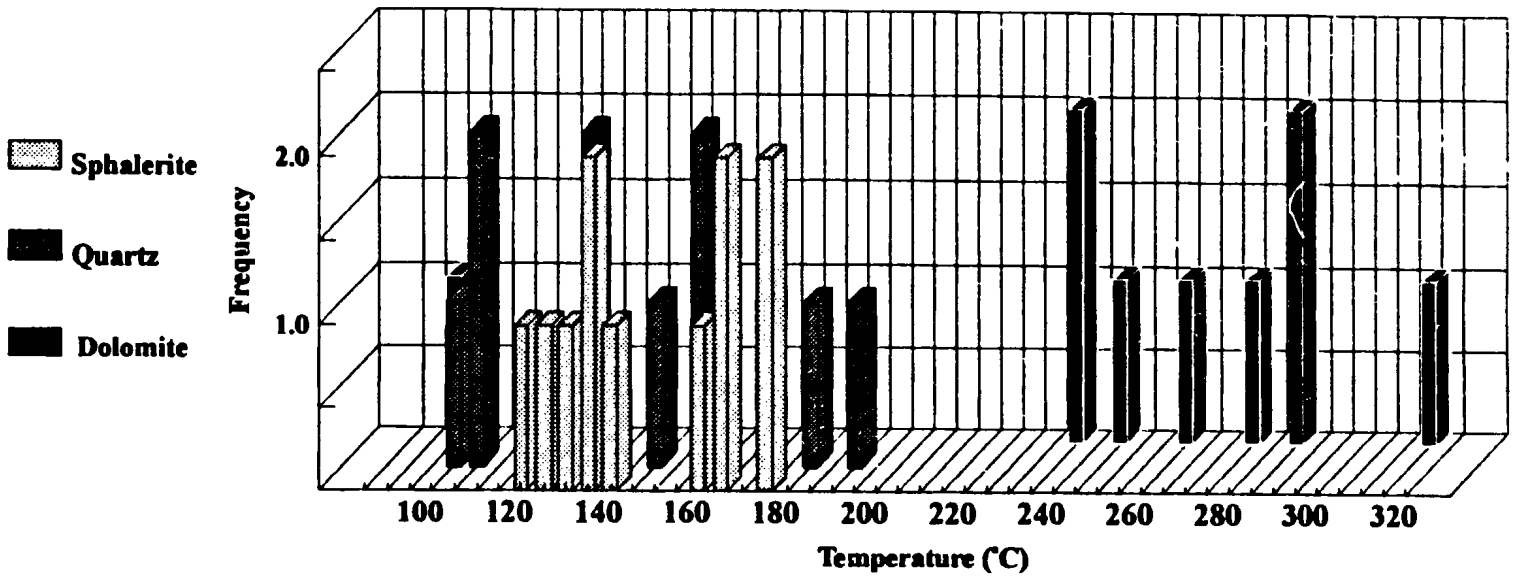

Fig. 4.15a: Homogenization temperatures for primary, pseudosecondary, and secondary fluid inclusions in sphalerite, quartz and dolomite. The high homogenization temperatures for the dolomite appear to be the result of greenschist facies overprinting.

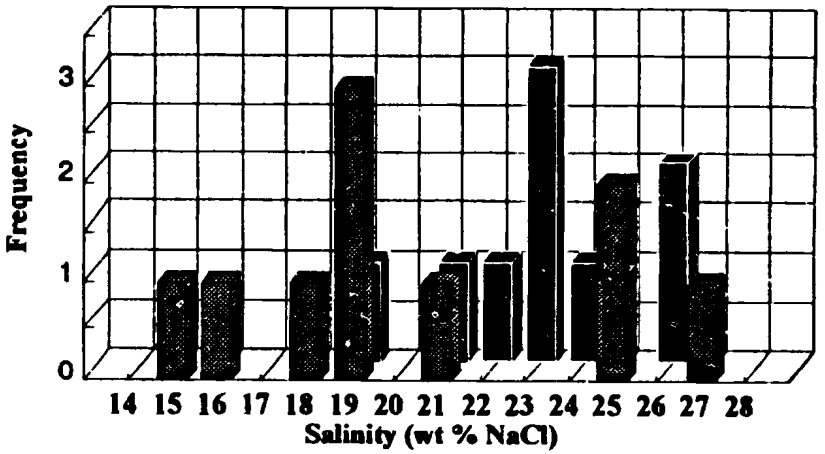

Fig. 4.15b: Salinity data for main-stage dolomite and quartz inclusions from primary and pseudosecondary fluid inclusions. Salinities for sphalerite were impractical due to the 2 to 4 μm size of the inclusions.

occurrence along distinct planes which terminated at crystal boundaries. The inclusions were two phased ($H_2O_{(l)}$-$CO_{2(g)}$), 4-11 μm by 2-3 μm, elongate, with constant liquid-vapour ratios. Homogenization temperatures ranged from 122.8 to 177°C. Salinity measurements were not performed due to the small size of the inclusions.

Ten inclusions were studied from the quartz gangue at the Panda Showing. Nine of the inclusions were primary, and one was secondary. The primary inclusions ranged from 6-12 μm, were two phased ($H_2O_{(l)}$-$CO_{2(g)}$), and were identified by their solitary nature, equant shapes, and constant liquid-vapour ratios. Homogenization temperatures ranged from 101.9 to 156.9°C and salinities of 15.9 to 26.9 equiv. wt. % NaCl. One inclusion gave a homogenization temperature of 183.8°C which was non-reproducible, suggesting the inclusion might have leaked. No daughter minerals were observed. One secondary inclusion gave a homogenization temperature of 190.7°C and a salinity of 14.3 equiv. wt. % NaCl. The inclusion was elongate (12μm long by 3μm wide) and was the largest inclusion in a trial which cut a crystal boundary.

Ten two phased ($H_2O_{(l)}$-$CO_{2(g)}$), fluid inclusions were studied from the main stage dolomite at the Saor Alba occurrence. Nine of the inclusions were secondary in nature with only one being primary. The secondary inclusions studied ranged in size from 6 to 14 μm (average of 8μm) , occurred as trials which cut crystal boundaries, and did not have constant liquid-vapour ratios. Homogenization temperatures ranged from 239.6 to 317.7°C, and salinities from 18.6 to 25.7 equiv. wt. % NaCl. No daughter minerals were observed. One large (10μm) primary inclusion was observed with a homogenization

temperature of 98.9°C, which decrepitated while the secondary inclusions were being heated.

Temperatures for the sphalerite and quartz inclusions are consistent with mineralization temperatures of 75° - 200°C reported for Mississippi Valley-type (MVT) deposits (Roedder, 1984; Leach and Sangster, 1993; Sangster *et al.*, 1994). The elevated temperatures for inclusions in the dolomite seem to indicate that they may have been reset (perhaps by necking) due to the sub-greenschist to greenschist facies metamorphism which affected the area. Several inclusions within the dolomite decrepitated before a homogenization temperature could be obtained, indicating that inclusion leakage may have occurred, resulting in elevated homogenization temperatures (cf. Roedder, 1976).

Salinity ranges from 15 - 27 weight percent sodium chloride equivalent (wt % equiv. NaCl) for quartz, to 19 - 26 wt % equiv. NaCl for dolomite (Figure 4.15b). The salinities of inclusions in dolomite would not be affected by leakage and they do not appear to have been adversely affected by metamorphic overprinting. The high salinities and lack of NaCl daughter minerals in the inclusions point to the fact that they must contain more than just NaCl (Roedder, 1976; 1984). Roedder (1962) showed that the lowest possible freezing point for a pure NaCl solution is -21.1°C (23.4 wt % NaCl), yet the minimum freezing temperatures within the quartz inclusions are -25.6°C. These low values can be explained by the presence of Mg and Ca salts in the ore forming solutions, although NaCl would still be the main solute (Roedder, 1962; 1976). Salinities of MVT

fluids are typically 10 - 30 wt % equiv. NaCl (Roedder, 1976, 1984; Leach and Sangster, 1993; Sangster *et al.*, 1994).

The fluid inclusion wafers were viewed under a fluorescence microscope to ascertain if any hydrocarbons were present within the inclusions, as several workers have noted the presence of such inclusions in carbonate hosted Pb-Zn mineral deposits (Price, 1976; Roedder, 1984; Gize and Hoering, 1980). No hydrocarbon inclusions were found in the sphalerite, possibly due to their small size, but some fractures that were subsequently annealed by later sphalerite mineralization show fluorescence. This fluorescence suggests that hydrocarbons were present during mineralization, but whether they were present in the actual ore fluid is difficult to say without further work.

4.6.4 Carbon Isotopes

Carbon isotopic analysis was used to characterise the black graphitic substance commonly found throughout the RBDM. Field observations indicated that the black to dark grey mineral had a hardness less than 2 (relative to Moh's scale), and X-ray diffraction analyses of 14 samples indicated that this material was graphite.

It is possible to define a possible carbon source by measuring the $^{13}C/^{12}C$ ratio (Hoefs, 1987). Carbon isotope data are expressed in the del, or delta, notation (similar to sulphur isotopes). Delta (δ) is defined as:

$$\delta^{13}C = \frac{\left(^{13}C/^{12}C\right)_{sample} - \left(^{13}C/^{12}C\right)_{standard}}{\left(^{13}C/^{12}C\right)_{standard}} \times 1000$$

Where the standard is the Peedee Belemnite (PDB), a cephalopod from the Cretaceous Peedee Formation in South Carolina, with a ^{13}C / ^{12}C ratio of 449.94 x 10^{-5} (Craig, 1957). Values for the $^{13}C/^{12}C$ ratio are expressed as parts per thousand, or per mil (‰). Typical $\delta^{13}C$ values in nature vary between +5 to -38‰, as illustrated in Figure 4.16. The large fractionation is caused by plants and animals preferentially incorporating the lighter ^{12}C isotope relative to ^{13}C.

Carbon isotopic analyses performed on 15 samples of the black, graphitic material defined $\delta^{13}C$ ratios between -14.6 to -31.6‰ (Table III.8, Appendix III), with an average of -28‰. These values are similar to sedimentary organic material or petroleum (Figure 4.17). Due to these very low $\delta^{13}C$ values, combined with their presence in vugs and fractures within the dolomite it seems reasonable to assume that this graphitic substance is actually a pyrobitumen product, i.e. a hydrocarbon which has undergone volatile loss. The pyrobitumen is very common at mineralized outcrops, leading to the conclusion that the hydrocarbons probably played a role in sulphide precipitation or transport. $\delta^{13}C$ for the pyrobitumen from the RBDM is consistent with observations from other Proterozoic rocks in Canada (Strauss, 1986), South Africa, Gabon, Australia, and USA (McKirdy and Imbus, 1988) which have values between -21 and -41.2‰.

Carbon-hydrogen-nitrogen analysis (Table III.9, Appendix III) performed on the pyrobitumen gave results which ranges from 51.95 - 75.85 wt. % carbon, 0.3 - 0.5 wt. % hydrogen, and 0.74 - 0.89 wt. % nitrogen. No oxygen data is available since the samples were combusted in the presence of oxygen. Hydrogen-carbon (H/C) ratios of 0.08 and

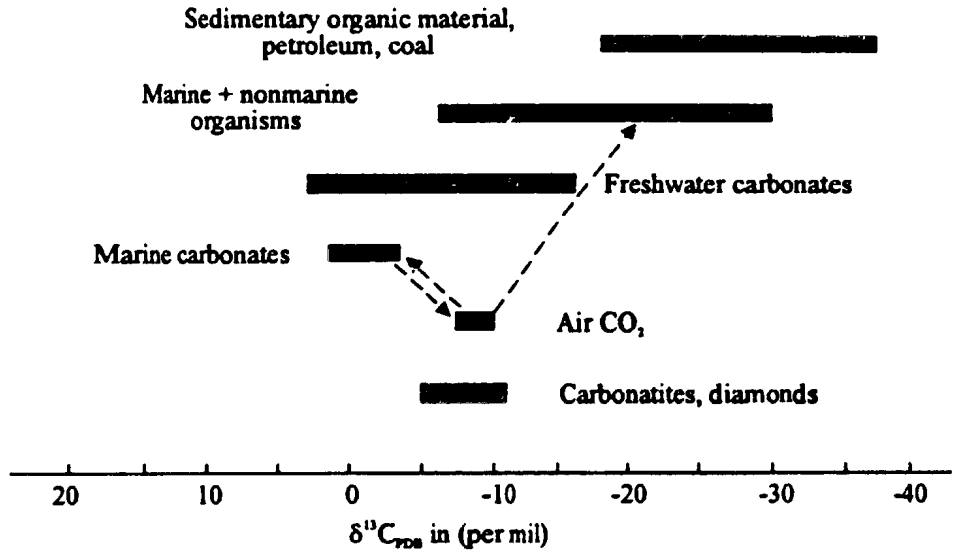

Fig. 4.16: The ranges of $\delta^{13}C$ values in natural, carbon-bearing samples. Data from Hoefs (1987).

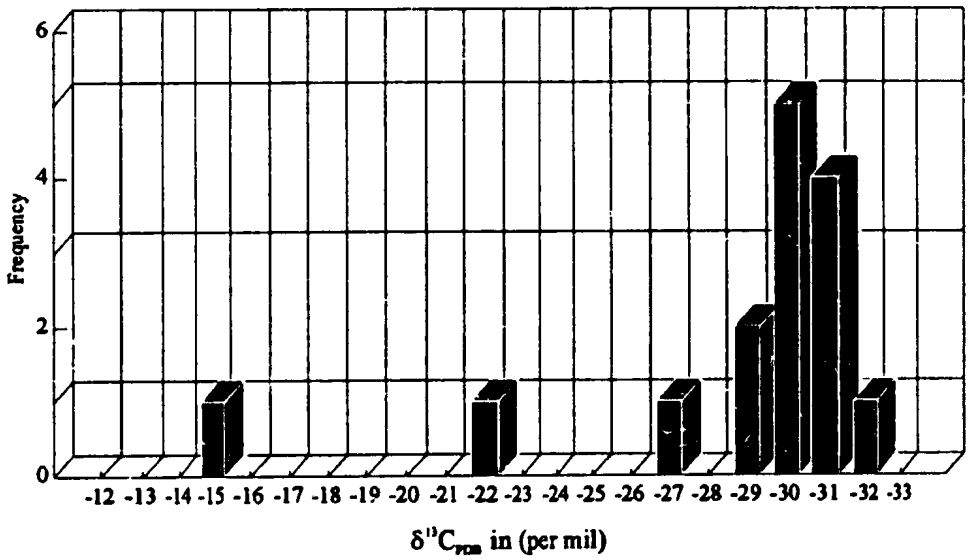

Fig. 4.17: Histogram for $\delta^{13}C$ values of carbonaceous material present within vugs in the RBDM.

0.05 were calculated for the pyrobitumen samples. These ratios differ dramatically when compared to an average crude oil (H/C = 1.8), Tissot and Welte (1978), or solid bitumens associated with MVT mineralization in Missouri (H/C = 1.4), Marikos *et al.* (1986). The low C/H ratios suggest that the samples have lost appreciable amounts of volatiles, resulting in graphitization of the hydrocarbons. Due to the volatile loss it was not possible to accurately calculate an empirical formula for the pyrobitumen (Table III.9, Appendix III).

4.6.5 Carbon and Oxygen Isotopes from Carbonates

Carbon and oxygen isotopes have been used successfully in determining the role and evolution of fluids in mineralizating processes since Engel *et al.* (1958). Oxygen isotope data are expressed in a similar manner to carbon isotopes, where δ is expressed as:

$$\delta^{18}O = \frac{\left(^{18}O/^{16}O\right)_{sample} - \left(^{18}O/^{16}O\right)_{standard}}{\left(^{18}O/^{16}O\right)_{standard}} \times 1000$$

The standard is Vienna Standard Mean Ocean Water (V-SMOW), a synthetic standard which is thought to best represent typical ocean water (Hoefs, 1987), with a $^{18}O/^{16}O$ ratio of 2005.2×10^{-6} (Baertschi, 1976). Values for the $^{18}O/^{16}O$ ratio are expressed as parts per thousand, or per mil (‰). Typical $\delta^{18}O$ values in nature vary between + 35 and - 40‰, illustrated in Figure 4.18.

Twenty-five samples of carbonate were analysed (Table III.10, Appendix III) from 5 groups: Warspite Fm. dolomite; RBDM dolomite host rock from mineralized areas; paragenetically early, fine-grained orange dolomite; main stage (pre-ore) dolomite; and post-ore calcite. These 5 groups are plotted on Figure 4.19. Overall $\delta^{18}O$ values range from 8.5 to 20.8‰, and $\delta^{13}C$ from -13.9 to 0.4‰. (Table III.10, Appendix III) The host dolomite (RBDM) exhibits a typical marine carbon signature with $\delta^{13}C$ values from -3.07 to -0.31‰, and $\delta^{18}O$ values from 17.02 to 20.8‰. The single sample of the Warspite Fm yields $\delta^{13}C$ and $\delta^{18}O$ values of 0.4‰ and 18.5‰ respectively. Early dolomite has the largest variation in both $\delta^{13}C$ and $\delta^{18}O$, with $\delta^{13}C$ values between -13.9 and -3.8‰, and $\delta^{18}O$ values between 8.5 and 18.6‰. Main stage (pre-ore) dolomite is generally tightly constrained, except for two points, with variations in $\delta^{13}C$ values between -7.8 and -2.9‰, and $\delta^{18}O$ between 8.5 and 19.7‰. Finally, post-ore calcite has $\delta^{13}C$ values between -6.6 and -3.4‰, and $\delta^{18}O$ values between 14.8 and 17.5‰.

The $\delta^{18}O$ and $\delta^{13}C$ values of carbonate appear to define a mixing line between the host dolomites (wall rock) and a source with low $\delta^{13}C$ and $\delta^{18}O$ values relative to the host dolomites (Figure 4.19). The postulated mixing line follows the same trend as the paragenetic sequence (early, and pre-ore dolomite, proceeded by post-ore calcite). A possible interpretation for the mixing line is the reaction of the mineralizing fluid with isotopically light $\delta^{13}C$ hydrocarbons (pyrobitumen), either *in situ* or transported, followed

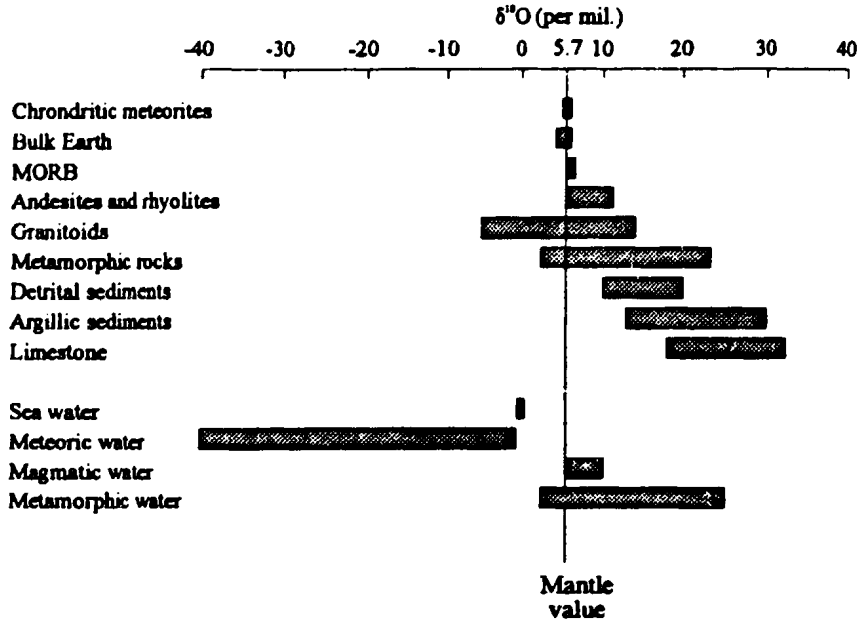

Fig. 4.18: Natural oxygen isotope reservoirs and their $\delta^{18}O$ values. Data from Hoefs (1987), and redrawn from Rollinson (1993).

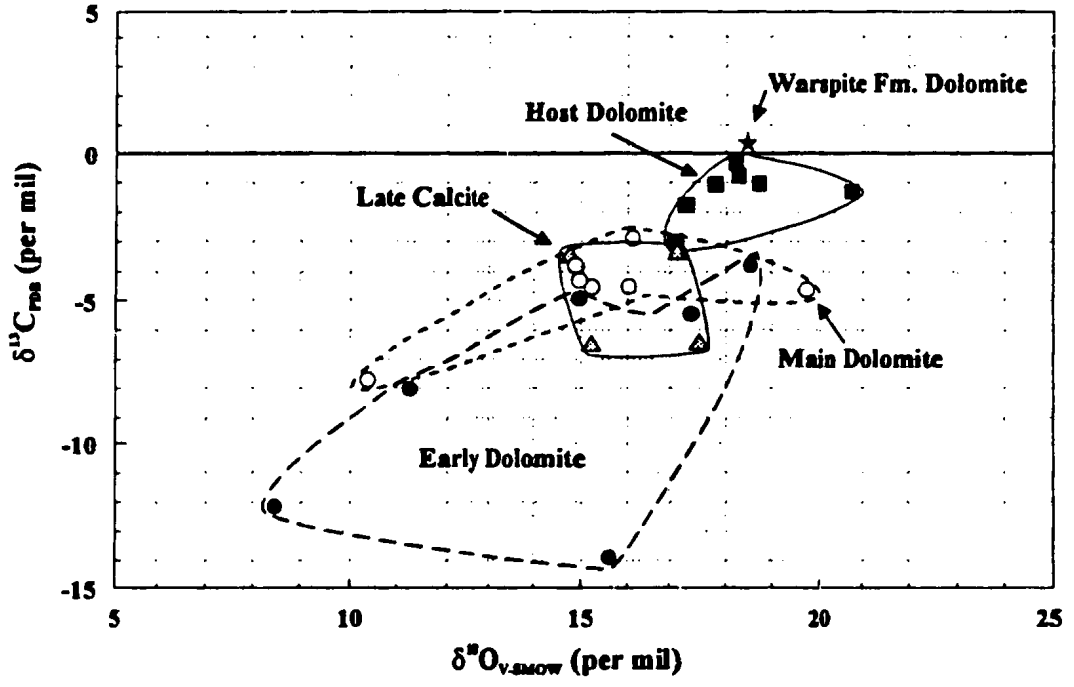

Fig. 4.19: $\delta^{18}O$ vs $\delta^{13}C$ plot for carbonates present in the RBDM. The paragenetic sequence is: host dolomite (RBDM), early dolomite, main (pre-ore) dolomite, and late calcite. The Warspite Fm. dolomite has been plotted for a comparison with the host RBDM.

by the progressive reaction and isotopic re-equilibrium of the fluid with carbonate wall rock.

The oxygen isotopic composition of the hydrothermal fluid(s) was calculated at a variety of temperatures (from fluid inclusions) using fractionation factors of O'Neil *et al.* (1969) for calcite, and Mathews and Katz (1977) for dolomite. The data are shown in Table III.10 (Appendix III) and illustrated in Figure 4.20. The data indicates that the oxygen isotopic composition of the fluids evolved from a $\delta^{18}O$ value of -9.1 to 0.9‰ (average, -3.2‰) for the early dolomite at 110°C, to -4.3 - 5.0‰ (average, 0.6‰) for the main stage dolomite at 140°C, and finally 1.9 - 4.6‰ (average, 3.2‰) for the late calcite at 140°C. The $\delta^{18}O$ values suggest that the oxygen isotopic composition of the fluid changed from an early meteoric water to a basinal brine, probably due to water-rock interaction (Taylor, 1974). The presence of meteoric water is consistant with the karstification of the host dolomite, and the evolution to a basinal brine is consistant with the fluid inclusions having a salinity of 17-27 eq. wt % NaCl

4.6.6 Sulphur Isotopes

Twenty-three sulphide samples were analysed from the showings present within the RBDM, and their $\delta^{34}S$ values are shown in Table III.1 (Appendix III), and illustrated in Figure 4.21. All values are quoted relative to CDT and are accurate to ± 0.2‰ Pyrite mineralization has $\delta^{34}S$ values from 8.3 - 31.8‰ (average, 20.5‰), galena from 10.6 - 32.9‰ (average, 17.5‰), and sphalerite from 6.3 - 33.8‰ (average, 19.7‰).

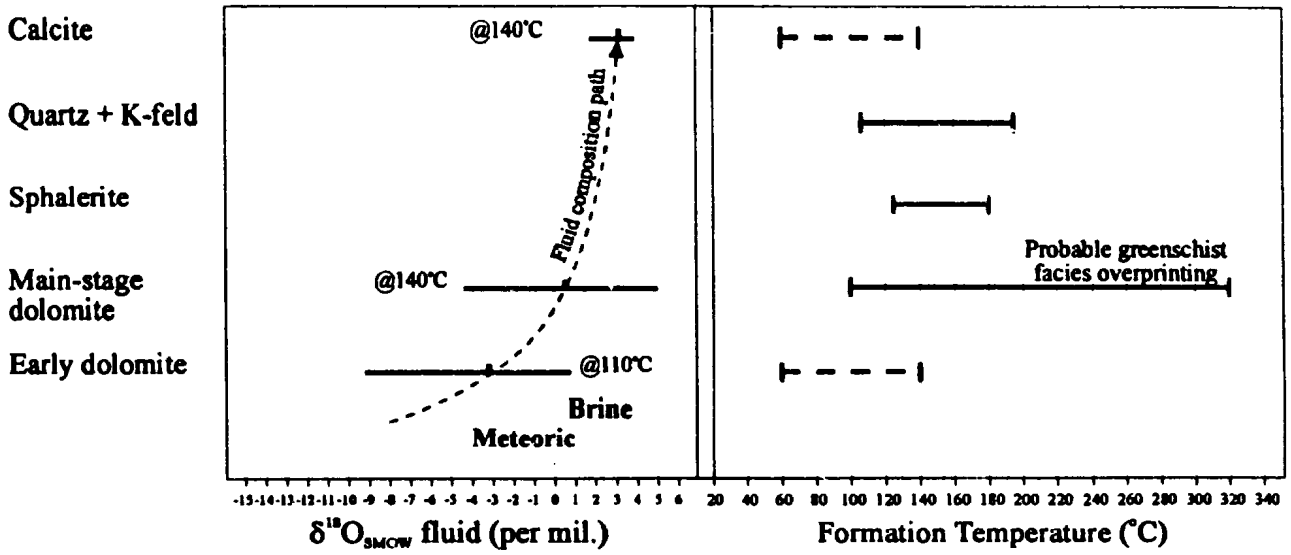

Fig. 4.20: Fluid composition path for mineralization within the RBDM. Temperatures derived from fluid inclusions and the average $\delta^{18}O$ values (bars on diagram) from oxygen isotope studies. Fluid compositions calculated from fractionation factors of O'Neil *et al.* (1969) and Mathews and Katz

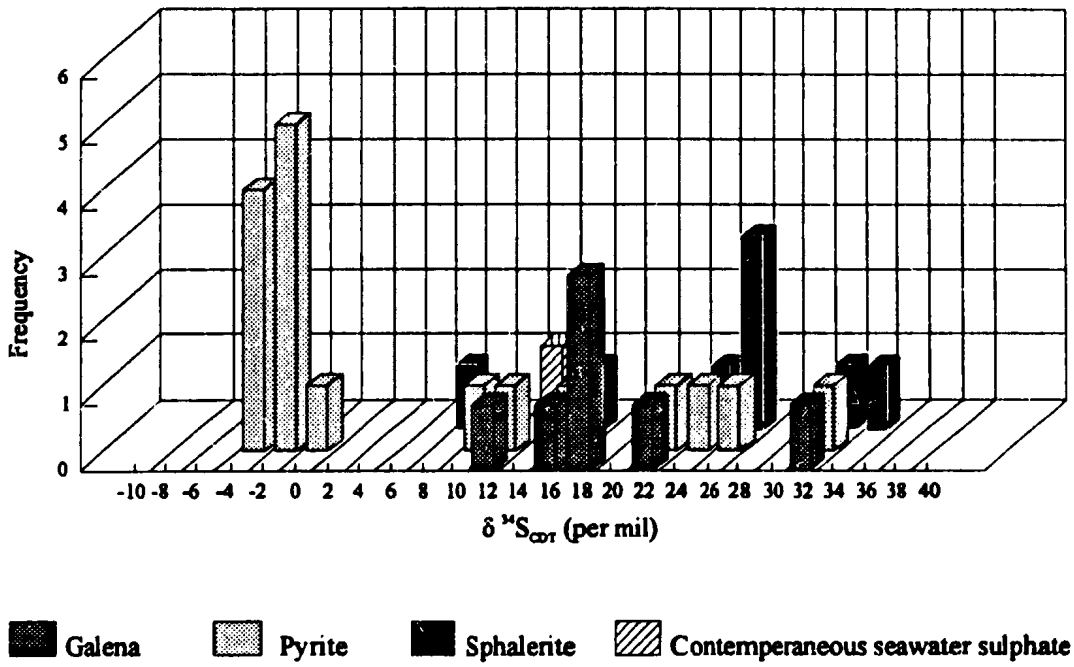

Fig. 4.21: Histogram of $\delta^{34}S$ for RBDM sulphides, and pyrite from the Nullataktok Fm. pyrite bed for comparison. Contemperaneous seawater of 12 per mil. is taken from Hayes *et al.*, 1992.

Mineral pairs were extracted in the hope of using them as isotope geothermometers (Ohmoto and Rye, 1979). Results were disappointing, as they demonstrated that the mineral pairs were not in isotopic equilibrium (large variations in temperatures). The conclusion drawn from this was that there must have been distinct "pulses" of mineralizing fluids which differed in their geochemistry, leading to the precipitation of the minerals.

Figure 4.21 illustrates that a broad range of values are present for the $\delta^{34}S$ values of the RBDM sulphides. Seawater sulphate has varied considerably through geological time, and during the Paleoproterozoic it is postulated to have been ~ 12‰ (Claypool *et al.*, 1980; Hayes *et al.*, 1992; Lambert and Donnelly, 1992). The high $\delta^{34}S$ values present in most of the RBDM mineralization requires a source of ^{34}S-rich sulphur. Seawater sulphate does not have high enough $\delta^{34}S$ values. As mentioned in section 5.3.3, the pyrite bed in the Nullataktok Fm. participated in a Rayleigh type fractionation process that preferentially removed ^{34}S from the basin to produce seawater sulphate with a $\delta^{34}S$ value of ~ +34‰ in the restricted Ramah Basin. This ^{34}S-enriched seawater was trapped as connate (formational) water providing a source of sulphur that could be expelled at a later date, probably as a result of the Torngat orogenic event (ca 1.86 Ga), to form the sulphides with high $\delta^{34}S$ values.

4.6.7 Lead Isotopes

Lead isotopes were analysed from galena separates to determine the possible source and model age of the lead. The results are shown in Table III.2 (Appendix III), and are illustrated in Figures 4.1 and 4.2. Model ages (Stacey and Kramers, 1975) for the galena mineralization range from 1559 - 1919 Ma (1813 Ma average), and Mu (μ) values from 6.507 - 7.037. The low μ values are very non-radiogenic (Figure 4.2), and suggest that the source area for the lead may have undergone uranium loss early in its history. The model ages appear to be slightly younger than the age of mineralization, which is constrained by the fact that blocks of quartz veined dolomite are present within the footwall of a thrust fault, south of Delabarre Bay (Plates 4.15 and 4.16). The thrust fault is thought to have formed during the crustal thickening of the Ramah Gp. between 1959 and 1853 Ma (Bertrand *et al.*, 1993), so it is reasonable to assume that veining of the dolomite occurred prior to the emplacement of the thrust fault. It would thus appear that the mixing and dilution of various sources has resulted in the formation of the model ages.

Ashwal *et al.* (1987) and Wilton (1991) suggest, from work in Proterozoic basins on the southern margin of the Nain Province, that similarly non-radiogenic lead indicates a uranium loss event probably occurred in the Archean basement similar to that observed in Greenland by Moorbath *et al.* (1973). It seems likely that the depleted lead (low μ) in the Ramah Gp. originated from a source region that had undergone uranium loss. A likely scenario for the source and formation of the lead would be: Protolith formation; metamorphic event depleting source area in uranium; decay of the remaining uranium (to

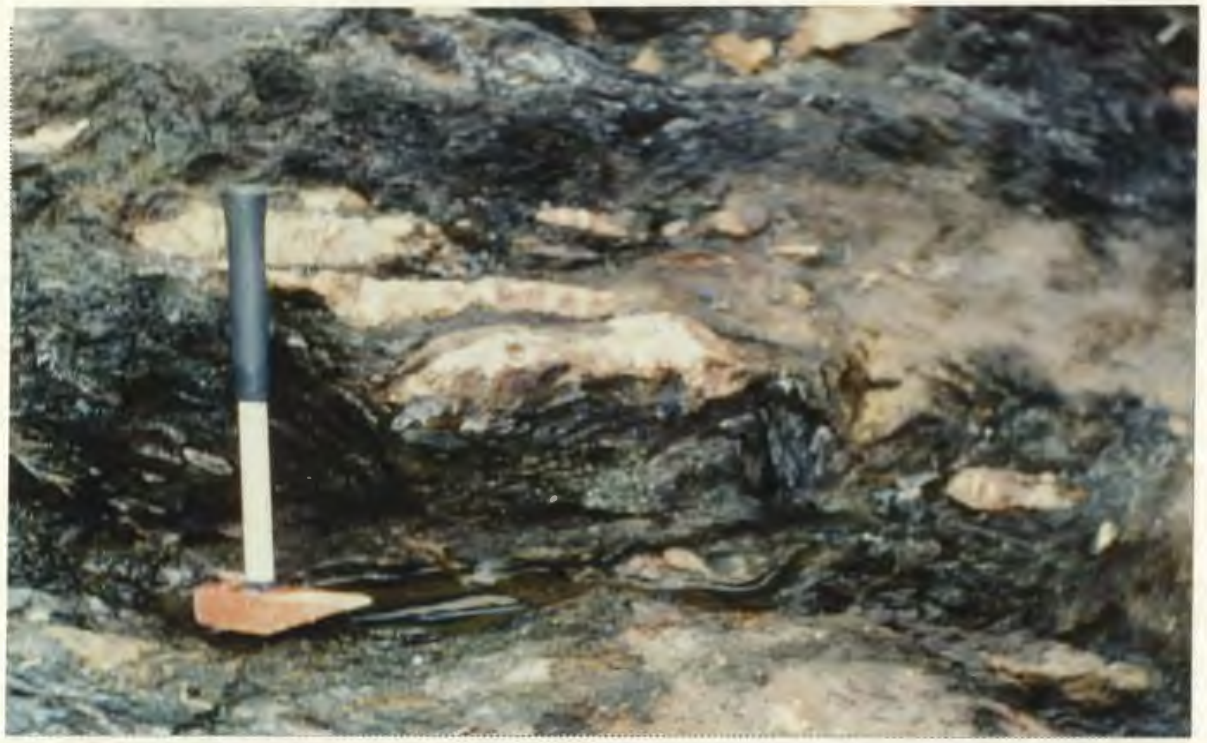

PLATE 4.15: Quartz-carbonate veined blocks of RBDM within a thrust fault plane at Delabarre Bay. The mineralized blocks indicate that the mineralization was pre- or syn-thrust faulting.

PLATE 4.16: Thrust zone at Delabarre Bay containing quartz-carbonate veined blocks of RBDM. Note the discoloration of the stream in the foreground caused by oxidation of the pyrite bed.

produce non-radiogenic lead); uplift, weathering and transportation to the Ramah basin; deposition in Ramah basin as shales; mobilization from the shales as a result of the collision between the Rae and Nain Provinces; mobilized fluid forms mineralization within the RBDM.

4.6.8 Related mineralization

A number of other showings and occurrences are present within the RBDM, brecciated parts of the Nullataktok chert bed, and also as a thin dolomite unit above the chert bed. These showings may have been formed from the same fluids that produced the mineralization present at the brecciated RBDM showings. The other showings present within the RBDM are the Loch Bears Gut and an occurrence 500m west of the Char showing which is nickel-rich (vaesite). Both showings appear to have been formed from remobilization of sulphides within the dolomite, due to faulting. Mineralization present within the chert is found at the Large (Gn, Sph), Adams Lake (Sph and Py illustrated in Plate 4.17), Sandman/Walsh (Sph, Gn), and the Gates (Sph) occurrences. These occurrences, when present as outcrop, are found in brecciated zones with a carbonate cement, near the top of the Nullataktok Fm. chert bed. This observation suggests that mineralizing fluid, rich in carbonate, caused brecciation, perhaps due to overpressuring and faulting.

Sulphur isotopes (Table III.1, Appendix III) of these showings and occurrences have $\delta^{34}S$ values similar to other RBDM-hosted mineralization, with the exception of the

very low $\delta^{34}S$ values for galena and pyrite at Loch Bears Gut (2.2 and -12.2‰ respectively), and sphalerite at Adams Lake (3.7‰). These values may be a result of deriving isotopically "light" sulphur from the pyrite bed, or ^{34}S loss due to remobilization.

Lead isotope data (Table III.2, Appendix III; Figures 4.1 and 4.2) for the Loch Bears Gut showing closely resemble the non radiogentic leads from other galena samples within the Ramah Gp.. Stacey and Kramers' (1975) model ages for the galena are 1832 and 1772 (with μ values of 6.537 and 6.730 respectively). Similarly the samples plot below the crustal growth curves of Zartman and Doe (1981), suggesting a source area isotopically similar to the mixed Nuk and Uivak gneisses to the east of the Ramah Gp.

4.7 Other Occurrences

Other minor occurrences include gabbroic to diabasic sill mineralization (Butter and Butter Extension), and quartz vein-hosted galena mineralization (Wilton No.2 showing).

The Butter and Butter Extension showings are present where a diabase sill has intruded the Nullataktok Fm., and consist of quartz veins with pyrite, chalcopyrite, and malachite. Petrographical examination indicates that the chalcopyrite occurs either at the centre of pyrite blebs, or within quartz veins with minor sphalerite (Plate 4.18). The sulphur isotopic ratio for the chalcopyrite is 3.5‰ (Table III.1, Appendix III), inconclusively indicating that the sulphur may be derived from either an igneous source (~0‰), the nearby pyrite - pyrrhotite bed (~ 6.3‰), or the diagenetic pyrite within the

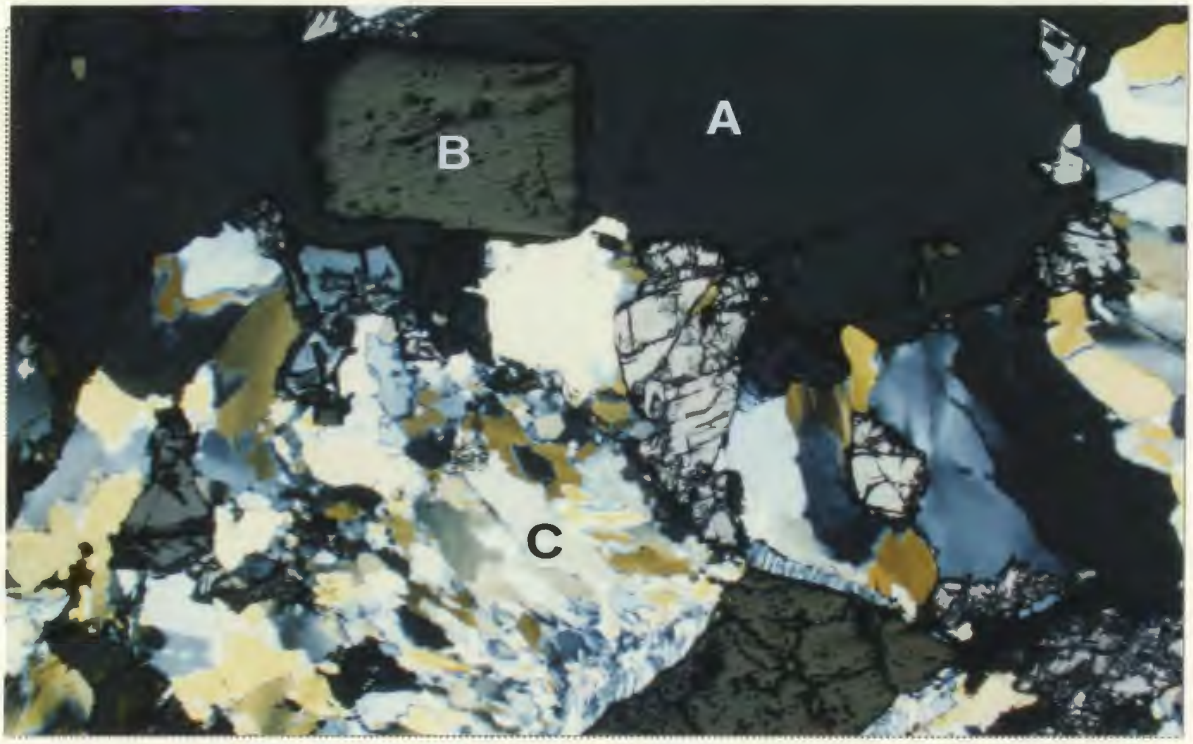

PLATE 4.17: Sphalerite (A) and pyrite (B) within remobilized chert (C) at the Adams Lake Showing. Note the undulose extinction present within the chert, and the recystallized pyrite. x 2.5 magnification, transmitted and reflected light with the polarizer in.

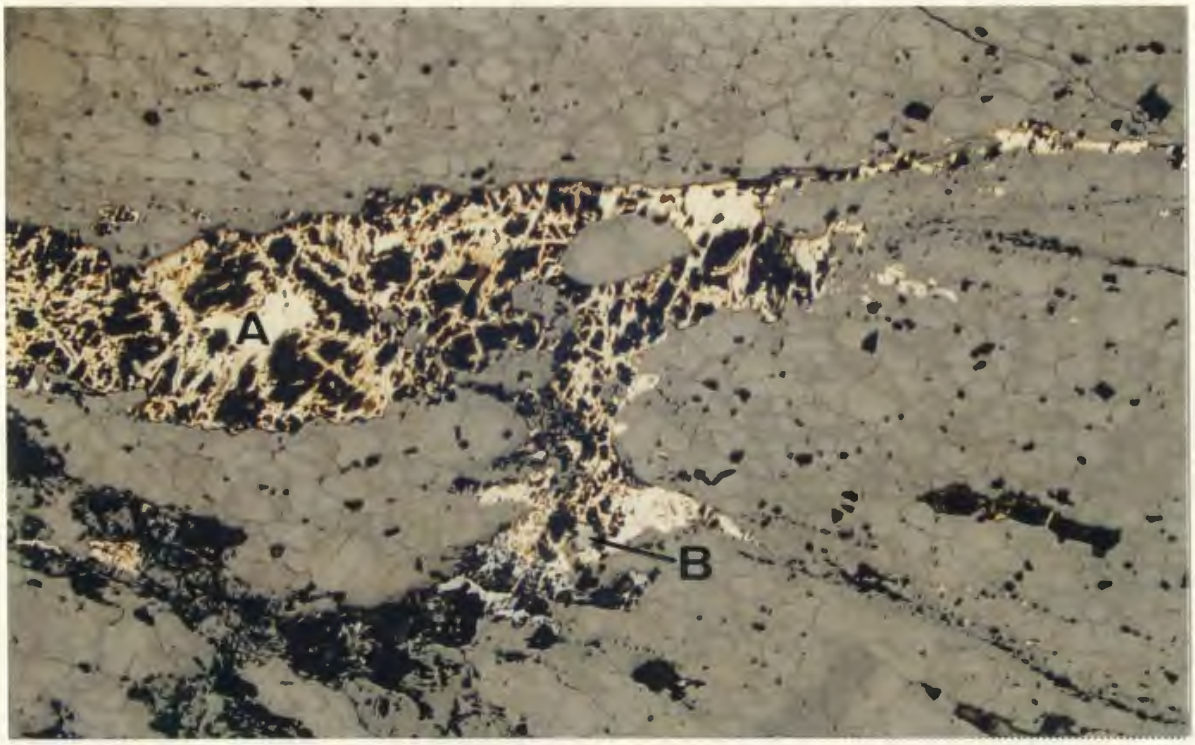

PLATE 4.18: Chalcopyrite (A) and minor sphalerite (B) present within a recrystallized quartz vein at the Butter Showing. x 2.5 magnification, reflected light.

shale (generally greater than 0‰). The most likely scenario is that the emplacement of the sill resulted in circulation of hot, copper-rich fluid through the shales, resulting in the reaction with diagenetic pyrite to produce the sulphides.

The Wilton No. 2 galena showing is a quartz vein cutting the Warspite Fm. dolomites. The vein has been deformed, indicating emplacement prior to deformation. Galena is generally disseminated sporadically through the centre of the vein. Lead isotope analyses of the galena (Table III.2, Appendix III) indicate that the lead is non-radiogenic with a Stacey and Kramers (1975) model age of 1833 Ma, and a μ of 7.117 (Figures 4.1 and 4.2). The mineralization may be a product of overpressuring of late stage fluids during the formation of the RBDM mineralization.

CHAPTER 5

METALLOGENIC MODELS AND CONCLUSIONS

The aim of this chapter is to synthesize all of the data presented in the previous chapters and to propose a metallogenic model for the genesis of mineralization within the Ramah Group based on the data. The mineralization will be described geochronologically as the mineralization is not necessarily contemporaneous with stratigraphy.

5.1 Archean Mineralization

The potentially oldest mineralization occurs in the Archean gneisses of the Nain Province to the east of the Ramah Gp. and this polymetallic mineralization must form an integral component in any metallogenic explanation of the area because the base metals may have been deposited prior to the deposition of the Ramah Gp.. Sulphur isotope signatures of ~ 0‰ are very different from mineralization within the RBDM (~ 10 to 30‰), probably indicating a different sulphur source. Lead isotope ratios show that the galena is very non-radiogenic indicating derivation from a uranium depleted source. The lead isotope data from these showings yielded Stacey and Kramers (1975) model ages of 2460 and 2446 Ma which are distinctive compared to the model ages of 1559 to 1919 Ma for galena from RBDM showings. Taken together, the sulphur and lead isotope data suggest that the lead and the sulphur were probably locally derived and may have resulted from magmatic activity in, and metamorphism of, the Archean gneisses.

Stream sediment data from northern Labrador indicate that the Archean gneisses to the east of the Ramah Gp. are enriched in lead and zinc with respect to the Archean rocks to the west (Figures 5.1 and 5.2) (Hornbrook and Friske, 1991; Davenport, pers. comm., 1994). Thus, if detritus from the Archean was transported into the early Ramah basin then the resulting sediment might be expected to be enriched in these elements. Paleoflow directions (Knight and Morgan, 1981) throughout the deposition of the Ramah Gp. indicate that the basin sediments were derived from the east (Archean basement). The shale-rich Nullatakok Formation sequence has elevated lead and zinc content (98 ppm, and 791 ppm respectively), relative to Vine and Tourtelot's (1970) average black shale compositions, with Pb and Zn concentrations of 20 ppm and 300 ppm, respectively. The shale sequences in the Nullataktok and Typhoon Peak formations, together with the basal clastics of the Rowsell Harbour Formation, could act as potential Cu, Zn, or Pb source rocks for any subsequent mineralizing fluids (Maynard, 1983, 1991; Brown, 1992).

The Archean basement also contains a number of mafic and ultramafic intrusive rocks as well as volcanic rocks incorporated into the gneisses during deformation and metamorphism. Weathering of these rocks during the initial deposition of the Rowsell Harbour Formation led to the formation of sandstones and conglomerates rich in detrital hematite and magnetite. The green staining within the basal formation is interpreted to reflect the presence of fuchsite, indicating that the ultramafic rocks in the basement provided chromium mica to the sediments deposited in the early Ramah Gp..

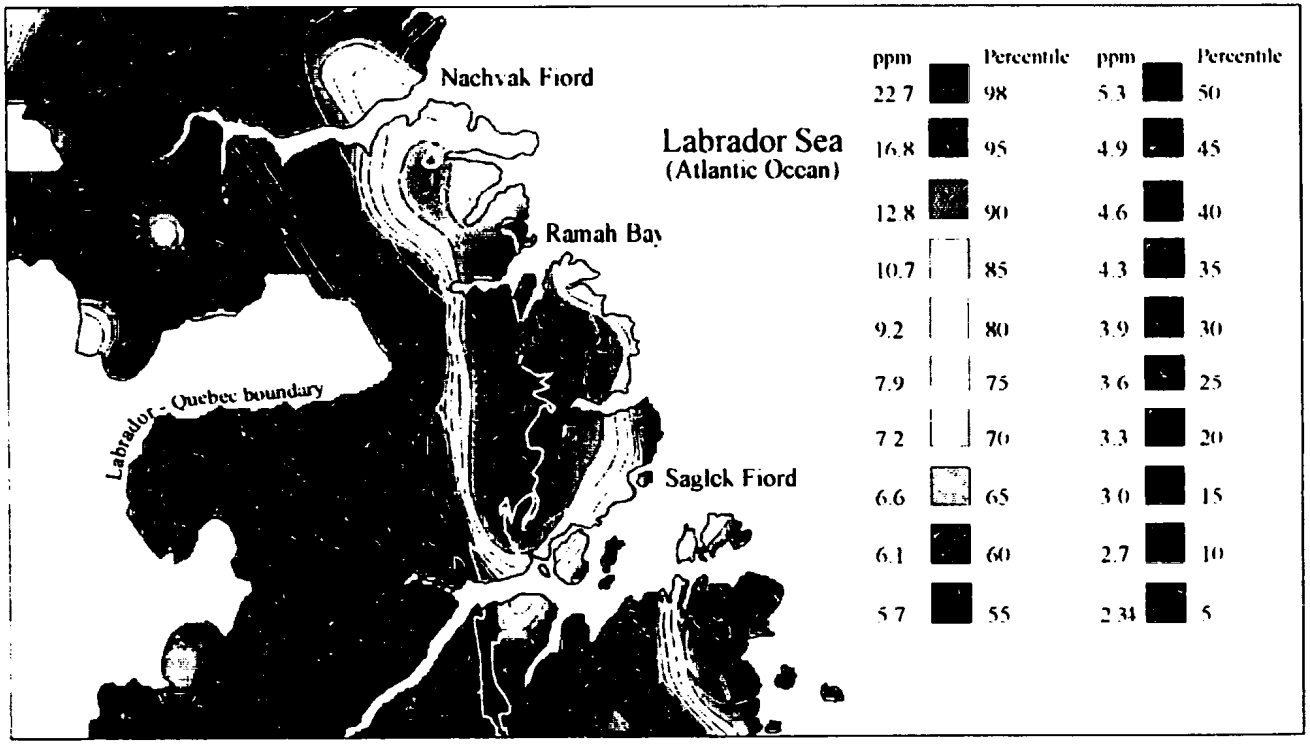

Figure 5.1. Stream sediment geochemistry data for lead between Nachvak and Saglek Fiords. Note that the Ramah Gp. and the Archean basement to the east are enriched in lead, while the Tasiuyak Terrane gneisses are depleted. The conclusion drawn from this data, together with the Pb-Pb isotope data, suggests that the source for the lead within the Ramah Gp. was the result of Paleoproterozoic erosion of the Nain gneisses, and the transportation of the metal into the Ramah basin. Data from Hornbrook and Friske (1987).

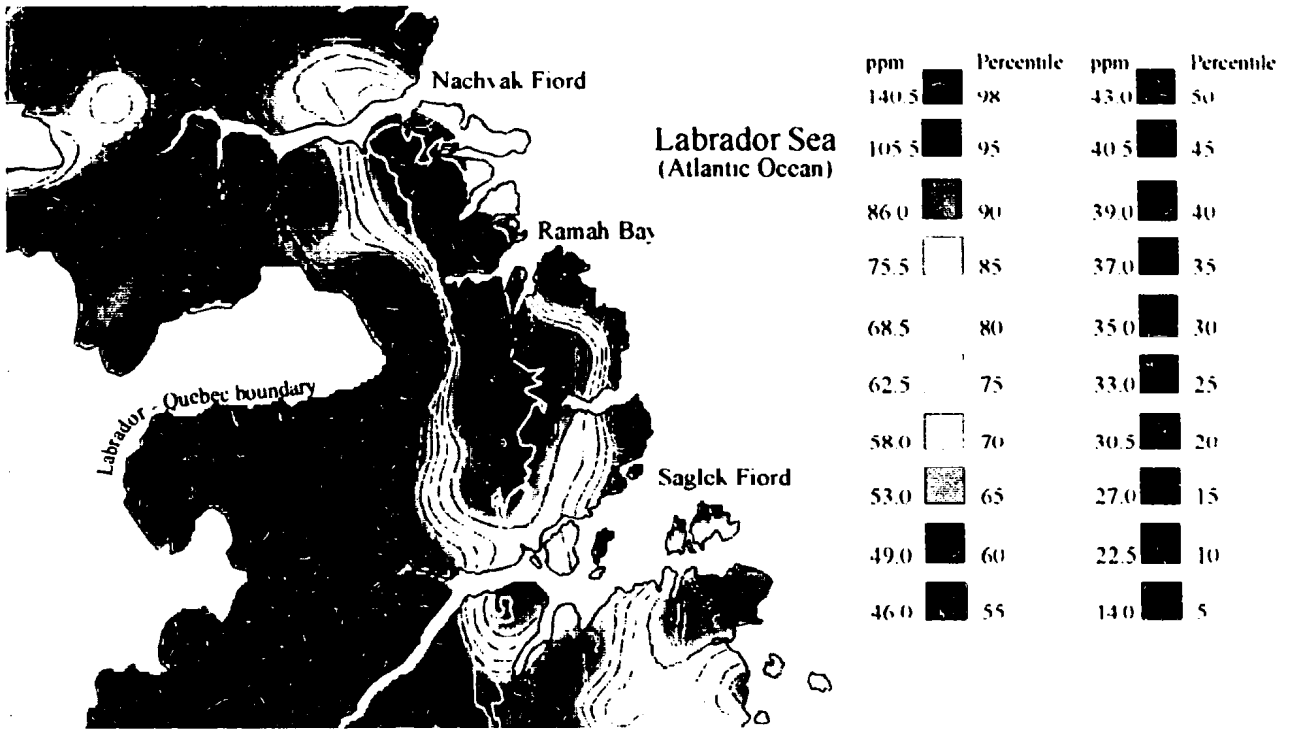

Figure 5.2: Stream sediment geochemistry data for zinc between Saglek and Nachvak Fiords. The Ramah Gp and the Archean gneisses in the Saglek area are enriched in zinc, while the rocks to the west of the Ramah Gp. are relatively depleted. The Ramah Gp. is outlined by the thick white line. Data from Hornbrook and Friske (1987)

5.2 Rowsell Harbour Mineralization

Submarine and subaerial extrusion of alkali basalts resulted in the formation of the Rowsell Harbour Volcanic Member (RHVM). Hydrothermal convection of seawater through the 10m thick volcanic unit caused the mobilization of Cu and Fe within the basalt, and their subsequent precipitation to form the chalcopyrite mineralization present at the Zambia Occurrence. The extrusion of the basalt suggests tension within, or close to, the Ramah basin.

5.3 Pyrite-Pyrrhotite Bed

It is clear from the previous information that the pyrite-pyrrhotite bed formed as the result of biogenic activity in the Ramah Gp. basin ca 2.0 Ga. The biogenic nature of the pyrite-pyrrhotite bed is supported by the fine-grained and banded appearance of the pyrite and the Co-Ni ratios which indicate that there is no volcanogenic component present within the pyrite. The trace element characteristics of the unaltered pyrite bed are typical for pyrite; chalcophile element (V, Cr, Ni, Cu, and Zn) enrichment resulted from contact metasomatism induced by intrusion of the diabase-gabbroic sills. All the evidence suggests that the unit formed as the result of anoxia in the Ramah Basin. The basin must have been well supplied by nutrients to account for the organisms that formed the thick and laterally extensive pyrite bed. Sulphur isotope data indicate that biogenic fractionation processes within the basin resulted in the enrichment of ^{32}S in the pyrite while the heavier isotope, ^{34}S, was enriched in the co-existing, basal anoxic seawater layer in the restricted

Ramah Basin. The enriched seawater was later incorporated into the shales as formation (connate) water or in deep water evaporites. It is reasonable to assume that the Ramah Basin was considerably larger than the present outcrop size, and that vast volumes of this connate water would have been trapped within the sedimentary package. Subsequent tectonic activity caused this water to migrate up-dip and towards the basin margins.

5.4 Intrusive Mineralization

The next form of metallic sulphide mineralization to occur was that of the copper and nickel associated with the gabbroic to diabasic intrusives. The mineralization is found as two types: as an immiscible liquid phase within the sills; and veinlets within the surrounding, organic-rich, host rocks. The cumulates have been described by Hussey (1994), and are not described here further. Mineralization in the surrounding host rock (i.e. Butter and Butter extension showings) consists of chalcopyrite with malachite staining. Sulphur isotope data indicate that the sulphur could have been derived from either a magmatic source or assimilation of the biogenic pyrite bed. Sill emplacement occurred prior to the Torngat Orogen (ca 1860 Ma), as the sills have been affected by the subsequent deformation.

5.5 Mississippi Valley-type Mineralization

The largest metallogenic effect on the region was undoubtedly caused by collision of the Rae and Nain Structural provinces (Torngat Orogen). The effect of this orogenic event was to cause the expulsion of fluids from the basin(s) that lay to the west of the present Nain craton in a similar manner to that first envisaged by Oliver (1986) for the Appalachian-Ouachita Orogen. Oliver (1986) believed that hydrocarbons and Pb-Zn rich fluids were expelled from Laurentian foreland basins during collision with the Gondwanan continent .

The most important characteristics of MVT lead-zinc deposits have been described by Ohle (1959,1980), Servjensky (1986), Anderson and Macqueen (1988), and Leach and Sangster (1993). These features include:

1. Occurrence principally in dolostone, rarely in limestone or sandstone.
2. Epigenetic and strata-bound.
3. No association with igneous activity.
4. Occurrence at shallow depths at flanks of basins.
5. Occurrence in platform-carbonate sequences, located either in relatively undeformed rocks bordering foredeeps, or in foreland thrust belts.
6. Occurrence over wide areas, localized to form "districts" by geological features that permit upward migration of ore-forming fluids. Examples of these features include breccias, depositional margins of shale units, facies tracts, faults, and basement highs.

7. Occurrence just below shelf sequence boundaries (unconformities).

8. Temperature of deposition is low (75°-200°C), but typically higher than the expected local geothermal gradient.

9. Mineralogically simple: dominant minerals are sphalerite, galena, pyrite, marcasite, dolomite, calcite, and quartz.

10. Sulphide textures are extremely varied, with ores ranging from coarsely crystalline to fine grained and from massive to disseminated.

11. Associated alteration consists mainly of dolomitization, dissolution of host rock, and dissolution and crystallization of feldspar and clay.

12. Evidence for dissolution of the carbonate host rocks, manifested as slumping, collapse, brecciation, or some combination of these.

13. Ore fluid compositions match dense basinal brines, typically containing 10-30 wt.% salts.

14. Carbon and oxygen isotopic compositions of the host rocks are normal for such rocks but are lowered adjacent to ore, which suggest that the host rocks were recrystallized in the presence of a fluid.

15. Sulphur isotopic compositions of ore sulphides less than contemporaneous seawater.

16. Presence of hydrocarbons.

Mineralization within the RBDM has a number of diagnostic features including: presence within the dolomite; simple mineralogy (sphalerite, galena, pyrite); presence of pyrobitumen; no contemporaneous igneous activity; presence with secondary dissolution pores; and common brecciation of host rock. These are some of the ubiquitous features of Mississippi Valley-type (MVT) deposits as characterized by Ohle (1959,1980), Sverjensky (1986), and Anderson and Macqueen (1988).

It is proposed here, based on these macroscopic features, as well as the petrographic and geochemical data, that the RBDM mineralization represents a Paleoproterozoic example of this class of mineral deposit. Geochemical evidence supporting the MVT model for the origin of the RBDM mineralization includes: sulphur, oxygen, carbon, and lead isotope data; SEM analyses; as well as petrographic studies using reflected and cathodoluminescence microscopy. Fluid inclusions have also constrained the fluid temperature and geochemistry.

5.5.1 Sulphur Source

It is generally believed that MVT mineralization results from the mixing of sulphur from an enriched source with sulphur from a less enriched source (Sverjensky, 1986; Ohmoto et al., 1990; Ghazban et al., 1990; Leach and Sangster, 1993). A problem arises in the RBDM mineralization with how to evolve such a ^{34}S enriched solution. The broad range in $\delta^{34}S$ values of some classic MVT deposits and districts is shown in Figure 5.3 (Upper Mississippi Valley- Ault and Kulp, 1960; Pickney and Rafter, 1972; McLimans,

1977: Viburnum Trend- Sverjensky, 1981: Pine Point, NWT- Evans et al., 1968; Sasaki and Krouse, 1969; Macqueen and Powell, 1983: Nanisivik- Ghazban et al., 1990). Even during the Phanerozoic, when seawater sulphate was highly variable, sulphides from these deposits and districts do not reach the $\delta^{34}S$ values that are present in the Ramah Gp. In the majority of the classic MVT districts, there is considerable evidence to suggest that evaporites played a significant role in their formation. The only lithological evidence to support the presence of evaporite minerals in the RBDM would be the dissolution present within the unit. However, psueodomorphs of evaporitic minerals such as gypsum, anhydrite, or halite have not been identified by any workers in the Ramah Gp.. Sulphur isotope work on the RBDM mineralization indicates that there are large ranges in $\delta^{34}S$ values for the galena, sphalerite and pyrite (Figure 5.3). These sulphides have extremely high $\delta^{34}S$ values (sphalerite ~ 34‰, galena ~ 33‰, pyrite ~ 32‰) which cannot be explained by contemporaneous seawater sulphate being the sole or main source of sulphur without some modification. Contemporaneous Paleoproterozoic seawater sulphate (Figure 5.4) is believed to have had a composition of ~ 12‰ (Hayes *et al.*, 1992), which is too low to account for the high values obtained within the RBDM. In the previous chapter the elevated $\delta^{34}S$ values were suggested to result from sulphur-reducing bacteria isotopically enriching the basin in ^{34}S as a result of Rayleigh-type fractionation during the deposition of the Nullataktok pyrite bed. The ^{34}S enriched seawater became trapped within the pores of the Nullataktok shales. Knight and Morgan (1981) believed that the source for the basin sediments was derived from the east and that the basin probably

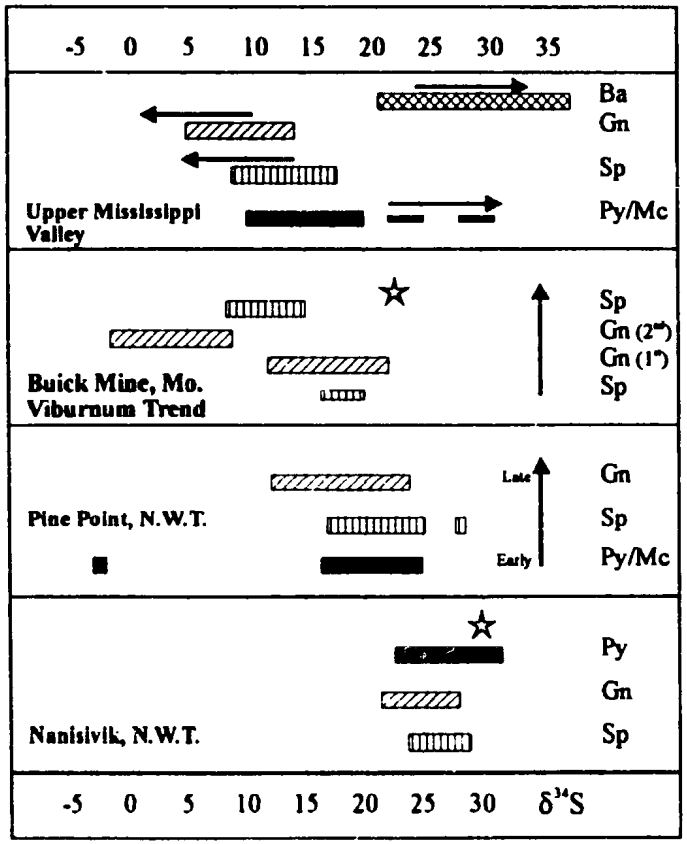

Fig. 5.3: $\delta^{34}S$ values for classic Phanerozoic and Proterozoic MVT deposits. Arrows indicate early to late mineralization, stars indicate contemperaneous seawater sulphate. See text for original references.

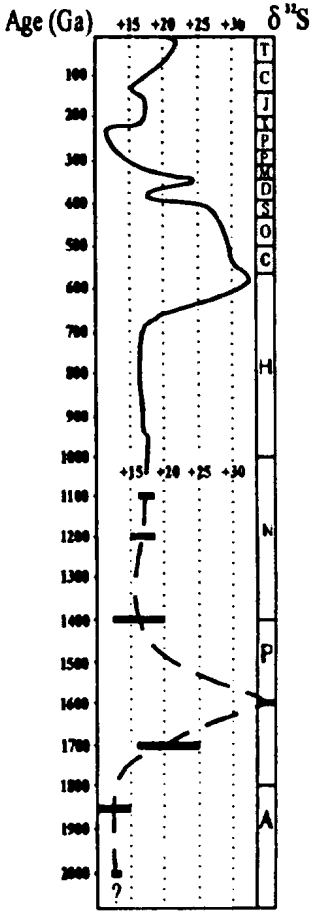

Fig. 5.4: Variation of seawater sulphate ($\delta^{34}S_{CDT}$)through geological time. Data for Phanerozoic from Claypool *et al.* (1980) and Proterozoic from Hayes *et al.* (1992).

deepened to the west. It is suggested here that the Nullataktok Formation thickened to the west, and therefore could act as a large reservoir for ^{34}S enriched connate water.

Another possible mechanism that could form high $\delta^{34}S$ values for sulphides within the RBDM is a method proposed by Hall *et al.* (1994) for pyrite ($\delta^{34}S$ 36.5 - 42.1‰) within the Late Precambrian Bonahaven Dolomite, Argyll, Scotland. Hall *et al.* (1994) propose that the enrichment was a result of the reduction of evaporitic sulphate during progressive regional metamorphism up to greenschist facies grade. The reaction can be represented nominally by:

$$CaSO_4 + 2C_{organic} + H_2O \longrightarrow CaCO_3 + H_2S + CO_2$$

$$2FeO_{silicate} + 4H_2S + C_{organic} \longrightarrow 2FeS_2 + 2H_2O + CH_4$$

The model proposed by Hall *et al.* (1994) is supported by the findings of Fairchild (1985) who suggested that quartz-calcite nodules present within the Bonahaven Dolomite could represent psuedomorphs after anhydrite. No quartz-calcite nodules have been identified within the Ramah Gp., and the only evidence to support the presence of evaporites is thebrecciation of dolomite at the Panda Showing. It is possible that during the biogenic deposition of the Nullataktok Formation pyrite bed, evaporites formed in deep water, or in shallow water at the basin margins, in a manner similar to evaporites from the Permian Castile Formation, New Mexico (Anderson, *et al.*, 1972; Kendall, 1984). To account for the ^{34}S enriched evaporites (if present) a Rayleigh-type fractionation process, due to biogenic activity, is still the favoured mechanism.

5.5.2 Pyrobitumen (hydrocarbon) Source

Nullataktok Formation shales have carbon contents between 1.7 and 2.8 wt. % (Hayashi *et al.*, 1994), while Typhoon Peak Formation shales have carbon contents between 0 to 0.3%. The values for the Nullataktok Formation are very close to those in carbonaceous and bituminous mudrocks which typically contain 3 - 10% organic carbon (Tucker, 1992). High carbon contents result from the accumulation of organic matter in areas where low rates of water circulation cause insufficient oxygen to reach the bottom sediments for decomposition of the organic matter. As a result of poor circulation the water becomes stratified and the sea may become dysaerobic (oxygen deficient) or totally anoxic. Anoxic bottom waters are characterised by accumulation of pyrite at the sediment-water interface. The presence of pyrite and high carbon contents within the Nullataktok Formation indicate that the Ramah basin had restricted, or more likely, euxinic circulation, and therefore had good potential for hydrocarbon generation. Organic-rich sediments contain high concentrations of Cu, Pb, Zn, Mo, V, U, and As, which are adsorbed on organic matter and clay minerals (Tucker, 1992). Hence, it is likely that the Nullataktok Formation could have acted as a source for the base metals developed in the Ramah Gp..

Maturation of the bituminous shales is suggested due to the presence of what appears to be pyrobitumen (thermally altered hydrocarbons) within the RBDM. The average $\delta^{13}C$ value for the pyrobitumen is -28‰, and is analogous to organic carbon found in petroleum (Hoeffs, 1987, Waples, 1981). Assuming that the Ramah basin had a

pre-erosional thickness of 2.5km (present estimated thickness is 1.7km), and a continental geothermal gradient of 30°C/km, it is possible that the Nullataktok shales reached a temperature of 75°C, but the temperature may have been even higher as sill emplacement occurred before thickening and deformation. The 75°C temperature is well within the oil generation zone window (60-150°C), depending on the original kerogen type (Allen and Allen, 1990). The hydrocarbons probably formed during basin dewatering due to compaction, or during the Rae-Nain Structural Province collision, resulting in the thickening of the Ramah basin and subsequent hydrocarbon migration to the basin margins. Hydrocarbons accumulated within the porous RBDM, forming a hydrocarbon reservoir.

Field observations of the pyrobitumen suggest the hydrocarbons formed contemporaneously with the quartz-carbonate veins which post-date the sulphide mineralization. Fluorescence petrographic studies of sphalerite indicate that inclusions within the sphalerite do not contain hydrocarbons (no fluorescence observed), but that fractures, subsequently annealed, did show fluorescence. This evidence implies that hydrocarbons might indeed have been present during mineralization.

5.5.3 Source of Metals

Stream sediment data for northern Labrador indicate that the Archean orthogneisses to the east of the Ramah Gp. are enriched with respect to Pb and Zn, relative to paragneisses to the east. The lead isotope ratios of galena within the basement

gneiss (Morgan vein Showing) and the RBDM imply a common low μ source, but subsequent remobilization has resulted in different Stacy and Kramers (1975) model ages. This information, together with the paleoflow data (Knight and Morgan, 1981), suggest that the probable Pb and Zn source for the Ramah basin was the Archean gneisses. The transported Pb and Zn was integrated into black shales due to anoxic conditions that prevailed during their deposition (Figures 5.5a and 5.5b).

5.5.4 Composition and Transport of the Ore Fluid(s)

Oxygen isotope ratios, in conjunction with estimated fluid compositions from fluid inclusion analyses of gangue minerals, suggest that the pre-ore fluid(s) was/were meteoric in origin (low $\delta^{18}O$ values) and became progressively connate brine-rich (high $\delta^{18}O$ values). Transportation of the metals within the ore-forming fluid(s) would have been as chloride complexes in the presence of dissolved sulphates (Anderson, 1975; Anderson and Macqueen, 1988) as indicated by the high salinity (15-27 wt. % equiv. NaCl) of fluid inclusions. Concentrations of 3 ppm Zn and 1.6 ppm Pb have been calculated at 150°C, and 25 wt. % equiv. NaCl for fluids in the Upper Mississippi Valley district, USA (McLimans, 1977), and it is proposed that similar fluid compositions would have been present within the Ramah Gp.. Studies by Burst (1969) of shale sequences in the Gulf Coast, USA, indicate that high salinity pore water is released between about 10°C and 90°C, and further water is released by the conversion of expandable to non-expandable

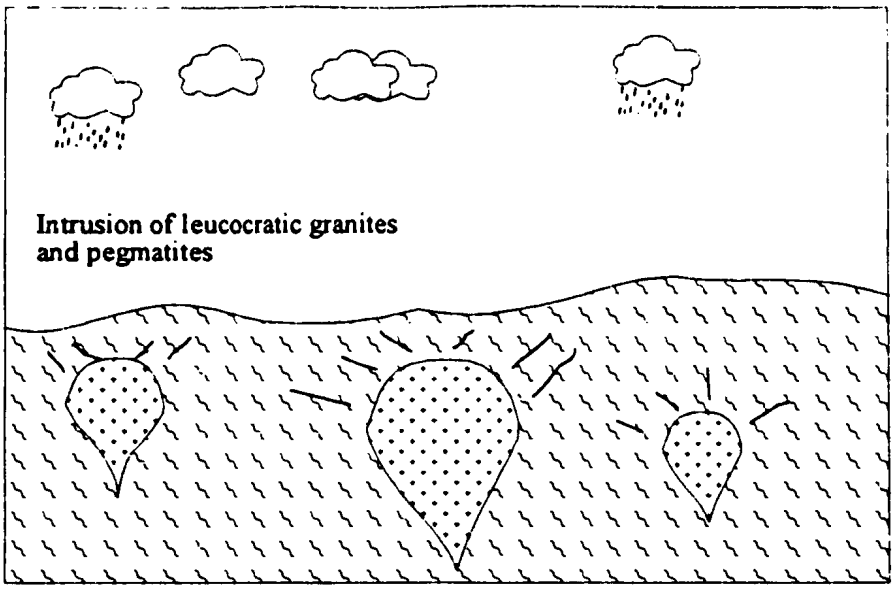

Fig. 5.5a: Formation of basement mineralization. Metamorphism of protolith resulting in a uranium loss event (low μ values), intrusion of leucocratic granites and pegmatites, followed by further metamorphism.

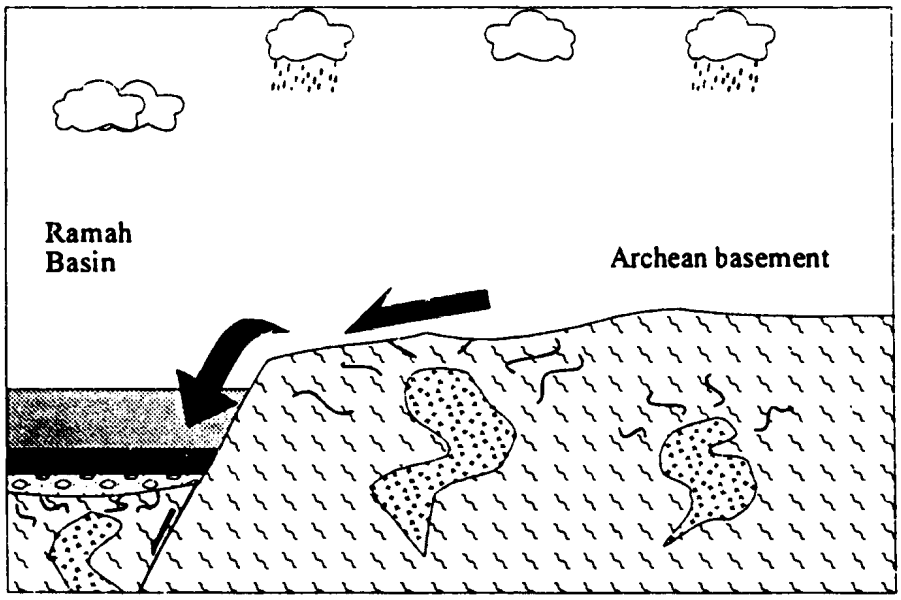

Fig. 5.5b: Erosion of Archean gneiss and deposition of the resulting sediments within the Ramah Basin. Most metals would be concentrated within black shales, such as those of the Nullataktok and Typhoon Peak formations.

clays (e.g. montmorillonite —› illite). The second dehydration is the beginning of base metal leaching (Figure 5.6).

The mineralizing fluid(s) had three possible flow routes (Figure 5.7): through sandstone aquifers within the Rowsell Harbour and Reddick Bight formations; through the porous RBDM; or through Nullataktok Fm. shales, either above or beneath the chert bed. Fluid flowing through the Rowsell Harbour Fm sandstones would tend to be enriched in Pb (due to the leaching of feldspars within the formation), relative to zinc, similar to those of southeast Missouri (Sverjensky, 1986). Although flow rates through the sandstone aquifers would have been relatively high, a conceptual problem then arises as to how the mineralizing fluid ascended into the RBDM. The only evidence to support fluid flow within the Rowsell Harbour Fm. was chalcopyrite found at the Normore Showing. This mineralization indicates that small volumes of overpressurized, Cu-rich fluids did exist. No Pb and Zn mineralization was observed in the formation, but this may be due to an unfavourable precipitation mechanism. Fluid migration through the RBDM is possible due to its enhanced porosity, proximity to the overlying Nullataktok shale, and the presence of mineralization within the unit. If the basin did deepen to the west, it is likely that the sabkha-like environment in which the RBDM formed would discontinue and give way to deep water conditions forming shales. The migration of fluids later in the history of the Ramah Gp. would likely have occurred along the dolomite horizon where fluid was forced into the dolomite at a pinch-out structure. Unfortunately, there is no way of proving that the RBDM pinched-out to the west. Immediately above the Reddick Bight Formation is a

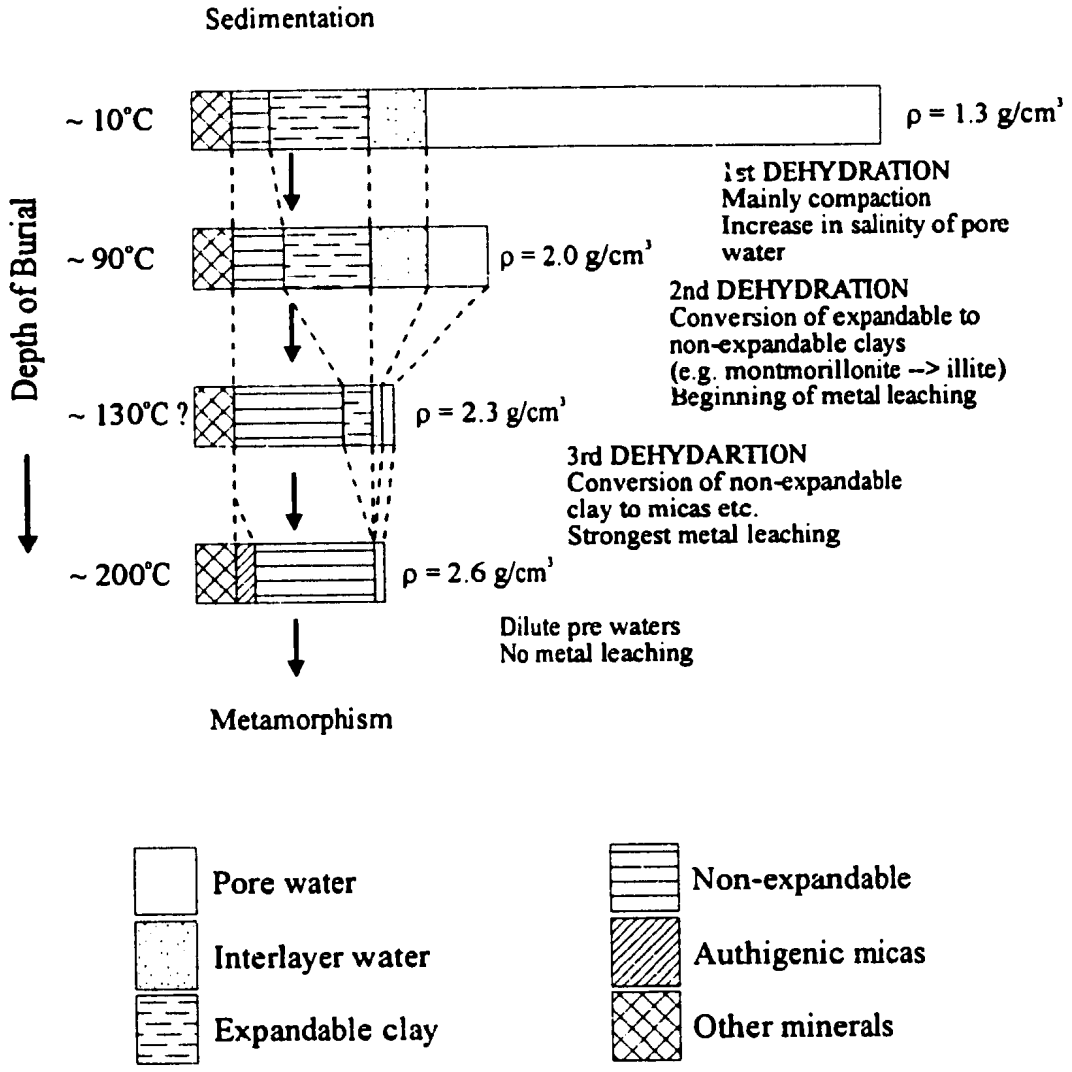

Fig. 5.6: Schematic illustration of the change in marine shale bulk composition during compaction and dehydration (after Burst, 1969). ρ refers to density.

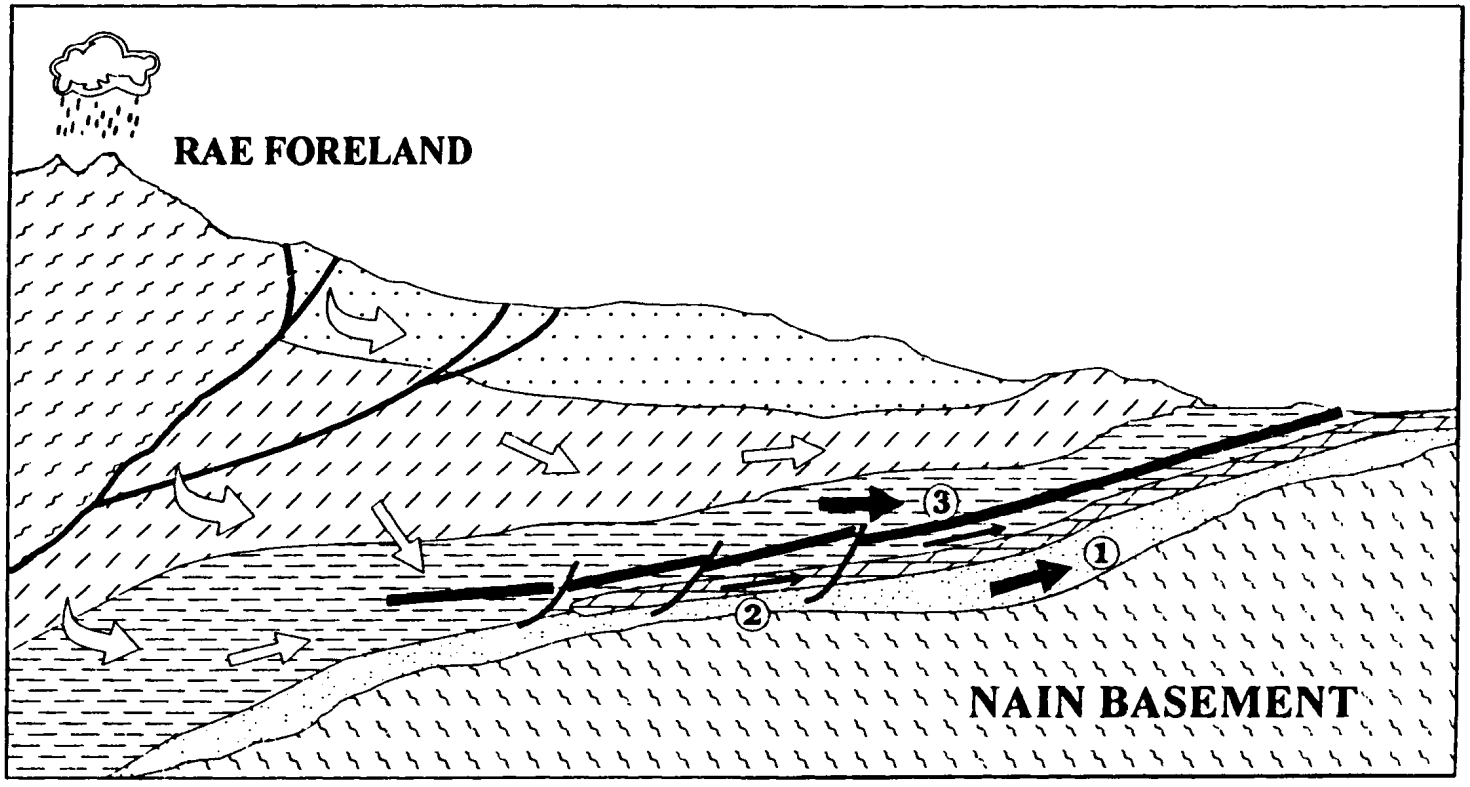

Fig. 5.7: Possible flow routes of the MVT mineralization fluid. Expelled fluids from the Ramah basin have three possible flow routes; (1) through the Rowsell Harbour and Reddick Bight formation clastics; (2) through the RBDM; or (3) Above or beneath the Nullataktok Fm chert bed (heavy black line). Fracturing of the chert bed maybe due to peripheral bulge formation (cf. Mitchell, 1985). Model modified after Garven and Freeze (1984).

50-70m thick unit of pyritic and graphitic shale, capped by the pyrite and chert beds. It is conceivable that this shale unit could have acted as an aquifer for migrating fluids originating in the west, and that the overlying chert bed (up to 30m in thickness) could have acted as an aquitard/aquiclude. This would have caused fluids to become overpressured and forced them into the more porous RBDM. Overpressuring is suggested at a number of localities where the chert bed has been brecciated and recemented by dolomite, sometimes resulting in mineralization (Large, Sandman/Walsh, Gates and Adams Lake showings). Evolved brines from the upper portions of the Nullataktok Formation would have had to descend into the lower formation. This fluid descent may have taken place due to early fracturing of the chert bed to the west as a result of the early Rae-Nain collision, causing a peripheral bulge to develop. This is similar to the model of Mitchell (1985) for Irish Carboniferous mineralization due to the Variscan/Hercynian Orogeny (Late Carboniferous) in Europe.

5.5.5 Sulphide Deposition

There are three basic models proposed for the mechanisms of precipitation for Mississippi Valley-type sulphides (Table 5.1) including: fluid mixing, cooling and changes in pH brought on through wall-rock alteration, and various sulphate reduction processes. To address the question of which mechanism was the most likely for the RBDM, it is important to consider the mineralogy, paragenetic sequence of the ore minerals, and the geochemistry and temperature of the fluids. Key concerns which must be addressed

Table 5.1: Geochemical models for the transportation and precipitation of base metals and sulphur in Mississippi Valley-type deposits (Sverjensky, 1981).

Transportation of ore-forming constituents	Precipitation mechanisms
I. *Mixing models*	a) Mixing with fluids containing H_2S
Base metals transported by fluids without	b) Replacement of diagenetic iron disulphides
significant sulphur contents	c) Thermal degradation of organic compounds releasing sulphur
II. *Sulphate reduction models*	a) Reduction of sulphate by reactions with
Base metals transported together with sulphate in same solutions	organic matter or methane
III. *Reduced-sulphur model*	a) Changes of pH
Base metals transported together with	b) Dilution
reduced sulphur in the same solutions	c) Decrease of temperature

include: carbon and oxygen isotopic values for the mineralized zones; ^{34}S-enriched fluids to produce isotopically heavy sulphides; presence of hydrocarbons (pyrobitumen); and the role of meteoric water. The chosen mechanism must satisfactorily account for many, if not all, of the textures, mineralogy, and geochemistry of the mineralization.

The presence of pyrobitumen within the RBDM suggests hydrocarbons were present and is therefore consistent with the mixing and sulphate reduction models (models I and II in Table 5.1) (Anderson, 1975; Beales and Jackson, 1966; Anderson, 1983; Barton, 1967; Macqueen and Powell, 1983). A decrease in temperature of the ore fluid is suggested by the presence of late stage quartz within the dolomite. Quartz solubility is largely a function of temperature, with quartz precipitation occurring with substantial cooling. Oxygen isotope studies indicate the existence of several different fluid chemistries, so it appears likely that a fluid mixing model accompanied by cooling is most appropriate to explain the presence of the pyrobitumen and quartz.

The simplest model to explain the mineralization within the RBDM is a sulphate reduction model (Table 5.1). This model assumes that metals (as chloride complexes) and sulphates are transported in the same ore solution, and mix with organic matter such as petroleum or methane (Helgeson, 1969; Anderson and Garven, 1987; Anderson and Macqueen, 1988). The sulphate reduction model has been used to explain mineralization at several MVT deposits including Pine Point (Macqueen and Powell, 1983) and Nanisivik (Ghazban *et al.*, 1990). The resulting carbon oxidation, sulphate reduction, and metal deposition can therefore be summarized by the following equations:

$$CH_{4\,(aq)} + SO_4^{2-}{}_{(aq)} + 2H^+ = CO_{2\,(g)} + H_2S_{(aq)} + 2H_{2\,(l)} \quad (1)$$

$$\text{and } ZnCl_4^{2-}{}_{(aq)} \text{ (or } PbCl_4^{2-}) + H_2S_{(aq)} = ZnS_{(s)} + 2H^+{}_{(aq)} + 4Cl^-{}_{(aq)} \quad (2)$$

This model is probably oversimplified as it does not account for the abundant dolomite gangue present in the RBDM.

A model which does account for the presence of dolomite prior to and contemporaneous with the sulphides is that of Anderson and Garven (1986). In their model Anderson and Garven (1987) suggest the principle reaction is:

$$SO_4^{2-} + CH_4 = H_2S + CO_3^{2-} + H_2O \quad (3)$$

The stoichiometry of the reaction will depend on the nature of the organic matter, here assumed to be methane for simplicity. This reaction can occur through direct chemical reduction or bacterial reduction. Carbon dioxide liberated from equation (3) is then free to react with the dolomite host rock via

$$CaMg(CO_3)_2 + 2H_2CO_3 = Ca^{2+} + Mg^{2+} + 4HCO^{3-}. \quad (4)$$

An interesting point from the above reaction reaction (4) is that half of the carbon atoms in the product bicarbonate come from dolomite and the other half from CO_2 (which was ultimately derived from the organic matter). Anderson and Garven (1987) suggest that if such a process was in effect the $\delta^{13}C$ values for the fluid would be intermediate in composition between the host rock and the organic matter. Such as process is noted in the early, main, and post-ore carbonates within the RBDM where carbonates become progressively heavier in ^{13}C as time progresses until approaching host rock values. Dolomite precipitation can occur either by the reversal of reaction (4) through an increase

in carbonate alkalinity as a result of sulphate reduction, or through as suggested by Anderson and Garven (1987), a variation of reaction (3), namely

$$2CaSO_4 + Mg^{2+} + 2CH_4 = CaMg(CO_3)_2 + Ca^{2+} + 2H_2S + 2H_2O \quad (5)$$

where $CaSO_4$ might be assumed to be in solution as ion pairs. While there is no direct evidence within the Ramah Gp. for the former presence of abundant gypsum or anhydrite in the host rock, an equivalent reaction involving solute species of Ca^{2+} and SO_4^{2-} may have been important for the precipitation of the large quantities of dolomite associated with the mineralization.

Sulphide precipitation is associated with the liberation of hydrogen ions (Anderson and Garven (1987) through the following reaction:

$$Me^{2+} + H_2S = 2H^+ + MS \quad (6)$$

The hydrogen ions are further consumed in further dissolution of the dolomite,

$$CaMg(CO_3)_2 + 4H^+ = Ca^{2+} + Mg^{2+} + 2CO_2 + 2H_2O, \quad (7)$$

and the resultant CO_2 can react with water to liberate more H^+ and thus continue the process. A key point which Anderson and Garven (1987) emphasize is that sulphides do not precipitate at the same time as dolomite. This chemical control may account for the alternating sparry dolomite and sulphides seen at many Mississippi Valley-type deposits (Leach and Sangster, 1993).

This model is favoured for the RBDM mineralization as it accounts for the presence of pyrobitumen (hydrocarbon); early low $\delta^{13}C$ values evolving to higher values in the dolomite gangue, suggesting mixing of an organic carbon source with an inorganic

source; widespread dissolution of the host rock due to production of acidic solutions; salinities of fluid inclusions implying metal transport as chloride complexes; the distinct banding of the sulphides and the gangue minerals; and the high $\delta^{34}S$ values for the sulphides derived from ^{34}S-enriched pore fluids formed by Rayleigh-type fractionation. To account for the high $\delta^{34}S$ values it is assumed that fractionation between sulphate and sulphide was minimal (i.e. the ^{34}S-enriched sulphate produced ^{34}S-enriched H_2S which was subsequently incorporated into the sulphides). Late stage quartz, feldspar, and calcite formation was probably a function of cooling.

It is interesting to compare the paragenetic sequence of the RBDM mineralization with data obtained for an experimental study for precipitation mechanisms in MVT deposits by Plumlee *et al.* (1994). The experimental paragenetic sequence, Figure 5.8, is identical to the observed sequence of the RBDM. The model of Plumlee *et al.* evokes the mixing of a limestone-staturated (Ca-rich) brine with a dolomite-saturated (Mg-rich) brine of the same salinity, but with differing temperatures, Ca/Mg ratios, H_2S, and metal contents. The inadequacies of the experimental model however, to explain geochemical and field observations for the RBDM are many, and include: the meteoric signature within the early dolomite when the model requires a brine-like signature; the need for H_2S to be present in each solution as opposed to evidence which suggests dissolved sulphate; and the mixing of a low temperature limestone-saturated solution with a higher temperature dolomite-saturated solution, when the dolomite saturated brine should be present within the RBDM.

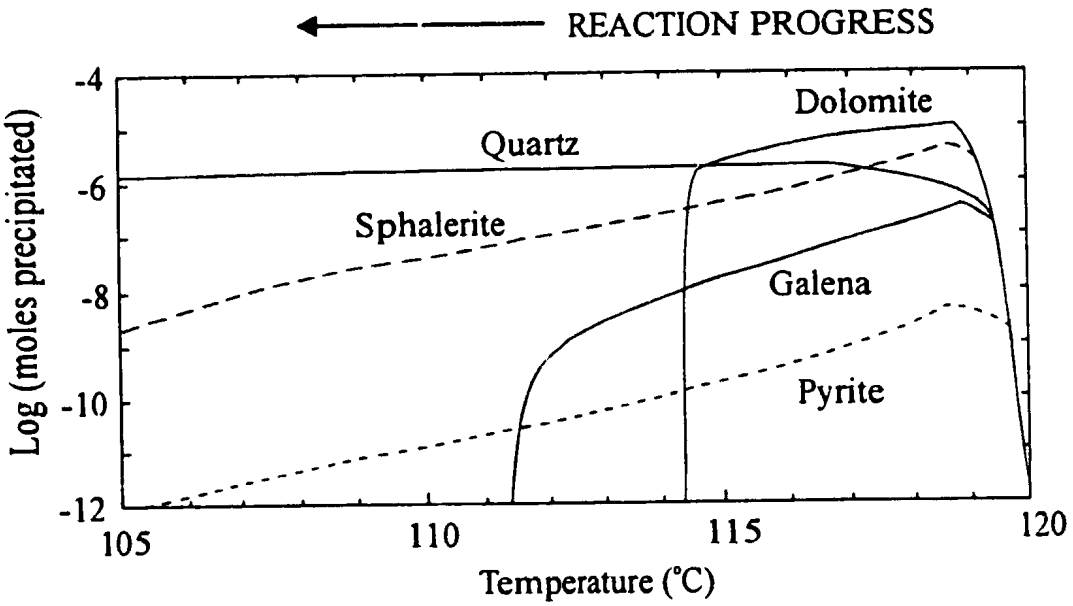

Fig 5.8: Reaction path diagram showing minerals precipitated during mixing of a 120°C brine (10^{-4} *m* H_2S) with a 100°C, limestone-saturated, high H_2S (1.5×10^{-2} *m*) brine of the same total salinity. Taken from Fig. 13, Plumlee et al. (1994).

Timing of the mineralization is difficult due to the lack of minerals which can be dated within the Ramah Gp., but it appears from field relationships that it predates deformation caused by the Torngat Orogeny. Evidence that the mineralization was pre-deformational occurs on the south shore of Delabarre Bay where a thrust plane contains quartz-carbonate veined Reddick Bight dolomite blocks (Plates 4.14 and 4.15). These blocks indicate veining must have occurred prior to the propagation of the thrust faults. While mineralization occurred in the east, progressive deformation between the Nain and Rae Structural Provinces was taking place to the west. The deformation front progressed to the east and resulted in folding, thrusting, and thickening of the Ramah Gp.. During deformation, sulphides were remobilized from the RBDM along fault planes. An example of the remobilization would be the Loch Bears Gut showing, where polymetallic sphalerite, galena, and pyrite veins occur within the RBDM, proximal to a thrust fault.

5.5.6 Other Epigentic mineralization related to basin compaction

Mineralization at the Normore Showing, at the base of the Rowsell Harbour Fm., is somewhat problematic in terms of interpretation, due to the limited extent of the outcrop. From field observations it appears that the vein may have resulted from fracturing caused by dewatering of the basal clastic sequence (Rowsell Harbour and Reddick Bight formations) during the Torngat Orogenic event (Van Kranendonk *et al.*, 1993). This scenario is postulated due to the mineralogy of the showing (Cu-rich), and the orientation of the vein (096/54°N) because; (1) copper-rich fluids would be expected

to have been derived from the clastic basal sequences (Brown, 1992), and (2) the S_1 stress orientation of the Torngat Orogen corresponds closely to the trend of the quartz vein.

It is probable that the Wilton No.2 Showing, cutting the Warspite Fm., is a result of epigenetic mineralization derived from the same MVT forming fluids precipitating quartz and galena as vein type mineralization. The veins were subsequently deformed by the progressing deformation due to the Torngat Orogen.

5.5.7 Geological Implications

Sangster (1990) noted that although the Proterozoic represents six times the length of Paleozoic time, MVT deposits are relatively scarce. He also suggested that "All the 'normal' ingredients considered necessary to generate MVT deposits in Palaeozoic rocks - carbonate platforms, unconformities, shale basins, sea-water sulphate, hydrocarbons, etc. - were present in the Proterozoic, yet deposits are anomalously lacking in rocks of Proterozoic age". Prior to this study, only five MVT deposits were known within Proterozoic rocks (Figure 5.9): Vazante, Brazil (Thorman *et al.*, 1979); Gayna River, Canada (Hewton, 1982); Nanisivik, Canada (Olsen, 1984); Coxco, Australia (Walker *et al.*, 1983); and Pering, Transvaal District, South Africa (Wheatley *et al.*, 1986; Martini, 1990; Duane *et al.*, 1991). Only the Transvaal District is believed to be of Paleoproterozoic age; the Coxco Deposit is Paleoproterozoic to Mesoproterozoic in age. Some doubt exists over the classification of the Proterozoic Black Angel deposit in Greenland (Pedersen, 1980), and the Balmat-Edwards deposit in the USA (Whelan *et al.*,

1984). Most workers now believe that these ore bodies belong to the SEDEX class of mineralization (Sangster, 1990).

Figure 5.9 illustrates the geographical and temporal distribution of MVT mineralization, and includes the mineralization from the RBDM. MVT mineralization within the Ramah Gp.has all of Sangster's (1990) "normal" ingredients, including: a thin carbonate sequence; an unconformity marking the change from a shallow shelf sequence to a deep water shale basin; seawater sulphate, modified due to bacterial reduction; and hydrocarbons. All of these basic "ingredients" have been integrated during the early stages of the Torngat Orogeny, ca 1860 Ma (Van Kranedonk *et al.*, 1993), resulting in MVT mineralization, via a process similar to the gravity model of Garven and Freeze (1986). The uniqueness of the Ramah Gp. MVT mineralization lies in the proposed biogenically reduced sulphate model. Although this model is not new, it is the only model that can account for the very high (~ 30‰) $\delta^{34}S$ values of sulphides from contemperaneous seawater with a $\delta^{34}S$ of 12‰ (Hayes, 1992). The Ramah Gp. mineralization is the first documented case where MVT sulphides formed as the sole consequence of biogenic activity, and not due to the process of normal evaporite formation. MVT mineralization present within the Ramah Gp. represents the second oldest form of this style of mineralization described to date, and is the oldest described from Laurentia.

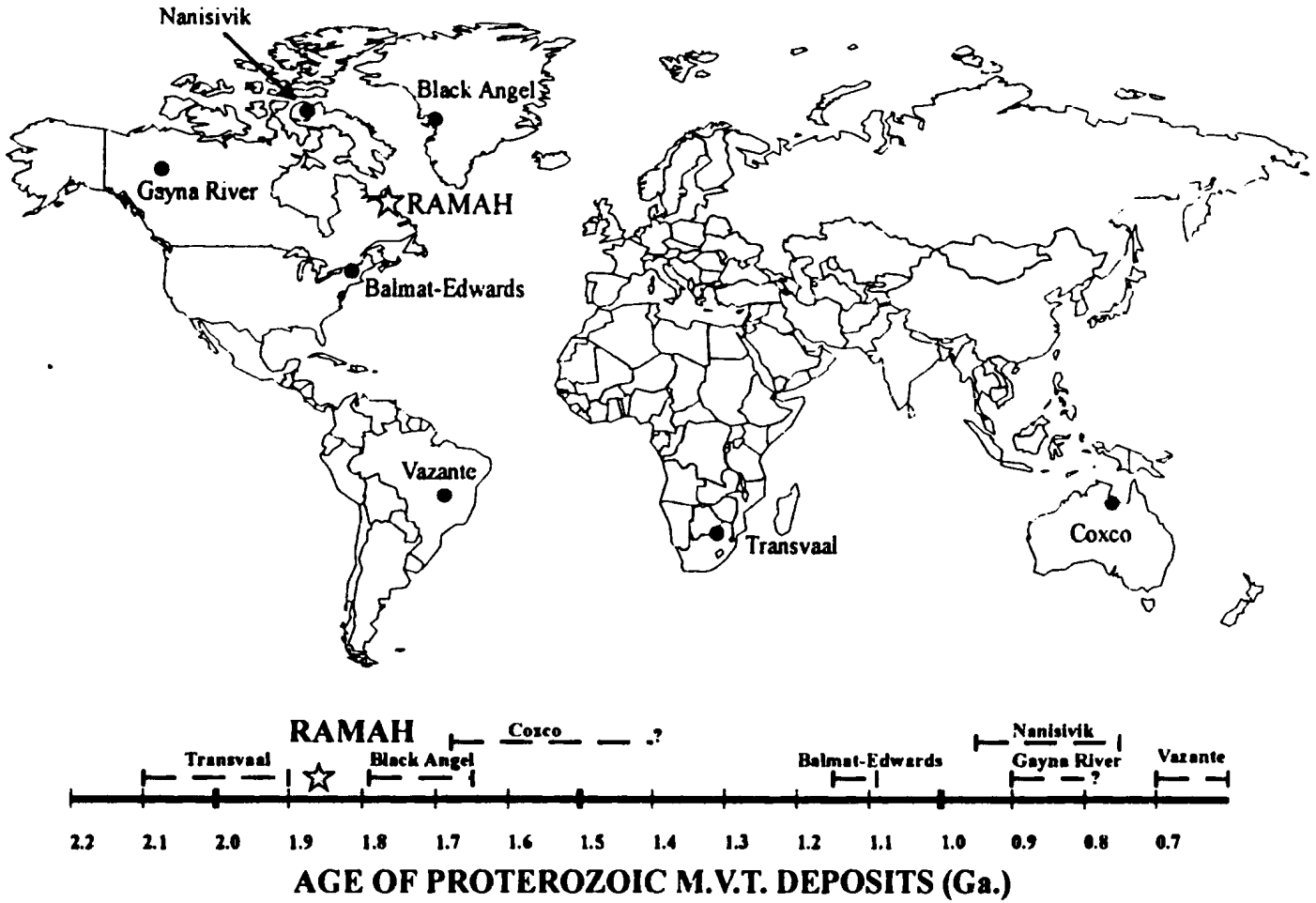

Fig 5.9: Temporal and spacial distribution of Mississippi Valley-type mineralization from rocks of Proterozoic age. The mineralization present within the RBDM may represent the oldest example of MVT mineralization in Laurentia, with a lower age limit of approx. 1.86 Ga. Mineralization within the Transvaal sequence is composed of several deposits making up a mining district. Black Angel and Balmat-Edwards may represent the SEDEX class of ore deposits

5.6 Recommendations for future work

Future work which needs to be addressed within the Ramah Group to further clarify the proposed model should include: detailed sampling of the Nullataktok Formation for diagenetic pyrite to validate the presence of Rayleigh-type fractionation; detailed mapping of brecciated zone within the RBDM to clearly define the paragenetic sequence of the host carbonates and the accompanying mineralization; cathodoluminescent micro-stratigraphy on most of the RBDM mineralized outcrops would identify the extent and number of fluids responsible for the carbonate mineralization; further carbon and oxygen isotopic measurements on the RBDM gangue minerals to resolve the fluid composition and temperture (feldspar-quartz mineral pairs): Ar-Ar or K-Ar dating of muscovite associated with sphalerite in the RBDM to constrain the age of mineralization.

5.7 Conclusions

As with all metallogenic models, the processes of plate tectonics are the overall controlling factors, and mineralization within the Ramah Group resulted from two episodes of plate movement: rifting to form the Ramah basin, and expulsion of brines from the basin during the Torngat Orogen.

Rifting of the Nain craton (ca 2.0 Ga) resulted in what is interpreted to have been a passive continental margin, and the deposition of the Rowsell Harbour and Reddick Bight formations in a shallow shelf environment. The RBDM is stratigraphically the highest within the shelf sequence and exhibits sub-aerial features such as tepee structures and

dissolution breccias. Rapid deepening of the basin occurred following Reddick Bight Dolomite Member deposition, and resulted in the formation of anoxic bottom waters, enriched in organics, transgressing the shelf sequence. A two metre thick pyrite bed, formed as a result of sulphur-reducing bacteria, led to the formation of ^{34}S-enriched seawater within the restricted basin. This enriched water was subsequently incorporated into the pore fluids of the shales due to further sedimentation. Deep water sedimentation continued, resulting in the formation of the carbonate-rich Warspite Formation, the shale-rich Typhoon Peak Formation, and greywacke-rich Cameron Brook Formation. Following sedimentation, the Ramah Group was intruded by numerous gabbro-diabase sills, resulting in the formation of Cu and Ni mineralization within or adjacent to the sills.

The most extensive mineralization within the Ramah Group resulted from fluid migration as a consequence of the Torngat Orogeny (1860 Ma) (Bertrand *et al.*, 1993). The collision of the Nain and Rae Structural Provices resulted in the expulsion of evolved brines containing metal chloride complexes, and ^{34}S-enriched pore water. These brines migrated along areas of significant porosity and permeability where they mixed with hydrocarbons present within the Reddick Bight Dolomite Member. Precipitation of sulphides occurred by sulphate reduction in areas of increased porosity such as collapse breccia zones within the dolomite, or in the thin dolomite unit above the chert bed, as a result of overpressuring of the mineralizing fluids. As the Torngat orogen deformation front progressed eastwards sulphides were remobilized within fault zones.

The style of mineralization present within the Reddick Bight Dolomite Member is comparable to the Mississippi Valley-type (MVT), and as such represents the second oldest occurrence of this style of mineralization identified to date.

REFERENCES

Anderson, G.M. 1975. Precipitation of Mississippi Valley-type ores. Economic Geology, **70**, 937-942.

Anderson, G.M. 1983. Some geochemical aspects of sulfide precipitation in carbonate rocks. *In* G. Kisvarsanyi, S.K. Garven, W.P. Pratt, and J.W. Koenig (eds.), Proceedings of International Conference on Mississippi Valley Type Lead-Zinc Deposits. University of Missouri-Rolla Press, Rolla, MO, 61-76.

Anderson, G.M., and Garven, G. 1987. Sulfate-sulfide-carbonate associations in Mississippi Valley-type lead-zinc deposits. Economic Geology, **82**, 482-488.

Anderson, G.M., and Macqueen, R.W. 1988. Mississippi Valley-type lead-zinc deposits. *In* Ore Deposit Models Geoscience Canada Reprint Series 3, 79-90.

Anderson, R.Y., Dean, W.E., Kirkland, D.W., and Snider, H.I. 1972. Permian Castile varved evaporite sequence. West Texas and New Mexico. Geological Society of America Bulletin, **83**, 59-86.

Ashwal, L.D., Wooden, J.L., and Emslie, R.F. 1987. Sr, Nd, Pb isotopes in Proterozoic intrusives astride the Grenville front in Labrador: Implications for crustal contamination and basement mapping. Geochemica et Cosmochimica Acta, **50**, 2571-2585.

Assereto, R.L.A.M. and Kendall, C.G.St.C. 1977. Nature, origin and classification of peritidal tepee structures and related breccias. Sedimentology, **24**, 153-210.

Ault, W.V., and Jesen, M.L. 1963. Summary of sulfur isotope standards. *In* Jesen, M.L. (ed.), Biochemistry of sulfur isotopes. National Science Foundation, Symposium Proceedings, Yale University, April 12-14.

Ault, W.V., and Kulp, J.L. 1960. Sulfur isotopes and ore deposits. Economic Geology, **55**, 73-100.

Baertschi, P. 1976. Absolute ^{18}O content of Standard Mean Ocean Water. Earth and Planetary Science Letters, **31**, 341.

Bajwah, Z.U., Seccombe, P.K., and Offler, R. 1987. Trace element distribution, Co:Ni ratios and genesis of the Big Cadia iron-copper deposit, New South Wales, Australia. Mineralium Deposita, **22**, 292-300.

Barton, P.B., Jr. 1967. Possible role of organic matter in the precipitation of the Mississippi Valley ores. *In* J.S. Brown (ed.) Genesis of Stratiform Lead-Zinc-Barite-Fluorite Deposits in Carbonate Rocks. Economic Geology Publishing Co., Lancaster, PA, Monograph 3, 371-377.

Barton, P.B., Jr., and Bethke, P.M. 1987. Chalcopyrite disease in sphalerite: pathology and epidemiology. The American Mineralogist, 72, 451-467.

Beales, F.W., and Jackson, S.A. 1966. Precipitation of lead-zinc ores in carbonate reservoirs as illustrated by Pine Point ore field, Canada. Institute of Mining and Metallurgy, Transactions, Section B, 75, B8278-B8285.

Bell, R. 1884. Observations on the geology, mineralogy, zoology and botany of the Labrador coast, Hudson Strait and Bay. Geological Survey of Canada, Report of Programs, 1882-1885.

— 1895. The Labrador peninsular. Scottish Geography Magazine, 11, 335-361.

Berg, J.H. 1981. Stratigraphic comparison of the Snyder and Falls Brook Groups with the Mugford Group. *In* The Nain Anorthosite Project, Labrador: Field Report 1981, Morse, S.A. (Ed). Contribution Number 40, Department of Geology and Geography, University of Massachusetts, 16-22.

Bertrand, J. -M., , Van Kranendonk, M.J., Hanmer, S., and Roddick, J.C. 1990. Structural and metamorphic geochronology of the Torngat Orogen in the North River-Nutak transect area, labrador: preliminary results of U-Pb dating. Geoscience Canada, 17, 297-301.

Bertrand, J. -M., Roddick, J.C., Van Kranendonk, M.J., and Ermanovics, I. 1993. U-Pb geochronology of deformation and metamorphism across a central transect of Early Proterozoic Torngat Orogen, North River map area, Labrador. Canadian Journal of Earth Sciences, 30, 1470-1489.

Blackwell, J.D. 1976. Ramah reconnaissance. Cominco Limited, Unpublished Report, 20pp.

Bottomley, D.J., Veizer, J., Nielsen, H., and Moczydlowska, M. 1992. Isotopic composition of disseminated sulfur in Precambrian sedimentary rocks. Geochemica et Cosmochimica Acta, 56, 3311-3322.

Bralia, A., Sabatini, G., and Troja, F. 1979. A revaluation of the Co/Ni ratio in pyrite as geochemical tool in ore genesis problems. Mineneralium Deposita, 14, 353-374.

Bridgewater, D., and Schiøtte, L. 1991. The Archean gneiss complex of northern Labrador. A review of current results, ideas and problems. Bulletin of the Geological Society of Denmark, **39**, 153-166.

Brown, A.C. 1992. Sediment-hosted stratiform copper deposits. Geoscience Canada, **19**, 125-141.

Brown, J.S. 1967. Genesis of Stratiform Lead-Zinc-Barite-Fluorite Deposits in Carbonate Rocks. Economic Geology Publishing Company, Lancaster, PA, Monograph 3, 443pp.

Burst, J.F. 1969. Diagenesis of Gulf Coast clayey sediments and its possible relation to petroleum migration. Bulletin of the American Association of Petroleum Geologists, **53**, 73-93.

Calon, T.J. and Jamison, W. 1992. Structural evolution of the eastern borderland of the Torngat Orogen, Kiki Lake transect, Saglek Fiord area, northern Labrador. Eastern Canadian Shield Onshore-Offshore Transect (ECSOOT), LITHOPROBE Report **32**, 90-112.

Calon, T.J. and Jamison, W. 1993. Structural evolution of the eastern borderland of the Torngat Orogen, Kiki Lake transect, Saglek Fjord area, northern Labrador: progress report for 1993. Eastern Canadian Shield Onshore-Offshore Transect (ECSOOT), LITHOPROBE Report **34**, 89-99.

Cameron, E.M. and Garrels, R.M. 1980. Geochemical composition of some Precambrian shales from the Canadian Shield. Chemical Geology, **28**, 181-197.

Carlsson, G. 1901. Report on iron pyrites property, Rowsels Harbour, Labrador, Nfld. Unpublished Report, 8pp.

Carter, W.C. 1902. Labrador Rowsell's Habrour pyrite. Unpublished Report, 2pp.

Christie, A.M. 1952. Geology of the northern coast of Labrador, from Grenfell Sound to Port Manvers, Newfoundland. Geological Survey of Canada, Paper **52-22**, 16pp.

Class, C., Altherr, R., Volker, F, Eberz, G., and McCulloch, M.T. 1994. Geochemistry of Piocene to Quaternary alkali basalts from the Huri Hills, northern Kenya. Chemical Geology, **113**, 1-22.

Claypool, G.E., Holser, W.T., Kaplan, I.R., Sakai, H., and Zak, I. 1980. The age curves of sulfur and oxygen isotopes in marine sulfate and their mutual interpretation. Chemical Geology, **28**, 199-260.

Coleman, A.P. 1921. Northeastern part of Labrador, and New Quebec. Geological Survey of Canada, Memoir **124**, 66pp.

Collerson, K.D., Meroz, Y., Gill, C., and Nutman, A.P. 1992. Early crustal growth in the North Atlantic craton: new field and isotopic constraints from Labrador American Geophysical Union Fall Meeting, Program Abstracts, EOS, **72**, 542.

Craig, H. 1957. Isotopic standards for carbon and oxygen and correction factors for mass spectrometric analysis of carbon dioxide. Geochemica et Cosmochimica Acta, **12**, 133-149.

Daly, R.A. 1902. The geology of the northeast coast of Labrador. Bulletin of Harvard University, Museum of Comparative Zoology, Volume 38, Geological Series, **5**, 205-270.

Delabarre, E.B. 1902. Report of the Brown-Harvard expedition to Nachvak, Labrador, in the year 1900. Geographical Society of Philadelphia, Bulletin, **3**, 65-212.

Doe, B.R., and Zartman, R.E. 1979. Plumbotectonics. *In* H. Barnes, (ed.), Geochemistry of Hydrothermal Ore Deposits. Wiley, New York, Chapter 2, 22-70.

Douglas, G.V. 1953. Notes on localities visted on the Labrador coast in 1946 and 1947. Geological Survey of Canada, Paper **53-1**, 67pp.

Duane, M.J., Kruger, F.J., Roberts, P.J., and Smith, C.B. 1991. Pb and Sr isotopes and origin of Proterozoic base metal (fluorite) and gold deposits, Transvaal Sequence, South Africa. Economic Geology, **86**, 1491-1505.

Engel, A.E.J., Clayton, R.N., and Epstein, S. 1958. Variation in isotopic composition of oxygen and carbon in Leadville limestone (Mississippian, Colorado) and in its hydrothermal and metamorphic phases. Journal of Geology, **66**, 374-393.

Ermanovics, I.F. 1993. Geology of Hopedale block, southern Nain Province, and the adjacent Proterozoic terranes, Labrador, Newfoundland. Geological Survey of Canada, Memoir **431**, 161pp.

Ermanovics, I.F., Van Kranendonk, M.J., Corriveau, L., Mengel, F., Bridgewater, D., and Sherlock, R. 1989. The boundary between zone of the Nain-Churchill provinces in the North River-Nutak map areas, Labrador. *In* Current Research, Part C, Geological survey of Canada, Paper **89-1C**, 385-394.

Evans, T.L., Campbell, F.A., and Krouse, H.R. 1968. A reconnaissance study of some western Canadian lead-zinc deposits. Economic Geology, **63**, 349-359.

Fairchild, I.J. 1985. Petrology and carbonate chemistry of some Dalradian dolomitic metasediments: preservation of diagenetic textures. Journal of Geological Society of London, **142**, 167-18.5

Faure, G. 1986. Priciples of Isotope Geology. 2nd edition, Wiley, New York.

Fogwill, W.D. 1966. Rowsell Harbour pyrite prospect in northern Labrador. Newfoundland and Labrador Corporation Limited, Unpublished report, 12pp.

Garven, G., and Freeze, R.A. 1984. Theoretical analysis of the role of groundwater flow in the genesis of stratabound ore deposits. 2: Quantitative results. American Journal of Science, **284**, 1125-1174.

Ghazban, F, Schwarcz, H.P., and Ford, D.C. 1990. Carbon and sulfur isotope evidence for *in situ* reduction of sulfate, Nanisivik lead-zinc deposits, Northwest Territories, Baffin Island, Canada. Economic Geology, **85**, 360-375.

Gize, A.P., and Hoering, T.C. 1980. The organic matter in Mississippi Valley-type deposits. Carnegie Institution, Washington Year Book, **79**, 384-388.

Goldschmidt, V.M., 1958. Geochemistry. Oxford University Press, London, 730pp.

Goodwin, A.M. 1991. Precambrian Geology: The Dynamic Evolution of the Continental Crust. Academic Press, London, 666pp.

Green, B.A. 1972. Geological map of Labrador. Newfoundland Department of Mines, Agriculture and Resources, Mineral Resources Division.

Hall, A.J., McConville, P., Boyce, A.J., and Fallick, A.E. 1994. Sulphides with high $\delta^{34}S$ from the Late Precambrian Bonahaven Dolomite, Argyll, Scotland. Mineralogical Magazine, **58**, 486-490.

Hayes, J.M., Lambert, C.J., and Strauss, H. 1992. The sulfur-isotopic record. *In* Schopf, J.W., and Klein, C. (eds.), The Proterozoic Biosphere. Cambridge University Press, Cambridge, 129-132.

Hayashi, K., Fujisawa, H., Ohmoto, H., and Holland, H.D. 1994. Geochemistry of Proterozoic (~ 1.9 Ga) sedimentary rocks from the Labrador district, Canada. Mineralogical Magazine, **58A**, 398-399.

Helgeson, H.C. 1969. Thermodynamics of hydrothermal systems at elevated temperatures and pressures. American Journal of Science, **267**, 729-804.

Hewton, R.S. 1982. Gayna River: A Proterozoic Mississippi Valley-type zinc-lead deposit. *In* R.W. Hutchinson, C.D. Spence, and J.M. Franklin (eds.), Precambrian Sulphide Deposits, Geological Association of Canada, Special Paper 25, 667-700.

Hoefs, J. 1987. Stable Isotope Geochemistry. 3rd edition, Springer-Verlag, Berlin.

Hoffman, P.F. 1988. United plates of America, the birth of a craton: Early Proterozoic assembly and growth of Laurentia. Annual Reveiw of the Earth and Planetary Sciences, **16**, 543-603.

Hofmann, A.W. 1988. Chemical differentiation of the Earth: the relationship between mantle, continental crust and oceanic crust. Earth and Planetary Science Letters, **90**, 297-314.

Holmden, C., and Muehlenbachs, K. 1993. The $^{18}O/^{16}O$ ratio of 2-billion-year-old seawater inferred from ancient oceanic crust. Science, **259**, 1733-1736.

Hornbrook, E.H.W., and Friske, P.W.B. 1987. Regional stream sediment and water geochemical data, Labrador, 1986. Geological Survey of Canada, Open File 1354.

Huerta-Diaz, M.A., and Morse, J.W. 1992. Pyritization of trace metals in anoxic marine sediments. Geochemica et Cosmochimica Acta, **56**, 2681-2702.

Hussey, A.M. 1994. Petrography, Geochemistry, and Economic Potential of Stratiform Sills in the Aphebian Ramah Group, Northern Labrador. B.Sc. (Hons.) thesis, Memorial University of Newfoundland, St. John's, 111pp.

Kendall, C.G.St.C. and Warren, J. 1987. A reveiw of the origin and setting of tepees and their assiciated fabrics. Sedimentology, **34**, 1007-1027.

Knight, I. and Morgan, W.C. 1976. Stratigraphic subdivision of the Aphebian Ramah Group, northern Labrador. Geological Survey of Canada, Paper **77-15**, 31pp.

Knight, I. and Morgan, W.C. 1981. The Aphebian Ramah Group, northern Labrador. Geological Survey of Canada, Paper **81-10**, 313-330.

Lambert, I.B., and Donnelly, T.H. 1992. Global oxidation and a supercontinent in the Proterozoic: evidence from stable isotope trends. *In* M. Schidlowski, S. Golubic, M.M. Kimberley, D.M. McKirdy, P.A. Trudinger (eds.), Early Organic Evolution: Implications for Mineral and Energy Resources. Springer-Verlag, 408-414.

Land, L.S. 1985. The origin of massive dolomite. Journal of Geological Education, **33**, 112-125.

Large, D.E. 1983. Sediment-hosted massive sulphide lead-zinc deposits: an empirical model. Mineralogical Association of Canada Short Course Notes, **8**, 1-29.

Lazenby, M.E.C. 1980. Prehistoric sources of chert in northern Labrador: Fieldwork and preliminary analyses. Arctic, **33**, 247-259.

Laznicka, P. 1988. Breccias and Coarse Fragmentites: petrology, environments, associations, ores. Developments in Economic Geology, 25. Elsevier, Amsterdam, 832pp.

Leach, D.L., and Sangster, D.F. 1993. Mississippi valley-type lead-zinc deposits. *In* Kirkham, R.V., Sinclair, W.D., Thorpe, R.I., and Duke, J.M. (eds.), Mineral Deposit Modeling. Geological Association of Canada, Special Paper 40, 289-314.

Loftus-Hills, G., and Solomon, M. 1967. Cobalt, nickel and selenium in sulphides as indicators of ore genesis. Mineralium Deposita, **2**, 228-242.

Macqueen, R.W., and Powell, T.G. 1983. Organic geochemistry of the Pine-Point lead-zinc orefield and region, North West Territories, Canada. Economic Geology, **78**, 1-25.

McConnell, J.W. and Honarvar, P. 1993. First-year results of detailed stream-sediment and water geochemical surveys in northern Labrador. Newfoundland Department of Mines and Energy, Geological Survey Branch, Open File Report **LAB/0969**.

McConnell, J.W. 1994. Detailed Survey of stream-sediment and water geochemistry, northern Labrador. *In* Current Research, Newfoundland Department of Mines and Energy, Geological Survey Branch, Report **94-1**, 313-326.

McKirdy, D.M., and Imbus, S.W. Precambrian petroleum: a decade of changing perceptions. *In* M. Schidlowski, S. Golubic, M.M. Kimberley, D.M. McKirdy, P.A. Trudinger (eds.), Early Organic Evolution: Implications for Mineral and Energy Resources. Springer-Verlag, 147-175.

McLean, S. 1991. Report on prospecting and lithogeochemical surveys on reserved licence 104R held by Falconbridge Limited, Saglek Fiord property, Labrador, N.T.S. 14L/11, 14, August 1990. Unpublished Report.

McLimans, R.K. 1977. Geologic, fluid inclusion, and stable isotope studies of the Upper Mississippi Valley zinc-lead district, southwest Wisconsin. Ph.D. Thesis, the Pennsylvania State University (unpublished), 175pp.

Machado, N., Goulet, N., and Gariépy, C. 1989. U-Pb geochronology of reactivated Archean basement and Hudsonian metamorphism in the northern Labrador Trough. Canadian Journal of Earth Sciences, **26**, 1-15.

Machel, H.G. 1985. Cathodoluminescence in calcite and dolomite and its chemical interpretation. Geoscience Canada, **12**, 139-147.

MacLeod, J.L. 1984. Report on the reconnaissance geological and geochemical surveys, Ramah Bay, Labrador. Esso Minerals Canada, Unpublished Report, 34pp.

MacLeod, J.L. 1985. Assessment report on the reconnaissance geological surveys of the Saglek Fiord-Delabarre Bay area, Labrador. Esso Minerals Canada, Unpublished Report, 44pp.

Macnamara, J., and Thode, H.G. 1950. Comparison of the isotopic constitution of terrestrial and meteoric sulfur. Physical Reviews, **78**, 307-308.

Macqueen, R.W., and Powell, T.G. 1983. Organic geochemistry of the Pine Point lead-zinc ore field and region, Northwest Territories, Canada. Economic Geology, **78**, 1-25.

Marikos, M.A., Laudon, R.C., and Leventhal, J.S. 1986. Solid insoluble bitumen in the Magmont West orebody, southeast Missouri. Economic Geology, **81**, 1983-1988.

Marshall, D.J. 1988. Cathodoluminescence of Geological Materials. Unwin Hyman, London, Chapter 7, 76-93.

Marsters, J.L. 1954. Report on Rowsell's Harbour pyrites property, Labrador. Unpublished Report, Brinex G54016, 17pp.

Martini, J.E. 1990. The Genadendal Zn-Pb-Mn mineralization, South Africa: A possible early Proterozoic alkaline hydrothermal system. Economic Geology, **85**, 1172-1185.

Mathews, A., and Katz, A. 1977. Oxygen isotope fractionation during the dolomitization of calcium carbonate. Geochemica et Cosmochimica Acta, **41**, 1431-1438.

Maynard, J.B. 1983. Geochemistry of Sedimentary Ore Deposits. Springer-Verlag, New York, 305pp.

Maynard, J.B. 1991. Shale-hosted deposits of Pb, Zn, and Ba: Syngenetic deposition from exhaled brines in deep marine basins. *In* Sedimentary and Diagenetic Mineral Deposits: A Basin Analysis Approach to Exploration. Reviews in Economic Geology, **5**, 177-185.

Medlin, W.L. 1961. Thermoluminescence in dolomite. Journal of Chemical Physics, **34**, 672-677.

Medlin, W.L. 1968. The nature of traps and emission centers in thermoluminescent rock minerals. *In* McDougall, D.J. (ed.), Thermoluminescence of Geological Materials. Academic Press, New York, 193-223.

Mengel, F. 1988. Thermotectonic evolution of the Proterozoic-Archaean boundary in the Saglek area, northern Labrador. Ph.D. thesis, Memorial University of Newfoundland, St. John's. 349pp.

Mengel, F., Rivers, T., and Reynolds, P. 1991. Lithotectonic elements and tectonic evolution of Torngat Orogen, Saglek Fiord, northern Labrador. Canadian Journal of Earth Sciences, **28**, 1407-1423.

Meyer, J.R. and Dean, P.L. 1988. Industrial minerals and follow-up lake- and stream-sediment geochemical anomalies in Labrador. *In* Current Research, Newfoundland Department of Mines and Energy, Mineral Development Division, Report **88-1**, 247-259.

Mitchell, A.H.G. 1985. Mineral deposits related to tectonic events accompanying arc-continent collision. Transactions of the Institute of Mining and Metallurgy (Section B: Applied earth science), **94**, B115-B125.

Moorbath, S., O'Nions, R.K., and Pankhurst, R.J. 1973. Early Archean age for the Isua iron-formation, West Greenland. Nature, **245**, 138-139.

Morgan, W.C. 1975. Geology of the Precambrian Ramah Group and basement rocks in the Nachvak Fiord-Saglek Fiord area, north Labrador. Geological Survey of Canada, Paper 74-54, 42pp.

— 1978. Ramah Group volcanics - Labrador. *In*: Wanless, R.K. & Loveridge, W.D. (eds.) Rubidium - Strontium isochron age studies, Report 2. Geological Survey of Canada, Paper 77-14, 56-61.

— 1979a. Geology, Nachvak Fiord-Ramah Bay, Newfoundland-Quebec. Geological Survey of Canada, Map 1469A, scale 1:50 000.

— 1979b. Geology, Bears Gut-Saglek Fiord, Newfoundland. Geological Survey of Canada, map 1478A, scale 1:50 000.

Nunn, G.A.C., Heaman, L.M., and Krough, T.E. 1990. U-Pb geochronological evidence for Archean crust in the continuation of the Rae Province (eastern Churchill Province), Grenville Front Tectonic Zone, Labrador. Geoscience Canada, 17, 259-265.

Nutman, A.P., Fryer, B.J., and Bridgewater, D. 1989. The early Archaean Nulliak (supracrustal) assemblage, northern Labrador. Canadian Journal of Earth Sciences, 26, 2159-2168.

Nutman, A.P. and Collerson, K.D. 1991. Very early Archean crustal-accretion complexes preserved in the North Atlantic craton. Geology, 19, 791-794.

Oder, C.R.L., and Hook, J.W. 1950. Zinc deposits in the southeastern states. *In* Snyder, F.G. (ed.), Symposium on Mineral Resouces of the Southeastern United States. University of Tennessee Press, Knoxville, Tennessee, 72-87.

Ohle, E.L. 1959. Some considerations in determining the origin of ore deposits of the Mississippi Valley-type - Part I. Economic Geology, 54, 769-789.

— 1980. Some considerations in determining the origin of ore deposits of the Mississippi Valley-type - Part II. Economic Geology, 75, 161-172.

Ohmoto, H., Kaiser, C.J., and Geer, K.A. 1990. Systematics of sulphur isotopes in recent marine sediments. *In* H.K. Herbert, and S.E. Ho (eds.), Stable Isotopes and Fluid Processes in Mineralization. Geology Department and University Extension, the University of Western Australia Publication No. 23, 70-120.

Ohmoto, H., and Rye, R.O. 1979. Isotopes of sulfur and carbon. *In* Barnes, H.L. (ed.), Geochemistry of Hydrothermal Ore Deposits, 2nd Edition, Wiley, New York, 509-567.

Olsen, R.A. 1984. Genesis of paleokarst and stratabound zinc-lead sulfide deposits in a Proterozoic dolostone, northern Baffin Island, Canada. Economic Geology, **79**, 1056-1103.

O'Neil, J.R., Clayton, R.N., and Mayeda, T.K. 1969. Oxygen isotope fractionation in divalent metal carbonates. Journal of Chemical Physics, **51**, 5547-5558.

Oliver, J. 1986. Fluids expelled tectonically from orogenic belts: Their role in hydrocarbon migration and other geologic phenomena. Geology, **14**, 99-102.

Osmond, R. 1992. Report on prospecting and lithogeochemical surveys on reserved licence 104R held by Falconbridge Limited, Saglek Fiord property, Labrador, N.T.S. 14L/11, 14, July, 1992. Unpublished Report, 10pp.

Pandalai, H.S., Majumder, T., and Chandra, D. 1983. Geochemistry of pyrite and black shales of Amijhore, Rohtas District, Bihar, India. Economic Geology, **78**, 1505-1513.

Pedersen, F.D. 1980. Remobilization of the massive sulfide ore of the Black Angel mine, Central West Greenland. Economic Geology, 75, 1022-1041.

Pickney, D.M., and Rafter, T.A. 1972. Fractionation of sulfur isotopes during ore deposition in the Upper Mississippi Valley zinc-lead district. Economic Geology, **67**, 315-328.

Plumlee, G.S., Leach, D.L., Hofstra, A.H., Landis, G.P., Rowan, E.L., and Virts, J.G. 1994. Chemical reaction path modeling of ore deposition in Mississippi Valley-type Pb-Zn deposits of the Ozark region, U.S. Midcontinent. Economic Geology, **89**, 1361-1383.

Price, L.C. 1976. Aqueous solubility of petroleum as applied to its origin and primary migration. American Association of Petroleum Geology Bulletin, **60**, 213-244.

Raiswell, R., and Plant, J. 1980. The incorporation of trace elements in pyrite during diagenesis of black shales, Yorkshire, England. Economic Geology, **75**, 684-699.

Roedder, E. 1962. Studies of fluid inclusions. I: low-temperature application of a dual-purpose freezing and heating stage. Economic Geology, **57**, 1045-1061.

Roedder, E. 1976. Fluid-inclusion evidence on the genesis of ores in sedimentary and volcanic rocks. *In* K.H. Wolf (ed.), Handbook of Strata-bound and stratiform ore deposits: I. Principles and General Studies. Elsevier Scientific Publishing Company, Amsterdam, 67-110.

Roedder, E. 1984. Fluid Inclusions. Mineralogical Society of America, Reviews in Mineralogy Volume 12, 644pp.

Rollinson, H. 1993. Using Geochemical Data: Evaluation, Presentation, Interpretation. Longman Scientific and Technical, Harlow, 352pp.

Ryan, A.B., Martineau, Y., Bridgewater, D., and Schiøtte, L. 1983. The Archean-Proterozoic boundary in the Saglek Fiord area, Labrador, Report 1. *In* Current Research, Part A. Geological Survey of Canada, Paper **83-1A**, 297-304.

Ryan, A.B., Martineau, Y., Korstgård, J, and Lee, D. 1984. The Archean-Proterozoic boundary in northern Labrador, Report 2. *In* Current Research, Part A. Geological Survey of Canada, Paper **84-1A**, 545-551.

Ryan, A.B., Krough, T.E., Hearman, L. Schärer, U., Phillipe, S., and Oliver, G. 1991. On recent geochronological studies in the Nain Province, Churchill Province, and the Nain plutonic suite, north-central Labrador. *In* Current Research (1991). Newfoundland Department of Mines and Energy, Geological Survey Branch, Report **91-1**, 257-261.

Rye, R.O., and Ohmoto, H. 1974. Sulfur and carbon isotopes and ore genesis: a review. Economic Geology, **69**, 826-842.

Sasaki, A., and Krouse, H.R. 1969. Sulfur isotopes and the Pine Point lead-zinc mineralization. Economic Geology, **64**, 718-730.

Sangster, D.F. 1968. Relative sulphur isotope abundances of ancient seas and strata-bound sulphide deposits. The Geological Association of Canada. Proceedings, **19**, 79-91.

Sangster, D.F. 1990. Mississippi Valley-type and SEDEX lead-zinc deposits; a comparative examination. Transactions of the Institute of Mining and Metallurgy (Section B: Applied earth science), **99**, B21-B42.

Sangster, D.F., Nowlan, G.S., and McCracken, A.D 1994. Thermal comparison of Mississippi Valley-type lead-zinc deposits and their host rocks using fluid inclusion and conodont color alteration index data. Economic Geology, **89**, 493-514.

Schidlowski, M. 1989. Evolution of the sulphur cycle in the Precambrian. *In* P. Brimblecombe and A. Yu. Lein (eds.) Evolution of the Global Biogeochemical Sulphur Cycle. J. Wiley & Sons, New York, 3-19.

Schiøtte, L., Compston, W., and Bridgewater, D. 1989. Ion probe U-Th-Pb zircon dating of polymetamorphic orthogneisses from northern Labrador, Canada. Canadian Journal of Earth Sciences, **26**, 1533-1556.

Smyth, W.R. 1976. Geology of the Mugford Group, northern Labrador. *In* Report of Activities for 1976, Gibbons, R.V. (ed); Newfoundland Department of Mines and Energy, Mineral Development Division, Report **77-1**, 72-79.

Smyth, W.R. and Knight, I. 1978. Correlation of the Aphebian supracrustal sequences, Nain Province, northern Labrador. *In* Newfoundland Department of Mines and Energy, Mineral Development Division, Report **78-1**, 72-79.

Snelgrove, A.K. 1938. Minerals and mineral resources of Newfoundland. Geological Survey of Newfoundland. Information Circular, **4.**

Speer, J.A. 1976. The stratigraphy and metamorphism of the Snyder Group, Labrador. Ph.D. thesis (unpublished), Virginia Polytechnique Institute and State University, Virginia.

St-Onge, M.R., Lucas, S.B., and Parrish, R.R. 1992. Terrane accretion in the internal zone of the Ungava orogen, northern Quebec, Part I. Tectonostratigraphic assemblages and their tectonic implications. Canadian Journal of earth Sciences, **29**, 746-764.

Stacey, J.S., and Kramers, J.D. 1975. Approximation of terrestrial lead isotope evolution by a two-stage model. Earth and Planetary Science Letters, **26**, 207-221.

Stienhauer, H. 1814. Notice relative to the geology of the coast of Labrador. Geological Society of London, Transactions, **2**, 488-494.

Strauss, H. 1986. Carbon and sulfur isotopes Percambrian sediments from the Canadian Shield. Geochemica et Cosmochimica Acta, **50**, 2653-2662.

Sverjensky, D.A. 1981. The origin of a Mississippi Valley-type deposit in the Viburnum Trend, Southeast Missouri. Economic Geology, **76**, 1848-1872.

Sverjensky, D.A. 1986. Genesis of Mississippi Valley-type lead-zinc deposits. Annual Review of Earth and Planetary Sciences, **14**, 177-199.

Sverjensky, D.A., Rye, D.M., and Doe, B.R. 1979. The lead and sulfur isotopic compositions of galena from a Mississippi Valley-type deposit in the New Lead Belt, southeast Missouri. Economic Geology, 74, 149-153.

Swinden, H.S., Wardle, R.J., Davenport, P.H., Gower, C.F., Kerr, A., Miller, R.R., Nolan, L., Ryan, A.B., and Wilton, D.H.C.. 1991. Minerali exploration opportunities in Labrador: A perspective for the 1990's. Current Research (1990), Newfoundland Department of Mines and Energy, Geological Survey Branch, Report 94-1, 349-390.

Tallman, P. 1995. Report on claims staked in the Ramah Group, northern Labrador. Unpublished report.

Taylor, B.E. 1987. Stable isotope geochemistry of ore-forming fluids. Mineralogical Association of Canada, Short Course in Stable Isotope Geochemistry of Low Temperature Fluids, **13**, 357-445.

Taylor, F.C. 1969. Reconnaissance of a part of the Precambrian Shield, northeastern Quebec and northern Labrador. Geological Survey of Canada, Paper **68-43.**

Taylor, F.C. 1970. Reconnaissance geology of a part of the Precambrian Shield; northeastern Quebec and northern Labrador; Part 2. Geological Survey of Canada, Paper **70-24**.

Taylor, F.C. 1971. A revision of Precambrian structural provinces in northeastern Quebec and northern Labrador. Canadian Journal of Earth Sciences, **8**, 579-584.

Taylor, F.C. 1974. *In* Age Determinations and Geological Studies, K-Ar Isotopic Ages., Report 12, Geological Survey of Canada, Paper **74-2**.

Taylor, H.P. 1974. The application of oxygen and hydrogen isotope studies to problems of hydrothermal alteration and ore deposition. Economic Geology, **69**, 843-883.

Thorman, C.H., and Nahass, S. 1979. Reconaissance geologic study of the Vazante zinc district Minas Gerais, Brazil. U.S. Geological Survey Professional Paper **1126-I**, I1-I12.

Tissot, B.P., and Welte, D.H. 1978. Petroleum formation and occurrence, a new approach to oil and gas exploration. Springer-Verlag, New York, 539 pp.

Tucker, M.E. 1992. Sedimentary Petrology: and introduction to the origin of sedimentary rocks. Blackwell Scientific Publications, Oxford. 260 pp.

Van Kranendonk, M.J. 1990. Structural history and geotectonic evolution of the eastern Torngat Orogen in the North River map area, Labrador. *In* Current Research, Part C, Geological Survey of Canada Paper, **90-1C**, 81-96.

Van Kranendonk, M.J. 1992. Geological Evolution of the Archean Nain Province and the Early Proterozoic Torngat Orogen as seen along a Transect in the North River-Nutak Map Area, Northern Labrador, Canada. Ph.D. thesis, Queen's University, Kingston, Ontario, 477pp.

Van Kranendonk, M.J., St-Onge, M.R., and Henderson, J.R. 1993. Paleoproterozoic tectonic assembly of northeastern Laurentia through multiple indentations. Precambrian Research, **63**, 325-347.

Viets, J.B., and Leach, D.L. 1990. Genetic implications of regional and temporal trends in ore fluid geochemistry of Mississippi Valley-type deposits in the Ozark region. Economic Geology, **85**, 842-861.

Vine, J.D., and Tourtelot, E.B. 1970. Geochemistry of black shale deposits - summary report. Economic Geology, **65**, 253-272.

Walker, R.N., Gulson, B, and Smith, J. 1983. The Coxco deposit – a Proterozoic Mississippi Valley-type deposit in the McArthur River District, Northern Territory, Australia. Economic Geology, **78**, 214-249.

Wapples, D.W. 1981. Organic Geochemistry for exploration Geologists. Burgess Publishing, Minneapolis, Minnesota.

Wardle, R.J. 1983. Nain-Churchill Province cross-section, Nachvak Fiord, northern Labrador. *In* Current Research, Newfoundland Department of Mines and Energy, Report **83-1**, 68-89.

Wardle, R.J. 1984. Nain-Churchill Province cross-section, Rivière Baudancourt-Nachvak Lake. *In* Current Research, Newfoundland Department of Mines and Energy, Report **84-11**, 1-11.

Wheatley, C.J.V., Whitfield, G.G., Kenny, K.J., and Birch, A. 1986. The Pering carbonate-hosted zinc-lead deposit, Griqualand West. *In* C.R. Anhaeusser and S. Maske (eds.), Mineral Deposits of Southern Africa (Vol I & II), Geological Society of South Africa, Johannesburg, 867-874.

Whelan, J.F., Rye, R.O., and De Lorraine, W. 1984. The Balmat-Edwards zinc-lead deposits – synsedimentary ore from Mississippi Valley-type fluids. Economic Geology, **79**, 239-265.

Wilson, M. 1989. Igneous Petrologenesis. A Global Tectonic Approach. Chapman and Hall, London, 466pp.

Wilton, D.H.C. 1991. Metallogenic and tectonic implications of Pb isotope data for galena separates from the Labrador Central Mineral Belt. Economic Geology, **86**, 1721-1736.

Wilton, D.H.C. 1994. The Mugford Group, northern Labrador, revisited: notes from a continuing study. *In* Current Research, Newfoundland Department of Mines and Energy, Geological Survey Branch, Report **94-1**, 409-414.

Wilton, D.H.C. and Phillips, D. 1992. Preliminary report on examination of sulphide-rich zones within the Proterozoic Snyder, Group, Labrador, and the SEDEX potential of these units. *In* Current Research, Newfoundland Department of Mines and Energy, Geological Survey Branch **92-1**, 431-439.

Wilton, D.H.C., Archibald, S.M., Hussey, A.M., and Butler, Jr., R.W. 1993. Report on metallogenic investigations on the north Labrador coast during 1993. Newfoundland Department of Mines and Energy, Geological Survey Branch, Open File **LAB/0996**, 19pp.

Wilton, D.H.C., Archibald, S.M., Hussey, A.M., and Butler, Jr., R.W. 1994. Metallogeny of the Ramah Group: Discovery of a new Pb-Zn exploration target, northern Labrador. *In* Current Research, Newfoundland Department of Mines and Energy, Geological Survey Branch, Report **94-1**, 415-428.

Wilton, D.H.C., Churchill, R.A., and Saunders, G.K. 1993. Stratigraphy and metallogeny of the Cod Island and Calm Cove formations, Mugford Group, northern Labrador. *In* Current Research, Newfoundland Department of Mines and Energy, Geological Survey Branch, Report **93-1**, 91-102.

Zartman, R.E., and Doe, B.R. 1981. Plumbotectonics - the model. Tectonophysics, **75**, 135-162.

APPENDIX I

Table I.1: Lithological description of samples with grid references

Sample No.	Description	UTM	
SA 93-		Easting	Northing
001	Nullataktok shale containing pyrite and dolostone	486300	6525800
002	Malachite in Warspite Fm. dolomite (Wilton No. 1)	486300	6525800
003a	Galena in quartz vein cutting Warspite Fm. (Wilton No. 2)	486520	6526900
003b	Quartz vein cutting Warspite Fm.	486855	6526900
004	Quartz and calcite vein	487200	6527550
005	Dark quartzitic rock in Nullataktok Fm.	487200	6527500
006	Massive pyrite and chert (deformed pyrite bed)	481100	6523700
007	Chalcopyrite in quartz vein (Butter Showing)	481400	6523500
008	Chalcopyrite, pyrite, and pyrrohotite in quartz vein (Butter Showing)	481400	6523500
009	Dolomite from Warspite Fm.	486600	6525900
010	Pyrite in Warspite Fm. dolomite	486600	6525900
011	Chert with pyrite at margins	487100	6532600
012	Purple sandstone in Reddick Bight Fm.	487200	6532000
013	Compact cherty shale containing pyrite	487200	6531900
014	Massive pyrite with quartz veining (float)	487200	6531850
015	Brecciated chert containing sphalerite (Sandman/Walsh Occurrence)	487200	6531800
016a	Manganesse stained gossan	487000	6531600
016b	Chert with pyrobitumen	487150	6531650
017a	Green clay within chert bed	487000	6531400
017b	Bedded pyrite with 2 generations of pyrite	487150	6531650
018	Iron stained impure chert	487000	6531350
019	Black chert	487150	6531250
020	Massive bedded pyrite (Sandman Occurrence)	487150	6531250
021	Gritty sanstone within chert bed	487150	6531250
022	Green shale beneath pyrite bed	487150	6531250
023	Basal conglomerate (Rowsell Harbour Fm.)	488950	6532300
024	Fuchsite stained quartzite boulder (Rowsell Harbour Fm.)	488950	6532350
025	Base of Rowsell Harbour Volcanic Member (RHVM)	489100	6530850
026	Middle of RHVM with chalcopyrite (Zambia Occurrence)	489100	6530850
027	Top of RHVM	489100	6530850
028	Pyrite in Nullataktok Fm. chert lenses	488000	6530000
029	Quartz vein thought to contain sphalerite (Nullataktok Fm.)	488150	6530100
030	Galena in Archean gneiss	489600	6529990
031	Sphalerite in Archean gneiss	489600	6529990
032	Archean gneiss hosting samples SA93- 031/032	489600	6529990
033	Quartz-carbonate vein with pyrobitumen in RBDM	481500	6535900
034	RBDM	481500	6535900
035	Course grained dolomite (RBDM)	481230	6536400
036	Nodular mudstone with pyrite	480550	6536450
037	Granular pyrite and graphitic shale beneath chert bed	480550	6536450
038	Green-grey siltstone beneath pyrite bed	480550	6536450

Table I.1 (cont.): Lithological description of samples with grid references

Sample No.	Description	UTM
039	Black and white chert (70cm above pyrite bed)	480550 6536450
040	Chert immediately above pyrite bed	482900 6532900
041	Massive pyrite bed	482900 6532900
042	Secondary pyrite and quartz veins	482900 6532900
043	Green-grey siltstone beneath pyrite bed	482900 6532900
044	Pyrobitumen in RBDM	486100 6533450
045	Warspite Fm. shale with pyrite	482150 6525450
046a	Quartz vein cutting Warspite Fm. shales containing pyrite and pyrobitumen	482500 6525400
046b	Light grey siltstone with pyrite (Typhoon Peak Fm.)	482600 6525400
047a	Shale with pyrite (Typhoon Peak Fm.)	482700 6525400
047b	Pillow lava of the RHVM	489100 6522450
048a	Glass around pillow rim (RHVM)	489250 6621850
048b	Pillow lava of the RHVM	489250 6521850
049	Chert nodule with green mineral from Nullataktok Fm.	488600 6521050
050	Pyrite in RBDM	488750 6521150
051	Recrystallized pyrite from pyrite bed	488150 6521550
052	Fine bedded pyrite with secondary pyrite	488150 6521550
053	Quartz vein with pyrite cutting pyrite bed	488150 6521550
054	Green siltstone beneath pyrite bed	488150 6521550
055	Chert bed	488150 6521550
056	Ultrabasic pod	487500 6512150
057	Thermally metamorphosed pyrite bed	489600 6508950
058	Sphalerite and pyrite in RBDM (Panda Showing)	489900 6508700
059	Pyrite-pyrrhotite bed	489600 6508500
060	Sphalerite, chalcopyrite, and pyrite in RBDM (Saor Alba Occurrence)	488650 6503800
061	Pyrobitumen in RBDM	480650 6503800
062	Chert bed	488520 6503650
063	Pyrrhotite-pyrite bed (Near Miss Showing)	488520 6503650
064	Green siltstone beneath pyrrhotite-pyrite bed	488520 6503650
065	Pyrrhotite-pyrite bed	489050 6502550
066	Sphalerite and pyrite in RBDM (3-0 Occurrence)	489000 6500400
067	Leached quartzite (Reddick Bight Fm.)	489000 6500400
068	Sphalerite in quartz-dolomite vein in RBDM (Galloway Occurrence)	488850 6499850
069	Massive sphalerite, with minor galena (Blackjack Showing)	488600 6499600
070	Hematite conglomerate float (Rowsell Harbour Formation)	474350 6545730
071	Pyrite and pyrobitumen in RBDM	474100 6543850
072	Sphalerite, pyrite, and chert boulder (Adams Lake Showing)	474200 6543700
073a	Massive poorly bedded pyrite bed	479500 6540700
073b	Secondary pyrite in pyrite bed	479500 6540700
074	Nullataktok Fm. shale with pyrite	479500 6540700
075	RBDM boulders with quartz veining in thrust plane	479500 6540700
076	Pyrrhotite and chalcopyrite within veined RBDM	484700 6486700

Table I.1 (cont.): Lithological description of samples with grid references

Sample No.	Sample description	UTM	
W93-		Easting	Northing
014	Malachite with chalcopyrite in dyke (Butter extension Showing)	481070	6523590
015	Representative sample of upper quartzite in the Reddick Bight Fm	486650	6532540
016	Hematite spotted sandstone	486400	6532300
016a	Dolomite with secondary porosity	486400	6532200
017a	Pyrite nodule	486050	6532040
017b	Pyite in shale	486050	6532040
017c	Pyrite in quartz vein	486050	6532040
017d	Pyrite nodule	486050	6532040
017e	Nullataktok Fm. shale	486050	6532040
018	Pyrite bed	485955	6532145
019a	Two generations of pyrite in chert	485955	6532145
019b	Chert with Pyrrhotite	485955	6532145
019c	Sphalerite and pyrrhotite in chert (Gates Occurrence)	485955	6532145
020a	Pyrite in Warspite Fm.	484930	6529590
020b	Flow (?) in Warspite	484930	6529590
021	Dolomite from the Typhoon Peak Fm.	486250	6530410
022	Chert with Pyrite	486490	6531900
023a	Chalcopyrite and Pyrite in quartz vein (Normore Showing)	489350	6529500
023b	Host quartzite to 23a	489350	6529500
024	Rowsell Harbour Volcanic Member	489260	6529740
025a	Galena and chalcopyrite in Archean vein	486460	6529900
025b	Galena in Archean vein	486460	6529900
025c	Galena, sphalerite and chalcopyrite in Archean vein	486460	6529900
026a	Sphalerite and pyrobitumen (Pine Harbour Showing)	484805	6534100
026b	Pyrobitumen in RBDM	484805	6534100
027	Slate with quartz vein and calcite cemented shale breccia	481040	6533240
028	Disseminated pyrite in Nullataktok Fm. slate	479360	6531280
029	Leucogneiss with large garnets (3cm)	477840	6531470
030	Chert	476630	6531200
031a	Chert nodule and pyrite	483120	6532970
031b	Chert	483120	6532970
031c	Massive pyrite	483120	6532970
032	Reddick Bight dolomite	486075	6533455
033	Sphalerite, pyrite and pyrobitumen in RBDM (Reddick Bight N. Shore)	486075	6533455
034a	RBDM	488050	6528130
034b	Chert fragment in RBDM	488100	6528200
035	Nullataktok Fm. slate	479140	6529150
036a	Nullataktok Fm. slate	478930	6529460
036b	Pyrobitumen in RBDM	478930	6529460
036c	Dolomitic sandstone from Reddick Bight Fm.	478930	6529460
036d	Sphalerite, galena, and pyrite in RBDM. (McLeod #1 Showing)	478930	6529460

Table I.1 (cont.): Lithological description of samples with grid references

Sample No.	Description	UTM	
037a	Pyrite bed	480390	6526830
037b	Chert bed	480390	6526830
037c	Diabase sill	480390	6526830
038	Sphalerite and pyrite within brecciated chert bed (Large Showing)	488050	6513050
039	Diabase sill	487680	6510000
039a	Sphalerite, galena, and pyrite in the RBDM (Panda Showing)	489855	6508935
039b	Galena and sphalerite in the RBDM (Daniel's Point Showing)	490255	6508540
039c	Brecciated dolomite (RBDM)	489855	6508935
039d	Pyrobitumen in RBDM	489855	6508935
039e	Black quartzite beneath RBDM	489855	6508935
040	Galena in RBDM (V-8 Showing)	489395	6510735
041a	Galena in quartz-carbonate vein	488300	6498450
041b	Pyrobitumen in RBDM	488300	6498450
041c	Secondary calcite	488300	6498300
041d	RDBM (possible stromatolites)	480300	6498250
041e	Pyrobitumen in RBDM	488300	6498200
041f	Sphalerite, galena, and pyrite vein cutting RBDM (Loch Bears Gut Showing)	488330	6498180
041g	Thrust gouge (Loch Bears Gut Showing)	488330	6498180
041h	Nullataktok Fm. Shale	488330	6498180
042	RHVM	490038	6503260
043	Fuchsite in Rowsell Harbour Fm. quartzite	474250	6545050
044	Pyrobitumen in RBDM	473980	6543790
045	Black chert	474005	6543600
046	Pyrobitumen in RBDM	474030	6542170
047	Quartzite (+talcy substance)	479460	6540800
048	Chert and massive pyrite	479450	6540580
049	Native sulphur in Nullataktok Fm. shale	479650	6540220
049a	Nullataktok Fm. shale (host to sulphur)	479650	6540220
050	Pyrobitumen in RBDM	480380	6539480
051	Pyrobitumen in RBDM	481320	6540490
052	Quartz pebble conglomerate (Rowsell Harbour Fm.)	481750	6541600
053	Galena (Pyrite and chalcopyrite) in RBDM (Char showing)	485775	6486985
054a	Diabase sill	484700	6486985
054b	Pyrite bed	484700	6486985
054c	Chert bed	484700	6486985
055a	Sphalerite in RBDM (Godot Showing)	481230	6534760
055b	Pyrite in RBDM (Godot Showing)	481230	6534760
055c	Pyrobitumen in RBDM	481230	6534760
056a	Galena in RBDM (Blue Sky Showing)	478575	6530850
056b	Sphalerite and pyrite (Blue Sky Showing)	478575	6530850

APPENDIX II

Table II.1: Assay data from selected samples from occurrences in the Ramah Group, northern Labrador

Showing	Sample No.	% Cu	%Pb	% Zn	Ag (ppm)	As (ppm)	Ba (ppm)	Cd (ppm)	Ni (ppm)
Pine Harbour	W93-26A	0.004	0.004	5	5	31	--	78	2,828
Macleod No. 1	W93-36D	--	0.97	8.1	5.6	21	--	130	--
	W93-36D1	--	0.74	1.1	4.8	18	--	17	--
Reddick Bight North shore	W93-33	--	0.001	0.004	0.2	1.5	64	--	--
Sandman/Walsh float	SA93-015	0.005	0.012	0.91	0.3	6	--	--	18
Large	W93-038	0.002	0.018	0.34	0.4	--	--	--	--
Panda	Panda 1	0.003	0.002	14.0	1.4 (5.0)	13	--	370	22
	Panda 2	--	1.05	3.7	1.3 (3.0)	5.2	--	96	--
	Panda 3	0.003	0.006	14.0	0.4	12	--	330	--
Daniel's Point	W93-39B	--	4.3	0.3	3.1 (2)	2.3	--	10	--
V-8	W93-40	--	0.42	0.067	0.5	--	--	--	--
Loch Bears Gut	LBG	0.004	3.3	0.84	7.2 (7.0)	119	--	24	85
	W93-41A	0.006	0.39	13.0	3.1 (4)	122	--	420	120
Black Jack	Black Jack 1		0.021	31.0	15 (15)	3.9	--	1350	--
	Black Jack 2	--	15.0	18.0	40 (93)	4.2	--	710	--
Char	W93-53	0.005	1.98	0.006	6.8 (22)	245	4,201	--	38
Adams Lake	SA93-072	0.019	0.05	0.99	3	74	--	130	51
Butter	SA93-007	0.48	0.0[illegible]	0.005	3.1	0.8	--	--	--
Nearmiss	AH93-012	0.024	--	0.007	0.3	3.6	--	--	150
	AH93-015	0.075	0.013	0.065	0.9	8.8	150	6	470
Godot*	W93-55a	4.68PPM	--	1424.34PPM	NA	--	--	NA	5.62
Blue Sky*	W93-56a	--	731.11	1563.7	NA	--	41.59	NA	--
	W93-56b	--	10.13PPM	1983.79	NA	--	25.79	NA	--

All data analysed by Newfoundland Dept. Natural Resources, St. John's, except for samples marked with an asterisk (*) which were analysed at MUN using XRF methods, -- below detection limits, ( ) repeat samples.

Table II.2: XRF data for samples from the Ramah Group

ppm rock	Na2O	MgO	Al2O3	SiO2	P2O5	S	Cl	K2O	CaO	Sc	TiO2	V	Cr	MnO	Fe2O3T
SA93-001	1.39%	3.95%	17.60%	60.17%	0.05%	2250	45	4.76%	0.06%	12	0.55%	80	126	0.00%	5.22%
SA93-002	0.27%	4.04%	12.19%	61.39%	0.08%	1461	169	3.71%	0.41%	17	0.77%	704	171	0.02%	10.89%
SA93-004	0.09%	3.76%	2.40%	30.37%	0.02%	610	115	0.14%	42.74%	25	0.28%	27	107	0.06%	1.80%
SA93-005	6.11%	6.00%	10.64%	78.94%	0.08%	618	100	0.16%	0.16%	4	0.14%	10	44	0.00%	0.19%
SA93-006	0.03%	0.17%	0.11%	27.62%	0.01%	267594	40	0.02%	0.18%	3	0.01%	10	6	0.00%	33.16%
SA93-007	0.00%	0.02%	0.12%	97.30%	0.02%	4024	27	0.01%	0.04%	4	0.03%	2	24	0.00%	1.49%
SA93-010	0.36%	0.63%	2.57%	25.28%	0.02%	247230	163	0.76%	0.91%	6	0.23%	19	48	0.01%	38.95%
SA93-011	0.12%	1.75%	0.95%	84.41%	0.01%	21627	35	0.25%	2.82%	5	0.04%	45	10	0.07%	4.76%
SA93-012	0.11%	1.33%	7.36%	79.66%	0.03%	446	37	3.27%	1.22%	2	0.12%	9	24	0.02%	4.43%
SA93-013	3.11%	4.44%	6.35%	39.31%	0.04%	70536	28	0.46%	10.69%	34	0.63%	93	30	0.14%	17.88%
SA93-014	0.08%	0.00%	0.41%	68.77%	0.01%	141648	87	0.18%	2.46%	1	0.03%	17	9	0.02%	14.51%
SA93-015	1.40%	0.96%	1.78%	54.90%	0.04%	111662	25	0.10%	3.74%	14	0.16%	25	44	0.03%	19.42%
SA93-016A	0.59%	0.40%	2.43%	27.61%	0.06%	2582	82	1.22%	0.13%	5	0.61%	771	56	0.00%	55.06%
SA93-016B	0.00%	4.90%	0.08%	78.96%	0.01%	3987	36	0.03%	7.61%	3	0.01%	17	11	0.22%	2.44%
SA93-017A	0.07%	8.03%	9.96%	37.19%	0.24%	26125	35	3.29%	0.93%	19	0.85%	172	43	0.06%	24.00%

ppm rock	Ni	Cu	Zn	Ga	As	Rb	Sr	Y	Zr	Nb	Ba	Ce	Pb	Th	U
SA93-001	4.64	15.24	41.22	20.34	5.11	146.79	12.20	7.87	116.21	7.94	1492.30	11.05	20.08	9.19	3.41
SA93-002	186.44	6411.77	152.02	18.30	0.00	121.13	6.32	10.69	116.25	6.27	1043.71	38.13	19.03	5.97	23.09
SA93-004	4.87	3.74	6.38	2.53	7.38	3.07	229.77	11.17	41.53	3.74	8.02	12.26	4.17	1.96	0.00
SA93-005	0.00	0.00	0.00	5.56	4.22	3.73	22.57	9.93	238.34	3.50	56.01	12.48	17.89	1.14	1.28
SA93-006	240.60	174.59	950.90	2.21	86.00	0.61	2.07	0.54	5.73	0.52	0.00	1.75	49.59	3.09	5.64
SA93-007	0.00	961.52	0.00	0.95	8.68	0.00	1.75	0.50	5.53	1.57	0.00	12.80	0.00	0.00	0.00
SA93-010	158.91	649.85	791.84	8.39	0.00	23.62	1.90	2.14	37.46	4.41	105.37	6.80	286.70	5.39	0.00
SA93-011	1.61	11.55	0.00	3.46	7.75	2.88	14.47	2.33	13.30	1.93	45.87	12.07	17.17	1.14	1.74
SA93-012	13.62	3.04	3.40	6.21	13.73	55.26	36.54	4.75	94.34	4.79	581.94	73.95	6.55	2.59	0.20
SA93-013	36.38	97.74	7922.93	22.63	1.30	9.59	250.72	6.84	59.90	3.58	71.25	10.61	66.51	2.24	0.50
SA93-014	81.73	29.38	9.39	0.37	273.56	0.43	38.34	2.71	3.16	1.60	45.21	16.31	3.45	0.00	1.73
SA93-015	57.85	105.05	18162.97	14.31	84.88	1.13	118.57	10.38	16.87	1.44	4.61	19.10	448.34	1.25	0.00
SA93-016A	12.36	66.83	27.07	4.56	3407.01	7.67	8.14	15.54	88.06	7.20	308.50	133.43	79.16	3.06	5.07
SA93-016B	3.41	3.46	0.00	0.00	7.29	0.00	19.06	0.91	2.91	0.98	0.00	0.00	0.00	0.00	0.68
SA93-017A	0.00	104.26	89.21	36.30	0.00	47.00	19.38	14.84	125.96	12.81	579.82	45.66	6.00	1.39	1.72

All values in ppm unless otherwise indicated. Values of 0% or 0ppm indicate that concentrations were below the limits of detection.

Table II.2 (cont.): XRF data for samples from the Ramah Group

ppm rock	Na2O	MgO	Al2O3	SiO2	P2O5	S	Cl	K2O	CaO	Sc	TiO2	V	Cr	MnO	Fe2O3T
SA93-017B	0.07%	0.37%	1.32%	35.64%	0.01%	260260	46	0.85%	1.60%	2	0.12%	179	36	0.02%	26.42%
SA93-018	0.72%	1.91%	3.23%	26.39%	0.03%	1427	42	0.41%	0.59%	9	0.22%	51	6	1.12%	60.07%
SA93-019	0.01%	0.08%	0.26%	91.30%	0.00%	40342	130	0.09%	0.60%	0	0.01%	37	11	0.00%	4.64%
SA93-020	0.34%	0.00%	2.11%	30.16%	0.01%	318248	23	0.99%	0.04%	0	0.08%	131	9	0.00%	28.12%
SA93-020A	0.02%	0.00%	0.32%	1.29%	0.00%	455395	53	0.14%	0.02%	0	0.05%	97	9	0.00%	37.49%
SA93-021	0.99%	9.43%	4.11%	60.54%	0.02%	23123	39	1.42%	8.70%	17	0.08%	338	43	0.21%	8.04%
SA93-022	3.60%	13.04%	13.93%	45.02%	0.17%	13469	39	0.74%	0.30%	55	2.44%	515	173	0.04%	13.28%
SA93-023	0.07%	4.69%	9.73%	54.76%	0.00%	798	82	3.62%	7.94%	15	0.22%	71	6942	0.26%	9.37%
SA93-024	0.07%	0.56%	14.65%	74.13%	0.01%	455	53	4.72%	0.02%	0	0.13%	28	176	0.00%	1.53%
SA93-028	0.26%	0.52%	5.09%	46.45%	0.01%	196922	25	1.89%	0.02%	0	0.28%	121	241	0.00%	21.99%
SA93-031	0.80%	0.69%	19.03%	63.90%	0.08%	600	88	5.16%	1.28%	0	0.26%	25	12	0.05%	3.27%
SA93-032	3.76%	0.39%	17.75%	69.25%	0.07%	811	135	4.46%	0.29%	0	0.27%	22	7	0.02%	2.18%
SA93-036	0.32%	15.28%	9.72%	26.43%	0.30%	8457	59	1.50%	11.19%	48	2.16%	450	16	0.49%	24.10%
SA93-037	0.13%	0.00%	0.29%	51.15%	0.01%	213042	0	0.04%	0.03%	0	0.17%	20	18	0.00%	21.53%
SA93-038	0.06%	18.74%	11.57%	45.85%	0.05%	649	0	5.25%	0.17%	50	0.92%	300	583	0.05%	15.13%

ppm rock	Ni	Cu	Zn	Ga	As	Rb	Sr	Y	Zr	Nb	Ba	Ce	Pb	Th	U
SA93-017B	221.72	132.79	161.78	3.11	397.82	4.99	18.32	1.89	12.15	2.49	213.80	0.00	62.05	2.49	2.87
SA93-018	56.28	88.79	155.04	3.79	12.11	10.30	25.58	10.63	110.05	15.30	39.59	0.00	10.91	0.00	0.35
SA93-019	2.80	12.50	0.00	0.90	25.81	0.45	4.32	0.15	6.31	1.72	36.21	0.00	4.26	0.45	0.10
SA93-020	168.82	63.41	15.87	5.03	540.25	3.35	4.31	1.12	8.71	3.32	189.57	0.00	62.69	0.00	0.00
SA93-020A	330.17	66.66	14.84	4.16	863.73	1.39	2.41	0.00	8.61	2.28	0.00	0.00	112.90	0.00	6.33
SA93-021	0.00	38.65	22.44	15.68	0.00	20.05	67.88	3.48	23.46	1.34	92.46	0.00	0.00	0.00	0.00
SA93-022	35.39	150.70	160.62	28.09	0.00	11.16	15.18	37.75	215.81	13.83	84.19	0.00	0.00	0.00	5.97
SA93-023	604.15	36.98	39.69	17.75	0.00	70.91	169.96	3.77	12.46	5.53	1226.83	0.00	0.00	0.00	0.00
SA93-024	6.67	0.00	0.00	8.84	0.00	60.59	17.57	3.48	121.12	2.10	561.11	0.00	0.00	14.15	0.00
SA93-028	61.59	33.99	15.55	7.03	246.84	19.33	1.89	1.50	23.61	3.00	258.79	0.00	16.62	3.67	0.00
SA93-031	0.00	20.40	686.78	23.61	0.00	93.98	26.34	1.83	157.44	2.52	1386.74	52.81	910.16	4.34	0.00
SA93-032	0.00	0.00	76.59	22.42	0.00	102.08	188.31	1.29	168.32	3.26	1192.84	44.36	112.06	10.32	0.00
SA93-036	28.18	197.10	79.62	23.65	0.00	22.50	72.55	44.90	181.40	12.46	77.91	48.12	5.94	0.00	0.00
SA93-037	159.97	19.28	53.31	0.00	641.85	0.00	0.00	5.40	14.70	2.79	40.90	0.00	11.39	0.00	0.00
SA93-038	122.91	172.20	70.10	14.65	25.11	107.34	3.52	9.21	49.57	3.42	101.13	0.00	0.00	0.00	0.00

All values in ppm unless otherwise indicated. Values of 0% or 0ppm indicate that concentrations were below the limits of detection.

Table II.2 (cont.): XRF data for samples from the Ramah Group

ppm rock	Na2O	MgO	Al2O3	SiO2	P2O5	S	Cl	K2O	CaO	Sc	TiO2	V	Cr	MnO	Fe2O3T
SA93-039	0.00%	0.01%	0.00%	98.53%	0.00%	662	0	0.01%	0.02%	0	0.00%	0	10	0.00%	0.11%
SA93-040	0.03%	1.13%	0.45%	91.33%	0.00%	14138	66	0.13%	1.41%	0	0.03%	34	17	0.03%	2.81%
SA93-041	0.02%	0.00%	0.26%	1.39%	0.00%	441013	0	0.10%	0.02%	0	0.03%	68	13	0.00%	37.77%
SA93-042	0.22%	0.04%	2.95%	36.42%	0.02%	279323	45	1.17%	0.09%	0	0.33%	398	150	0.00%	26.46%
SA93-043	1.60%	8.31%	12.81%	55.73%	0.16%	7566	55	3.76%	3.58%	39	1.58%	375	225	0.11%	9.31%
SA93-046B	1.13%	5.37%	17.56%	60.73%	0.07%	5878	405	4.98%	0.55%	22	0.67%	224	167	0.02%	4.52%
SA93-047A	1.48%	3.68%	9.98%	70.95%	0.12%	12578	117	2.49%	0.17%	17	0.62%	130	131	0.00%	4.71%
SA93-049	0.59%	4.09%	6.57%	77.49%	0.03%	650	53	0.72%	0.05%	11	0.24%	83	52	0.02%	5.31%
SA93-050	0.10%	10.68%	7.70%	37.16%	0.04%	22075	101	3.13%	18.12%	18	0.27%	88	69	0.21%	10.83%
SA93-051	0.29%	0.16%	1.71%	29.08%	0.02%	260698	30	0.80%	0.04%	9	0.20%	283	79	0.00%	29.83%
SA93-052	0.03%	0.00%	0.66%	2.04%	0.00%	406578	15	0.27%	0.02%	0	0.03%	157	28	0.00%	36.35%
SA93-053	1.15%	9.82%	8.49%	44.22%	0.12%	17904	40	2.48%	8.18%	41	1.24%	395	126	0.37%	14.74%
SA93-054	0.00%	0.00%	0.51%	47.48%	0.00%	245537	57	0.22%	0.05%	0	0.05%	84	19	0.00%	24.21%
SA93-055	0.00%	0.25%	0.00%	92.01%	0.00%	814	26	0.01%	4.22%	0	0.00%	10	18	0.03%	0.27%
SA93-056	0.11%	28.42%	4.78%	39.46%	0.04%	1209	218	0.04%	4.15%	13	0.36%	83	1709	0.14%	16.64%

ppm rock	Ni	Cu	Zn	Ga	As	Rb	Sr	Y	Zr	Nb	Ba	Ce	Pb	Th	U
SA93-039	0.00	0.00	0.00	0.00	0.00	0.00	0.00	0.00	0.00	1.61	0.00	0.00	0.00	0.00	0.00
SA93-040	0.00	10.40	0.00	0.00	25.27	0.99	3.94	0.79	8.44	1.90	25.17	0.00	0.00	0.00	0.00
SA93-041	368.20	76.64	27.21	3.36	855.85	0.00	0.00	0.00	5.86	1.79	0.00	0.00	72.98	0.00	0.00
SA93-042	201.18	49.99	357.31	3.91	758.37	5.49	3.88	4.75	15.34	4.82	80.13	0.00	29.39	0.00	0.00
SA93-043	25.10	114.69	101.73	22.49	0.00	44.22	49.91	21.46	110.78	6.96	326.60	0.00	0.00	0.00	0.00
SA93-046B	18.24	27.63	51.32	22.30	0.00	161.96	25.39	10.71	181.63	8.35	831.08	0.00	19.63	7.78	0.00
SA93-047A	6.85	16.94	38.93	10.64	0.00	81.46	19.79	22.29	119.78	7.92	361.62	0.00	37.03	4.18	0.00
SA93-049	11.19	51.91	113.79	7.13	0.00	12.71	4.12	2.03	12.01	2.70	90.68	0.00	35.95	0.00	0.00
SA93-050	44.66	25.83	0.00	10.59	81.57	64.47	23.69	11.43	92.04	13.88	542.53	0.00	108.47	0.00	27.67
SA93-051	231.67	354.10	310.92	5.02	612.42	7.61	4.42	2.24	24.41	3.06	73.58	0.00	44.07	4.00	0.00
SA93-052	353.57	96.09	35.04	5.29	853.30	2.91	1.78	2.20	7.53	2.46	0.00	0.00	243.92	0.00	0.00
SA93-053	73.70	198.40	100.57	14.70	0.00	34.07	102.59	37.81	111.19	8.65	324.49	0.00	0.00	0.00	0.00
SA93-054	274.72	168.89	300.63	0.00	382.05	0.00	0.00	2.94	9.30	3.29	0.00	0.00	20.29	0.00	0.00
SA93-055	0.00	0.00	0.00	0.00	0.00	0.00	35.42	0.00	0.00	1.50	0.00	0.00	0.00	0.00	0.00
SA93-056	599.01	55.63	66.51	8.17	0.00	4.23	13.19	7.62	33.60	1.99	0.00	0.00	0.00	0.00	0.00

All values in ppm unless otherwise indicated. Values of 0% or 0ppm indicate that concentrations were below the limits of detection.

Table II.2 (cont.): XRF data for samples from the Ramah Group

ppm rock	Na2O	MgO	Al2O3	SiO2	P2O5	S	Cl	K2O	CaO	Sc	TiO2	V	Cr	MnO	Fe2O3T
SA93-057	0.03%	0.11%	1.56%	14.25%	0.01%	336217	24	0.63%	0.12%	10	0.18%	360	59	0.01%	38.87%
SA93-059	0.04%	0.25%	1.92%	18.87%	0.02%	297246	48	0.88%	0.18%	8	0.21%	582	69	0.01%	37.84%
SA93-062	0.13%	0.06%	0.11%	87.82%	0.01%	990	1150	0.01%	0.02%	0	0.00%	0	27	0.00%	0.97%
SA93-063	0.08%	1.44%	1.45%	9.62%	0.01%	269132	94	0.34%	1.22%	0	0.15%	239	42	0.05%	46.86%
SA93-064	1.35%	10.25%	9.60%	49.01%	0.20%	5277	605	0.31%	0.93%	37	2.30%	481	98	0.19%	19.85%
SA93-065	0.06%	0.40%	2.17%	22.45%	0.02%	263379	218	0.81%	0.28%	0	0.18%	380	58	0.01%	40.53%
SA93-066	0.26%	15.99%	0.65%	37.78%	0.02%	12997	701	0.28%	24.37%	16	0.01%	8	12	0.15%	6.31%
SA93-067	0.08%	24.91%	1.45%	49.15%	0.30%	368	238	0.07%	24.34%	8	0.02%	9	7	0.08%	1.63%

ppm rock	Ni	Cu	Zn	Ga	As	Rb	Sr	Y	Zr	Nb	Ba	Ce	Pb	Th	U
SA93-057	495.83	303.95	347.12	0.00	43.19	5.20	9.52	5.48	29.82	3.29	28.12	0.00	70.84	5.36	7.19
SA93-059	497.50	243.83	763.23	5.95	100.24	11.89	7.25	10.34	43.09	4.58	0.00	0.00	70.86	5.94	14.01
SA93-062	0.00	7.33	0.00	0.00	0.00	0.00	0.00	0.00	0.00	1.03	0.00	0.00	0.00	0.00	0.00
SA93-063	508.70	586.51	821.75	0.00	151.98	1.55	20.65	5.70	21.23	2.77	30.11	0.00	173.77	0.00	5.66
SA93-064	14.74	155.93	97.13	21.92	0.00	3.79	18.65	21.17	185.02	13.25	55.64	0.00	17.87	0.00	0.00
SA93-065	387.22	428.69	473.70	0.00	62.41	8.48	7.90	7.66	36.57	3.70	32.30	0.00	92.88	0.00	8.42
SA93-066	0.00	9.45	2653.99	0.00	0.00	3.00	158.02	9.62	10.94	0.00	439.66	0.00	92.76	0.00	0.00
SA93-067	0.00	0.00	63.52	0.00	0.00	1.16	103.22	1.30	20.41	1.40	57.33	0.00	0.00	0.00	0.00

All values in ppm unless otherwise indicated. Values of 0% or 0ppm indicate that concentrations were below the limits of detection.

Table II.2 (cont.): XRF data for samples from the Ram..n Group

ppm rock	Na2O	MgO	Al2O3	SiO2	P2O5	S	Cl	K2O	CaO	Sc	TiO2	V	Cr	MnO	Fe2O3T
W93-14	0.00%	0.05%	0.11%	88.68%	0.01%	4486	24	0.01%	4.59%	0	0.01%	0	40	0.09%	1.09%
W93-15	0.16%	0.68%	3.59%	93.06%	0.01%	337	111	0.74%	0.71%	0	0.01%	0	17	0.01%	0.27%
W93-16	0.27%	1.30%	13.40%	65.92%	0.04%	288	71	5.56%	0.02%	10	0.44%	46	77	0.06%	8.92%
W93-17B	0.64%	2.07%	7.44%	75.67%	0.11%	27900	175	2.37%	0.24%	9	0.70%	584	90	0.01%	5.33%
W93-17D	0.45%	0.08%	3.62%	40.71%	0.00%	269461	0	1.14%	0.02%	0	0.10%	57	30	0.00%	25.00%
W93-17E	2.62%	2.63%	20.63%	59.66%	0.01%	2776	64	5.52%	0.02%	17	0.80%	388	161	0.01%	1.95%
W93-19B1	0.00%	0.00%	0.00%	99.66%	0.00%	520	0	0.01%	0.01%	0	0.00%	0	0	0.00%	0.04%
W93-19B2	0.06%	1.86%	1.59%	77.62%	0.01%	9666	0	0.24%	9.13%	13	0.04%	84	17	0.08%	4.77%
W93-19C	0.00%	1.12%	0.25%	91.69%	0.00%	1848	28	0.07%	1.88%	0	0.01%	19	15	0.04%	1.06%
W93-20A	0.14%	3.02%	5.03%	21.10%	0.08%	10585	27	1.51%	46.57%	39	0.34%	192	117	0.45%	5.24%
W93-20B	2.58%	5.32%	13.98%	58.36%	0.05%	46982	25	2.65%	0.62%	25	0.57%	340	205	0.04%	6.84%
W93-22	0.00%	0.00%	0.00%	96.31%	0.00%	1750	0	0.01%	0.03%	0	0.00%	0	22	0.00%	0.43%
W93-22A	0.00%	0.00%	0.08%	98.01%	0.00%	2459	206	0.03%	0.01%	0	0.00%	0	8	0.00%	0.49%
W93-22B	4.44%	0.14%	16.07%	69.33%	0.01%	86	79	3.66%	0.85%	0	0.12%	8	9	0.02%	0.97%
W93-28	1.24%	2.98%	17.74%	56.50%	0.02%	24829	0	5.16%	0.02%	31	0.96%	249	200	0.02%	8.28%

ppm rock	Ni	Cu	Zn	Ga	As	Rb	Sr	Y	Zr	Nb	Ba	Ce	Pb	Th	U
W93-14	0.00	3851.17	21.89	0.00	0.00	0.00	23.16	1.66	1.28	0.89	0.00	0.00	11.02	0.00	0.00
W93-15	0.00	4.20	0.00	0.00	28.56	7.43	6.70	1.27	30.69	1.30	42.10	0.00	11.39	0.00	0.00
W93-16	48.59	7.38	21.83	13.83	0.00	112.45	28.54	12.49	307.68	17.97	708.41	53.41	7.51	7.41	0.00
W93-17B	91.34	52.06	61.94	9.75	113.25	44.32	6.09	19.51	113.61	19.15	1099.24	44.16	11.32	0.00	9.98
W93-17D	124.83	33.13	92.95	3.27	501.95	10.09	1.60	3.61	16.24	3.26	71.01	0.00	49.69	5.03	0.00
W93-17E	7.02	0.00	14.94	24.02	15.12	81.96	11.07	9.51	168.86	9.87	1096.29	74.07	0.00	3.20	0.00
W93-19B1	0.00	0.00	0.00	0.00	17.51	0.00	0.00	0.00	0.00	2.11	0.00	0.00	0.00	0.00	0.00
W93-19B2	0.00	9.24	0.00	3.06	0.00	3.00	126.01	2.17	14.11	1.72	20.65	0.00	14.06	0.00	0.00
W93-19C	0.00	0.00	0.00	0.00	0.00	1.00	13.93	0.71	2.49	1.38	0.00	0.00	0.00	0.00	0.00
W93-20A	26.88	7.03	522.50	6.30	105.49	41.89	169.56	27.31	35.42	3.37	255.61	44.22	25.19	0.00	0.00
W93-20B	110.90	88.90	34.81	16.04	0.00	77.51	45.10	18.86	103.83	8.07	326.91	0.00	24.54	4.89	6.70
W93-22	0.00	0.00	0.00	0.00	0.00	0.00	0.00	0.00	0.00	1.37	0.00	0.00	0.00	0.00	0.00
W93-22A	0.00	1738.68	0.00	0.00	0.00	0.00	1.51	0.00	0.00	1.51	0.00	0.00	0.00	0.00	0.00
W93-22B	0.00	42.69	4.24	17.82	0.00	66.81	194.57	0.00	57.85	1.83	990.44	0.00	38.38	0.00	0.00
W93-28	91.99	42.62	59.90	25.85	0.00	163.45	36.22	18.20	178.89	22.58	431.10	0.00	30.93	7.94	0.00

All values in ppm unless otherwise indicated. Values of 0% or 0ppm indicate that concentrations were below the limits of detection.

Table II.2 (cont.): XRF data for samples from the Ramah Group

ppm rock	Na2O	MgO	Al2O3	SiO2	P2O5	S	Cl	K2O	CaO	Sc	TiO2	V	Cr	MnO	Fe2O3T
W93-30.1	0.00%	0.26%	1.81%	93.96%	0.00%	99	27	0.56%	0.01%	0	0.02%	6	30	0.00%	0.40%
W93-30.2	0.03%	0.09%	1.67%	94.48%	0.02%	130	69	0.45%	0.04%	0	0.01%	0	22	0.00%	0.08%
W93-31B	0.01%	8.00%	0.00%	57.68%	0.00%	232	62	0.00%	15.55%	10	0.00%	0	28	0.49%	6.57%
W93-31C	0.12%	0.00%	0.96%	5.17%	0.00%	395812	94	0.42%	0.04%	0	0.05%	163	40	0.00%	34.87%
W93-34B	0.02%	7.50%	0.00%	74.02%	0.04%	5306	68	0.01%	9.60%	0	0.00%	22	43	0.13%	1.98%
W93-35	1.54%	3.20%	18.47%	55.29%	0.04%	1045	53	4.36%	0.03%	27	0.76%	252	207	0.02%	11.71%
W93-36A	0.79%	2.61%	17.28%	64.99%	0.00%	1154	50	5.00%	0.04%	10	0.30%	379	129	0.01%	0.49%
W93-36C	0.10%	22.03%	1.75%	5.21%	0.03%	665	300	0.81%	37.80%	16	0.03%	9	0	0.56%	4.43%
W93-37A	0.16%	1.01%	1.85%	13.28%	0.01%	333758	0	0.53%	0.09%	12	0.19%	440	55	0.01%	40.43%
W93-52	0.09%	0.86%	11.26%	78.54%	0.02%	317	128	2.73%	1.17%	0	0.18%	47	75	0.02%	1.94%
W93-41E	0.05%	18.19%	1.87%	14.56%	0.04%	5113	203	0.69%	33.55%	31	0.21%	651	260	0.37%	7.95%
W93-43	0.04%	0.63%	9.56%	81.99%	0.00%	225	79	2.95%	0.06%	0	0.05%	12	59	0.00%	0.88%
W93-45	0.00%	0.14%	0.06%	96.53%	0.00%	9652	0	0.00%	0.14%	0	0.00%	0	0	0.00%	1.43%
W93-47	0.09%	2.15%	23.69%	59.17%	0.02%	184	127	7.50%	0.05%	13	0.54%	53	184	0.02%	2.54%
W93-48	0.03%	0.00%	0.53%	32.78%	0.03%	308067	158	0.25%	0.53%	0	0.02%	40	11	0.00%	27.27%

ppm rock	Ni	Cu	Zn	Ga	As	Rb	Sr	Y	Zr	Nb	Ba	Ce	Pb	Th	U
W93-30.1	0.00	0.00	0.00	0.00	0.00	11.69	1.30	0.00	58.34	1.46	112.58	0.00	0.00	0.00	0.00
W93-30.2	0.00	0.00	0.00	0.00	0.00	5.63	0.00	0.98	38.56	1.54	86.04	0.00	0.00	0.00	0.00
W93-31B	0.00	0.00	0.00	0.00	0.00	0.00	53.91	1.57	0.00	0.00	0.00	0.00	0.00	0.00	0.00
W93-31C	367.44	177.27	87.53	0.00	1268.48	1.80	2.74	2.56	7.32	2.21	52.58	0.00	72.52	0.00	0.00
W93-34B	0.00	0.00	0.00	0.00	24.86	0.00	59.97	13.95	3.82	0.85	0.00	0.00	10.23	0.00	0.00
W93-35	46.39	30.55	74.84	26.22	0.00	137.89	40.33	17.04	163.98	18.79	315.13	0.00	72.55	7.67	4.07
W93-36A	0.00	0.00	4.28	19.40	0.00	71.25	12.10	0.00	76.52	6.07	605.86	0.00	0.00	0.00	0.00
W93-36C	0.00	0.00	8.02	3.02	0.00	10.79	46.61	11.47	84.06	15.30	93.07	0.00	0.00	5.02	0.00
W93-37A	640.71	1027.23	427.88	0.00	152.07	4.53	6.63	6.43	27.48	3.86	75.18	0.00	37.89	0.00	0.00
W93-52	0.00	0.00	0.00	8.19	0.00	37.07	20.09	6.13	167.74	4.03	541.46	116.20	4.02	29.95	0.00
W93-41E	0.00	0.00	12.35	10.44	21.88	15.47	72.71	21.96	33.32	2.61	777.62	0.00	11.15	3.52	0.00
W93-43	0.00	0.00	0.00	5.23	0.00	39.23	4.10	0.79	91.46	1.73	679.41	0.00	0.00	0.00	0.00
W93-45	0.00	25.03	0.00	0.00	0.00	0.00	0.00	0.00	1.52	1.68	0.00	0.00	0.00	0.00	0.00
W93-47	19.73	0.00	22.58	23.80	0.00	190.29	24.44	11.51	399.59	10.23	2964.78	164.66	0.00	14.51	0.00
W93-48	72.69	76.74	0.00	0.00	366.27	5.61	3.99	2.71	6.59	2.70	21.76	0.00	177.73	0.00	5.26

All values in ppm unless otherwise indicated. Values of 0% or 0ppm indicate that concentrations were below the limits of detection.

Table II.2 (cont.): XRF data for samples from the Ramah Group

ppm rock	Na2O	MgO	Al2O3	SiO2	P2O5	S	Cl	K2O	CaO	Sc	TiO2	V	Cr	MnO	Fe2O3T
W93-49A	0.06%	0.10%	2.49%	44.57%	0.01%	260361	210	1.03%	0.09%	8	0.10%	612	32	0.00%	23.75%
W93-53	0.07%	19.32%	2.24%	24.67%	0.34%	2520	323	0.89%	29.72%	16	0.04%	32	15	0.14%	3.02%
W93-54B	0.19%	0.68%	1.40%	11.70%	0.01%	302563	86	0.30%	0.25%	0	0.16%	358	73	0.01%	43.65%
W93-54C	0.00%	0.05%	0.00%	98.85%	0.00%	388	0	0.01%	0.05%	0	0.00%	0	7	0.00%	0.36%
W93-55A	0.06%	1.48%	0.69%	51.05%	0.01%	4204	118	0.25%	31.01%	9	0.90%	86	27	0.41%	1.26%
W93-56A	0.19%	23.52%	0.25%	7.76%	0.03%	1492	99	0.08%	37.96%	17	0.01%	0	9	0.32%	1.86%
W93-56B	0.19%	22.08%	0.39%	3.80%	0.01%	2075	154	0.20%	38.67%	16	0.01%	6	10	0.65%	5.44%
Ramah Q1	0.00%	0.11%	0.00%	96.34%	0.00%	2435	0	0.01%	0.11%	0	0.00%	0	18	0.00%	0.57%
Ramah Q2	0.00%	0.00%	0.00%	95.69%	0.00%	510	0	0.00%	0.03%	0	0.00%	0	16	0.00%	0.09%
Ramah Ch't	0.00%	0.00%	0.03%	99.12%	0.01%	1489	0	0.03%	0.03%	0	0.00%	0	10	0.00%	0.26%

ppm rock	Ni	Cu	Zn	Ga	As	Rb	Sr	Y	Zr	Nb	Ba	Ce	Pb	Th	U
W93-49A	368.78	74.83	501.18	3.63	651.90	9.41	2.67	1.52	14.46	4.09	41.66	0.00	32.60	3.86	0.00
W93-53	0.00	0.00	6.44	0.00	0.00	12.38	36.63	6.36	40.18	1.31	1193.75	0.00	18.97	0.00	14.13
W93-54B	489.70	282.64	467.78	0.00	177.82	1.92	13.09	6.30	20.95	2.38	97.79	0.00	61.69	0.00	9.00
W93-54C	0.00	2.13	0.00	0.00	19.59	0.00	0.00	0.00	0.00	1.64	0.00	0.00	0.00	0.00	0.00
W93-55A	5.62	4.68	1424.34	0.00	0.00	3.38	371.61	10.42	0.00	0.00	0.00	0.00	0.00	0.00	0.00
W93-56A	0.00	0.00	1563.70	4.48	0.00	1.23	70.02	8.00	13.35	4.02	41.59	0.00	731.11	0.00	0.00
W93-56B	0.00	0.00	1983.79	0.00	0.00	2.72	78.06	9.67	18.75	10.41	25.79	0.00	10.13	0.00	0.00
Ramah Q1	0.00	5.08	0.00	0.00	16.48	0.00	1.77	0.00	0.00	1.01	0.00	0.00	0.00	0.00	0.00
Ramah Q2	0.00	0.00	0.00	0.00	0.00	0.00	0.00	0.00	0.00	1.02	0.00	0.00	0.00	0.00	0.00
Ramah Ch't	0.00	4.56	0.00	0.00	0.00	0.00	0.00	0.00	3.78	2.66	0.00	0.00	5.44	0.00	0.00

Values of 0% or 0 ppm indicate that concentrations were below the limits of detection. Samples analysed at the Department of Earth Sciences, Memorial University

Table II.3: Geochemistry of the Rowsell Harbour Volcanic Member

Sample	SiO2 (%)	TiO2 (%)	Al2O3 (%)	Fe2O3* (%)	MnO (%)	MgO (%)	CaO (%)	Na2O (%)	K2O (%)	P2O5 (%)	Cr (ppm)	Ni (ppm)	Sc* (ppm)	V (ppm)
SA93-025	52.98	2.12	13.60	16.20	0.15	5.13	5.78	2.54	0.41	0.20	72	72	35	414
SA93-026	51.05	2.00	13.32	13.95	0.20	5.43	9.63	0.00	2.99	0.19	70	54	36	426
SA93-027	42.91	2.32	14.81	17.42	0.23	6.88	10.38	0.00	4.03	0.25	78	64	40	488
SA93-048A	64.09	1.28	9.26	21.04	0.07	0.32	0.05	0.00	3.01	0.05	49	38	31	306
SA93-048B	50.42	2.36	15.24	18.13	0.16	4.24	2.50	3.34	3.27	0.21	77	78	38	447
W93-24	48.08	2.71	17.42	16.24	0.17	3.62	5.33	0.06	4.44	0.29	255	64	49	314
W93-42	51.98	1.00	14.50	14.09	0.19	7.61	8.29	1.72	0.13	0.07	85	115	45	452
931	46.46	1.58	14.74	0.00	0.19	10.41	10.74	2.79	0.65	0.24	536	196	31	0
902	46.08	1.97	14.90	0.00	0.19	8.85	0.79	2.56	0.79	0.32	341	134	32	0

Sample	Cu (ppm)	Zn (ppm)	Rb (ppm)	Ba (ppm)	Sr (ppm)	Ga (ppm)	Ta* (ppm)	Nb (ppm)	Hf* (ppm)	Zr (ppm)	Tl (ppm)	Y* (ppm)	Th* (ppm)	U* (ppm)
SA93-025	255	227	10	97	255	25	1.53	14.1	3.35	183	12709	17	2.67	0.58
SA93-026	383	90	52	808	265	19	1.01	13.3	2.89	163	12014	12	2.42	0.50
SA93-027	16	68	75	1007	227	24	0.78	13.7	4.14	174	13890	18	2.59	0.72
SA93-048A	38	85	67	424	14	19	1.39	13.5	1.29	155	7662	8	3.12	0.40
SA93-048B	5	181	64	411	123	25	1.13	15.4	3.33	199	14172	16	2.98	0.50
W93-24	126	77	4	29	161	15	0.39	2.6	0.94	52	16240	17	0.34	0.09
W93-42	0	14	99	1018	69	28	1.13	17.9	4.77	231	5971	17	3.46	0.67
931	0	0	9	268	372	0	1.41	24.0	2.10	101	9472	21	1.12	0.24
902	0	0	15	1171	473	0	1.98	29.0	2.10	107	11810	22	1.57	0.37

Sample	La* (ppm)	Ce* (ppm)	Pr* (ppm)	Nd* (ppm)	Sm* (ppm)	Eu* (ppm)	Gd* (ppm)	Tb* (ppm)	Dy* (ppm)	Ho* (ppm)	Er* (ppm)	Tm* (ppm)	Yb* (ppm)	Lu* (ppm)
SA93-025	18.62	43.10	5.55	23.95	5.46	1.55	5.96	0.63	3.61	0.67	1.89	0.28	1.84	0.28
SA93-026	17.04	40.40	5.17	23.41	4.97	1.49	5.12	0.54	2.90	0.49	1.47	0.22	1.50	0.23
SA93-027	14.69	36.50	4.80	21.91	5.13	1.36	5.49	0.65	3.83	0.73	2.30	0.29	2.19	0.32
SA93-048A	47.19	80.45	8.74	33.41	5.39	1.70	4.72	0.39	1.77	0.33	0.88	0.12	0.93	0.17
SA93-048B	22.81	54.97	6.91	32.03	7.08	1.72	7.07	0.71	3.67	0.67	1.87	0.26	2.00	0.28
W93-24	4.36	11.29	1.60	7.45	2.08	0.79	2.95	0.52	3.50	0.68	2.16	0.29	2.21	0.29
W93-42	24.93	59.62	7.81	32.67	6.54	1.51	4.55	0.58	3.52	0.71	2.11	0.35	2.35	0.38
931	12.60	26.00	0.00	14.00	3.56	1.32	3.30	0.64	0.00	0.70	0.00	0.34	1.75	0.30
902	15.40	33.00	0.00	19.00	4.48	1.55	4.60	0.81	0.00	0.90	0.00	0.46	1.85	0.26

Oxides and trace elements determined by XRF analysis and elements denoted by * have been determined by ICP-MS at the Department of Earth Sciences, Memorial University of Newfoundland. Values of 0% or 0 ppm indicate that the elements were not analysed or were below the limits of detection. Samples 931 and 902 are taken from Class et al. (1994). Sample W92-24 may represent a late diabase sill.

APPENDIX III

Table III.1: Sulphur isotope data

Sample	Mineral	$\delta^{34}S_{CDT}$ (‰)	Classification
W93-17A	Py	14.7	1
W93-20A	Py	14.7	1
W93-20B	Py	-3.9	1
W93-31A	Py	0.2	1
SA93-028*	Py	27.1	1
SA93-045	Py	3.7	1
SA93-046B	Py	6	1
SA93-047A	Py	8.7	1
SA93-074	Py	10.1	1
W93-19B	Py	18.6	2
SA93-011	Po	38.3	2
SA93-013	Py	18.1	2
SA93-040	Py	-0.6	2
SA93-053	Py	-3.7	2
SA93-006	70%Po,30%Py	6.3	3
SA93-010	50%Po,20%Py	5.2	3
SA93-020	Py	-1.9	3
SA93-041	Py	-3.2	3
SA93-052	Py	-3.9	3
SA93-052*	Py	-3.6	3
SA93-052*	Py	-3.8	3
SA93-053	Py	-3.7	3
SA93-057	Py	-4.2	3
SA93-059	30% Po,10% Py	-4.6	3
SA93-063	Py	-4.5	3
SA93-065	Po	-2.7	3
W93-54B	Py	-4.2	3
W93-25A	Gn	-0.4	4
W93-25B	Gn	-0.1	4
W93-025C	Sph	2	4
W93-025C	Gn	-1.2	4
SA93-030	Py	1.3	4
W93-038	Sph	32.3	5
SA93-013	Sph	25.3	5
SA93-015	Sph	25.4	5
W93-041A	Gn	14	6
W93-041F	Gn	2.2	6
W93-041F	Sph	13.2	6
W93-041F	Py	-12.2	6
SA93-072	Py	19.3	6
SA93-072	Sph	3.7	6
SA93-076	35%Po,15%NiS	11	6

Sample	Mineral	$\delta^{34}S_{CDT}$ (‰)	Classification
SA93-050	Py	23.3	7
SA93-058	Sph	30.1	7
SA93-058	70%Py,30%Sp	27.1	7
SA93-060	Sph	24.7	7
SA93-060	Py	11.1	7
SA93-066	Py	8.3	7
SA93-068	Sph	6.3	7
SA93-069	Sph	15.5	7
SA93-069	Gn	15.4	7
SA93-071	Py	25.8	7
W93-036D	Gn	16.7	7
W93-036D	Sph	24.3	7
W93-036D	Sph	24.2	7
W93-036D	Py	21.6	7
W93-039A	Sph	23.2	7
W93-039A	Gn	21.5	7
W93-039B	Gn	18	7
W93-040	Gn	17.6	7
W93-054	Gn	10.6	7
W93-054	Py	14.7	7
W93-056A	Gn	32.9	7
W93-056B	Sph	33.8	7
W93-056B	Py	31.8	7
SA93-007	Cpy	3.5	8
SA93-026	Cpy	12	9
NBS-123	Sph	16.9	standard

Key: * Repeat sample. 1 - pyrite nodules; 2 - pyrite in chert bed; 3 - pyrite bed; 4 - Archean vein sulphides; 5- Zn mineralized chert; 6 - vein mineralization in the Reddick Bight Dolomite Member; 7 - Mineralized breccia and vugs in the Reddick Bight Dolomite Member; 8 - Veins associated with the diabase and gabbro sills; 9 - sulphide present in the Rowsell Harbour Volcanic Member. Py - Pyrite, Gn - Galena, Sph - Sphalerite, Po - Pyrrhotite, NiS - Vaesite

Table III.2: Lead isotope data

Sample	$^{206}Pb/^{204}Pb$	$^{207}Pb/^{204}Pb$	$^{208}Pb/^{204}Pb$	Mu (μ)	Model Age (Ma)	Showing
SA93-003A	14.329	14.658	34.178	7.117	1833	*Wilton #2*
SA93-030	13.473	14.459	33.69	7.469	2460	*Archibald Archean*
SA93-069	14.163	14.561	34.029	6.672	1809	*Black Jack*
W93-25A	13.462	14.446	33.652	7.363	2446	*Archean Vein*
W93-36D	14.152	14.582	34.27	6.84	1871	*Macleod*
W93-39A	14.092	14.546	34.146	6.671	1861	*Panda*
W93-39B	14.137	14.548	34.121	6.617	1810	*Panda*
W93-40	14.524	14.636	34.117	6.722	1559	*V-8*
W93-41A	14.071	14.523	33.979	6.537	1832	*Loch Bears Gut*
W93-41F	14.24	14.585	34.09	6.73	1772	*Loch Bears Gut*
W93-53	14.011	14.506	33.923	6.507	1867	*Char*
W93-56	14.168	14.612	34.366	7.037	1919	*Bluesky*

Key: Mu values calculated from Zartman and Doe (1981); model ages calculated from Stacey and Kramer (1981). Errors for all ratios are 0.05% amu.

Table III.3: Cobalt / Nickel ratios for pyite bed

Sample	Co (ppm)	Ni (ppm)	Co/Ni
W93-31C	38	367	0.1
W93-37A	120	641	0.2
W93-54B*	102	490	0.2
SA93-006	27	241	0.1
SA93-010	213	159	1.3
SA93-017B	80	222	0.4
SA93-020A	74	330	0.2
SA93-037	106	160	0.7
SA93-041	71	368	0.2
SA93-051	108	239	0.5
SA93-052	70	368	0.2
SA93-057*	80	496	0.2
SA93-059*	99	498	0.2
SA93-063*	96	509	0.2
SA93-065*	239	387	0.6
SA93-073	169	146	1.2
SA93-073B	129	39	3.3
SA93-074	86	479	0.2

Note: Co values obtained by ICP-ES (NDME) and Ni obtained by MUN XRF. * indicates pyrrhotite rich.

Table III.4: Semi-quantitative sphalerite composition from selected showings.

Sample	Zn weight % (atomic %)	Fe weight % (atomic %)	Cu weight % (atomic %)	Cd weight % (atomic %)	S weight % (atomic %)
W93-25C	69.65 (54.13)	2.83 (2.57)	0.23 (0.18)	0.1 (0.05)	27.18 (43.07)
W93-36D	64.26 (48.61)	5.53 (4.90)	0.14 (0.11)	0.00 (0.00)	30.07 (46.38)
W93-36D*	55.91 (40.76)	9.76 (8.33)	0.17 (0.13)	0.00 (0.00)	34.16 (50.78)
W93-38	56.52 (42.40)	13.16 (11.56)	0.46 (0.36)	0.00 (0.00)	29.86 (45.68)
W93-39A	71.43 (55.96)	2.16 (1.98)	0.16 (0.13)	0.00 (0.00)	26.25 (41.93)
W93-41F	65.79 (49.69)	3.59 (3.17)	0.00 (0.00)	0.00 (0.00)	30.62 (47.14)
W93-56B	72.90 (59.32)	5.33 (5.08)	0.37 (0.31)	0.17 (0.08)	21.23 (35.21)
W93-56B*	68.64 (53.27)	3.90 (3.54)	0.34 (0.27)	0.00 (0.00)	27.12 (42.91)
SA93-013	57.29 (42.08)	8.44 (7.26)	0.88 (0.67)	0.00 (0.00)	33.38 (49.99)
SA93-015	54.83 (40.81)	10.44 (9.10)	3.48 (2.67)	0.00 (0.00)	31.25 (47.42)
SA93-058	58.43 (41.44)	2.21 (1.84)	0.00 (0.00)	0.19 (0.08)	39.17 (56.64)
SA93-60	55.53 (39.45)	4.73 (3.93)	1.09 (0.80)	0.16 (0.06)	38.49 (55.75)
SA93-68	57.55 (40.48)	1.93 (1.59)	0.24 (0.17)	0.00 (0.00)	40.28 (57.76)
SA93-069	46.24 (32 62)	15.76 (13.02)	0.40 (0.29)	0.00 (0.00)	37.60 (54.07)
SA93-072	57.55 (40.48)	1.93 (1.59)	0.24 (0.17)	0.00 (0.00)	40.28 (57.76)

Key: * - repeat sample of a different grain due to partial oxidation of surface. Sulphur totals relative to the metals are a result of a higher X-ray absorbance than the less absorbant metals.

Table III.5: Fluid inclusion data for dolomite

Inclusion number	Homogenization Temp. (°C)	Freezing Temp. (°C)	Salinity (NaCl wt%)
1 (S)	264.8	-14.7	18.6
2 (P)	98.9	-	-
3 (S)	239.6	-18.4	21.5
4 (S)	280	-23.4	25.1
5 (S)	317.7	-19.3	22.1
6 (S)	239.1	-24.1	25.7
7 (S)	-	-20.4	22.9
8 (S)	247.9	-17.7	21
9 (S)	288.5	-20.5	23
10 (S)	289	-19.3	22.1

Key: - fluid inclusion broke before homoginization temperature was reached or inclusion was too small to observe a freezing temperature. P -primary, PS -pseudosecondary, S -secondary.

Table III.6: Fluid inclusion data for quartz

Inclusion number	Homogenization Temp. (°C)	Freezing Temp. (°C)	Salinity (NaCl wt%)
1 (P)	156.9	-14.9	18.7
2 (P)	156.9	-14.6	18.5
3 (P)	147.5	-14.1	18.1
4 (P)	101.9	-22.4	24.4
5 (P)	109	-22.1	24.2
6 (P)	130.5	-11.8	15.9
7 (S?)	190.7	-10.2	14.3
8 (P)	183.8	-13.4	17.4
9 (P)	108	-25.6	26.9
10 (P)	134.9	-17.4	20.7

Table III.7: Fluid inclusion data for sphalerite

Inclusion number	Homogenization Temp. (°C)
1 (PS)	133.2
2 (PS)	176.8
3 (PS)	177
4 (P?)	170
5 (PS)	122.8
6 (PS)	137.4
7 (PS)	142.2
8 (P?)	126.8
9 (PS)	139.8
10 (PS)	169.7
11 (PS)	162.2

Table III 8: Carbon isotope

Sample	$\delta^{13}C_{PDB}$ (‰)
W93-41	-14.6
W93-26	-30.9
SA93-061	-29.9
SA93-044	-29.3
PANDA	-30.5
W93-26a	-30.7
SA93-033	-29.9
W93-51	-29.8
W93-39D	-21.1
W93-26b	-28.2
W93-044	-31.6
W93-46	-28
W93-50	-29.3
PANDAN	-30.1
SA93-046	-27

Table III.9: Carbon-Hydrogen-Nitrogen analyses of RBDM pyrobitumen

Sample number	wt % Carbon	wt % Hydrogen	wt % Nitrogen	Empirical Formula
W93-28b	75.85	0.51	0.88	$C_{100}H_xO_yNS_z$
W93-28b*	65.92	0.3	0.77	$C_{100}H_xO_yNS_z$
W93-44	51.59	-	0.74	$C_nH_xO_yNS_z$
W93-44*	54.95	-	0.77	$C_nH_xO_yNS_z$
W93-44*	59.85	-	0.89	$C_nH_xO_yNS_z$

The samples were combusted in the presence of O_2, hence no O_2 data is available. * repeat, - below limits of detection.

Table III.10: Carbon and oxygen isotopic data

Sample and showing name	Carbonate type	$\delta^{13}C_{PDB}$ (‰)	$\delta^{18}O_{SMOW}$ (‰)	Temperature (°C)	$\delta^{18}O$ fluid (‰)
W93-016 Reddick Bight N.S.	1	-1	18.7	25	-12.5
W93-056B Blue Sky	1	-3.1	17	25	-14.2
W93-36D Macleod No. 1	1	-1.1	17.8	25	-13.4
SA93-033	1	-1.3	20.8	25	-10.5
SA93-060 Saor Alba	1	-1.8	17.3	25	-14
W93-039 Panda	1	-0.8	18.3	25	-13
W93-039 Panda	1	-0.3	18.3	25	-13
SA93-009 Warspite (rep. sample)	1	0.4	18.5	25	-12.7
W93-039 Panda	2	-3.9	18.6	110	1
W93-039 Panda	2	-5	15	110	-2.7
SA93-068 Galloway	2	-13.9	15.6	110	-2
W93-036D Macleod No. 1	2	-5.5	17.4	110	-0.3
W93-039 Panda	2	-8.1	11.3	110	-6.3
W93-039 Panda	2	-12.2	8.5	110	-9.1
W93-039 Panda	3	-2.9	16.1	140	1.4
W93-039 Panda	3	-4.4	15	140	0.3
W93-039 Panda	3	-3.9	15	140	0.2
W93-036D Macleod No. 1	3	-4.7	19.7	140	5
W93-039 Panda	3	-4.6	15.2	140	0.5
W93-039 Panda	3	-4.6	16	140	1.3
W93-039 Panda	3	-7.8	10.4	140	-4.3
W93-036D Macleod No. 1	4	-6.5	17.5	140	4.6
W93-039 Panda	4	-6.6	15.2	140	2.3
SA93-058 Panda	4	-3.5	14.8	140	1.9
W93-016	4	-3.4	17.1	140	4.1
NBS19 TS Limestone	standard	-2.19	28.61	-	-

Key: Carbonate type: (1) Host RBDM, (2) Secondary dolomite, (3) Pre-ore dolomite, (4) Post-ore calcite. $\delta^{18}O$ of fluid calculated from Mathew and Katz (1977).

APPENDIX IV

Analytical Methods

IV.1 Stable isotope Studies

IV.1.1 Sulphur Isotopes

Sulphur isotopes have been used to eulicidate sulphide mineralization processes in a variety of different environments (Ohmoto and Rye, 1979; Ohmoto *et al.*, 1990). Hence to characterise the sulphide occurrences within the Ramah Gp. it was decided that sulphur isotope data should be utilized. Sixty-seven sulphide samples were analysed which fall into 9 categories, viz.: diagenetic pyrite nodules; pyrite present in the chert bed; sphalerite mineralization present at the top of the chert bed; pyrite-pyrrhotite bed; Archean vein mineralization; sulphide veins in the RBDM; sulphides associated with brecciation and vugs within the RBDM; mineralization associated with the diabase-gabbro sills; and mineralization associated with the RHVM.

The sulphides were removed by crushing and hand picking, and their purity determined by X-ray diffraction techniques. The sulphide separates were combusted at 1000°C with CuO to produce SO_2, in accordance with the technique described by Fritz *et al.* (1974). This SO_2 gas was collected in break seals and sent to the Ottawa-Carleton Geoscience Centre stable isotope facility where it was analysed. Samples from the pyrite bed were analysed using a VG 903 mass spectrometer at the Department of Earth Sciences, Memorial University. The data obtained are presented in Table III.1 (Appendix III), and are quoted relative to the Cañon Diablo Triolite (CDT) with an accuracy of 0.2‰.

IV.1.2 Carbon Isotopes

The black graphitic substance present within quartz-carbonate veins and vugs of the RBDM was thought to represent some type of organic substance. Characterisation between organic and inorganic compounds can easily be made by carbon isotope analysis. The samples were hand picked and purity determined by X-ray diffraction techniques. Any carbonate material present in the sample was reacted overnight with hydrochloric acid. The purified sample was comusted with CuO to produce CO_2, in accordance with the technique described by Craig (1957). The CO_2 gas was analysed by a Finigan MAT 252 mass spectrometer at the Department of Earth Sciences, Memorial University. Data obtained are presented in Table III.8 (Appendix III), and are quoted relative to the Pee Dee Belemnite (PDB) standard, with an accuracy of 0.1‰.

IV.1.3 Carbon and Oxygen Isotopes

A combined study of carbon and oxygen isotopes in carbonates is a powerful means of distinguishing between carbonates with different origins. Five types of samples were collected; host dolomite to mineralization within the RBDM; fine crystalline, orange secondary dolomite; coarse crystalline dolomite pre-dating mineralization; coarse calcite, post-dating mineralization; dolomite from the Warspite Fm.. The samples were slabbed to a thickness of 5mm before carefully being chiselled and broken to remove the carbonate. Slabbing assured the samples were unweathered and did not contain any late veining. X-ray diffraction techniques were used to assure the purity of the sample, before CO_2 extraction

was performed by the method of McCrea (1950). Evolved CO_2 gas was analysed on a Finigan MAT 252 mass spectrometer at Memorial University. Values obtained were quoted relative to PDB and Vienna Standard Mean Ocean Water (V-SMOW), with an accuracy of 0.1‰. The data are presented in Table III.10 (Appendix III).

IV.2 Radiogenic Isotopes (Pb-isotopes)

Lead isotopes can be used to provide source areas and model ages to sulphide mineralization (Zartman and Doe, 1981). Twelve galena separates were carefully removed from their host rock. The samples represented mineralization from the Archean basement, with the majority of the samples from the sulphides in the RBDM. The samples were sent to the GEOTOP laboratory, University du Quebec à Montréal, where the Pb isotopes were analysed. Ratios for the isotopes (^{208}Pb, ^{207}Pb, ^{206}Pb, and ^{204}Pb), together with their Stacey and Kramers' (1975) model mu (μ) values and model ages are given in Table III.2 (Appendix III).

IV.3 Fluid Inclusions

Fluid inclusions are extremely useful in characterising the trapping temperatures and salinities of fluids present in many minerals (Roedder, 1984). Suitable samples of sphalerite, saddle dolomite, and quartz were taken from mineralized areas (Panda and Saor Alba showings), and wafers were cut and doubly polished. The quartz and dolomite samples were cut to a thickness of 400 μm, while the translucent sphalerite was cut to 200 μm.

Owing to and the small size of the inclusions (generally less than 2 μm) of other sections only 3 slides were analysed with 31 measurements taken from freezing and heating experiments. Heating and freezing experiments were performed at Memorial University on an adapted USGS stage with apparatus manufactured by Fluid Inc. USA. Sizes of the fluid inclusions varied from ~ 10 μm in the dolomite, ~ 8-10 μm in quartz, and 3-6 μm in sphalerite. Owing to the small size of the sphalerite inclusions, freezing temperatures were not conducted on these samples. Results are presented in Tables III.5, 6 and 7 (Appendix III). The sections were also viewed under a Carl Zeiss Photomicroscope 3, fitted with a 50 W mercury bulb, to detect fluorescence caused by hydrocarbons present within the inclusions or surrounding minerals.

IV.5 Scanning Electron Microscope (SEM)

Polished, carbon-coated, thin sections of sphalerite were examined in a Hitachi S570 Scanning Electron Microscope at an accelerating voltage of 20 kV to ascertain Zn, S, Fe, Cd, and Cu concentrations in the Biology Department at Memorial University. Backscattered electron imaging was obtained with a GW Electronics type 113 solid state Backscattered Electron Detector. Semi-quantitative X-ray analysis were performed with a Tractor Northern 5500 Energy Dispersive X-ray Analyser equipped with a Microtrace silicon X-ray spectrometer, Model 70152, with a spectral resolution of 145 eV. Element concentrations were calculated using Standardless Semi-Quantitative (SSQ) analysis models. Data collected are presented in Table III.4 (Appendix III).

IV.6 Cathodoluminescence

Uncoated, polished thin sections of carbonates from mineralized areas of the RBDM were analysed under luminescent light to look for changes in the carbonate cements. Samples where analysed using a Luminoscope® ELM 2B fitted with a Wild Leitz Photomakroskop M4000 photographic unit, at the Department of Earth Sciences, Memorial University of Newfoundland. Standard operating currents (~ 0.5 mA) and voltages (~ 8-10 kV) were used throught the experiment. Photographs were taken using an auto exposure Wild Photoautomat MPS 55, with average exposure times of 4-6 minutes.

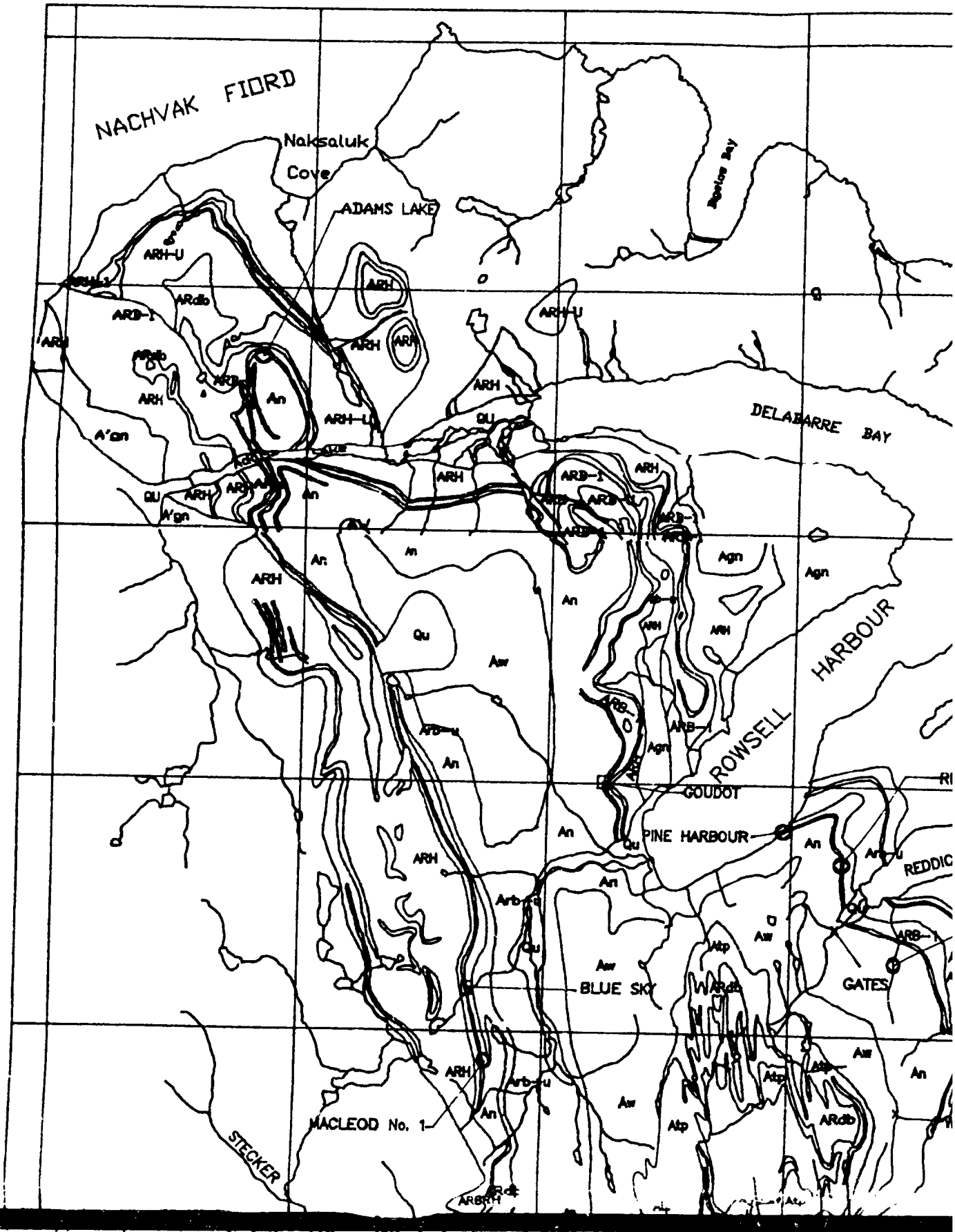
NACHVAK FIORD
Naksaluk
Cove
ADAMS LAKE
DELABARRE BAY
HARBOUR
ROWSELL
GOUDOT
PINE HARBOUR
REDDIC
BLUE SKY
GATES
MACLEOD No. 1
STECKER
ARH-U
ARH
ARB-1
ARdb
An
Agn
Aw
Qu
A'gn
Atp

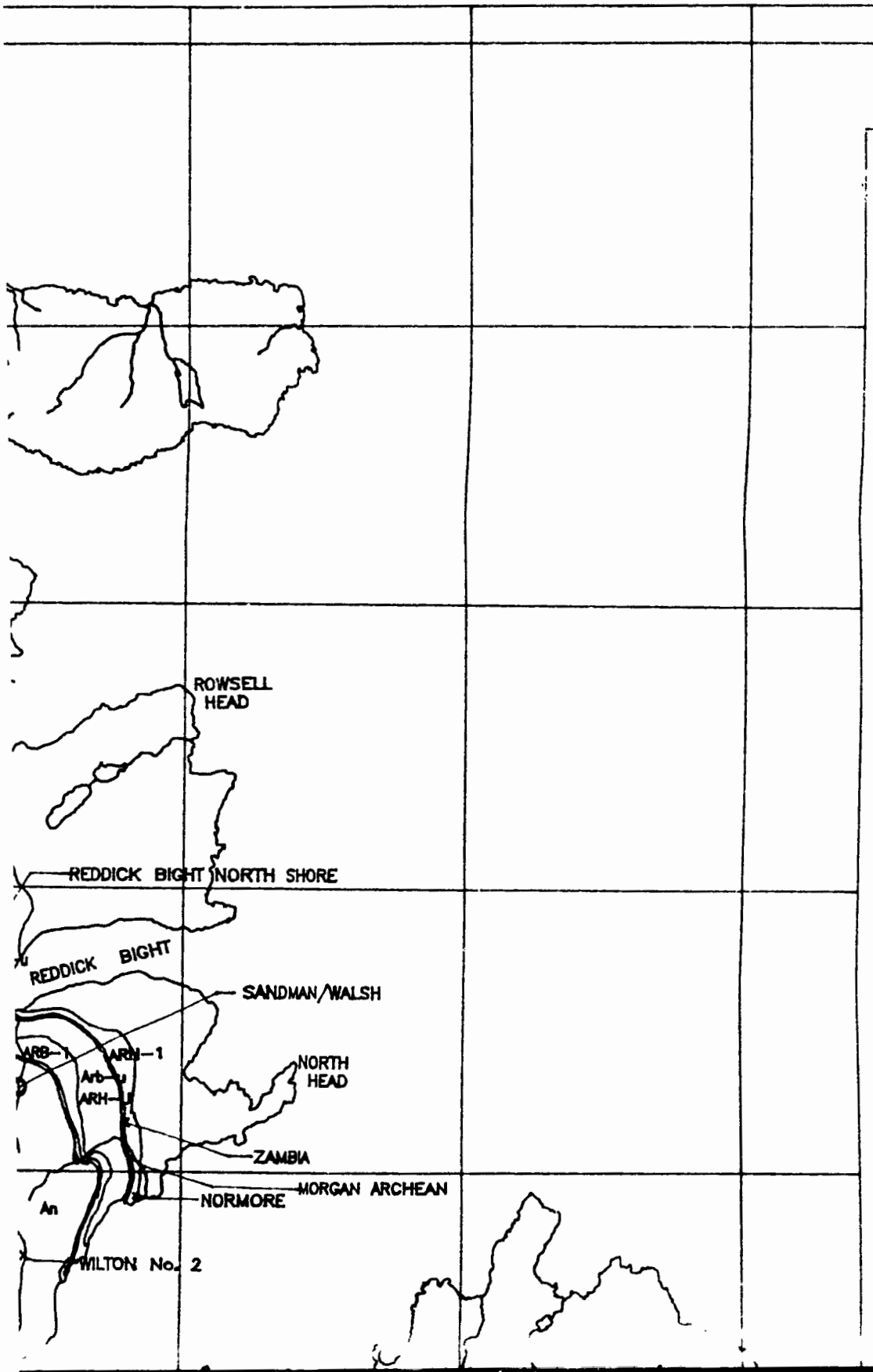

LEGEND

Ramah Gro

Qu	Quaternary
A_{Rum}	Ultramafic
A_{Rdb}	Massive alt
A_{cb}	Cameron B
A_{TP}	Typhoon P
A_W	Warspite F
A_N	Nullataktok
A_{RB}	Reddick Big
A_{RB-U}	Dolomite
A_{RB-L}	Quartzite
A_{RH}	Rowsell Har
A_{RH-U}	Upper Whi
A_{RH-V}	Volcanic
A_{RH-L}	Lower Whi

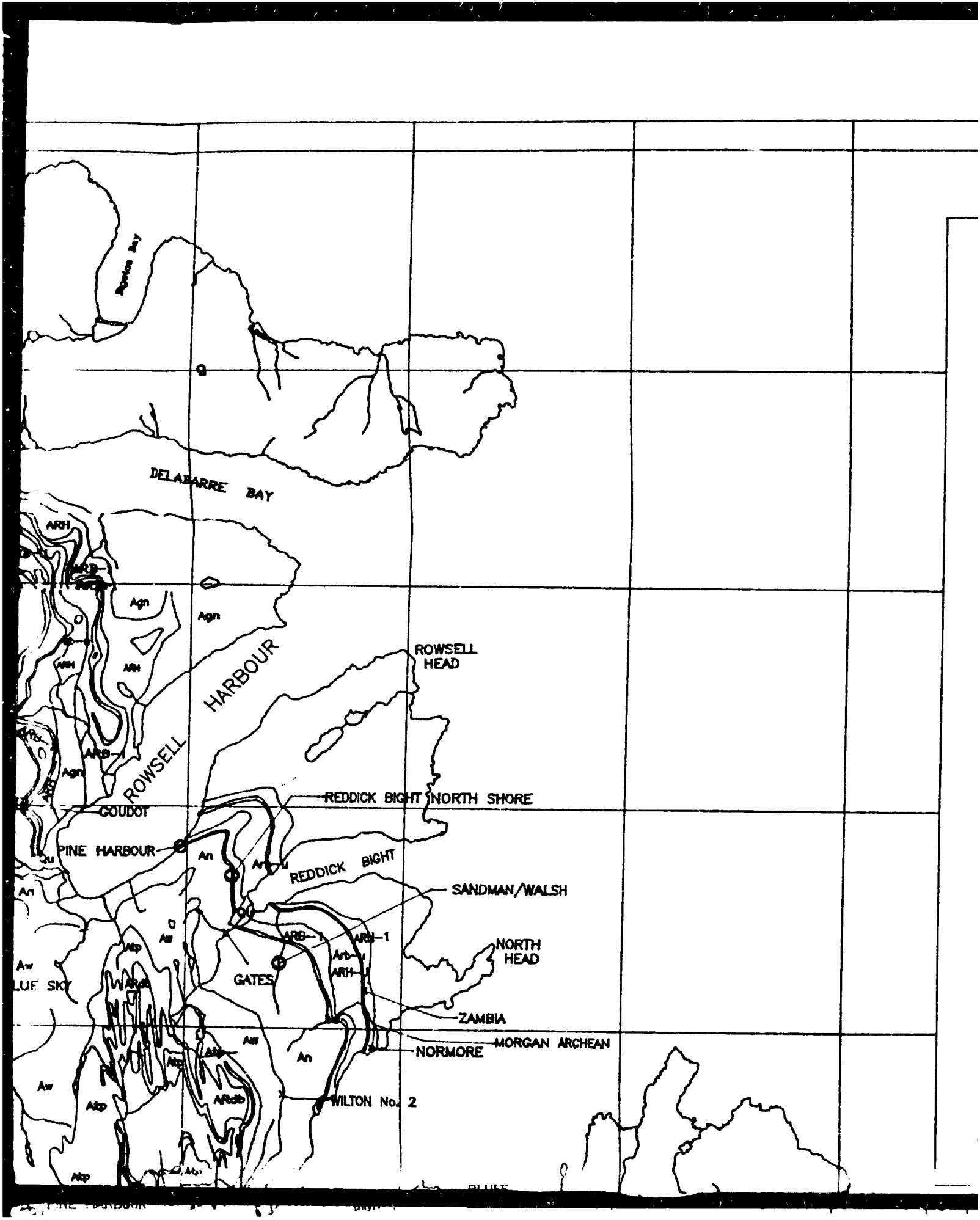
DELABARRE BAY
ROWSELL HEAD
HARBOUR
ROWSELL
REDDICK BIGHT NORTH SHORE
GOUDOT
PINE HARBOUR
REDDICK BIGHT
SANDMAN/WALSH
NORTH HEAD
GATES
ZAMBIA
MORGAN ARCHEAN
NORMORE
WILTON No. 2
ARH
ARB-1
Agn
An
Aw
Atp
ARdb

LEGEND
Ramah Group, Northern Labrador

- Qu — Quaternary
- A_{Rum} — Ultramafic Sills
- A_{Rdb} — Massive altered diabase and amphibolite sills
- A_{cb} — Cameron Brook Formation
- A_{TP} — Typhoon Peak Formation
- A_{W} — Warspite Formation
- A_{N} — Nullataktok Formation
- A_{RB} — Reddick Bight Formation (Undivided)
  - A_{RB-U} — Dolomite Member
  - A_{RB-L} — Quartzite Member
- A_{RH} — Rowsell Harbour Formation (Undivided)
  - A_{RH-U} — Upper White Quartzite Member
  - A_{RH-V} — Volcanic Member
  - A_{RH-L} — Lower White Quartzite Member

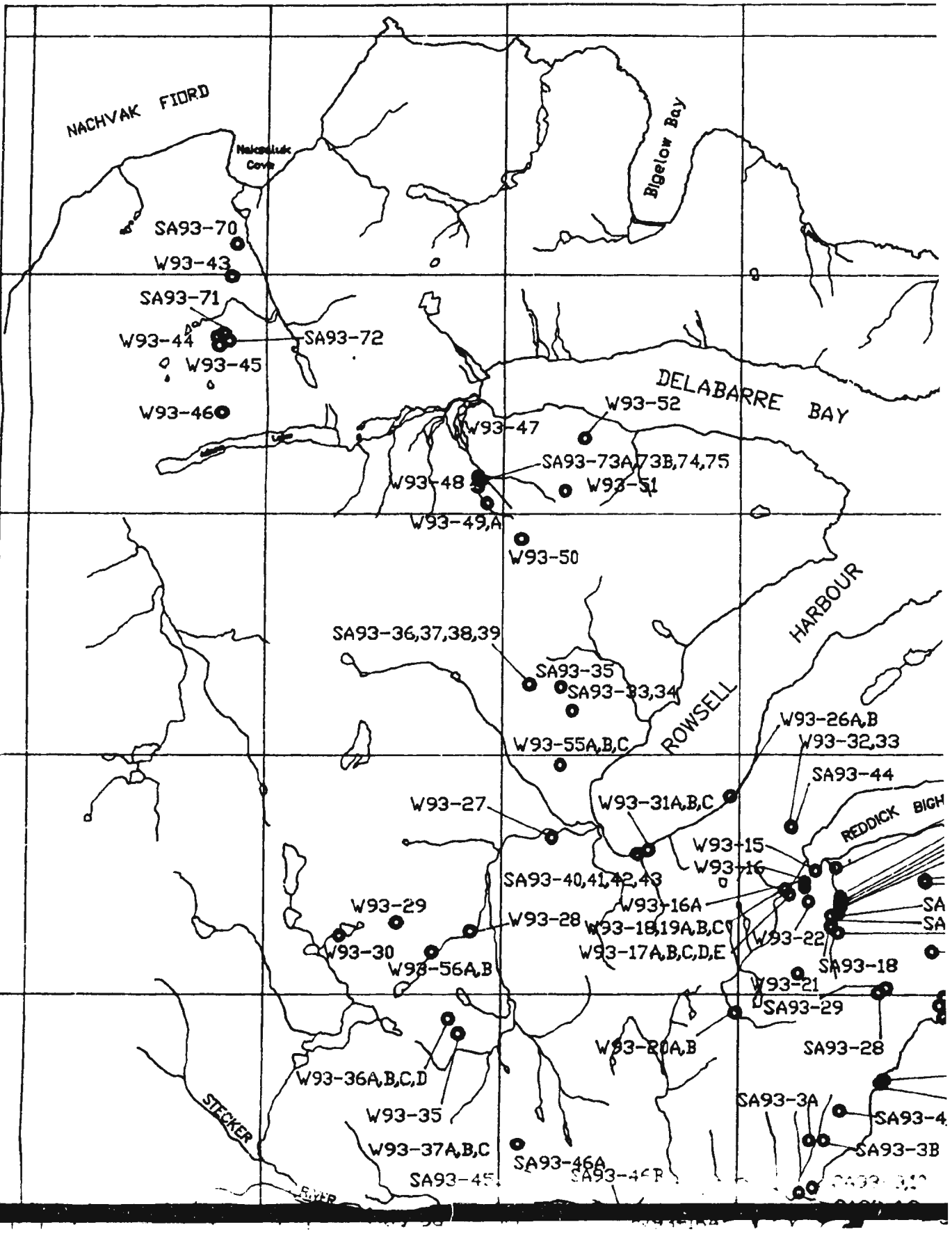
NACHVAK FIORD
Nakeeluk Cove
Bigelow Bay
SA93-70
W93-43
SA93-71
W93-44
SA93-72
W93-45
W93-46
DELABARRE BAY
W93-52
W93-47
SA93-73A,73B,74,75
W93-48
W93-51
W93-49,A
W93-50
HARBOUR
SA93-36,37,38,39
SA93-35
SA93-33,34
ROWSELL
W93-26A,B
W93-32,33
W93-55A,B,C
SA93-44
W93-27
W93-31A,B,C
REDDICK BIGH
W93-15
W93-16
SA93-40,41,42,43
W93-16A
W93-29
W93-28
W93-18,19A,B,C
W93-22
W93-30
W93-17A,B,C,D,E
W93-56A,B
SA93-18
W93-21
SA93-29
W93-20A,B
SA93-28
W93-36A,B,C,D
SA93-3A
W93-35
STECKER
W93-37A,B,C
SA93-46A
SA93-3B
SA93-45

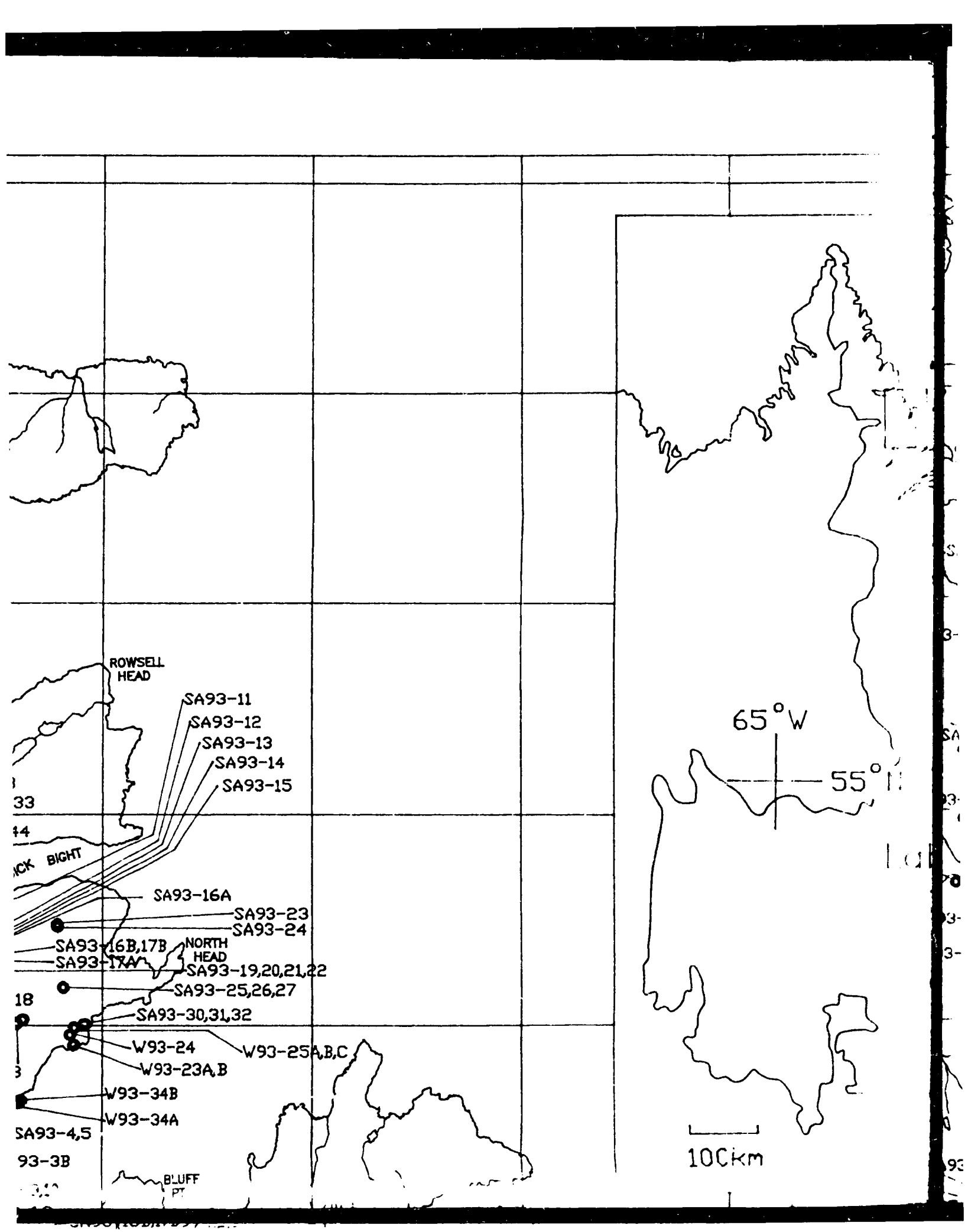
ROWSELL HEAD
SA93-11
SA93-12
SA93-13
SA93-14
SA93-15
SA93-16A
SA93-23
SA93-24
SA93-16B,17B
SA93-17A
NORTH HEAD
SA93-19,20,21,22
SA93-25,26,27
SA93-30,31,32
W93-24
W93-25A,B,C
W93-23A,B
W93-34B
W93-34A
SA93-4,5
93-3B
BLUFF PT
65°W
55°
100km

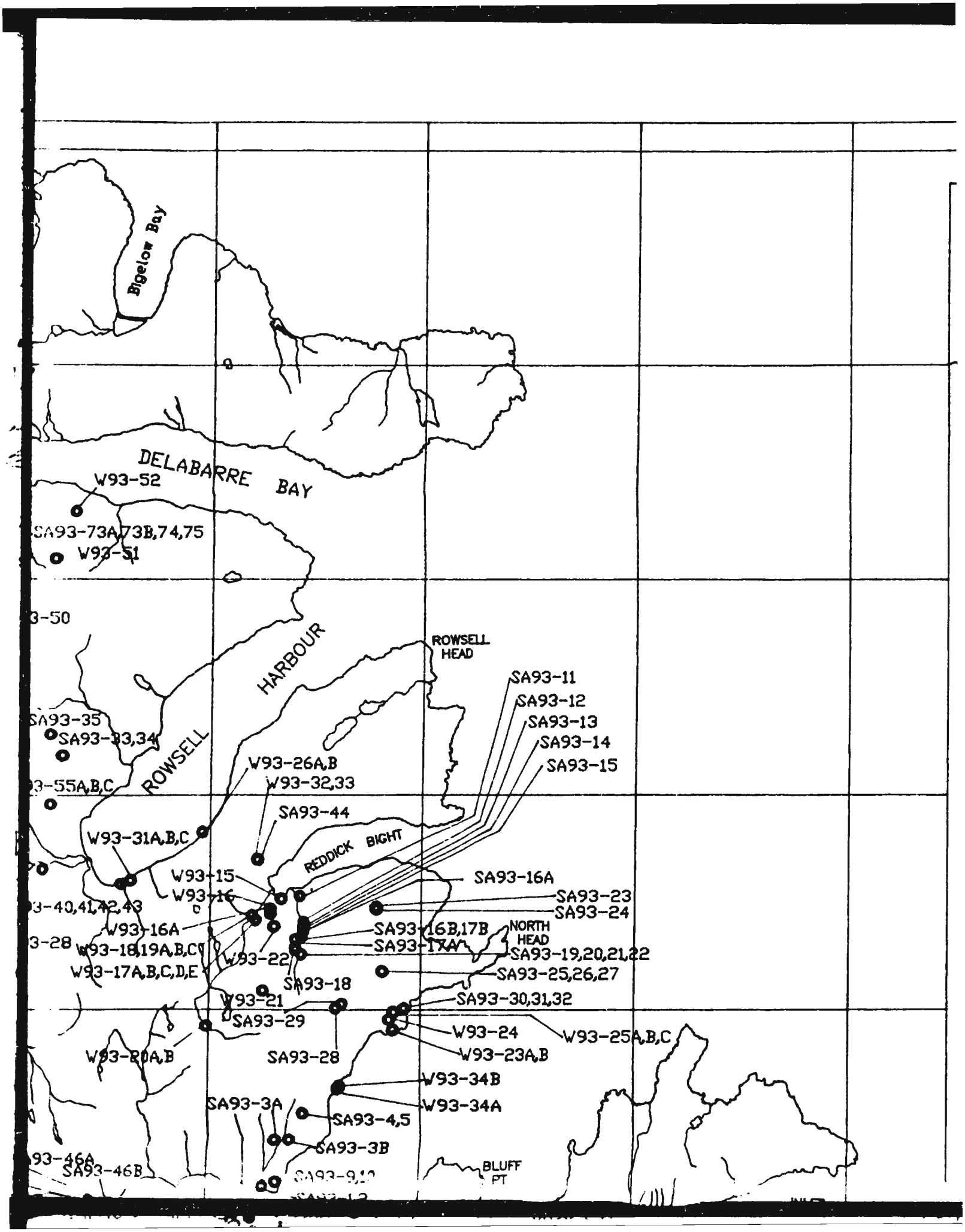
Bigelow Bay
DELABARRE BAY
W93-52
SA93-73A,73B,74,75
W93-51
3-50
HARBOUR
ROWSELL
ROWSELL HEAD
SA93-11
SA93-12
SA93-13
SA93-14
SA93-15
SA93-35
SA93-33,34
3-55A,B,C
W93-26A,B
W93-32,33
SA93-44
W93-31A,B,C
REDDICK BIGHT
W93-15
W93-16
SA93-16A
SA93-23
SA93-24
3-40,41,42,43
W93-16A
SA93-16B,17B
NORTH HEAD
3-28
W93-18,19A,B,C
SA93-17A
SA93-19,20,21,22
W93-22
W93-17A,B,C,D,E
SA93-25,26,27
SA93-18
W93-21
SA93-30,31,32
SA93-29
W93-24
W93-25A,B,C
W93-20A,B
SA93-28
W93-23A,B
W93-34B
SA93-3A
W93-34A
SA93-4,5
SA93-3B
93-46A
SA93-46B
BLUFF PT

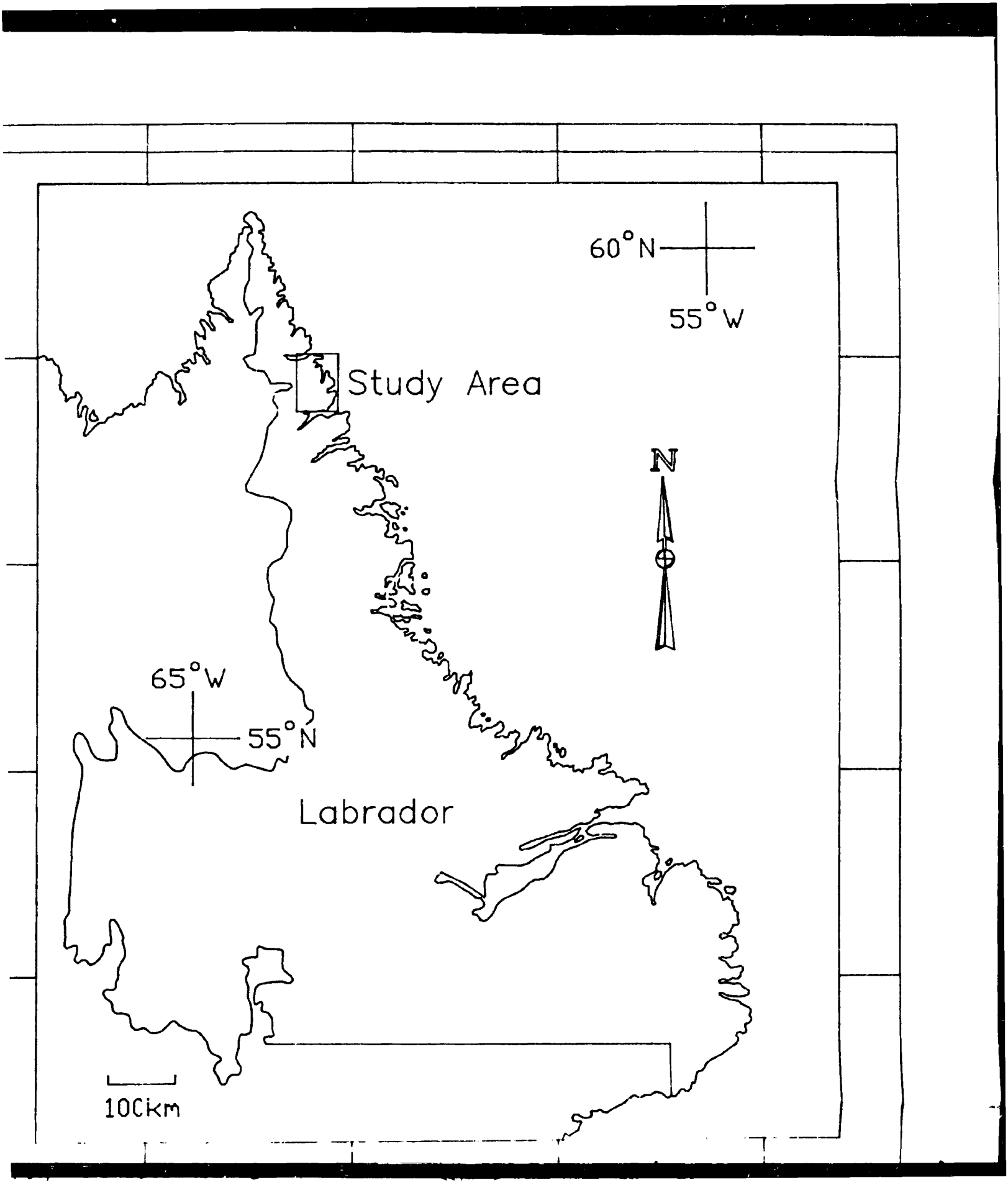
60°N
55°W
Study Area
N
65°W
55°N
Labrador
100km

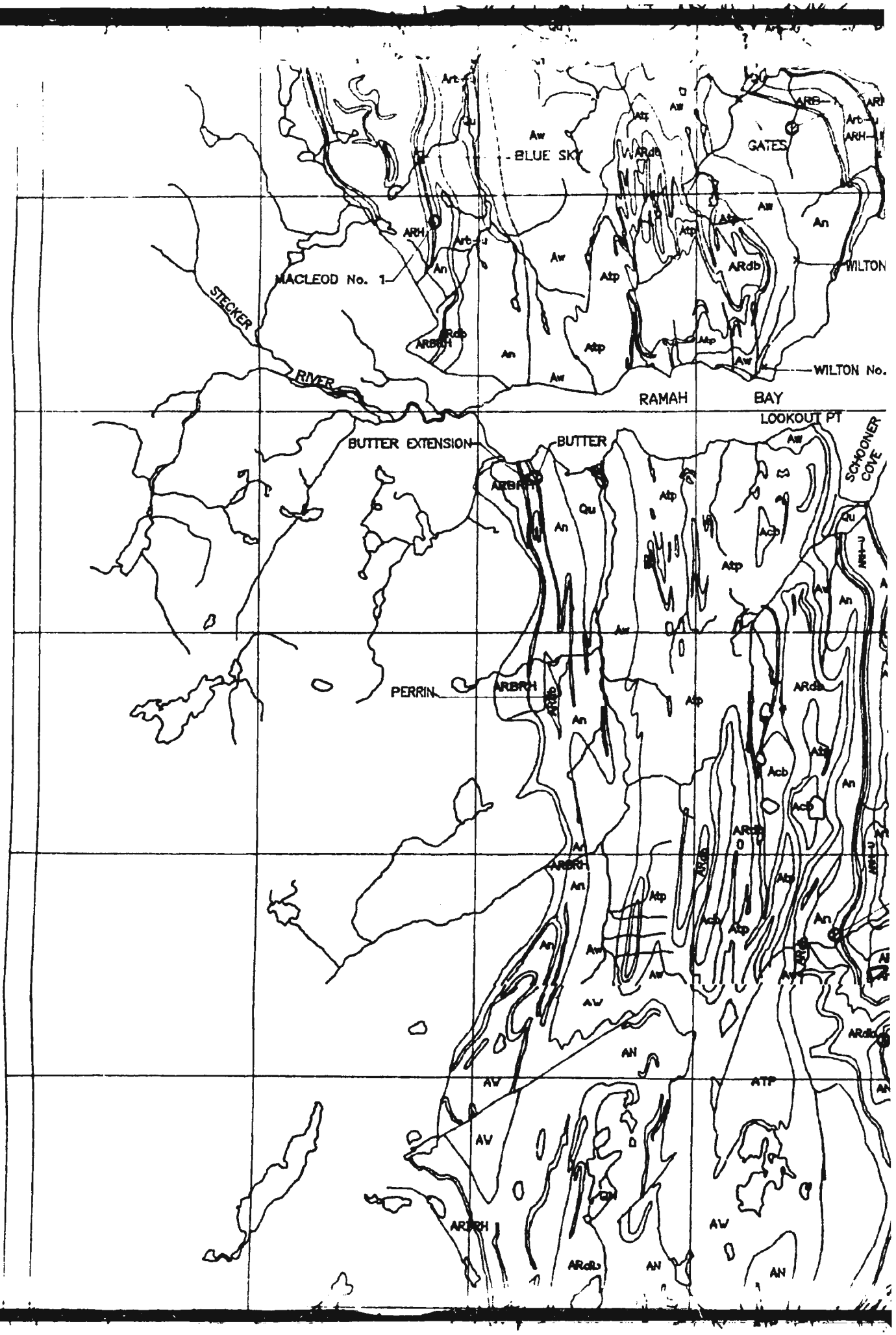
BLUE SKY
GATES
WILTON
MACLEOD No. 1
STECKER
RIVER
WILTON No.
RAMAH
BAY
LOOKOUT PT
SCHOONER COVE
BUTTER EXTENSION
BUTTER
PERRIN
Aw
An
Atp
ARdb
ARBRH
Acb
Qu
AV
AN
ATP

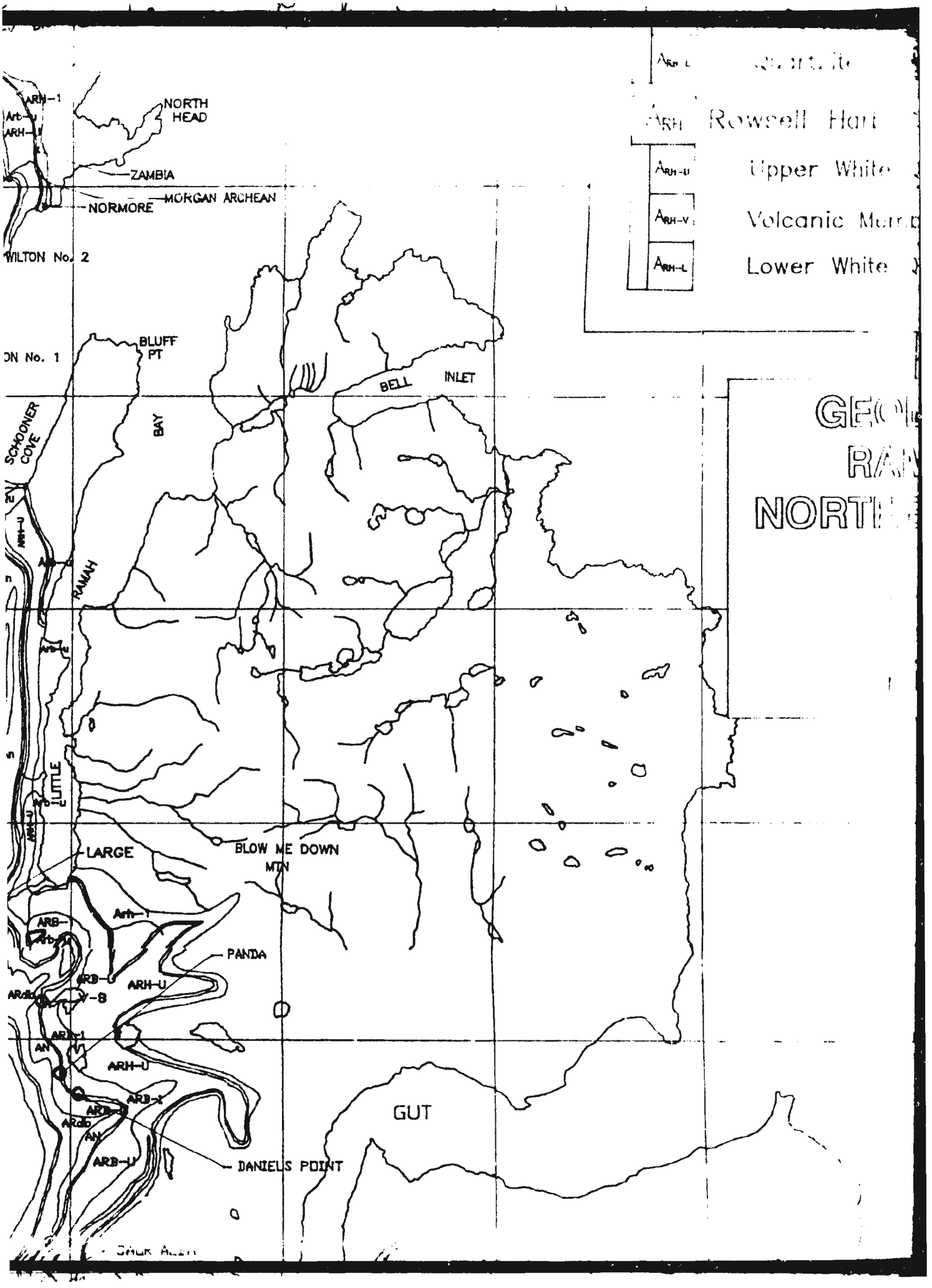
ARH Rowsell Hart
Upper White
Volcanic Mem
Lower White
NORTH HEAD
ZAMBIA
NORMORE
MORGAN ARCHEAN
WILTON No. 2
BLUFF PT
BELL INLET
SCHOONER COVE
BAY
RAMAH
LITTLE
LARGE
BLOW ME DOWN MTN
PANDA
GUT
DANIELS POINT
ARH-U
ARB
V-8

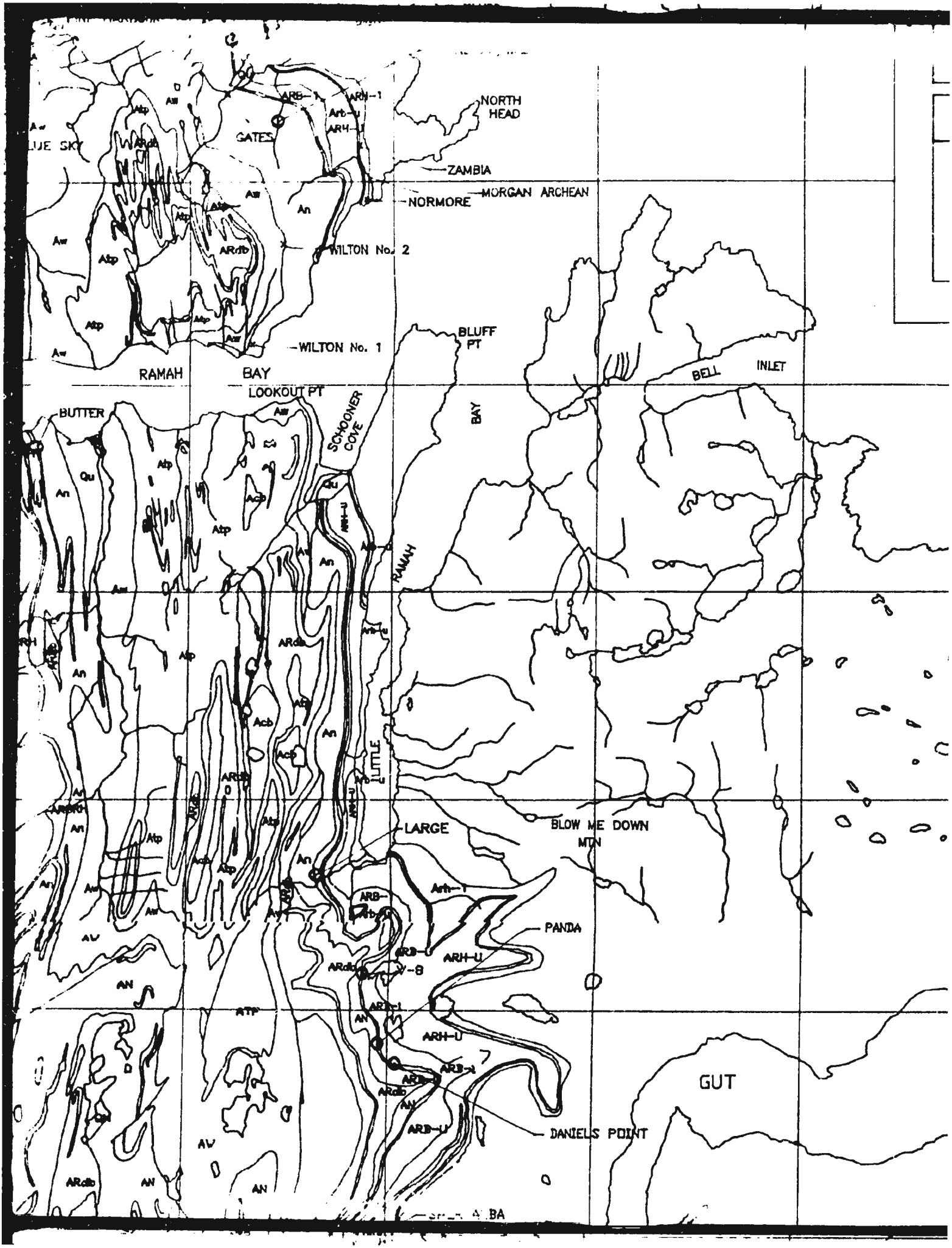
NORTH HEAD
GATES
ZAMBIA
NORMORE
MORGAN ARCHEAN
WILTON No. 2
WILTON No. 1
BLUFF PT
RAMAH BAY
LOOKOUT PT
BELL INLET
BUTTER
SCHOONER COVE
BAY
RAMAH
LITTLE
LARGE
BLOW ME DOWN MTN
PANDA
GUT
DANIELS POINT

Quartzite Member

A_{RH}	Rowseil Harbour Formation (Undivided)
A_{RH-U}	Upper White Quartzite Member
A_{RH-V}	Volcanic Member
A_{RH-L}	Lower White Quartzite Member

GEOLOGICAL MAP
RAMAH GROUP
NORTHERN LABRADOR

0 5

Kilometres

LABRADOR SEA

(ATLANTIC OCEAN)

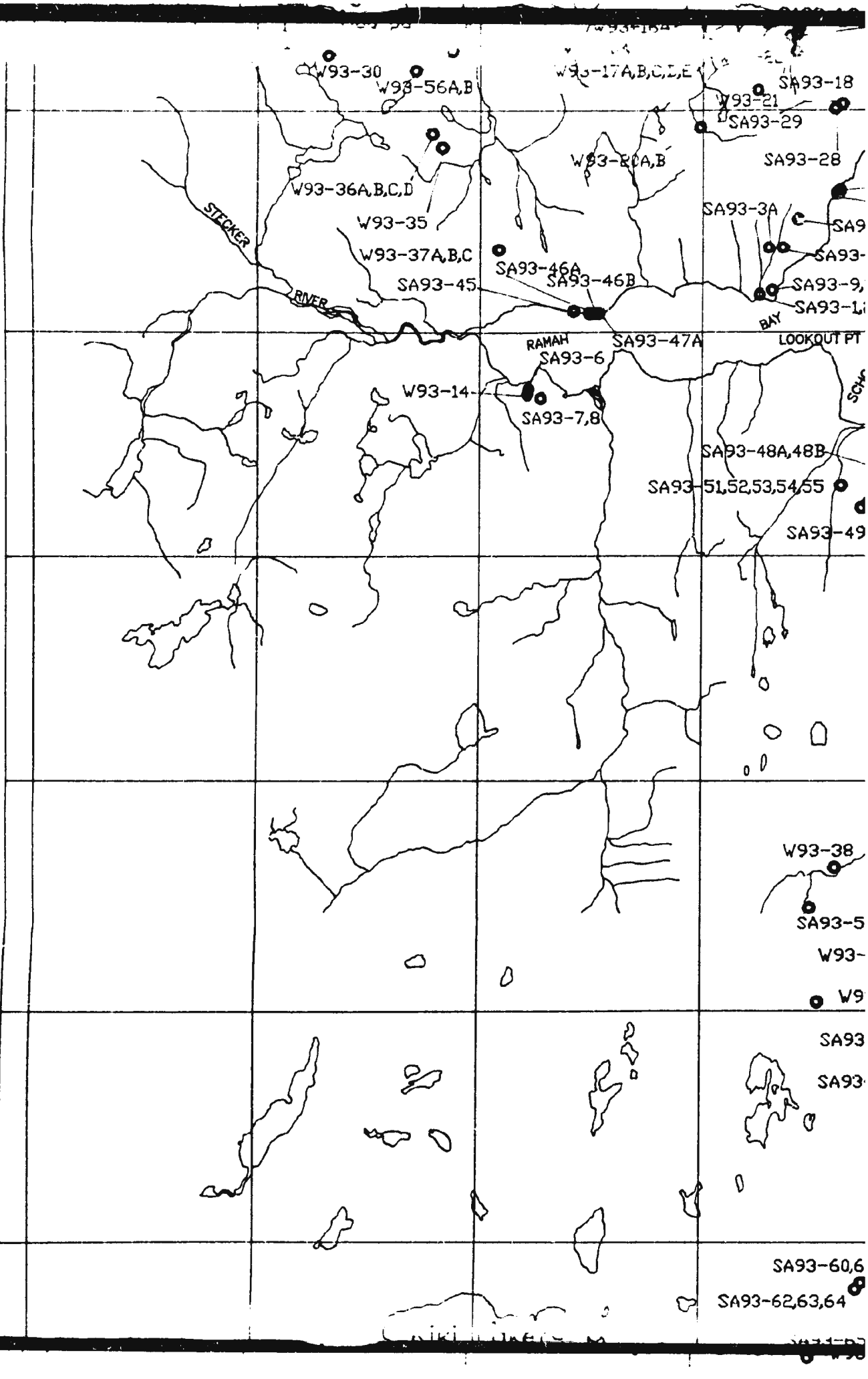
W93-30
W93-56A,B
W93-17A,B,C,D,E
SA93-18
W93-21
SA93-29
SA93-28
W93-8CA,B
W93-36A,B,C,D
STECKER
RIVER
W93-35
W93-37A,B,C
SA93-46A
SA93-46B
SA93-45
SA93-3A
SA93-9,
SA93-1
BAY
LOOKOUT PT
RAMAH
SA93-47A
SA93-6
W93-14
SA93-7,8
SA93-48A,48B
SA93-51,52,53,54,55
SA93-49
W93-38
SA93-5
W93-
W9
SA93
SA93
SA93-60,6
SA93-62,63,64

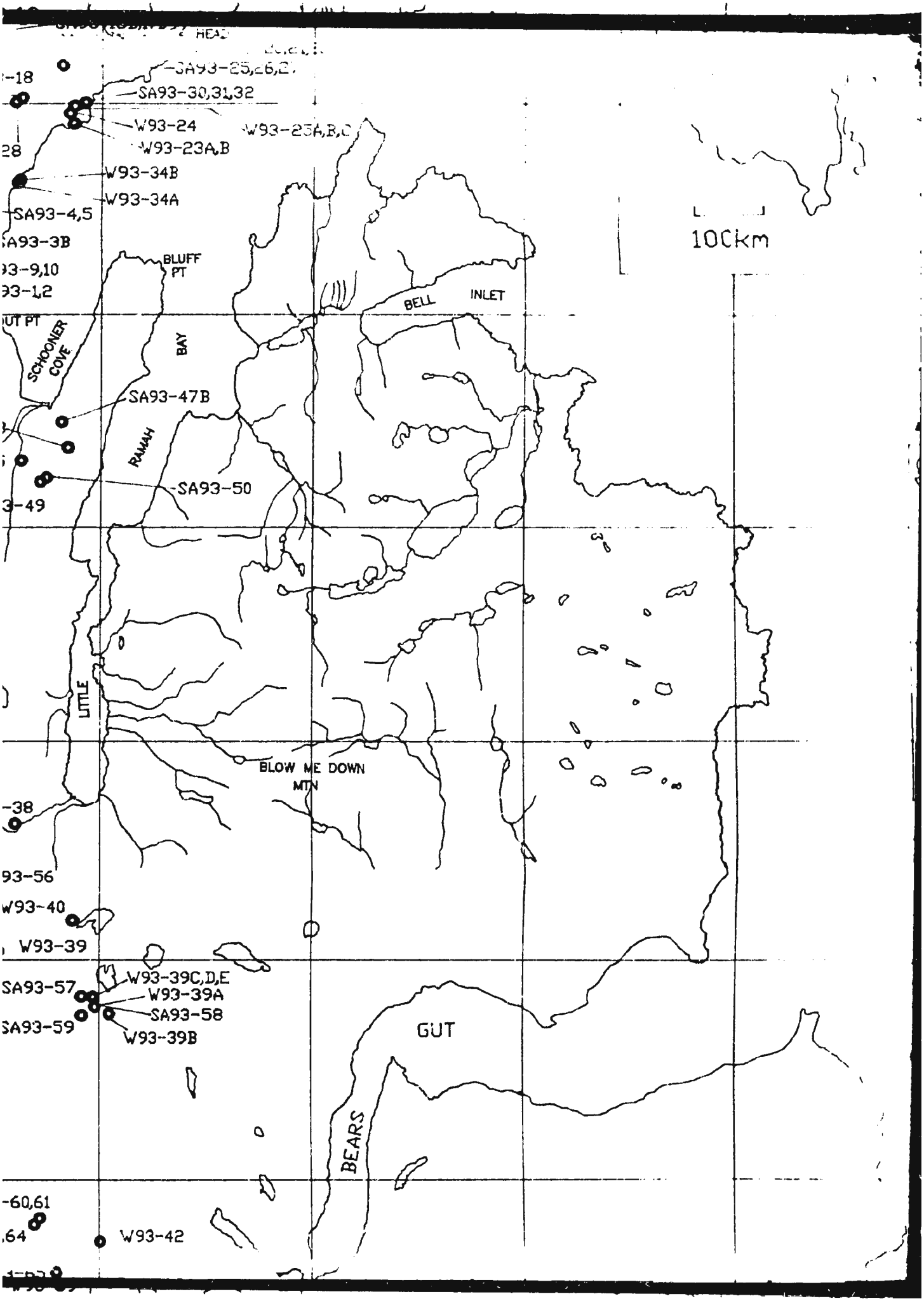
SA93-30,31,32
W93-24
W93-23A,B
W93-34B
W93-34A
SA93-4,5
BLUFF PT
BELL INLET
100km
SCHOONER COVE
BAY
SA93-47B
RAMAH
SA93-50
LITTLE
BLOW ME DOWN MTN
W93-40
W93-39
W93-39C,D,E
W93-39A
SA93-58
W93-39B
GUT
BEARS
W93-42

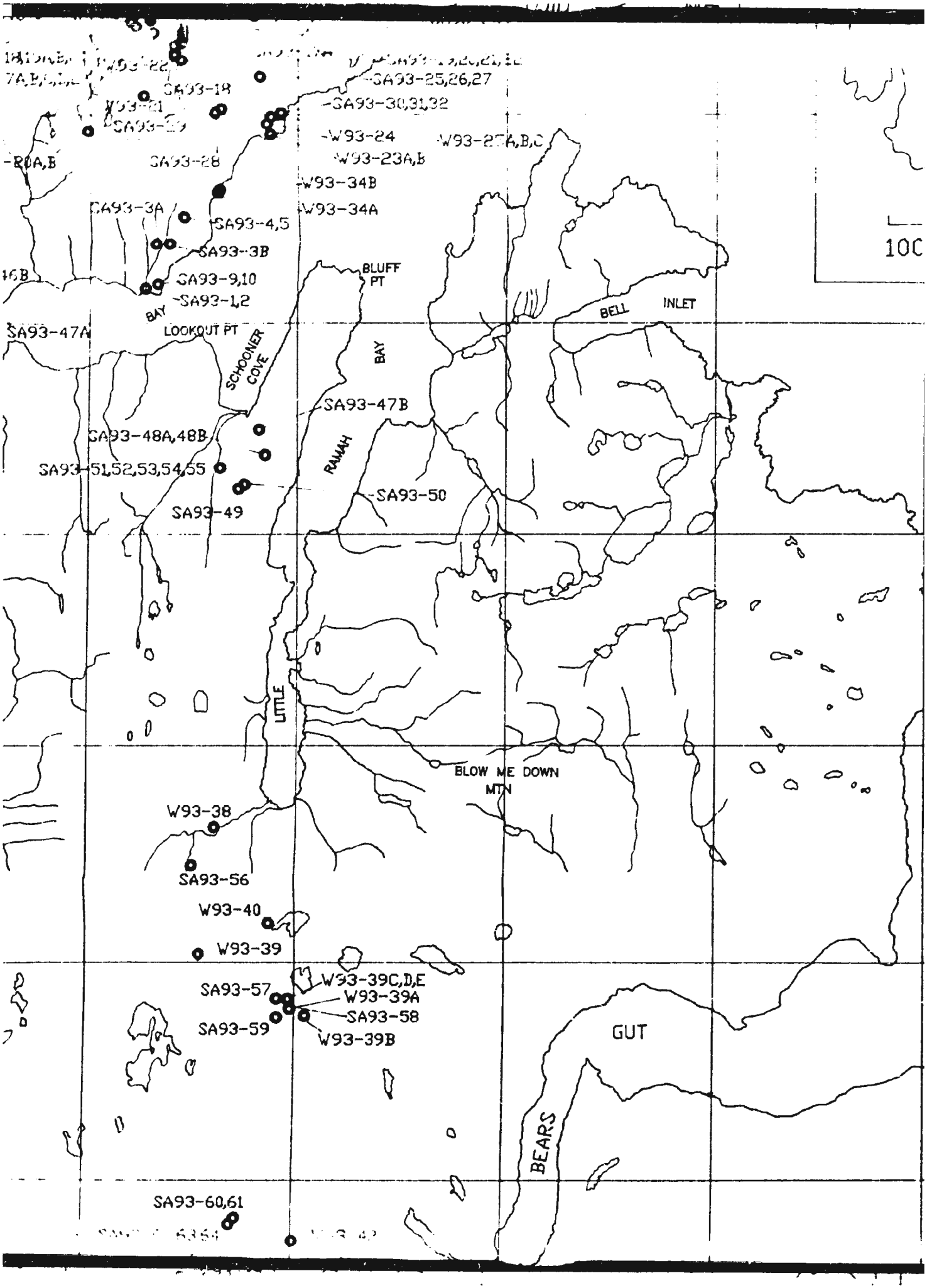
SA93-25,26,27
SA93-30,31,32
W93-24
W93-23A,B
W93-34B
W93-34A
SA93-28
SA93-3A
SA93-4,5
SA93-3B
SA93-9,10
SA93-1,2
BAY
LOOKOUT PT
SCHOONER COVE
BLUFF PT
BELL INLET
BAY
SA93-47A
SA93-47B
SA93-48A,48B
SA93-51,52,53,54,55
SA93-49
SA93-50
RAMAH
LITTLE
BLOW ME DOWN MTN
W93-38
SA93-56
W93-40
W93-39
W93-39C,D,E
W93-39A
SA93-57
SA93-58
SA93-59
W93-39B
GUT
BEARS
SA93-60,61

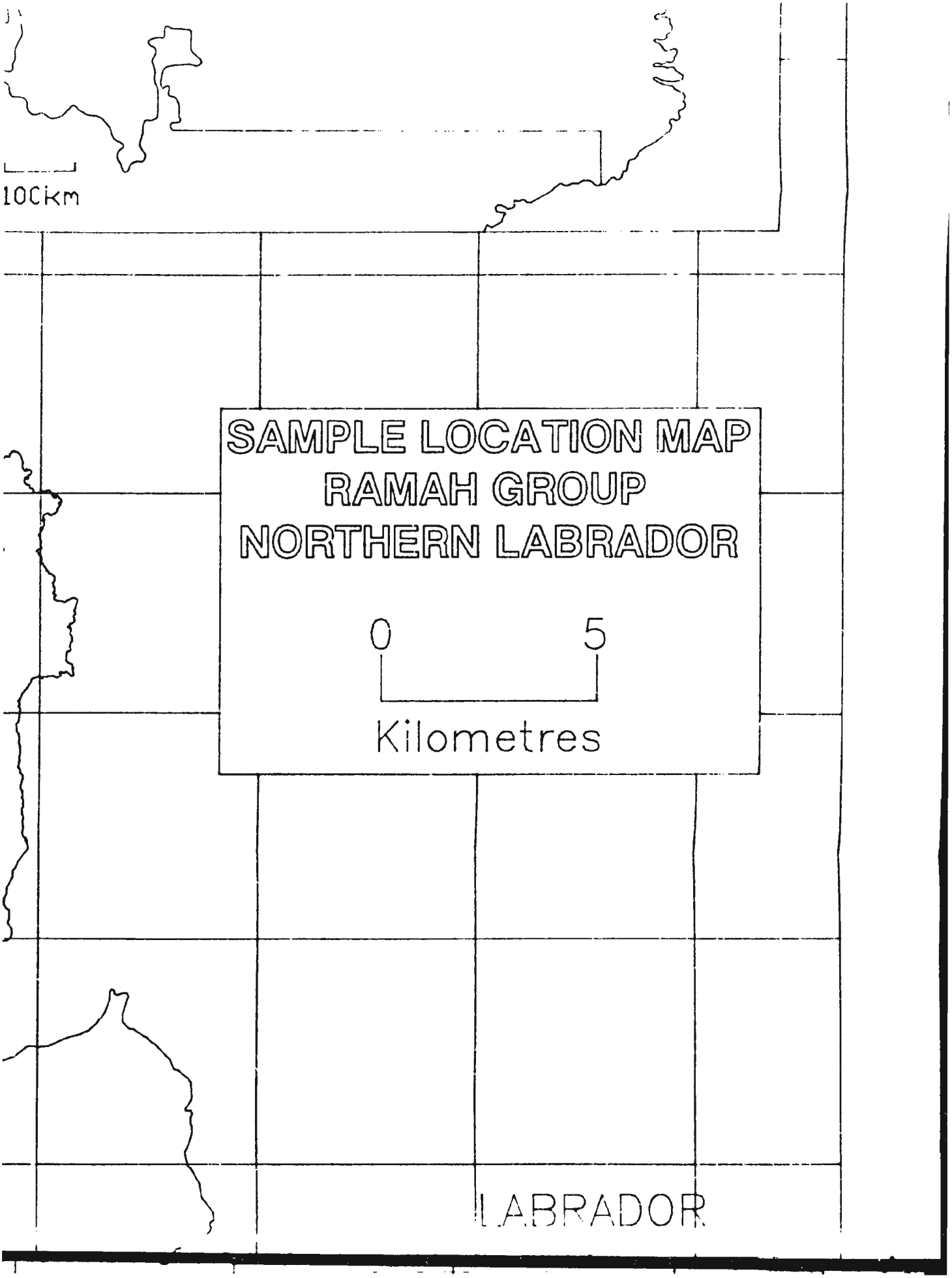
100km
SAMPLE LOCATION MAP
RAMAH GROUP
NORTHERN LABRADOR
0
5
Kilometres
LABRADOR

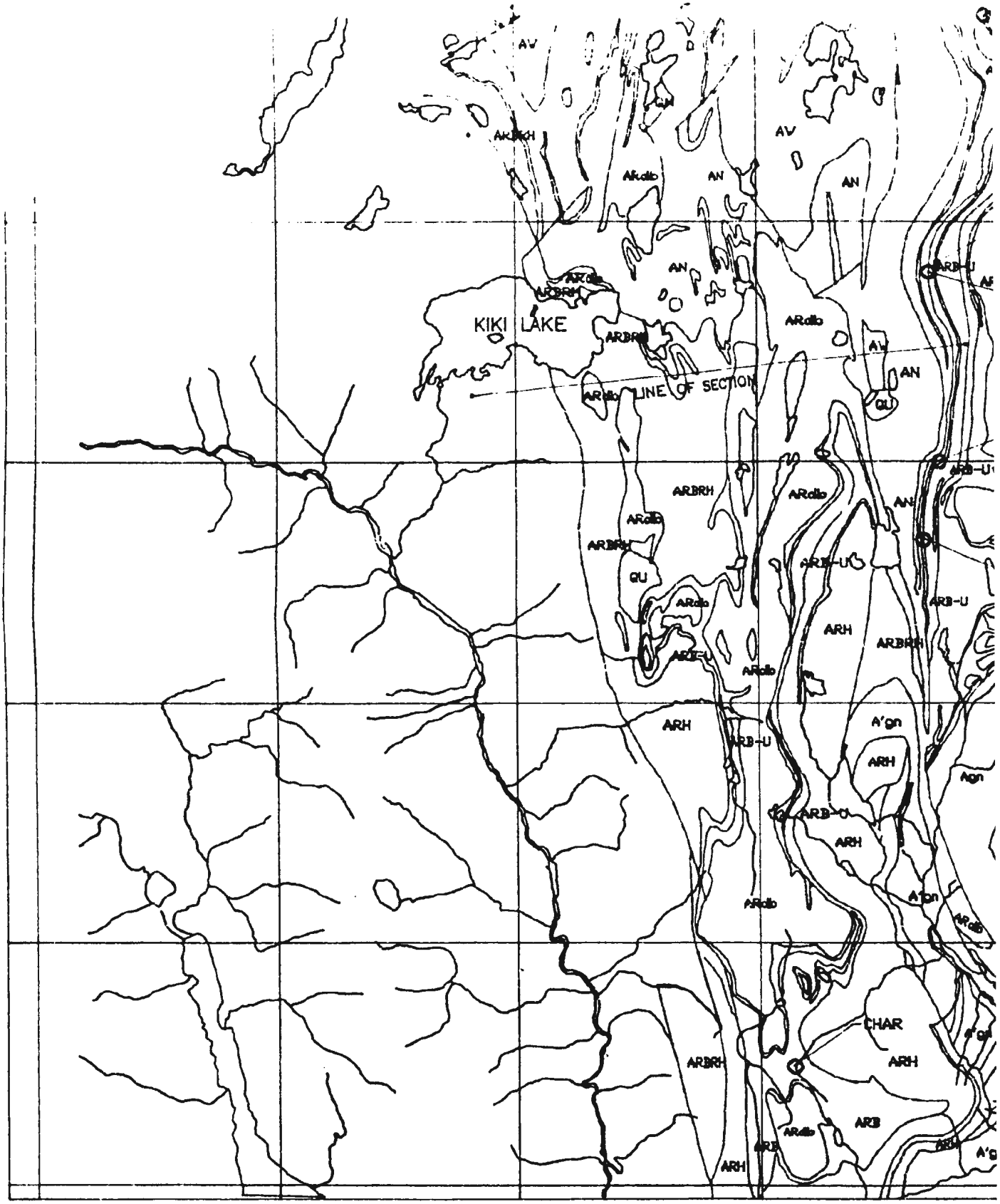
KIKI LAKE
LINE OF SECTION
AV
AN
ARdlo
ARBRH
ARH
ARB-U
QU
A'gn
CHAR
ARB

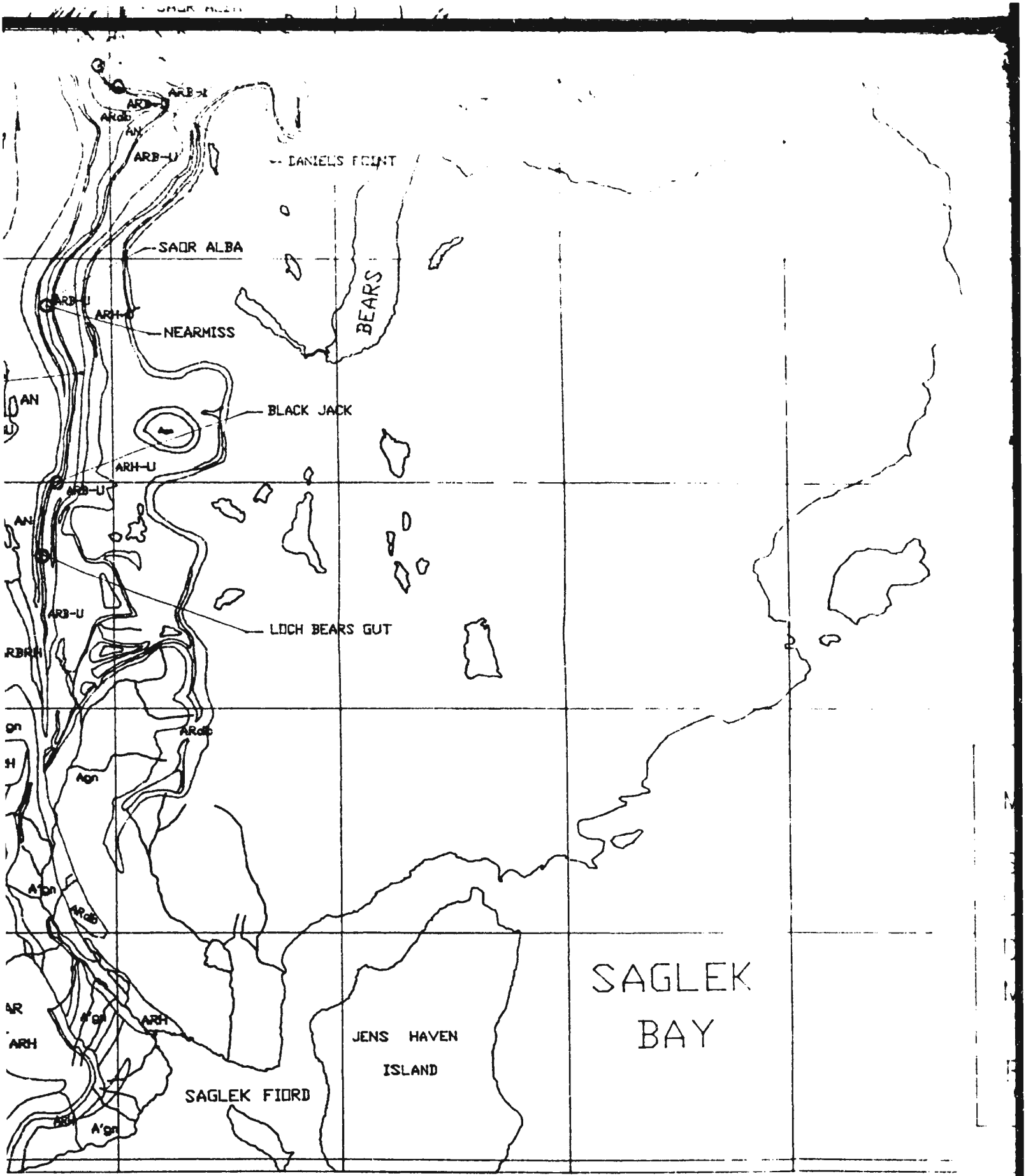
DANIELS POINT
SAOR ALBA
BEARS
NEARMISS
BLACK JACK
LOCH BEARS GUT
SAGLEK
BAY
JENS HAVEN
ISLAND
SAGLEK FIORD

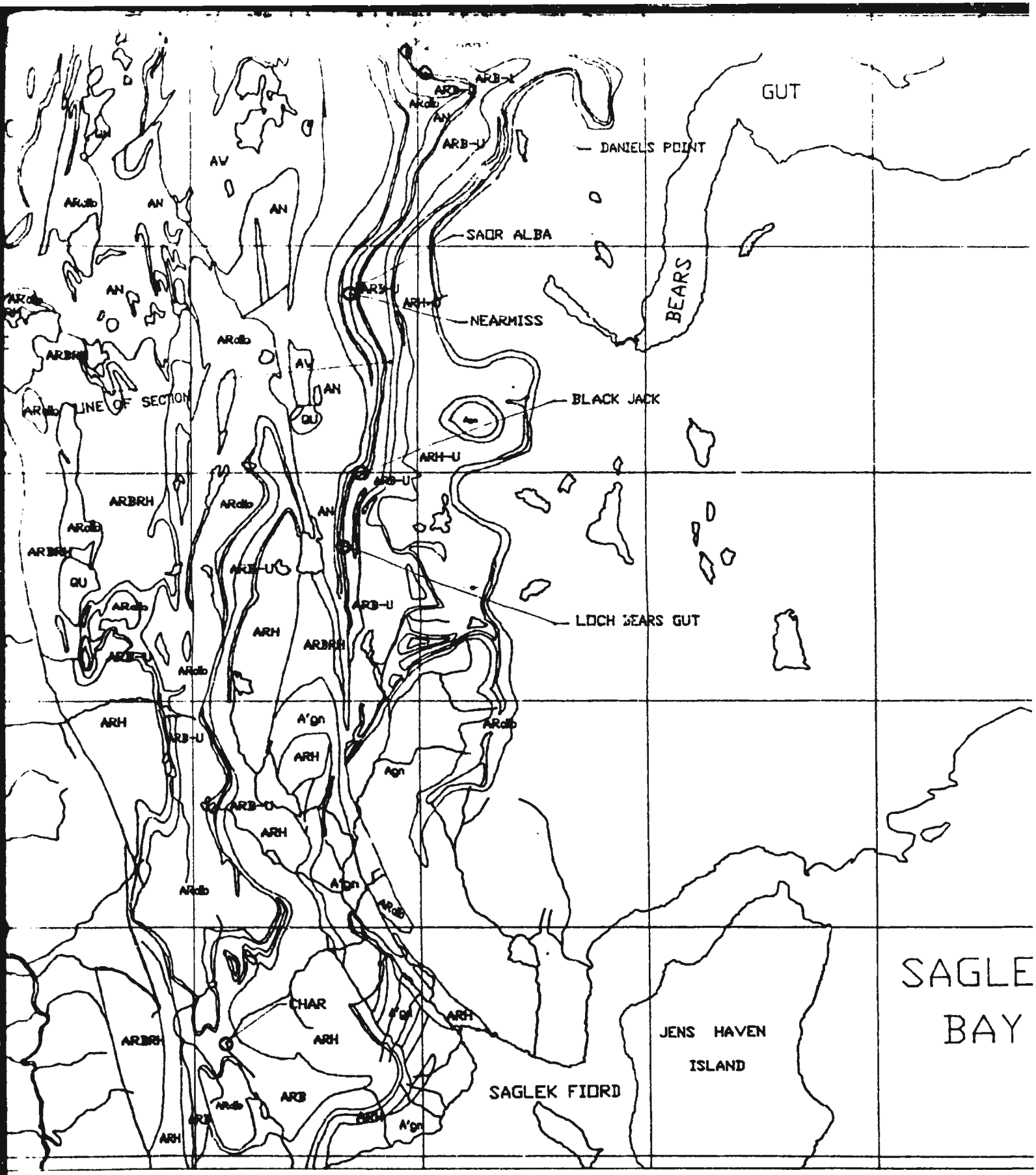
GUT
DANIELS POINT
SAOR ALBA
BEARS
NEARMISS
BLACK JACK
LINE OF SECTION
LOCH BEARS GUT
CHAR
SAGLEK FIORD
JENS HAVEN
ISLAND
SAGLE
BAY
AV
AN
QU
ARH
ARB-U
ARBRH
ARdlb
A'gn
Agn

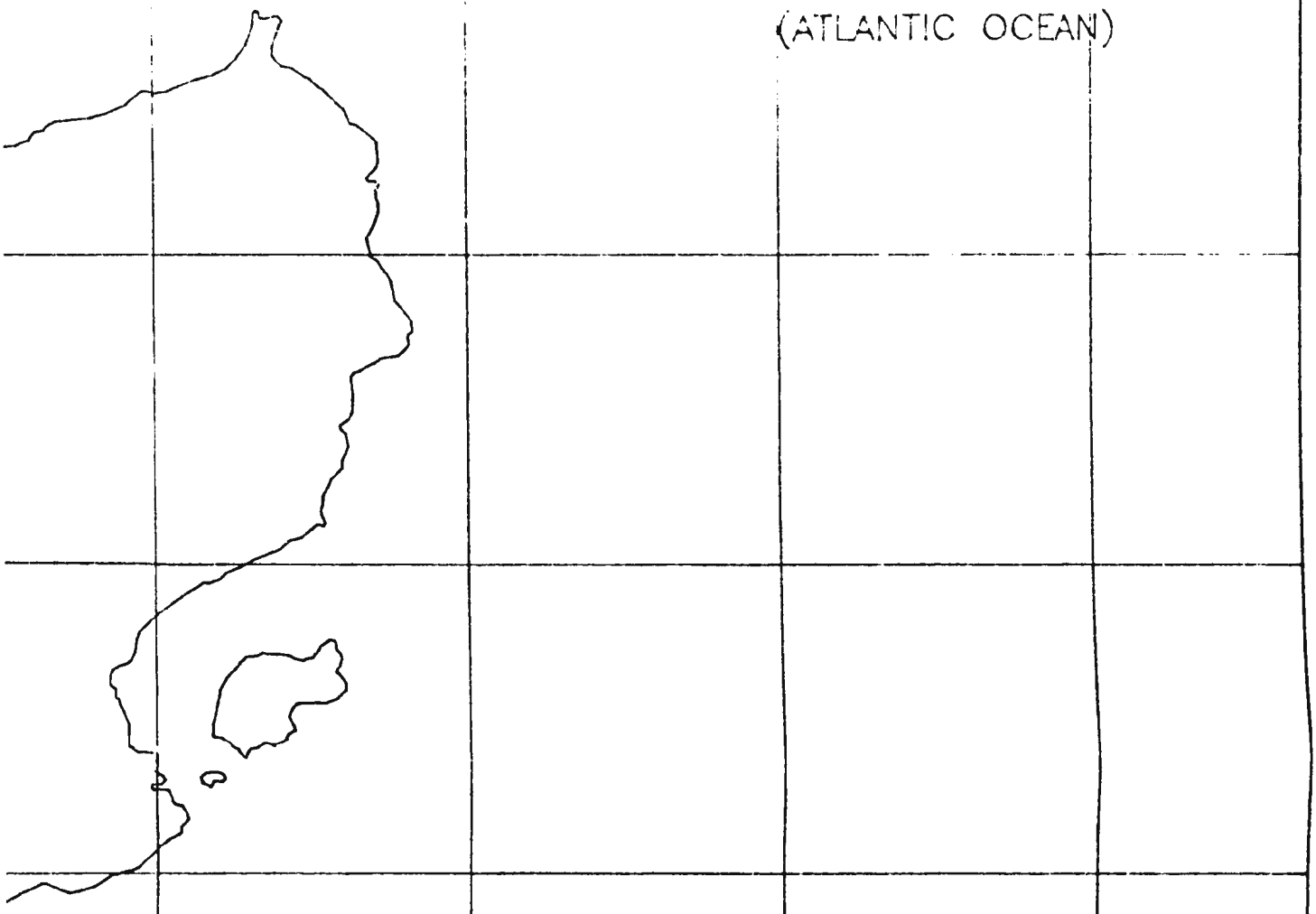

MAP 1: GEOLOGY AND SHOWINGS

S.M. Archibald
Unpublished M.Sc. thesis
Department of Earth Sciences
Memorial University of Nfld.

February 1995

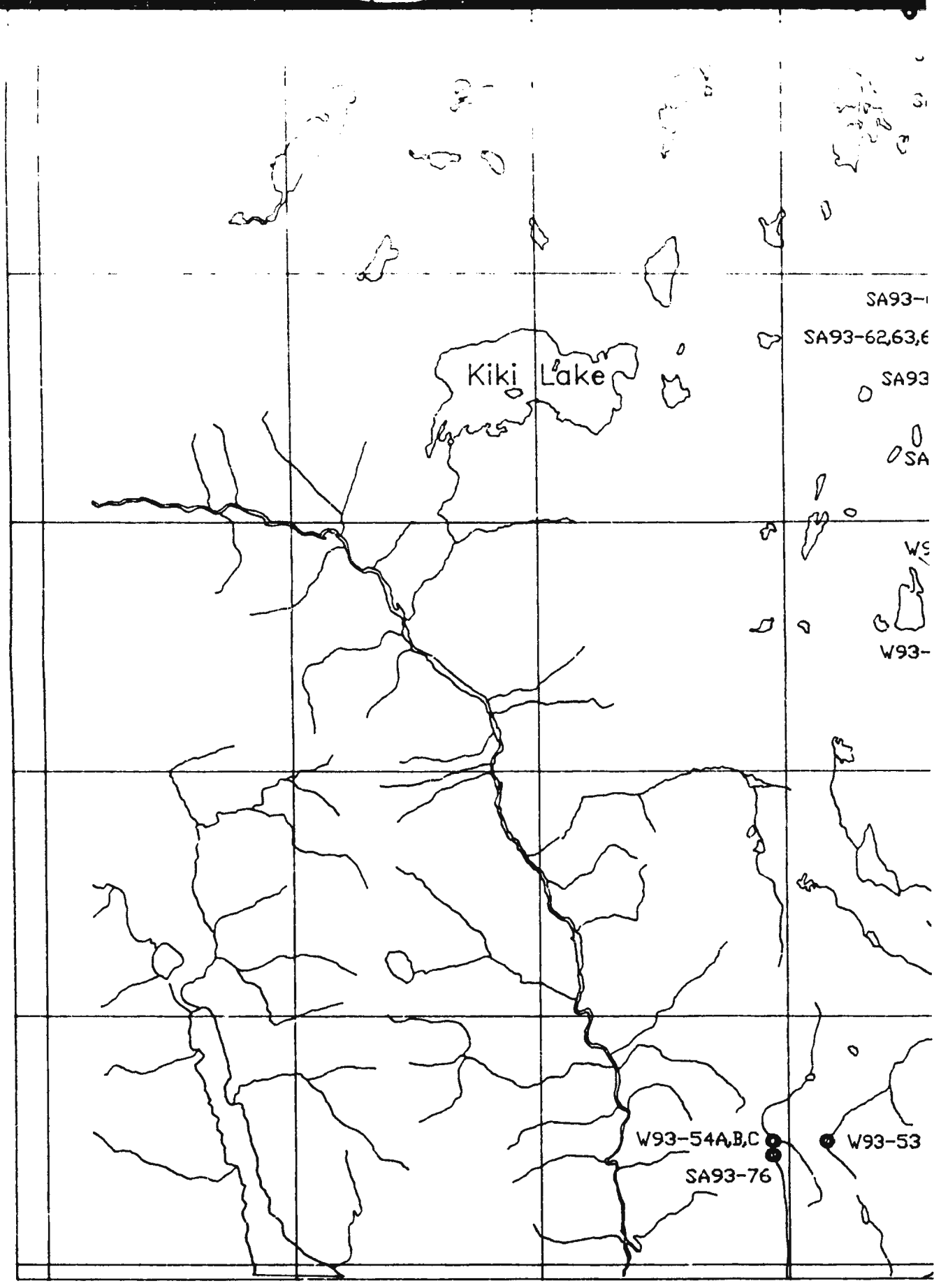
Kiki Lake
SA93-
SA93-62,63,
SA93
SA
W93-
W93-54A,B,C
SA93-76
W93-53

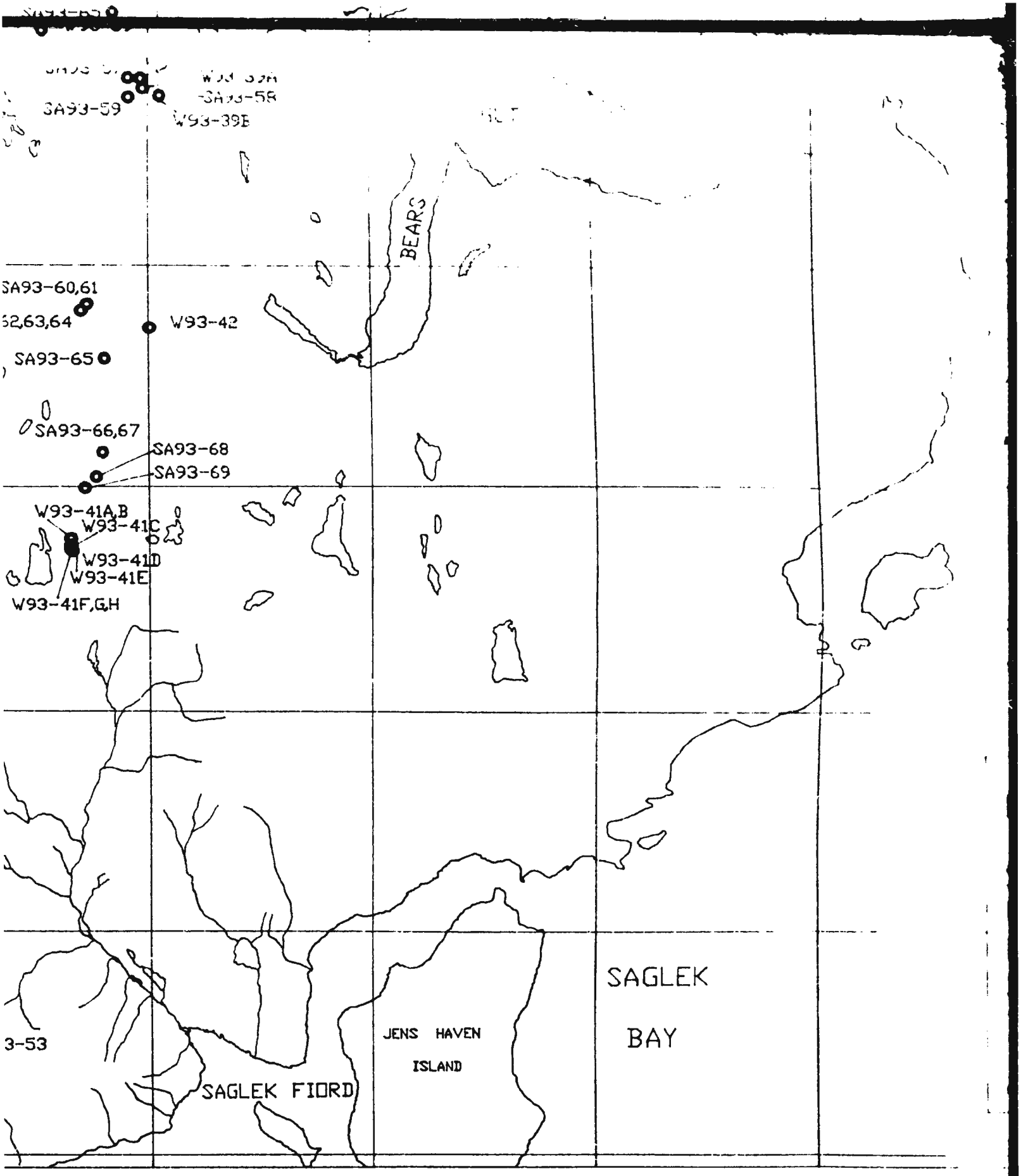
SA93-59
W93-39B
BEARS
SA93-60,61
62,63,64
W93-42
SA93-65
SA93-66,67
SA93-68
SA93-69
W93-41A,B
W93-41C
W93-41D
W93-41E
W93-41F,G,H
3-53
SAGLEK FIORD
JENS HAVEN
ISLAND
SAGLEK
BAY

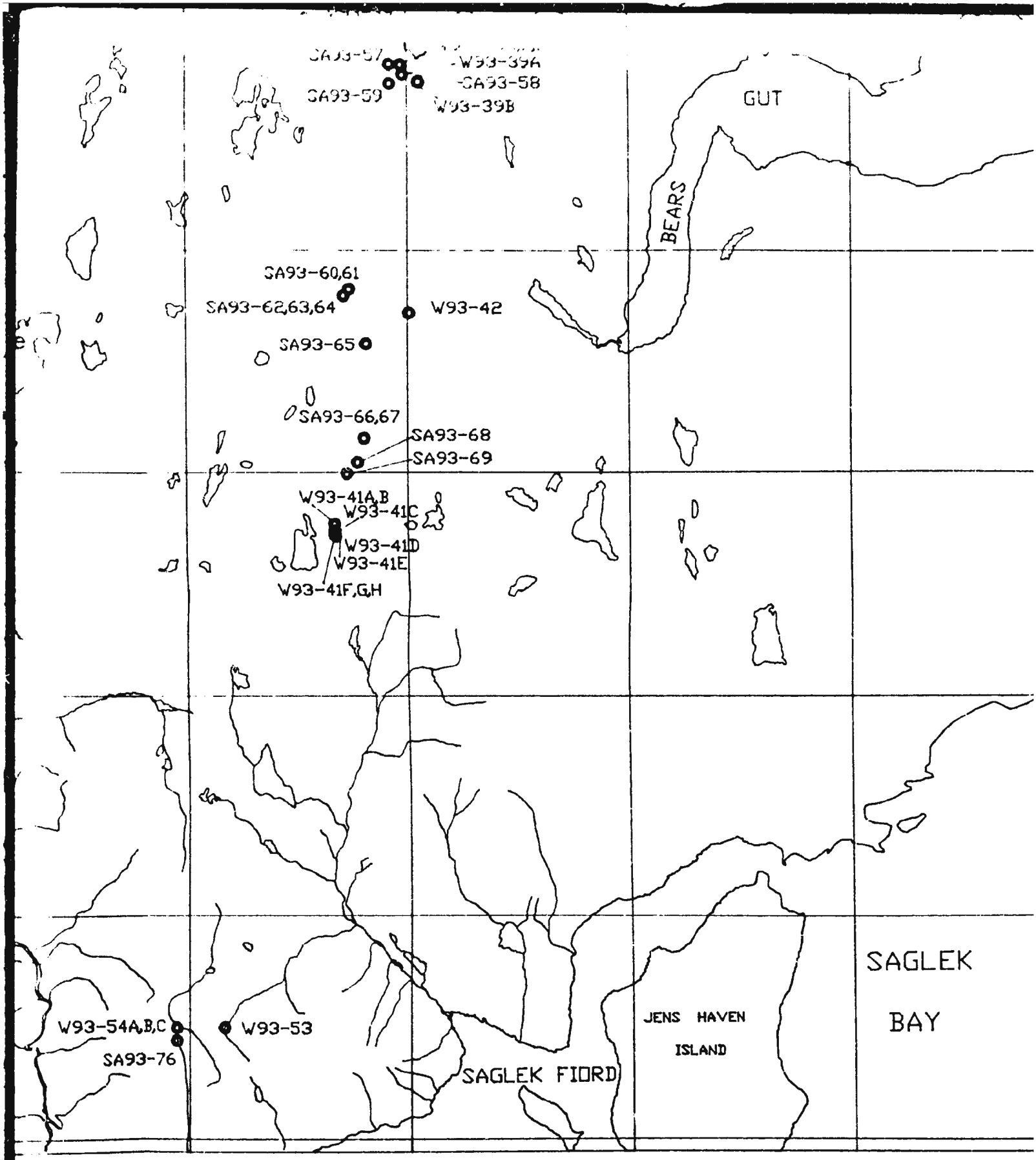
SA93-57
W93-39A
SA93-58
SA93-59
W93-39B
GUT
BEARS
SA93-60,61
SA93-62,63,64
W93-42
SA93-65
SA93-66,67
SA93-68
SA93-69
W93-41A,B
W93-41C
W93-41D
W93-41E
W93-41F,G,H
W93-54A,B,C
SA93-76
W93-53
SAGLEK FIORD
JENS HAVEN
ISLAND
SAGLEK
BAY

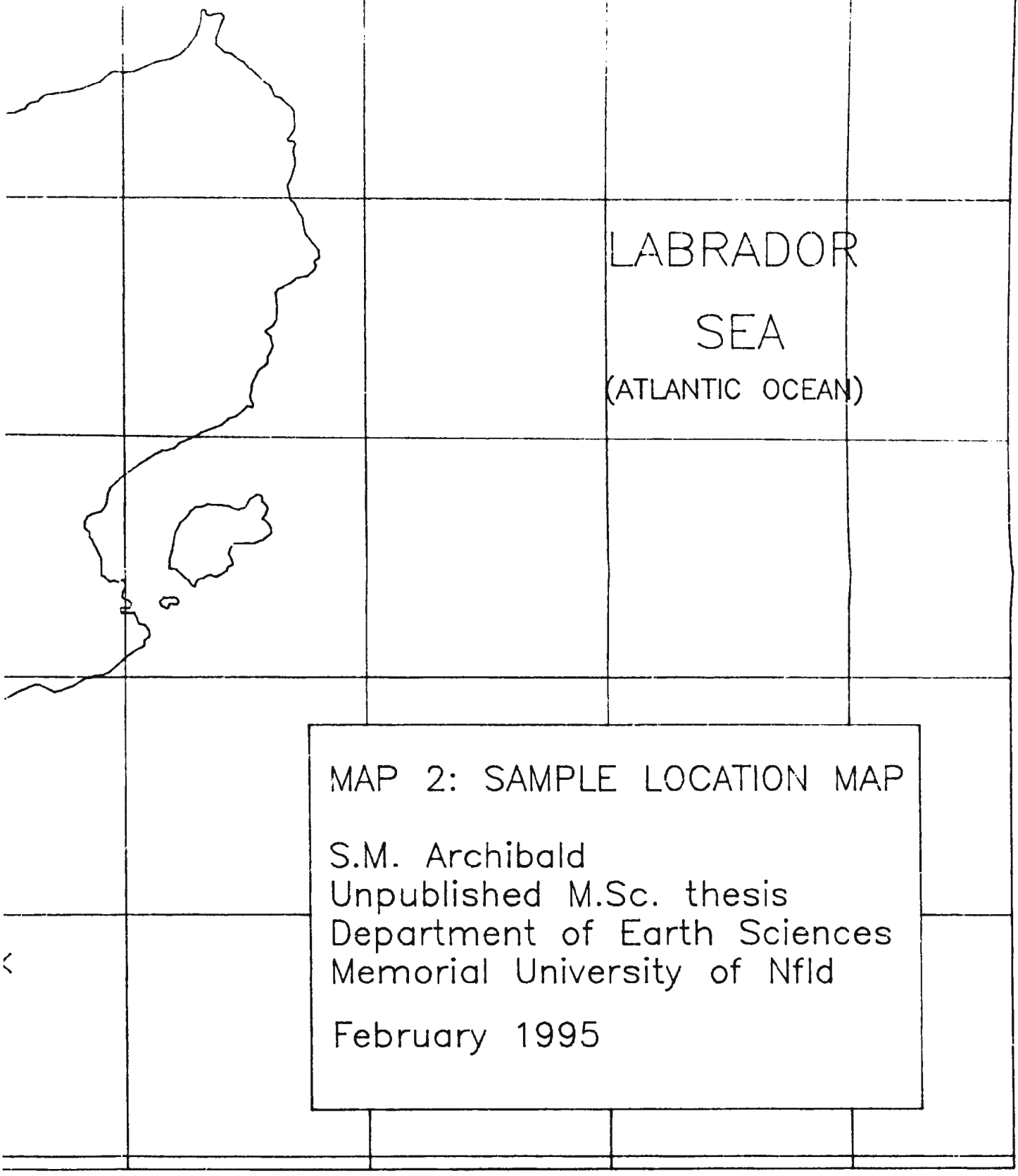

MAP 2: SAMPLE LOCATION MAP

S.M. Archibald
Unpublished M.Sc. thesis
Department of Earth Sciences
Memorial University of Nfld

February 1995